The Geology, Sedimentology, Geochronology and Palaeo-environmental Reconstruction of the Heelbo Hillslope Deposit, Free State Province, South Africa

Mary Yvonne Evans

Thesis submitted in fulfillment of the requirements for the
Degree of Doctor of Philosophy
University of the Witwatersrand
South Africa
2015

ABSTRACT

A multidisciplinary sedimentological, stratigraphic, mineralogical and geochronological analysis of a small, fossil-bearing, Holocene hillslope deposit, flanking a mesa, has enabled a reconstruction of the palaeo-environmental history of the region. The hillslope deposit, located on the farm Heelbo in the eastern Free State Povince, South Africa, overlies Jurassic mudrock and sandstone of the Elliot Formation, Karoo Supergroup. The deposit is located on a steep (~10°) slope and covers an area of ~7 km^2 in two separate sections. It extends ~475 m downslope and reaches a maximum thickness of at least 6-8 m towards the base.

Mineralogy indicates the deposit is sourced from the mesa but its fine grain size and location on a steep slope position Heelbo outside the scope of traditionally described alluvial fans or colluvial deposits. The hillslope deposit is described as an alluvial slope based on the morphology of the deposit and the grain size distribution against the slope gradient. The deposit comprises fine-sand to silt- grain size, but is found on a steep (~10°) slope. The source of the sediment is shown to be the sediment of the mesa, rather than input from an aeolian source. The grains are described as sub-angular and poorly sorted which also suggests a local provenance for the sediment.

Microscopic and XRF analysis confirm the derivation of the sediment from the Elliot Formation, with the lithic fragments derived from subarkoses to arkoses of the underlying bedrock of the Upper Elliot Formation (UEF) in the Karoo Supergroup. Secondary calcite was visible in only two of the thin sections, thus it is likely due to a diagenetic overprint that is constrained by depth from the surface or time and not to specific layers.

The deposit is cut by several mature and continuous gully networks with V-shaped profiles in the proximal slope, and combined V- and U-shaped profiles in the medial and distal sections. Gully formation is linked to both the sodium adsorption ratio (SAR_s), and high soil clay content, which facilitates swelling and shrinking.

The Heelbo deposit comprises two palaeosols (BT_1 and BT_2) and four sediment (B_1, B_2, RB and TS) horizons. Through luminescence dating, the ages were found to be approximately 6390 ± 740 years BP for the oldest Brown (B_1) horizon and 250 ± 170 years BP for the Red Brown (RB) horizon. The radiocarbon ages of the sediment were inconclusive, but the ^{14}C ages of the fossil bones were in agreement with the luminescence ages. The multiple palaeosol horizons identified suggest two cycles of deposition, pedogenesis and erosion of the alluvial succession. The palaeosols and the presence of calcareous nodules and rhizocretions, and smectite and mixed-layer clay minerals, together with the total absence of illite and kaolinite, suggest protracted, dry periods with intermittent short

periods of high rainfall. This is a similar climate regime to what the region experiences currently.

Main findings: The Heelbo alluvial slope comprises locally derived sediment, rather than an aeolian source. Heelbo suggests that the hillslope deposits classification system needs to be re-evaluated and opens opportunities for wider study of Pleistocene-Holocene hillslope deposits in central / northern South Africa. This study also contributes to climate change debates in the Holocene.

DECLARATION

I declare that this work has not been previously accepted in substance for any degree and is not being concurrently submitted in candidature for any degree. This thesis is the result of my own investigation, except where otherwise stated.

Signed..... (candidate)

Date .....

ACKNOWLEDGEMENTS

This PhD thesis could not have been completed without the love and support of my husband Graeme and the patience and tolerance of my children Ffion and Rhydian. I am deeply indebted to you.

The research was funded by the BHP Billiton Academic Fellowship Fund and I am grateful to Lulu Khumalo and Nomfundo Mqadi of BHP Billiton for their encouragement and support.

Many thanks go to the owners of the Heelbo Game Farm who allowed me to excavate their farm and use the facilities there. I am especially grateful to Mr Nel Human who always, at short notice, would accommodate us at the farm. *Baie dankie Oom Nel.*

Throughout the processes of researching and writing this thesis, I have encountered many people who have offered their support, advice, encouragement and help. And to all of them I say “thank you”: to my supervisors Prof. Terence McCarthy who guided me through the processes of fieldwork, sedimentology and general geology; and to Dr. Zubair Jinnah who supervised the completion of this thesis; to Dr George Susino for his help with the OSL dating techniques; to Dr Helen Roberts and Prof. Geoff Duller from the University of Aberystwyth, Wales and Dr Jan-Pieter Buylaert from the Risø National Laboratory, Denmark who were always ready to answer my distraught emails; to Profs. Paul Dirks and Gillian Drennan who started me on this path towards a doctoral degree; to Marcello Molezzi, Kahmani Gouden, David Lekota, Rhirandzu Marivate and Debra Colarossi for working on Heelbo and being good sports about getting stuck in the mud; to Dr. Ann Cameron for always lending a shoulder to cry on and constantly offering words of encouragement; to Lynda Whitfield and Diane du Toit for preparing the maps and diagrams; and to the staff of the School of Geosciences who were always willing to teach me a new technique or to help me along to the finish line.

I am deeply indebted to Dr. Zubair Jinnah. *I could not have done this without you. Thank you for going to Heelbo every field season; for keeping my spirits up with your words of wisdom ("always wear your sunscreen") and for all your hard labour in the field. Ten bottles of beer on the wall would not be enough.*

CONTENTS

ABSTRACT _____ i
DECLARATION _____ iv
ACKNOWLEDGEMENTS _____ v
CONTENTS _____ vi
LIST OF FIGURES _____ xi
LIST OF TABLES _____ xvi

CHAPTER 1

1.1 Introduction _____ 1
1.2 Water Erosion and Gullying _____ 3
1.3 Gullies and Topography _____ 5
1.4 Gullied Hillslopes in South Africa _____ 7
1.5 Research Aims _____ 10
1.6 Overview of Methodology _____ 10
1.7 Structure of Thesis _____ 14

CHAPTER 2 – RESEARCH CONTEXT

2.1 Introduction _____ 16
2.2 Previous work on Hillslope Deposits _____ 17
2.2.1 Types of hillslope deposits _____ 18
2.2.2 Classification of hillslope deposits _____ 29
2.3 Previous work on Gullies and Gully Erosion _____ 34
2.3.1 Defining gully erosion _____ 34
2.3.2 Classification of gullies _____ 35
2.3.3 Gully formation _____ 38
2.3.4 Factors that influence gully erosion _____ 41
2.3.5 Relationship between slope gradient and gullying ___ 50
2.3.6 Effect of local base level change on gullying _____ 54
2.4 Dating of fluvial sediments _____ 58

CHAPTER 3 – RESEARCH LOCALITY AND DESCRIPTION

3.1 Research Locality _____ 62

3.2 Regional Geology _____ 67

3.3 Regional Climate _____ 71

3.4 Site Descriptions and Characteristics _____ 74

3.4.1 Gully Erosion _____ 77

3.4.2 Stratigraphy _____ 79

3.4.3 Bone Bed _____ 81

3.4.4 Calcrete Nodules _____ 82

CHAPTER 4 – METHODS AND MATERIALS

4.1 Introduction _____ 83

4.2 Mapping and Field Descriptions_____ 84

4.3 Grain Size Analysis _____ 85

4.4 Soil and Sediment Analyses _____ 93

4.4.1 Soil dispersion test _____ 94

4.4.2 SAR_s, pH and EC analysis _____ 96

4.5 X-ray Diffraction _____ 97

4.6 X-ray Fluorescence _____ 101

4.7 Thin Section Preparation_____ 106

4.8 Optically Stimulated Luminescence Dating_____107

4.8.1 Sample collection _____ 114

4.8.2 Sample Preparation _____ 119

4.8.3 Instrumentation for measuring D_e _____ 122

4.8.4 Calibration of the Beta source _____125

4.8.5 Testing the appropriateness of the SAR protocol ___ 126

4.8.6 Determining the Equivalent Dose with SAR _____ 131

4.8.7 Sample preparation for Dose Rate acquisition _____ 133

4.9 Radiocarbon Dating _____141

4.9.1 Sample Preparation _____142

4.9.2 Radiocarbon conventional ages _____ 144

4.9.3 Calibration of ^{14}C ages _____ 145

CHAPTER 5 – RESULTS

5.1 Introduction_____146

5.2 Hillslope Morphology _____ 147

5.3 Stratigraphy _____153

5.3.1 Karoo Basement_____166

5.3.2 Brown Sediment Horizon (B_1) _____ 168

5.3.3 Black Turf Palaeosol (BT_1)_____170

5.3.4 Brown Sediment Horizon (B_2)_____174

5.3.5 Black Turf Palaeosol (BT_2) _____ 177

5.3.6 Red Brown Sediment Horizon (RB)_____ 180

5.3.7 Top Sediment Horizon (TS) _____183

5.3.8 The Bone Bed Section _____ 184

5.4 Grain Size Analysis_____ 186

5.4.1 The Top Sediment Horizon_____186

5.4.2 The Red Brown Horizon_____190

5.4.3 Bone Site and Vertical profiles at Areas 1 and 2____ 193

5.5 Mineralogy and Major Element Analysis_____196

5.5.1 Mineral concentrations by XRD and XRF_____196

5.5.2 Classification of the sedimentary horizons _____ 205

5.5.3 SAR_s, pH and EC _____ 208

CHAPTER 6 –RESULTS OF THE GEOCHRONOLOGY

6.1 Introduction_____222

6.2 The Radiocarbon Ages _____ 222

6.3 Optically Stimulated Luminescence Dating_____224

6.3.1 Infra-red depletion ratio_____ 224

6.3.2 Preheat and dose recovery test _____225

6.3.3 Determining the Equivalent Dose_____228

6.3.4 Graphical display methods _____ 231

6.3.5 Determination of the True Burial Dose (D_b)_____ 238

6.3.6 Determining the Annual Dose Rate _____243

6.3.7 The Luminescence Ages _____248

CHAPTER 7– GEOLOGY AND SEDIMENTOLOGY OF HEELBO

7.1 Introduction_____ 261
7.2 Origins of the hillslope deposit_____ 262
7.3 History of sedimentation and pedogenesis _____ 266
7.4 Comparison of the Heelbo deposit to alluvial fan types___ 276
7.4.1 Alluvial fan morphology _____276
7.4.2 Alluvial fan processes _____279
7.4.3 Problems with the classification of the Heelbo deposit _____284
7.4.4 Grain size, roundness and sorting _____287
7.4.5 Impact of vegetation on sheetflow versus concentrated channel flow _____ 290
7.5 Gully Formation at Heelbo_____ 294
7.5.1 Gully morphology_____ 294
7.5.2 Possible causes of the gullies_____ 295
7.6 Comparison of the ^{14}C and OSL Ages _____ 306

CHAPTER 8 – PALAEO-ENVIRONMENTAL HISTORY OF THE HEELBO ALLUVIAL SLOPE

8.1 Introduction_____310
8.2 A Record of Climate Change in Southern Africa_____311
8.3 Reconstruction of the Heelbo Palaeo-environment_____313
8.3.1 Assumptions for palaeo-environmental reconstruction of the Heelbo alluvial slope_____ 313
8.3.2 Palaeo-environmental significance of the Mineralogy_____315
8.3.3 Depositional history_____ 318

CHAPTER 9 – CONCLUSIONS

9.1 Summary of Key Findings_____330

9.2 Importance of this study and suggestions for future research_____336

REFERENCES _____339

APPENDIX A_____372

APPENDIX B _____ 373

APPENDIX C _____ 381

APPENDIX D _____ 385

LIST OF FIGURES

Figure 2.1 Interpreted radiogram longitudinal profile of the Blaue Gumpe talus cone 1 _____ 20

Figure 2.2 Simple schematic of alluvial fan morphology _____ 25

Figure 2.3 Modal textures versus average slope of alluvial fans _____ 33

Figure 2.4 Relationship between critical slope of soil surface and drainage area for gully development _____ 51

Figure 2.5 Schematic profile of relationship on alluvial fans _____ 55

Figure 2.6 Model of a geologically controlled river _____ 57

Figure 3.1 Location of Heelbo Game Farm _____ 63

Figure 3.2 Google Earth image of Heelbo research site _____ 64

Figure 3.3 Photograph facing southwards towards the Heelbo mesa _ 66

Figure 3.4 Outcropping area of Elliot Formation in South Africa and Lesotho _____ 68

Figure 3.5 Stratigraphy and lithology of Elliot Formation for section closest to Heelbo _____ 70

Figure 3.6 Average annual temperature, precipitation and potential evapo-transpiration of Bethlehem _____ 72

Figure 3.7 Mean rain-season duration over the Free StateProvince _ 73

Figure 3.8 Annual wind rose for Bloemfontein _____ 74

Figure 3.9 Google Earth image of location of sample points for hillslope gradient _____ 76

Figure 3.10 Gradient of the hillslope measured downslope _____ 77

Figure 3.11 Photograph of view from top of Heelbo ridge facing north showing network of gullies _____ 78

Figure 3.12 Fluting along the gully walls is indicative of a highly dispersive soil _____ 79

Figure 3.13 Well-preserved fossil bone bed _____ 81

Figure 3.14 Calcrete nodules and detrital calcrete _____ 82

Figure 4.1 Google Earth image showing position of cross section traverses that were mapped from proximal and distal sections of the hillslope deposit_____85
Figure 4.2(a) Google Earth image of sample location for grain size analysis at Area 1 and bone bed_____87
Figure 4.2(b) Google Earth image of sample location for grain size analysis at Area 2 _____88
Figure 4.3 Top sediment and red brown horizons sampled for grain size analysis at HB-09_____ 89
Figure 4.4 Udden-Wentworth grain-size scale, graphic illustration of sorting and roundness and sphericity estimate chart____93
Figure 4.5 Vertical section of the gully sampled to determine vertical changes in soil characteristics_____94
Figure 4.6 Degree of soil dispersion of a sample placed in distilled water_____95
Figure 4.7 Site location for samples collected for XRF analysis ____103
Figure 4.8 Schematic of the event being dated where minerals are exposed to low-level radioactivity_____109
Figure 4.9 Energy level representation of the luminescence process_____110
Figure 4.10 Location of sample sites for OSL and ^{14}C dating _____115
Figure 4.11 Equipment used for OSL sampling_____118
Figure 4.12 Riso TL/OSL Reader model DA-15_____ 122
Figure 4.13 Effect of radiation on a 100 µm quartz grain _____ 136
Figure 5.1 South west section of 1:50 000 topographic map of Paul Roux_____148
Figure 5.2 Aerial photographs of Heelbo deposit_____149
Figure 5.3 Gradient of the mesa slope is steep at 2.7°_____ 150
Figure 5.4 Cross-section through proximal, medial and distal sections of hillslope_____152
Figure 5.5(a) An example of a typical sedimentary package seen in the Heelbo stratigraphy _____154

Figure 5.5(b) Stratigraphy of the bone bed_____ 155
Figure 5.6 Photographs, stratigraphy and lithology_____164
Figure 5.7 A schematic of the depositional and erosional sequences of the Heelbo hillslope_____ 165
Figure 5.8 The relative altitudes of the surface of the deposit and the underlying bedrock_____166
Figure 5.9 Photomicrograph showing the bedrock material at Area 1 and Area 2_____168
Figure 5.10 Photomicrograph showing B_1 at Area 1 and Area 2_____170
Figure 5.11 Photomicrograph showing BT_1 at Area 1 and Area 2 ___ 172
Figure 5.12 Photomicrograph of BT_1 at HB-10_____ 173
Figure 5.13 Colour change in the B_2 horizon at site HB-06_____ 174
Figure 5.14 Photomicrograph showing B_2 at Area 1and Area 2 _____176
Figure 5.15 Photomicrograph of a large lithic fragment that has been fractured by roots in B_2 _____176
Figure 5.16 Photomicrograph of the thin section showing a calcite veinlet cross-cutting a lithic fragment in B_2 at HB-06_____ 177
Figure 5.17 Two distinct black turf palaeosols can be seen at HB-09_178
Figure 5.18 Photograph of thin section of BT_2 showing numerous cavities and yellow lithic fragments_____179
Figure 5.19 Black oxide coating found on lithic fragments and quartz grains noticeable in thin section _____180
Figure 5.20 Thin section photograph showing carbonate needles around edge of cavity_____182
Figure 5.21 Thin section photograph showing rhizocretions within a coarse matrix of TS _____184
Figure 5.22 Histograms showing grain size distribution for the TS sample_____ 187
Figure 5.23 Histograms showing grain size distribution for the RB ___190
Figure 5.24 Histograms showing grain size distribution for the preserved stratigraphy at the Bone Bed Site and a representative stratigraphy at Area 1 and Area 2_____194

Figure 5.25 XRD patterns for mineral identification for the basement material and RB at HB-02_____197
Figure 5.26 Chemical differences between the bedrock material and hillslope deposit_____ 202
Figure 5.27 Geochemical classification using log(SiO_2/Al_2O_3)-log(FeO_3/K_2O) _____207
Figure 5.28 Dispersion tests with samples placed in distilled water for 0, 5 and 30 minutes respectively _____ 210
Figure 5.29 Change in the sodium adsorption ratio down the slope__ 214
Figure 5.30 Change in pH down the slope_____ 214
Figure 5.31 Change in electrical conductivity down the slope_____215
Figure 5.32 Change in the sodium adsorption ratio with depth_____ 219
Figure 5.33 Change in pH with depth_____ 220
Figure 5.34 Change in electrical conductivity with depth_____221
Figure 6.1 Luminescence signal after IR stimulation of feldspars in disks 14, 32 and 47 respectively of sample OSL 3_____ 225
Figure 6.2 Equivalent dose measured at given preheat temperatures for samples OSL3, OSL4, OSL10 and OSL17_____ 226
Figure 6.3 Dose recovery determined by dividing the measured dose by the given dose for different preheat temperatures for samples OSL3, OSL4, OSL7 and OSL10_____ 227
Figure 6.4 Recycling ratio and associated errors for all the OSL samples._____ 230
Figure 6.5 Histograms of weighted mean showing central age model D_e values_____ 233
Figure 6.6 Radial plots for each of the samples showing the equivalent dose distribution_____237
Figure 6.7 Effect of water content on luminescence ages_____252
Figure 6.8 Luminescence ages (MAM) for two B_1 samples at the head of the hillslope deposit where the horizon was the thickest_____253

Figure 6.9 Luminescence ages (MAM) and relative depths of the units of the horizons at Area 1_____254
Figure 6.10 Luminescence ages for the stratigraphy at Area 2_____255
Figure 6.11 Luminescence ages of the RB, $BT_{2,}$ B_2 and B_1 horizons at the bone bed at the base of the hillslope deposit_____256
Figure 6.12 Luminescence ages of the channel-fill at the base of Area 1_____260
Figure 7.1 The amphitheatre-like architecture of the Karoo ridge channels sediment flow downslope onto the valley floor_264
Figure 7.2 Schematic of the depositional sequence of the deposit in Area 1_____267
Figure 7.3 Schematic model of the history of deposition, erosion and pedogenesis of the Heelbo deposit_____269
Figure 7.4 Correlation between mean annual precipitation and thickness of soil _____ 272
Figure 7.5 Factors controlling alluvial fan development_____278
Figure 7.6 Mean phi changes of the TS and RB horizons _____281
Figure 7.7 Change in mean grain size with slope gradient_____282
Figure 7.8 Modal textures versus average depositional slope of TS and RB_____ 285
Figure 7.9 Photos of piping at Heelbo_____305
Figure 8.1 OSL ages for Area 1 and 2 and the bone bed. The OSL ages for the RB horizon at the head of the slope are also shown_____320
Figure 8.2 Longitudinal section of the hillslope deposit at Area 1 with the depositional history_____321
Figure 8.3 Google Earth image of location of southern African palaeoclimate sites _____324

LIST OF TABLES

Table 2.1 Characteristics of four gully types identified by Imeson and Kwaad_____38

Table 4.1 Calculations used to determine statistical parameters and scales for sorting, skewness and kurtosis _____92

Table 4.2 Soil classification based on soil dispersion test_____ 95

Table 4.3 Sample numbers, location and altitude above sea level for XRD analysis _____ 97

Table 4.4 Standing time for the grain size separation_____98

Table 4.5 Site descriptions where samples were collected for XRF_102

Table 4.6 Major element calibration instrument parameters_____104

Table 4.7 Sample location for OSL and ^{14}C dating_____116

Table 4.8 Sequence to test for feldspar contamination in the quartz grains _____128

Table 4.9 Sequence to determine D_e for all samples based on the SAR protocol _____133

Table 5.1 Graphical mean, standard deviation, sorting and roundness characteristics of TS_____189

Table 5.2 Graphical mean, standard deviation, sorting and roundness characteristics of RB_____192

Table 5.3 Graphical mean, standard deviation, sorting and roundness of the bone bed, Area 1 and Area 2 stratigraphy_____195

Table 5.4 Major elements concentrations as determined by XRF__199

Table 5.5 Chemical index of alteration and plagioclase index of alteration_____205

Table 5.6 Guidelines to determine risk of dispersion, crusting and swelling of soils_____ 211

Table 5.7 Salinity or sodicity of soil based on SAR_s values _____212

Table 5.8 Cation concentrations of the soil sample taken down the slope from the RB horizon_____212

Table 5.9 The SAR_s, pH and EC for each sample down the hillslope_____213

Table 5.10 The SAR_s calculated in mmol/l for down slope samples_ 216
Table 5.11 Risk of dispersion, crusting and swelling of samples down slope_____217
Table 5.12 Cation concentrations of the soil sample taken through the vertical section_____218
Table 5.13 SAR_s, pH and EC of the vertical section including risk of dispersion, crusting and swelling of the vertical horizons which are more than 30% swelling clay _____218
Table 6.1 Radiocarbon ages for the palaeosols _____223
Table 6.2 Calibrated radiocarbon ages for the palaeosols _____223
Table 6.3 D_b values calculated for CAM, and MAM and overdispersion with associated errors _____243
Table 6.4 Concentration of U_{nat}, Th and K and associated errors__ 244
Table 6.5 Dose rate conversion factors for the thorium and uranium series_____246
Table 6.6 Dose rate data for potassium and rubidium_____246
Table 6.7 Correction factors for beta attenuation of quartz grains in the 180-212 µm grain size_____247
Table 6.8 Palaeodose, dosimetry, total dose rate and luminescence ages for CAM and MAM_____249
Table 7.1 Comparison of calibrated radiocarbon and OSL ages___ 307

CHAPTER 1

1.1 INTRODUCTION

The seasonality of rainfall and the occurrence of drought render semi-arid landscapes susceptible to erosion as the type and density of vegetation cover is altered (Foster *et al*., 2012). It is widely assumed that the large scale degradation of these semi-arid landscapes was the result of intensified agriculture in the 18th and 19th centuries through the introduction of European farming systems of grazing and rain-fed cereal cultivation (Foster *et al*., 2012). Parts of Australia (Wasson, 1994; Olley and Wasson, 2003), the USA (Montgomery, 2007; Follet, 2010) and South Africa (Foster *et al*, 2007; Boardman, 2014) have been affected by land-use practices that degrade the land resulting in badland environments. In South Africa a semi-arid climate, extended human occupation and the escalation of subsistence farming are often cited as the reason for the loss of soil resources (Meadows, 2003; Sonneveld *et al*., 2005) that have led to an accelerated rate of gully erosion (Berjak *et al*., 1986; Showers, 1989; Viljoen *et al*., 1993; Watson, 1996; 1997). Landscape degradation is often characterised by intensely dissected colluvial footslopes and by incised channels or gullies (locally referred to as *dongas*).

The South African Karoo typifies this situation and land degradation in this region of South Africa is highly debated with competing climatic and

overgrazing hypotheses (Hoffman *et al*., 1999; Hoffman and Ashwell, 2001). Herding of domestic livestock has been a significant component of the Karoo landscape for many years but it is unlikely that pre-colonial herders caused widespread irreversible damage to the landscape (Foster *et al*., 2012). They could have been responsible for localised overgrazing, but Fox (2000) suggested that European colonisation, which began in the second half of the 18th century, was responsible for the most dramatic increases in degradation in the last 200 years.

However, other research has shown that land degradation is not always a result of human occupation. Liggitt (1988) and Garland and Broderick (1992) state that the extent of the area of the erosion sites has decreased despite the development of agricultural zones, and that the effect of humans was limited to only small catchment areas, respectively. Sonneveld *et al*. (2005) conceded that soil erosion processes involve more complex interactions between land use, climate and soil properties than was previously assumed. Other studies have highlighted the role of intrinsic factors in soil erosion processes, such as the relationship between bedrock types and gullies (Botha, 1996), or that erodibility is strongly correlated with the exchangeable sodium percentage (ESP) and sodium adsorption ratio (SAR) (Rienks *et al*., 2000).

The extent and severity of soil erosion is also affected by environmental factors, for example soil erosion by wind and water is more severe in

dryland areas of arid to semi-arid environments with hot and dry climates compared to cold, humid climates. The impacts of soil degradation on these dryland areas are of great concern as drylands cover extensive areas, hosting an estimated 37% of the world's population with about one billion rural people dependent on this degraded land for agricultural production (Dobbie, 2001).

While wind erosion is significant in dryland areas owing to the sparse vegetation cover and low and unpredictable rainfall, with approximately 432 million hectares of Earth's arid to semi-arid regions susceptible to wind erosion (UNEP, 1992; Middleton and Thomas, 1997), water erosion has become a significant global concern as it affects almost 467 million hectares of land (Middleton and Thomas, 1997).

1.2 WATER EROSION AND GULLYING

Soil erosion by water can occur as rain-splash, sheet-wash erosion and concentrated flow as rill or gully erosion. Sheet-wash erosion occurs when the shear stress exerted by flowing water at the soil surface exceeds the shear strength of the soil, leading to the detachment and removal of a thin layer or sheet of the upper soil horizon (Dlamini *et al*., 2010). Rills and gullies form when sheet-wash becomes concentrated downslope, although gullies may also form through sub-surface processes. Gullies are defined as steep-sided water courses that experience ephemeral flows and are

generally larger and more permanent than rills, and associated with increased drainage density (Kirkby and Bracken, 2009).

Gullies have been researched extensively as they are responsible for decreasing the productivity of agricultural land and are often irreversible erosion structures (Crouch and Blong, 1989; Kakembo *et al*., 2009). By definition a gully is a linear incision within unconsolidated material that forms during intense periods of fluvial erosion (Torri and Borselli, 2003; Deschamps, 2006); and gully erosion is a reaction within the landscape to an instability or exceeded sensitivity caused by an intrinsic (i.e. slope aggradation) or extrinsic (i.e. climate) change in the system (Rowntree, 1988; Allison and Thomas, 1993; Billi and Dramis, 2003; Deschamps, 2006). Gullies are also characterised by headcutting or soil piping.

The effect of climate change on gully formation has not been adequately determined; however there is increasing research that shows that gully incision and sedimentation has occurred repeatedly during the late Quaternary related to or synchronous with major climatic changes (Dosseto *et al*., 2010). However, there is consensus that understanding the controls on past gully formation and the links with climate change is key to predicting the response of gullies to present and future climate change.

1.3 GULLIES AND TOPOGRAPHY

Gullies greatly enhance the connectivity between upland hillslopes and valley floors, providing conduits for the transport of sediment and water from these high-lying regions to the low-lying valleys (Harvey, 2002; Boardman, 2014). Soil degradation is characterised by the development of badlands on the foot slopes of the upland areas and by the presence of gully systems in the lowlands (Boardman, 2014). The formation of gullies in hillslope deposits has been widely recognised (Garland and Broderick, 1992; Foster *et al*., 2012) and these hillslope deposits that have accumulated at the base of mountain fronts are important sedimentary archives for palaeo-environmental research. These hillslope deposits have been studied extensively for reconstructing landscape responses to climate change as well as for a range of other hillslope processes of interest to geological and geomorphological research (see Bull, 1991; Harvey, 1997; Wilkinson and Humphreys, 2005). Bull (1991) suggests that environmental change greatly influences hillslope processes and the results may be recognised in the affected landforms. Changes in the amount and type of precipitation alter the magnitudes and rates of weathering, erosion, transportation, deposition and vegetation cover, thereby changing the hillslope morphology.

The existence of sedimentary material located on the foot slopes of soil catenas has been widely recognised (see Young, 1976; van Wambeke,

1992). However, the processes involved in its formation have often been disputed (Paton *et al*., 1995; Eriksson *et al*., 2000). More significantly, the time scales over which they have accumulated remain unclear. Hillslope deposits may be a result of slow-acting, continuous erosional and depositional processes acting on partially vegetated slopes, or may relate to phases of extreme erosion and deposition associated with land-use or climate changes (Eriksson *et al*., 2000). Geomorphological interpretation of these deposits is often inhibited by post-depositional pedogenic alteration.

Birkeland (1990) and Gerrard (1992) proposed a more integrated approach to the interpretation of hillslope deposits that combines geomorphology, pedology and stratigraphy to unravel these deposits. This integrated approach is necessary as most geomorphic systems are extremely complex and reflect the interrelationship between variables such as geology, climate, morphology, soils and vegetation. This approach also confirms the importance of the interplay between coeval erosional and depositional processes on hillslopes. These processes do not merely switch off but change in magnitude, extent and rate. The episodes of erosion and deposition are punctuated by periods of stability and pedogenesis, followed by renewed instability that results in the truncation and burial of soils on different parts of the slope (Eriksson *et al*., 2000).

The integrated approach as described by Birkeland (1990) and Gerrard (1992) has been used to detail Late Quaternary deposits in Australia (Prosser and Slade, 1994; Wasson *et al*., 1998). However, in tropical and sub-Saharan Africa and more specifically southern Africa, an integrated geomorphological / pedological and stratigraphical approach to studying these Late Quaternary colluvial and alluvial hillslope deposits, combined with absolute dating techniques, is less common (Watson *et al*., 1984; Botha *et al*., 1994; Eriksson *et al*., 2000; Tooth *et al*., 2013). Some studies in sub-Saharan Africa show evidence for periods of landscape instability and change interspersed with periods of stability and pedogenesis (Thomas and Thorp, 1980; Embrechts, 1986; Botha *et al.*, 1994).

1.4 GULLIED HILLSLOPES IN SOUTH AFRICA

Hillslope deposits cover large areas of the interior of South Africa and these exposures of colluvial sediments found in areas of KwaZulu-Natal, Free State and Northern Cape Provinces, in particular, have been identified by Botha (1996) to be discontinuous and poorly described and documented. Despite their discontinuous nature these hillslope sediments offer an opportunity for the reconstruction of their palaeo-environmental histories based on the depositional environments in which they had formed. These sedimentary deposits tend to be isolated exposures and their varied lithologies limit correlation on a regional basis. However, Botha (1996) suggests that, through an integrated analysis of their clay

mineralogy, associated high erodibility and gully erosion, and inferred ages, it is possible that these deposits can be correlated.

Botha (1996) noted that the lack of research into these hillslope deposits is possibly a result of the difficulties in mapping these sediments in the field and in determining their genesis and position in the stratigraphic column as well as the uncertainties in constraining their ages, as Fuchs and Lang (2009) noted that a prerequisite for the use of sediments as an archive of palaeo-processes is constraining their temporal evolution. The most extensive palaeo-environmental studies conducted on gullied hillslope deposits in southern Africa concentrated on hillslope colluviation in the KwaZulu-Natal region extending towards the Lesotho and Swaziland areas (Stocking, 1978; Dardis, 1988; Dardis and Beckedahl, 1988; Shakesby and Whitlow, 1991; Botha *et al.*, 1992). Botha (1996) went on to describe the distribution, morphology and nature of the colluvial hillslope deposits at selected sites in KwaZulu-Natal, the southeastern Free State and Swaziland.

The study by Botha (1996) focussed on the KwaZulu-Natal interior and extended into limited areas of southeastern Free State. A number of small-scale sedimentary deposits have since been identified on the hillslopes of remnant Karoo mesas and buttes in the interior of the Free State and more specifically around the towns of Rosendal, Senekal and Paul Roux. These hillslope deposits reveal a number of gully erosion

sites (see 1:50 000 topographic map of the area in APPENDIX A). These gullies, while not unusual to the area, are interesting in that they have not formed in an intensively farmed area. In fact for most of the year the land is uninhabited by any form of game or agriculture, yet the gullies are deeply entrenched into the landscape and the steep vertical side walls of the gullies have extensive piping and also reveal a well preserved stratigraphy that can be used to suggest a possible depositional history.

The sedimentary deposits on the hillslope located on the farm Heelbo, southeast of the town of Senekal, have been identified, and an integrated study of the geomorphology, soils and stratigraphy and geochronology, aided by the numerous gully exposures was conducted to understand these deposits. On the mountain front of a typical Karoo mesa is an accumulation of sediment that makes up the Heelbo sedimentary deposit. It is a small scale feature that extends across the entire apron of the mesa and is worth investigating because: a) the stratigraphy of the deposit has been exposed through gullying and, as such, the depositional history could be determined through the identification of the stratigraphic units and their mineralogy, b) the sediments could be analysed in terms of the chemical properties, c) the sedimentary packages could be dated using radiocarbon and optically stimulated luminescence dating techniques; and the deposit could provide a record of environmental change through an understanding of the sedimentary processes that occurred in the region.

1.5 RESEARCH AIMS

The rationale of this research project is to re-examine hillslope and alluvial fan classification to determine whether there is scope for new environments that do not fall into the existing classification. The aim is to describe the geology, sedimentology and stratigraphy of the hillslope deposit located on the mountain-front of the Karoo mesa found on the farm Heelbo in the Free State; and to determine the cause of gullying on the hillslope and the land-use implications of this. The research questions are:

- What type of landform is the sedimentary deposit and what are the distinguishing characteristics?
- What is the relationship between grain-size distribution and slope gradient and what were the depositional processes active on the hillslope?
- How did the gullies form which have incised the deposit?
- How old are the stratigraphic horizons preserved in the deposit?
- What is the palaeo-environmental history of the deposit?

1.6 OVERVIEW OF METHODOLOGY

This study is based on the integrated approach as proposed by Birkeland (1990) and Gerrard (1992) to interpret the processes - past and present - that may have altered this deposit over time, with attempts to reconstruct

its depositional history. Such a reconstruction is made possible by the exposure of the stratigraphic sequence by extensive gullying of the deposit; the preservation of the stratigraphic sequence in parts of the deposit; the identification of the mineralogy through X-ray fluorescence (XRF) and X-ray diffraction (XRD) analyses; and through the application of radiocarbon (^{14}C) and optically stimulated luminescence (OSL) dating techniques to constrain the timing of the depositional events.

To identify and describe the distinguishing characteristics of the sedimentary deposit, the fieldwork component of this project entailed the detailed mapping and description of the hillslope deposit and the entrenched gully systems; mapping of the stratigraphy exposed in the gully side walls; and measuring and mapping cross-section transects across the hillslope.

The fieldwork component of this project was undertaken over a three-year period (2008-2010) in sessions of mapping and sampling. The weather conditions during these sessions ranged from extremely hot and dry, to warm and very wet (saturated) and these conditions influenced the sampling protocols and had some effect on the samples collected.

Aerial photographs, the 1:50 000 topographic map and Google Earth images of the area were used to locate and measure the extent of the deposit and to determine the best locations for the sample sites and the

preferred slopes to describe, in the deeply-incised environment. The topographic cross-sections were measured and drawn across the slope in roughly a south-west to north-east direction (see Figure 4.1). Trimble differential GPS (dGPS) readings were taken at the surface and in the gullies to create the cross-section traverses and longitudinal profile. The altitude and co-ordinate position of the samples down slope were used to create a gradient profile of the slope. During the rainy season the handheld GPS (hGPS) was used to measure or locate sample points as the particular model of the dGPS could not be used in the rain. Sample sites were also recorded using either the dGPS or the hGPS and are referred to by the sample number assigned to each site.

Each site was described in terms of colour, grain sizes, root traces, textures, contacts and the reaction to 10% solution of HCl as described by Retallack (2001), and the individual layer thicknesses were measured and recorded. The samples were numbered according to the waypoint number recorded and the stratigraphic unit from which each was taken; and where there were two stratigraphic units that had a similar colour such as the brown and black turf layers, the sample number was recorded with a subscript 1 or 2 to distinguish them as older or younger, respectively.

The relationship between grain-size distribution and slope gradient of the sedimentary deposit was important to establish the depositional processes involved and the controlling environmental factors active during deposition.

The most continuous and least dissected slope down the length of the hillslope deposit was selected to collect samples for analysis, beginning at the head (where the proximal hillslope sediments meet with the ridge face) and ending downslope towards the distal margins of the deposit (see Figure 4.2a). It was clear in the aerial photograph that sampling the high-lying ridges on the outskirts of the deposit would lead to error because of the multiple sources of infill created by the basement highs that confine the deposit; therefore a section through the centre, and most continuous and undissected parts of the hillslope, was the most ideal. The remnants of the original deposits located within the gullies were also sampled even though they occur as isolated stacks scattered within the gullies.

To establish the cause of the gullies, samples were collected to test the dispersivity of the soil, which included tests for pH, SAR_s and EC. X-ray diffraction (XRD) was used to determine the clay minerals present in the palaeosols and their relationship to environmental factors during the formation of the Heelbo hillslope deposit. X-ray fluorescence (XRF) was used to determine the major and trace elements within the thickest layers of the deposit, and to determine whether leaching occurs in the deposit. Thin sections were used to analyse the soil texture in order to determine soil forming conditions.

The ages of the stratigraphic horizons were determined using relative and absolute dating techniques of radiocarbon (^{14}C) and optically stimulated

luminescence (OSL) dating on selected layers in the stratigraphic sequences. The ages were also used to reconstruct the palaeo-environmental history of the deposit by relating these to proxy data available for the given time.

1.7 STRUCTURE OF THESIS

This thesis has been organised into nine chapters to facilitate the coherent description of the research and includes chapters on the sedimentology and stratigraphy of the hillslope deposit; the relationship between grain size and slope gradient; and the effects of sodicity on gullying; and an analysis of the clay mineralogy, and the geochronology of selected deposits as determined by ^{14}C and OSL dating techniques.

Chapter 1 provides an introduction to the soil erosion problem on a global scale and with specific reference to gully erosion. The problems of gully erosion in South Africa are highlighted and the research aims of the study are stated. The research context for this study is expanded in **Chapter 2** with an overview of the literature on hillslope deposits and gully erosion presented. The location, geology and geomorphology of the research site are described in **Chapter 3** along with descriptions of the key characteristics of the area. The methodology and materials are discussed in **Chapter 4** with the results presented in **Chapter 5.** Because of the complexity of determining the geochronology of selected sites in the

deposit, the sampling protocols, treatment and results of the ^{14}C and OSL dating techniques are covered separately in **Chapter 6**. In **Chapter 7**, the geology, sedimentology and mineralogy of the deposit are discussed. The depositional history of the Heelbo deposit is discussed within the context of the past climates of southern Africa and the palaeo-environmental history of the hillslope succession is presented in **Chapter 8**, with a summary of the key findings and suggestions for further research discussed in **Chapter 9**.

CHAPTER 2: RESEARCH CONTEXT

2.1 INTRODUCTION

The accumulation of sedimentary deposits on the hillslopes of mountain fronts has long attracted the interests of geologists and geomorphologists (see Reneau *et al*., 1989; Mills and Alison, 1995; Roering *et al*., 2001; Lang, 2003; 2013). Hillslope deposits that have previously been described in the literature include colluvial deposits (Botha, 1996), alluvial fans (Blair and McPherson 1994; Harvey, 1984; 2011; van Dijk, 2012), talus slopes (Ballantyne and Harris, 1994; Sass and Krautblatter, 2007; de Blasio *et al*., 2014) and alluvial slopes (Smith, 2000). It is essential to establish a link between landform and process to understanding the dominant controls on the emergence of landscape characteristics and to interpret the relationship between environmental change and landform responses to these changes.

Hillslope deposits are often referred to as colluvium which describes sediments that are eroded from, and transported along hillslopes by running water or gravity, and that usually form a wedge-shaped deposit on the foot slope (Fuchs and Lang, 2009). These are distinguished from alluvial sediments which are transported in spatially confined channels over greater distances (Harvey, 2011). These hillslope deposits, whether colluvial or alluvial in nature are a valuable archive for geomorphic research particularly palaeo-environmental reconstructions.

2.2 PREVIOUS WORK ON HILLSLOPE DEPOSITS

Soil mantled hillslopes, where erosion rates do not exceed the rates at which bedrock is converted to soil, are found in hilly and mountainous landscapes throughout the world (Roering *et al*., 2001). Botha and Partridge (2000) suggested two basic morphological categories of slope forms as convex and concave. Convex slopes are less prominent in the South African landscape as they are associated with homogeneous lithologies that have been subjected to incisions by rivers under sub-humid or humid climatic conditions. Roering *et al*. (2001) recognised that the scarcity of overland flow erosion on convex hillslopes suggests that down slope soil creep is controlled by disturbance-driven processes (e.g. biogenic activity and wet/dry climate cycles), such that sediment transport rates should depend primarily on gravity and therefore hillslope gradient. Where soil mantled hillslopes tend to be convex near the crest and become increasingly planar down slope, they would decline in slope angle, with time leading to the overall lowering of the landscape (Botha and Partridge, 2000; Roering *et al*., 2001). Slope systems are self-limiting systems, for example as slope angle declines, so does the sediment yield.

Concave slopes tend to be more visible on the South African landscape and reflect the influence of resistant cap rocks such as the dolerite sills in the Karoo. Concave slopes tend to display the four distinct slope elements identified by King (1953), which are the crest, the scarp, the talus or debris slope and the pediment slope. Sediment flux is linearly related to hillslope

gradient at low angles and increases rapidly as slope angles approach a critical value related to the angle of repose (Roering *et al*., 2001). This behaviour has important implications for how hillslopes respond to changes in uplift rates and / or climate variables, and it has become accepted that landscapes tend to adjust their form such that erosion rates are spatially constant over a climatically uniform region (Whipple *et al*., 1998; Botha and Partridge, 2000; Roering *et al*., 2001). In the South African context, a model for hillslope development may include the accumulation of thick sandy sediment on lower slopes requiring an initial humid period of weathering of bedrock and talus to form thick soils and saprolite on hillslopes, stabilised by dense vegetation (Clarke *et al*., 2003). A subsequent shift to more arid conditions, with the related decrease in vegetation cover, would allow sheet wash from rain-storm events to transport weathered debris down slope and deposit it as colluvium on more stable slope positions associated with bedrock steps (Clarke *et al*., 2003).

2.2.1 Types of Hillslope Deposits

In mountainous landscapes, land-sliding and mass-wasting dominate sediment transport on hillslopes. The frequency and magnitude of these slope-dependent processes control hillslope morphology, as well as the time required for hillslopes to adjust to changes in the rate of channel incision or climate related transport efficiency (Roering *et al*., 2001). The

development of hillslopes is thus governed by local climatic conditions and is the result of sequential periods of geomorphic stability and activity (Clarke *et al*., 2003).

2.2.1.1 Talus slopes

Talus slopes are defined as steep valley-side slopes formed by the accumulation of debris at the foot of rockwalls (Ballantyne and Harris, 1994), or at the base of mountain cliffs (de Blasio *et al*., 2014) and may or may not be stratified. The term talus is used to describe both the slope and the accumulated material, and refers to any slope cover of mainly coarse debris. Although talus slopes predominate in periglacial environments, they also occur in areas where the products of rock weathering of upper slope segments have accumulated at the foot of a cliff as rockfall, whether discrete or catastrophic events, is the primary process for talus accumulation. In long profile talus slopes have an upper straight slope with a gradient of 35º - 36º (Ballantyne and Harris, 1994) or between 20º - 35º (Sass and Krautblatter, 2007) relative to the angle of repose of the sediment (frictional limit of the individual grains against each other) as well as having talus-specific factors like height, steepness, and dissection of rockwall height (Ballantyne and Harris, 1994; Sass and Krautblatter, 2007; de Blasio *et al*., 2014). The base of the talus slope is marked by a concavity if it has not been removed by erosion. A small convexity has also been noted at the crest of some features (Ballantyne and Harris,

1994). Another important feature of talus slopes is longitudinal grading, which is the increase of average block diameter with distance, from the fall zone. Sass (2006) has shown that talus slopes are made up of strata with different block sizes, and thus it appears that these slopes have a complex geometry, resulting from the history and dynamics of the falling blocks.

The accumulation of talus sheets and retreat of the associated rockwalls in the Late-glacial and Holocene terrane of Mynydd Du, Wales, revealed that the slopes of the sheets were constant (Sass & Krautblatter, 2007), with steep gradients of approximately 30º (Curry & Morris, 2004). The constant gradient of talus sheets may even overprint any undulating rockwall base making it independent of the underlying ground morphology (Figure 2.1).

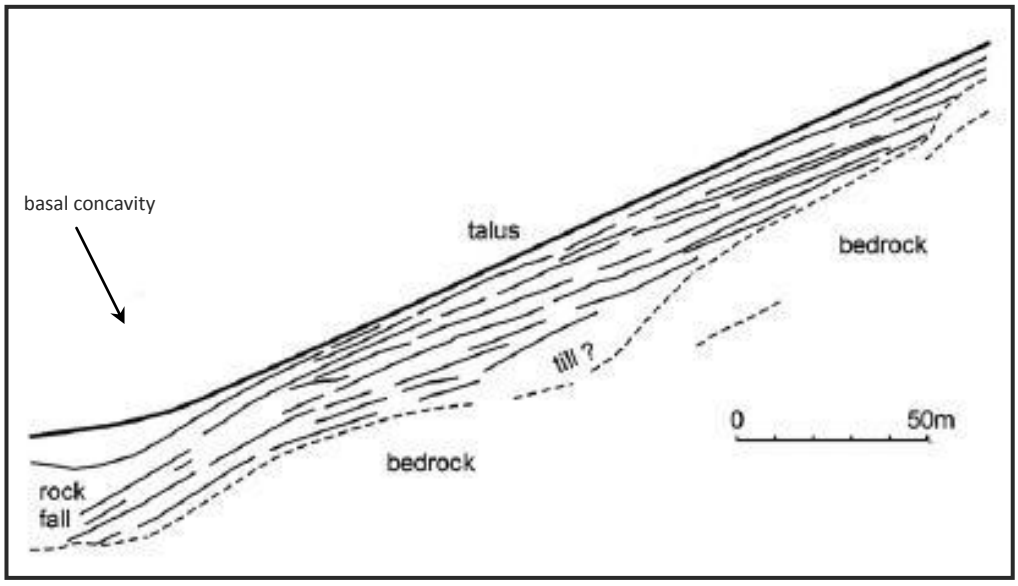


Figure 2.1 Interpreted radiogram longitudinal profile of the Blaue Gumpe Talus Cone 1 where the undulating bedrock morphology has no effect on the slope of the talus surface (after Sass & Krautblatter, 2007).

The talus slope may become gentler than described by Curry and Morris (2004). However, it may not be primary processes that create the changes in slope. Blank *et al.* (1996) interpreted the decreasing angle of a certain talus slope of the Buckskin Mountains in west-central Nevada, USA, as the result of a shrink-swell mechanism of a clay horizon below the talus sheet. This leads to thickening of the soil profile in that horizon and the talus sheet was rafted upward. The talus slope was not synformational as it became shallower as a result of secondary processes. However, the sheet still retained a constant gradient throughout its length (Blank *et al.,* 1996).

The constant slope of a talus sheet is only broken towards the distal reaches where a basal concavity is formed as the talus slope diminishes and the bedrock/low land sediment is exposed (Figure 2.1). Talus slopes are often modified by process such as debris flow activity in the form of both hillslope and valley confined flows. The overall effect of debris flows is to transport debris down slope, lowering the overall gradient and increasing the degree of slope concavity (Ballantyne and Harris, 1994). The lower reaches of the talus sheet may be similar to an alluvial fan profile but it is clear that these features only make up a relatively small part of the total morphology of the talus slope and the predominant feature remains the steep, constant gradient.

2.2.1.2 Colluvial deposits

The material moved down slope especially under the influence of gravity is called colluvium (Schaetzl and Anderson, 2005; Stoops *et al*., 2010; Lang 2013) and Price-Williams and Watson (1982) define colluvium as the product of the deposition of a mass movement of sediments rather than those deposited by fluvial processes i.e. by the transport mechanism of water. However, Pederson *et al.* (2000) use the term in a broad sense to mean detritus transported by various processes that is still adjacent to or on its source hillslope. Colluvial material ranges in size from fine-textured soils to large cobbles and boulders depending on the composition of the source material (Schaetzl and Anderson, 2005). Colluvial accumulation tends to be thinnest on the steepest slopes and thickest in the low-gradient deposition zones at the base of the slopes. Colluvial sediments are formed through processes on slopes that are spatially diffusive and are distinguished from alluvial sediments which are transported in spatially confined channels to form alluvial fans (Lang, 2013).

Botha and Partridge (2000) suggest that in southern Africa, however, the term colluvium refers to almost all slope sediments without indication of their origin or mode of deposition. The term therefore encompasses a wide range of deposits formed through many processes. The sediments commonly associated with colluvial deposits are coarse debris flows or mass wasting sediments, poorly sorted, poorly bedded sediments, and

products of soil creep. The slopes are often steep relative to their angle of repose of the sediment, with a rapid decrease in grain size down slope. However, in loess environments colluvium can occur on gentle slopes of about 7° (Stoops *et al*., 2010).

The colluvial hillslopes described by Botha (1996) are common in south-eastern South Africa and consist of sediment that was transported down slope due to gravitational forces and mass movement. Gully systems develop towards the shallower slopes on many of these colluvial hillslopes. During periods of stability, the hillslopes may form soil profiles which may overprint any previous sedimentary layering.

The greatest colluvial cover in eastern South Africa extends from northern and central KwaZulu-Natal (KZN), the eastern Free State and a small area in central Swaziland (Botha, 1996). A large part of the colluvial cover in southern Africa is located in areas which currently experience between 600 and 800 mm of annual rainfall (Botha, 1996). The extensive colluvial deposits in northern KZN are characterised by relatively thin layers containing little stratigraphic information. There are however, colluvial deposits in some places measuring up to 21 m thick (Wintle *et al.*, 1995a). The different cycles of gully erosion, colluviation and palaeosol formation during the late Quaternary has been described by Botha (1996) and Botha *et al.* (1994) with the most complete records taken from the St Paul's Mission in northern KZN (Wintle *et al*., 1995a; b).

Price-Williams and Watson (1982) suggest that during periods much drier than present, the colluvium was deposited as a series of fans which rested on the shallow pediment-slopes at the foot of the steeper valley sides. Furthermore, the decreased moisture availability which prevailed during these events was itself their cause, bringing about a reduction in the previous vegetation cover and thus promoting destabilization of parent sediments. Discrete horizons of calcium carbonate nodules in the colluvial deposits also point to climates drier than today. In contrast, certain horizons within the colluvial mantle have developed as vertisols which indicate periods of colluvial stabilization and pedogenesis when more moist conditions predominated (Price-Williams and Watson, 1982).

2.2.1.3 Alluvial Fans

Alluvial fans are landforms that develop where a channel exits a confined valley, and through avulsions and channel branching spreads sediment across an unconfined valley floor (Blair and McPherson, 1994; De Chant *et al*., 1999). Harvey (2011) suggests that these fans occur when confined streams emerge from mountain catchments into low-lying valleys or basins. Flow expansion causes a reduction in depth and velocity with a consequent loss of competence, leading to increased deposition. The cone apex is at the point where the stream flows from a steep channel on to a valley floor, where the flow becomes unrestricted (Figure 2.2) (Blair and McPherson, 1994; DeChant *et al*., 1999; van Dijk *et al*., 2012). The

mass is thickest at the point of origin and thins out rapidly in a downstream direction.

Alluvial fans are associated with a transition from a high-lying area where erosion and transportation are the dominant processes to a low-lying deposition basin. The catchment characteristics such as drainage basin area, relief and geology control the supply of water to the fan, and therefore the process regime on the fan (Harvey *et al*., 2005; 2011; van Dijk *et al*., 2012). The morphodynamics however, are associated with channel avulsion and sheet floods. Avulsion may be caused by ongoing sediment input and aggradation at the fan apex; and the overall fan gradient is determined by the sediment transport capacity and sediment supply (van Dijk *et al*., 2012).

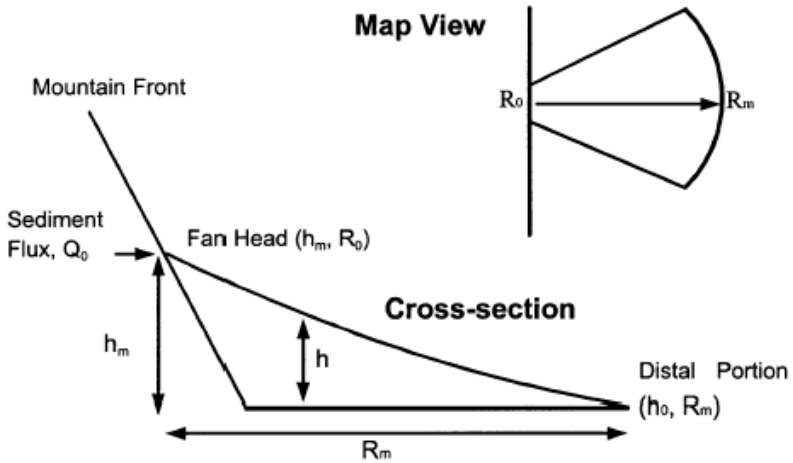


Figure 2.2 Simple schematic of alluvial fan morphology where the sediment flows out from the fan head and is deposited on the valley floor, terminating in the distal reaches at the fan toe (De Chant *et al*., 1999).

Alluvial fans are often less than a few kilometres wide, steep (2º - 25º) and semi-conical deposits. They can be found in any climate regime and can occur over great distances (up to 60 km) for fluvially dominated megafans (Harvey *et al*., 2005; Harvey, 2011). The assumptions about over-all coarsening-up sequences within alluvial fan sediment may be appropriate for distal fan environments, when the proximal fan sediments are being reworked by fan-head trenching (Harvey *et al*., 2005). The same assumptions however, are not appropriate for proximal environments on aggrading fans. Instead there would be an overall fining-up trend as the topography is buried over time (van Dijk *et al*, 2014).

Likewise, the over-simplistic association of wet /dry fans corresponding to wet / dry climates needs revision, as this concept relates to the debates on the relative roles of climate, tectonic activity and base level changes on alluvial fan sequences (Harvey *et al*., 2005; Harvey, 2011). Alluvial fans build highly varied stratigraphy in the absence of external forcing due to autogenic thresholds and process-form feedbacks that result in frequent channel switching and varied dispersal web (Nicholas and Quine, 2007). As such they are poor environments to use when investigating landscape responses to environmental change.

2.2.1.4 *Alluvial Slopes*

The difficulty in characterising hillslope deposits is further complicated when piedmonts lack the full morphology of an alluvial fan and/or where channelized stream flow persists across the width of the piedmont, where a gentle sloping fan is apparent near the channel. One of the terms suggested to describe such a deposit is *bajada* (Cooke and Warren, 1973; Bates and Jackson, 1987); but Summerfield (1991) and Harvey (1997) defined bajadas as coalesced alluvial fans. The concept of an *alluvial slope* was suggested by Bryan (1922) as a surface composed of alluvium which slopes down and away from the sides of the mountain and which merges with the broad valley floor. Bryan's (1922) definition and usage indicated the term alluvial slope to be inclusive of alluvial fans and piedmont streams lacking fan morphology (Smith, 2000). However, Hawley and Wilson (1965) restricted alluvial slope to a piedmont plain that lacks the surface morphology of one or several coalesced alluvial fans. Smith (2000) however, uses the term alluvial slope to describe stream flow dominated piedmonts. Alluvial slopes are more likely to form than alluvial fans where mountain fronts lack abrupt structural and topographic definition, which will most likely occur along tectonically inactive and embayed mountain fronts and on the hanging wall ramp side of half-grabens (Smith, 2000).

Hawley and Wilson (1965) recognised that gradations exist between alluvial fans and alluvial slopes but contend that the distinction of an alluvial slope is necessary because not all deposition in the piedmont can be related to alluvial fan morphology (Kuhle and Smith, 2001). The conditions which favour the development of alluvial slopes are not clearly defined but the topography of these slopes indicates that many non-entrenched piedmonts have relatively steep gradients of 0.01-0.04. They are also characterised by parallel drainage patterns extending from mountain front to basin floor without the development of alluvial fan morphologies (Hawley and Wilson, 1965; Kuhle and Smith, 2001). Channel depths are also relatively shallow, generally less than 1.5 m, and streams tend to be ephemeral with sediment transport flows being rapid, unsteady and shallow (Graf, 1988; Smith, 2000). Smith (2000) also notes that upper-flow-regime sedimentary structures and scour-and-fill structures should dominate the resulting deposit because of the steep slopes, shallow depths and unsteady flow.

One of the key features of an alluvial slope that distinguishes it from an alluvial fan is the nature of the channel network. The channel network of a fan, typically radiates out from a well-defined apex, whereas the channel network from an alluvial slope is dendritic, i.e. many smaller channels join to form fewer larger channels (Nicholas and Quine, 2007). Alluvial slopes appear to evolve through the accumulation of material deposited from

sheetwash which is subsequently reworked by a dendritic drainage (gully) network.

2.2.2 Classification of Hillslope Deposits

Semi-conical depositional landforms located along mountain fronts are generally referred to as alluvial fans, although the strict definition of alluvial fans is still contested. The effect of surface inclination may influence the definition of these deposits as very flat or very steep depositional landforms are usually referred to as floodplains or talus slopes respectively, rather than alluvial fans (Saito and Oguchi, 2005). This suggests that slope gradient is a key component to defining the morphological classification of the hillslope deposit.

Smith (2000) also highlighted the problems of defining piedmonts as alluvial fans or pediments. These definitions recognise the distinctive semi-conical morphology of a fan but not all research emphasises the physical processes producing the landform. Leeder (1978) noted that fully channelized streams and rivers can produce fan-shaped accumulations of sediment through the process of nodal avulsion where a single channel is present at any one time, deposition occurs and the depositional slopes remain low (<1°), such as the Kosi River fan. The single channel migration has also resulted in stream-flow dominated piedmont alluvial fan succession but according to Smith (2000) is not an alluvial fan deposit.

Blissenbach (1954) classified alluvial fans in semi-arid regions as steep (> 5°), gentle (2° to 5°) and flat (<2°) and suggested that landforms gentler that 1º are not alluvial fans but floodplains. Anstey (1965) however, pointed out that fans have slopes between 1° and 5°, from his work on over 4 000 fans in arid SW America and Pakistan. Whereas Hooke (1968) suggested that the slope of alluvial fans range from 2° to 12° and Boothroyd (1972) also defined semi-arid depositional landforms gentler than 1° as alluvial fans.

The definition of alluvial fans has been expanded into humid regions where gentle depositional landforms have been identified. Tomita (1951, in Saito and Oguchi, 2005) identified fans in Taiwan with the lowest slope values of 0.5° and Toya *et al*. (1971, in Saito and Oguchi, 2005) found fan slopes in Japan lower than 0.57°, where these fans have been formed by fluvial processes rather than debris flows. Other gentle sloping fans have been identified by Evans (1991) where the alluvial fan slopes ranging between 0.057° and 0.57° were found in the humid tropics. Davis (1898) recorded a very gentle fan slope formed by the Yellow River in China which is regarded as one of the largest alluvial fans in the world (Saito and Oguchi, 2005). Other large and gentle landforms have been identified as alluvial fans such as the Kosi River Fan at the foot of the Himalayas – 0.019° (Stanistreet and McCarthy, 1993); as well as the Okavango Fan in Botswana with a mean slope of 0.013° (McCarthy *et al*., 1991).

The description of such gentle depositional features as alluvial fans has been challenged by Blair and McPherson (1994) based on 237 piedmont depositional landforms which were classified as alluvial fans. They suggested that alluvial fans have average slopes between 1.5° and 25°, whereas rivers in sedimentary basins have gentle gradients not exceeding 0.4°. They based their classification on the morphology, sedimentary facies, hydraulics and sedimentary processes and assumed alluvial fans to be constructed mainly by catastrophic fluid gravity flows or sediment gravity flows (Blair and McPherson, 1994; Saito and Oguchi, 2005). According to the Blair and McPherson (1994) classification, 18 piedmont depositional landforms gentler than 0.4° were reclassified as rivers or river-deltas, including the gentle fans in Alaska – as gravel bedded rivers; the Kosi River Fan – as a sand-bedded river; and the Okavango Fan as a mud-dominated river (Figure 2.3).

Blair and McPherson (1994) also concluded that depositional slopes of 0.5° – 1.5° are not common in aggrading alluvial basins and referred to this interruption as the "natural depositional slope gap" (Figure 2.3). McCarthy and Cadle (1995) and Kim (1995) disputed the occurrence of the slope gap and ascribed it to the incomplete choice of data by Blair and McPherson. However, Blair and McPherson (1995) defended their inferences because they thought that the additional data presented by Kim (1995) and McCarthy and Cadle (1995) were inappropriate. Smith (2000) also argued that the fan-shaped accumulations of alluvium which have

been described as alluvial fans (such as by Stanistreet and McCarthy (1993)) should be considered both genetically and sedimentologically distinct from alluvial fans.

Saito *et al*. (2003) showed that almost all the fans of the 123 surveyed in Death Valley, California, were steeper than 1.5°, while their surrounding floodplains and playas are generally gentler than 0.5°, and using this isolated set of data they could support the notion of the depositional slope gap. However, Blair and McPherson (1994) suggested that their slope gap is universal and applicable to any climatic region.

Saito and Oguchi (2005) recognised that the presence or absence of a universal depositional slope gap is crucial for understanding the nature of fluvial sedimentation as well as the proper definition of alluvial fans. They (Saito and Oguchi, 2005) surveyed 490 fans in Japan, 71 in Taiwan and 129 in the Philippines and found that they could not be logically divided on the basis of their slope, because the fans followed the log-normal frequency distribution with respect to their slope gradients without any gaps. The log-normal distribution also applies to the area and relief ratio of the source basin, indicating that the fan/basin system varies gradually rather than abruptly. They concluded that this geomorphological continuity casts doubt on Blair and McPherson's (1994) concept of a natural depositional slope gap for humid regions at least.

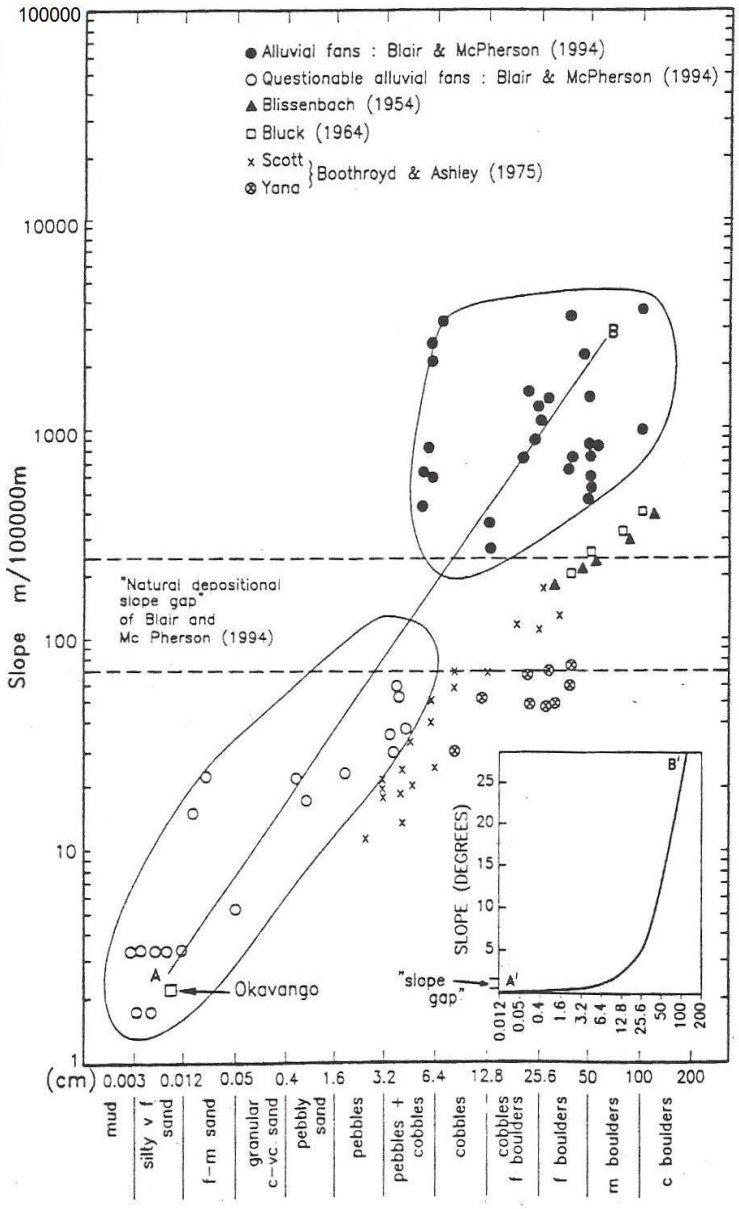


Figure 2.3. Modal textures versus average slope of alluvial fans showing the reclassification of deposits as true alluvial fans, the questionable fans as well as the Okavango Delta (modified after McCarthy and Cadle, 1995, pp47).

Hillslopes, regardless of their definitions may be susceptible to intensive gully erosion as water, either channelized or as sheet flow removes sediment from the high-lying uplands regions to the low-lying valleys.

2.3 PREVIOUS WORK ON GULLIES AND GULLY EROSION

2.3.1 Defining Gully Erosion

It is widely assumed that intensified agriculture in the 18th and 19th centuries, as well as the escalation of subsistence farming have led to an accelerated rate of gully erosion (Berjak *et al*., 1986; Showers, 1989; Viljoen *et al*., 1993; Watson, 1996; 1997; Boardman, 2014). However, research has also shown that this is not always the case and that gully erosion, especially in South Africa is not just an agricultural or contemporary issue resulting from land-use degradation, but has been occurring for at least the past 130 000 years (Price-Williams *et al*., 1982; Botha *et al*., 1994). Critical to resolving the debate on whether landscape changes are a result of natural or anthropogenic forcing is constraining the timing of gully formation. High resolution, reliable ages provides the basis for correlation of human and natural landscape activities. The resolution of the effect of human activities (e.g. overgrazing) and natural forces (e.g. climate change) has important implications for assessing the appropriateness of current soil erosion methods (Lyons *et al*., 2013).

Gullies are fluvially incised into the land surface and are characterised by steep sides and steeply sloping head scarps (Poesen and Govers, 1990; Torri and Poesen, 2014). Gully erosion is the movement of water across a soil surface, which then deepens into rivulets, and takes place either

where the concentrated runoff from a slope increases sufficiently in volume and velocity to cut deep incisions (gullies) into the land surface (Frankl *et al*., 2012); or where concentrated water continues cutting the same groove long enough to develop such incisions (Morgan, 2005).

Subsurface erosion such as soil piping and tunnelling has been recognised as an important control of gully development Valentin *et al*., 2005; Frankl *et al*., 2014). Crouch and Blong (1989) suggest that while most geomorphic studies have focussed attention on headward retreat as the main element in gully erosion and stabilization, many gully systems shed more sediment from sidewalls than from headwalls.

2.3.2 Classification of Gullies

Gullies are classified as being ephemeral, continuous or discontinuous, based on the drainage systems established on them (Leopoldt and Miller 1956; Nordström, 1988). Ephemeral gullies are temporary features that may occur annually but are easily removed through flash floods or sheetwash; hence the term ‘ephemeral’ refers to the permanence of their structure not to their flow (Bull, 1997). They form as micro-rills formed from overland flow which can enlarge into gullies downstream (Oostwoud Wijdenes *et al*., 1999; Deschamps, 2006). Ephemeral gullies are always topographically controlled and can be continuous or discontinuous and V-

or U-shaped in morphology (Grissinger, 1996; Vanderkerckhove *et al*., 1998; Nachtergale and Poesen, 1999; Deschamps, 2006).

Continuous gullies form because of surface runoff and are initiated where ground cover has become depleted and the main drainage lines become gullied by headward elongation (Heede, 1976; LeRoux *et al*., 2012). Continuous gullies begin with many small rills and usually start high up on the mountain side. The rills coalesce and cut downward into the channel increasing the depth of the gullies (LeRoux *et al*., 2012). These gullies form part of a drainage network and normally extend upslope from the main gully. The network pattern has a central gully whose depth increases in a downstream direction, ending in an abrupt gully mouth (Imeson and Kwaad, 1980).

Discontinuous gullies begin with an abrupt headcut and unlike continuous gullies can start anywhere in the landscape (Heede, 1976). They have a vertical headcut and a bed gradient less than that of the valley floor so that when and where the gully bed and the valley floor intersect a small depositional fan is formed (Leopold *et al*., 1964; Blong, 1970; Billi and Dramis, 2003, Deschamps, 2006).

As the discontinuous gullies extend into the drainage network it is possible for them to coalesce (Bocco, 1991). This gully fusion represents the early stages of the transformation of a discontinuous gully into a continuous

gully. A decline in discontinuous gullies shows that the gully system is nearing the end of an erosion cycle (Nordström, 1988; van Zijl, 2010); and often discontinuous gullies are linked to the main gully by piping and these will be classified as continuous gullies once the pipe roof caves in (van Zijl, 2010).

Gullies can also be classified according to their cross-section as either V or U-shaped (Nordström, 1988). V-shaped gullies initiate channels where no previous drainage path existed and these valley-sided gullies form on a substrate conducive to overland flow and which encourages runoff (Bocco, 1991). U-shaped gullies tend to be valley floor gullies and can erode by upstream extension into an existing channel, i.e. entrenchment and are prone to mass instability, piping and undercutting (Rowntree, 1991).

Gullies have also been classified according to the mechanism of their formation. Imeson and Kwaad (1980) identified 4 gully types (Table 2.1): Type 1 gullies develop from rill or wherever overland flow becomes concentrated (i.e. ephemeral); these gullies often have a V-shaped cross-section and form on a valley floor. Type 2 gullies develop from the upstream migration of plunge pools and often acquire a deep U-shape with steep walls. Type 3 is similar to type 2 but is associated more with subsurface water and piping and can often lead to the formation of badlands. Type 4 gullies develop within the alluvial sediments of the

valley floor by headcutting, are U-shaped and are often characteristic of discontinuous gullies.

Faber and Imeson (1982) distinguished between gullies caused by runoff and gullies formed by piping through subsurface flow; and since the morphology of the gully cross-section is dependent on the erosion process (Bocco, 1991), there is no fixed rule as to what shape a gully should have in accordance to its position in the landscape (Deschamps, 2006).

Table 2.1 Characteristics of four gully types identified by Imeson and Kwaad (1980, 432).

Gully Type	Gully Cross-section	Position in Landscape	Source of Run-off
Type 1	V-shaped	Anywhere, but mostly valley bottom	Overland flow
Type 2	U-shaped	Anywhere, but mostly valley bottom	Overland flow with subsurface water
Type 3	U-shaped	Anywhere but usually on lower slopes	Subsurface flow
Type 4	U-shaped	Valley bottoms	Overland flow from tributary gullies

2.3.3 Gully Formation

Studies on soil erosion have shown that gully formation is a complex, cyclical phenomenon that is governed by localised thresholds influenced by intrinsic and extrinsic variables (Keay-Bright and Boardman, 2009; van Zyl, 2010). The problem in identifying the causes for gully formation lies in the sensitivity of the geomorphic system, where small changes in any variable may force the destabilisation of the system which in turn may lead

to erosion. Gully formation, growth and shape are usually correlated with the landscape variables of relief, topography, climate, vegetation and human interaction with the landscape (Faber and Imeson, 1982; Beinart, 1984; Beavis, 2000).

Gully erosion is a threshold-dependent phenomenon that occurs only once the thresholds of key landscape variables (such as cultivation or overgrazing) are exceeded (Poesen *et al*., 2003; Valentin *et al*., 2005) and as such a systemic threshold rather than a single factor threshold is often applicable in understanding gully erosion. These thresholds, which will initiate erosion when exceeded, may include a combination of variables such as soil properties, slope gradients, rainfall intensities and vegetation cover (Bloem and Laker, 1994; Torri and Poesen, 2014). This means that all the factors affecting gully erosion hold the system close to equilibrium; and when this equilibrium is disturbed the response - gullying - will operate until a relative equilibrium is restored again.

This systemic approach to gully erosion was used by Nordström (1988) in studies of gullying in Lesotho, and by Kakembo (1997) in studies of gullies in the Peddie district in the former Ciskei. Kakembo (1997) noted that during the time period 1950 to 1970 a cumulative chain of events led to the rapid formation of gullies, implying a systematic threshold had been reached to initiate the gullies. The chain of events probably started in the

early 1900s and included land use changes, wet and dry climate cycles, and decreasing vegetative cover.

Nordström (1988) noted that the crossing of the threshold variables causes erosion to occur in cycles where the relative equilibrium of the system will be interrupted by periods of instability, leading to either aggradation or degradation. Such an erosion cycle of infill, relative stability and past gully entrenchment was described by Blong (1970) and by Shakesby and Whitlow (1991) in studies of gullies in Zimbabwe.

Nordström (1988) suggested that a gully system is near the end of the current cycle of erosion if there is a steep slope above the gully heads, a large percentage of the gully heads have extended into the bedrock, the system has a low extension/expansion ratio; there is a sharp decline in the rate of erosion; there is a decline in the absolute number of discontinuous gullies and there is a predominance of rectangular cross sections in the gully. For example, the extent of erosion in the Tugela catchment was considered by Garland and Broderick (1992) to be shrinking and possibly nearing the end of its current erosion cycle.

Garland *et al.* (2000) also noted that some gullies in South Africa appear to be getting shallower due to the foot slope accumulation of sediment. They concluded that as gully deepening has not been recorded in the recent literature on gullies in South Africa, that gullies have attained a

baseline, which suggests that gullies in general could be entering a period of infilling and deposition in the natural cycle of erosion, although different parts of the country may be at different stages. Nordström (1988) and Firth and Whitlow (1991) showed that different catchments can be in vastly different stages of the erosion cycle despite having the same climate.

2.3.4 Factors that Influence Gully Erosion

There are a number of variables that affect gully erosion, such as the soil properties which will determine whether water is able to infiltrate the soil or runoff and remove the soil; the aggregate stability of the soil, as well as those properties that will influence dispersion such as the organic carbon content of the soil, the amount of "free" Fe and Al present in the soil, the relative ratio of basic cations on the exchange sites, the cation exchange capacity (CEC), the dominant clay minerals, and the electrical conductivity (EC) and pH of the soil solution (Nelson *et al*., 1998; Amézketa, 1999; Bell and Walker, 2000; Rienks *et al*., 2000; Laker, 2004; Bronick and Lal, 2005).

2.3.4.1 Infiltration versus Run-off

Water infiltration rates into the soil and the soil's water holding capacity, the soil's grain size and the organic matter content are some of the factors controlling a soil's influence on runoff (van Zijl, 2010). If the infiltration rate

of the water is higher than the water addition rate to the land surface by rainfall, the runoff rate will be zero. However, if the water addition rate is greater than the rate of infiltration, runoff will occur which may lead to soil erosion. On steeper slopes both the amount and kinetic energy of the run-off will be greater than on gentle slopes (van Deventer *et al*., 2002; van Zijl, 2010) because there is less time for the water to infiltrate the soil. High intensity rain also allows little time for water infiltration and the high intensity thunderstorms which fall over most of southern Africa is thought to contribute greatly to the erosion problem in the region (Laker, 2004; van Zijl, 2010).

The infiltration of water into the soil is also influenced by soil texture, the tendency of soil to crust and the characteristics of precipitation. Water infiltrates quickly into coarse textured soils, but only a little water is retained in the soil; conversely fine-textured soils can hold more water but the infiltration rate is lower. The soil water content will favour run-off should it reach saturation levels, but promote infiltration if the water holding capacity is low (Laker, 2004; van Zijl, 2010).

In soils with relatively permeable topsoil abruptly overlying a low-permeable diagnostic horizon which is not a hardpan, the infiltration rate is governed by the low infiltration rates of the B horizon rather than the overlying topsoil. During a rainfall event, water will quickly infiltrate the A and E horizons but not the B horizon, and thus a perched water table will

form in the E horizon (van Zijl, 2010). If the saturation level reaches the soil surface, infiltration excess is reached and run-off will start. Van Zijl (2010) noted that the bigger problem in these soils is the lateral subsurface flow at the contact between the E and B horizon, as Rooyani (1985) suggested that the formation of soil pipes often starts here and when the soils are dispersive, this effect is aggravated.

2.3.4.2 Aggregate Stability and Dispersion

Dispersion in soil is caused either by physical raindrop impact or by chemical mechanisms where the clay platelets develop a similar charge which causes repulsion, bringing about deflocculation (Bell and Walker, 2000). The dispersed particles are moved along with water until the soil pores that they move into become too small and the pores become clogged. Thus a crust forms (Medinski, 2007), and the crusting significantly reduces the ability of water to infiltrate the soil (Hillel, 1980; van Zijl, 2010). Mills *et al*. (2006) showed that the dispersive particle size smaller than 0.1 mm determines the susceptibility of a soil to crusting.

Soil aggregation is the degree to which colloidal materials of different sizes in the soil remain associated when the soil is disturbed by tillage, raindrop impact or wetting and drying (Oades and Waters, 1991). The more stable the soil aggregate, the lower its potential for erosion. An aggregate hierarchy exists where micro-aggregates (<2 µm) consisting of clay

platelets and organic molecules bind together to form aggregates (< 250 µm) which in turn bond to form macro-aggregates (> 250 µm). The micro-aggregates are stabilised against disruption by several mechanisms wherein organo-mineral complexes play a central role (Tisdall and Oades, 1982). Oades and Waters (1991) showed that an aggregate hierarchy exists in soils where organic matter is the main stabilising agent of the aggregates; but it does not exist in oxisols where oxides are the main stabilising agents. If aggregates break down progressively then a hierarchy exists, but when an aggregate breaks up into silt and clay particles, no aggregate hierarchy exists (Oades and Waters, 1991).

The structural breakdown of the soil starts when the macro-aggregates disintegrate into micro-aggregates (Oades and Waters, 1991; Amézketa, 1999). However when the lowest order of soil structure is destroyed, the larger hierarchical orders are simultaneously destroyed (Dexter, 1988); the ultimate example of this is clay dispersion.

Clay dispersion occurs when the repulsive forces between clay particles exceed the forces of attraction, so that in the presence of pure water the particles repel each other to form a colloidal suspension (Bell and Walker, 2000). Dispersion is a time dependent chemical process (Amézketa, 1999), where there has to be sufficient water - soil contact for a sufficient amount of time, and Watts *et al*. (1996) found the critical amount of water needed for dispersion to be close to the plasticity limit. Unlike non-

dispersive soils where the individual particles will cling to each other and are only removed by water flowing with a certain erosive energy, dispersive soils have no threshold velocity for water flow and the particles will go into suspension even in quiet waters, and are thus highly susceptible to erosion and piping (Bell and Walker, 2000).

Bivalent cations such as Ca^{2+} and Mg^{2+} can form bridges between clay particles and organic matter and thus improve soil structure (Bronick and Lal, 2005). Sodium (Na^{+}) however, is a highly dispersive agent which directly enhances breakup of aggregates (Hanson, 1993; Bell and Walker, 2000; Bronick and Lal, 2005). The sodium ions originate from the weathering of sodium rich rocks, which in a sodic environment are usually granites (Pitty, 1979). These positively charged sodium ions in the soil attach themselves to clay particles, which decreases the ability of the clay particles to adhere to each other and causes the clay particles to swell when wet by increasing the osmotic potential of the soil. The soils become unstable and impermeable and when the soil dries it becomes flaky and easily eroded (Bell and Walker, 2000).

The effect of sodium in the soils is expressed as the two soil property parameters: the sodium adsorption ratio (SAR_s) and the exchangeable sodium percentage (ESP), which shows the ratio of Na^{+} to stabilising cations in the soil suspension and cation exchange positions respectively (Hanson, 1993; Bell and Walker, 2000). The SAR_s is used to quantify the

role of sodium where free salts are present in the pore water and if there are no free salts available then the use of SAR_s to define dispersive soils is not applicable, and the use of SAR_s is based on the assumption that soils are in equilibrium with their environment (Bell and Walker, 2000).

An ESP of 15% is used as the critical value above which a Natric horizon is defined in the Soil Taxonomy (Soil Survey Staff, 1999) and World Reference Base (IUSS Working Group WRB, 2007). A soil is considered to be sodic if it has a high percentage of exchangeable sodium and therefore a high pH value and these soils tend to be poorly drained and often crust on the surface (Davies *et al*., 2007). The drainage is affected because the sodium ions on clay particles can cause the soil to disperse, and because these soils are so dispersive they are easily eroded, which often results in a barren landscape (Davies *et al*., 2007). Rengasamy and Churchman (1999) however, suggest that soil dispersion or soil sodicity cannot be measured by a single parameter such as ESP or SAR_s, but that other soil characteristics such as pH and electrical conductivity should also be taken into account.

2.3.4.3 Exchangeable Cations

Although calcium and magnesium are often grouped together as similar ions in classifying soils, soils have been shown to be more susceptible to dispersion when Mg occupies more of the cation exchange sites,

especially in arid to semi-arid regions (Rahman and Rowell, 1979). This might be because of the smaller ionic radius and larger hydration number and ionic potential of Mg than Ca, which leads to a larger hydration shell and thus weaker bonds between the Mg ion and the clay particles (Zhang and Norton, 2002). Ca^{2+} is regarded as a stable cation and adds to aggregate stability when added to a soil by replacing Na and Mg on exchange sites (Armstrong and Tanton, 1992). According to Hofmeister's lyotropic series the decreasing order of cations enhancing dispersion is $Ca^{2+} < Mg^{2+} < K^{+} < Na^{+}$ (in Van Olphen, 1977).

Although magnesium is a divalent cation, there are studies to show that high Mg levels can be detrimental to soil structure. Sumner (1993) found that the Ca : Mg ratio could be an indicator of erodibility, with low Ca : Mg values corresponding to higher erodibility, whereas in the study of Bloem and Laker (1994) a Ca : Mg ratio of less than one was one of the probable causal properties of dispersive soils. Yadav and Girdhar (1981) also found an increase in soil dispersibility when the soil was leached with decreasing Ca:Mg ratio water.

Another way in which Mg influences soil dispersibility is by allowing more Na to be adsorbed onto the exchange sites than when Ca is the complementary cation (Curtin *et al*., 1994). Thus it is Na which is responsible for the higher dispersion, but Mg facilitates the adsorption of Na on the exchange sites. Nel (1989) warns that Mg will have a negative

impact on the physical condition of the soil if interlayered silicates or illite is the dominant clay mineral, the exchangeable Ca: Mg ratio is low, there are no $CaCO_3$ concretions in the soil, and iron or organic material has the most important influence on the stabilisation of soil aggregates.

The cation exchange capacity (CEC) of the soil arises due to the type and nature of the clay minerals present in the soil (Bell and Walker, 2000). Clay minerals that tend to be associated with dispersivity are 2:1 phyllosilicates and the CEC of these clays are usually in the range 40 to 150 meq/100 g clay. The CEC cannot alone be used to identify dispersive soils as other factors such as high organic content may contribute to high CEC values.

It has been shown that CEC and specific surface area are related to stable aggregates (Dimoyiannis *et al*., 1998) where polyvalent cations act as bridges between negatively charged clay particles and organic molecules, thereby reducing the repulsive electrostatic forces between them (Bronick and Lal, 2005). Clay minerals possess a layered structure and are considered host minerals; and are classified by differences in their layered structure (Nayak and Singh, 2007). There are several classes of clays such as smectites (montmorillonite and saponite), mica (illite), kaolinite, serpentine, pylophyllite (talc), vermiculite and sepiolite (Shichi and Takagi, 2000; Nayak and Singh, 2007). The adsorption capabilities of clay minerals result from a net negative charge on the structure of the minerals,

which give the clays the ability to adsorb positively charged species. However, their adsorption properties also come from their large surface area and high porosity (Alkan *et al*., 2004; Nayak and Singh, 2007). Montmorillonite for example has the largest surface area and highest cation exchange capacity (CEC).

Levy (1988) found that a soil's susceptibility to dispersion and crusting decreases in the order of dominant clay mineral of smectite → illite → kaolinite. Frenkel *et al*. (1978) showed that adding a little (2%) smectite to a kaolinitic soil led to increased dispersion of the clay particles. This effect was not clear in Levy's experiment, although he stated that small amounts of smectite in a kaolinitic or illitic soil probably did impede the water movement through it.

Stern (1990) investigated the effect of clay mineralogy on sheet erosion and found that "*smectite contaminated*" kaolinitic soils had final infiltration rates comparable to that of illitic soils, with pure kaolinitic soils' infiltration rates being about three times higher than the contaminated soils. Amorphous clay minerals, originating from volcanic rocks are very stable (Bronick and Lal, 2005). Even when these volcanic rocks weather, they form 1:1 clay minerals or oxides which are also very stable (Powers and Schlessinger, 2002).

Variations in the pH of the soil have been found to affect dispersion in many pure clay minerals (Chorom *et al*., 1994). Dispersion increases as the soil pH increases (Amézketa, 1999), because the negative charge on the clay particles also increases (Chorom *et al*., 1994). The results of the Chorom *et al*. (1994) study confirmed that clay dispersion and flocculation are dependent on net particle charge and pH, and that the net negative charge on clay systems is influenced by pH. In soils where pH-dependent charge clay minerals are dominant, the pH at the point of zero charge is the pH where the least amount of dispersion will occur (McBride, 1994). Calcareous soils have been found to be more stable than non-calcareous soils though (Yadav and Girdhar, 1981).

2.3.5 Relationship between Slope Gradient and Gullying

Gullies are common features of mountainous or hilly regions with steep slopes and Poesen *et al*. (2003, 108) state that "...in a landscape with a given climate and land use, there exists for a given slope gradient of the soil surface (S) a critical drainage area (A) necessary to produce sufficient runoff which will cause gully incision". This implies that as slope increases the drainage area required for gully erosion decreases. They compared 10 critical S-A data sets (as shown in Figure 2.4) which show the critical slope of soil surface in relation to the drainage area for incipient gully development in a variety of environments. This topographic threshold for gully initiation has also been explained in terms of the relationship

between soil surface gradient and critical drainage area by Vanderkerckhove *et al*. (2000) and Kakembo *et al*. (2009). The specific sediment yield increases when the frequency of gullies increases in the catchment, but decreases when the catchment area increased (Descroix *et al*., 2008).

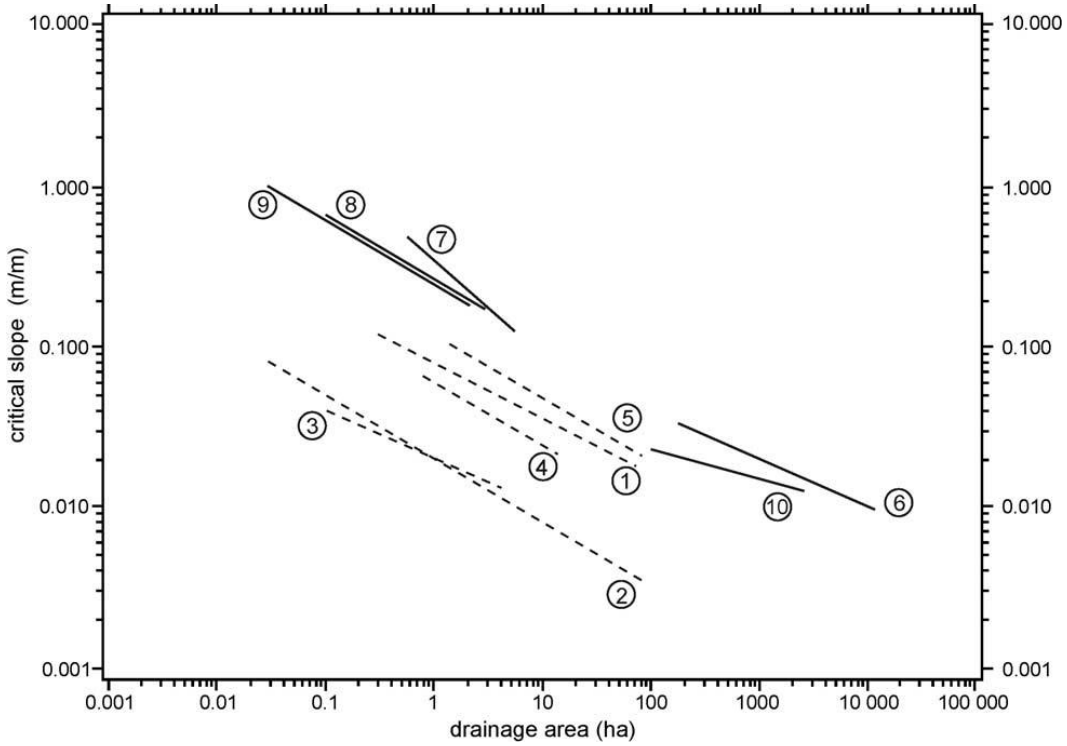


Figure 2.4 The relationship between critical slope of soil surface and drainage area for incipient gully development in a variety of environments. The dotted lines indicate threshold conditions for ephemeral gully development in cultivated cropland (1–5). Solid lines indicate threshold conditions for gully head development in non-cultivated land (6 = sagebrush and scattered trees; 7 = open oak woodland and grasslands; 8 = coastal prairie; 9 = logged forest and 10 = swampy, reed-covered valley floors) (Poesen *et al.*, 2003).

Steep slopes promote high runoff velocity and thus rill and gully initiation (Valentin *et al*., 2005). In a given climate, steep slopes can produce lower runoff volumes than gentler slopes, which is a function of the lower crusting rate on steep slopes. Because soil crusts usually develop on gentle slopes generating higher runoff, the slope threshold for rill initiation can be as low as 1% (Valentin *et al*., 2005). However this threshold value is specific to a given site and cannot be applied to other settings where local environmental conditions may be different.

Vanderkerckhove *et al*. (1998) showed that this relationship cannot explain gully initiation in isolation, as only a weak correlation exists between them. Kakembo *et al*. (2009) found a predominance of gully sites in the concave lower hillslope of the Eastern Cape with slope angles of 5° - 9° indicating a markedly preferential topographic threshold for gully formation. This gentle slope range for gully location is supported by Poesen *et al*. (2003) who noted that as the slope steepens, the critical drainage area for gully initiation decreases and vice versa. Keay-Bright and Boardman (2006) also showed that, in the central Karoo, gullying occurs mainly on footslope areas where colluvial material is available. In China, Li *et al*. (2004) reported critical slope gradients of 2°, 5° and 8° for rills (<0.3 m deep), shallow gullies (0.3 - 2 m deep) and deep gullies (>2 m deep) respectively (Valentin *et al*., 2005).

Sodic soils are dispersive and easily eroded, and when found on flat land will not allow rainwater to drain, which leads to water-logging on the surface. However on sloping terrain, rainwater carrying dissolved ions is lost through lateral drainage and the soil can lose its sodicity (Dye, 1977; Chappell, 1992). Sodic soils on sloping lands are also subject to water erosion which forms little furrows that can eventually lead to the development of gullies. Dispersive soils have sparse vegetation cover as the soil becomes hard and impermeable and cannot sustain good plant growth (Chappell, 1992; Khomo and Rogers, 2005). A catena profile is also common in some sodic environments, which implies that the soil profile and chemistry will vary along a slope and, with this variation in soil chemistry there will be a variation in the vegetation cover along the slope (Dye, 1977; Chappell, 1992; Gerrard, 1992*).*

Erosion tends to be greater at inflection points in the landscape where the hillslope profile form changes from convex to concave or vice versa (Knighton, 1998; Kakembo *et al*., 2009). Schaetzl and Anderson (2005) noted that the curvature of the slope largely controls the direction of the water and the sediment transport. Dlamini *et al*. (2010) found no correlation between sheet erosion and slope gradient, and between slope gradient and soil loss, although they did report that slope gradient does have some effect on these variables.

Gullies end where the transporting capacity of the concentrated runoff drops or where the erosional resistance to the topsoil increases significantly (Poesen *et al*., 2003). Thus a lowering of slope gradient with increasing drainage area may cause a drop in the transporting capacity and thus a decrease in the gully channel depth.

2.3.6 Effect of Local Base Level Change on Gullying

On many alluvial fans base level is stable, therefore the fan dynamics are controlled by context and climatic factors alone (Harvey, 2002). A change in local base level can have an effect on both alluvial fan morphology and dynamics, and if resulting in incision, this incision may be propagated up through the fan. Harvey (2002) suggests three possible scenarios for base level change: 1) where the base level is stable the fan deposit will prograde and bury the surfaces in front of the fan (Figure 2.5a); 2) Base level may change, but the gradient change may be insufficient to cause fan dissection (Figure 2.5b) and the fan will then prograde onto the newly exposed surface. If base level rises but does not cause any frontal erosion, sediments may prograde into the water body and form a fan delta. 3) Base level may fall and cause incision into the distal section of the fan (Figure 2.5c) provided the gradients are sufficient to initiate incision. However, dissection of the toe of a fan may also result from a rise in base level which may cause erosion, and fan profile foreshortening and steepening, causing distal incision.

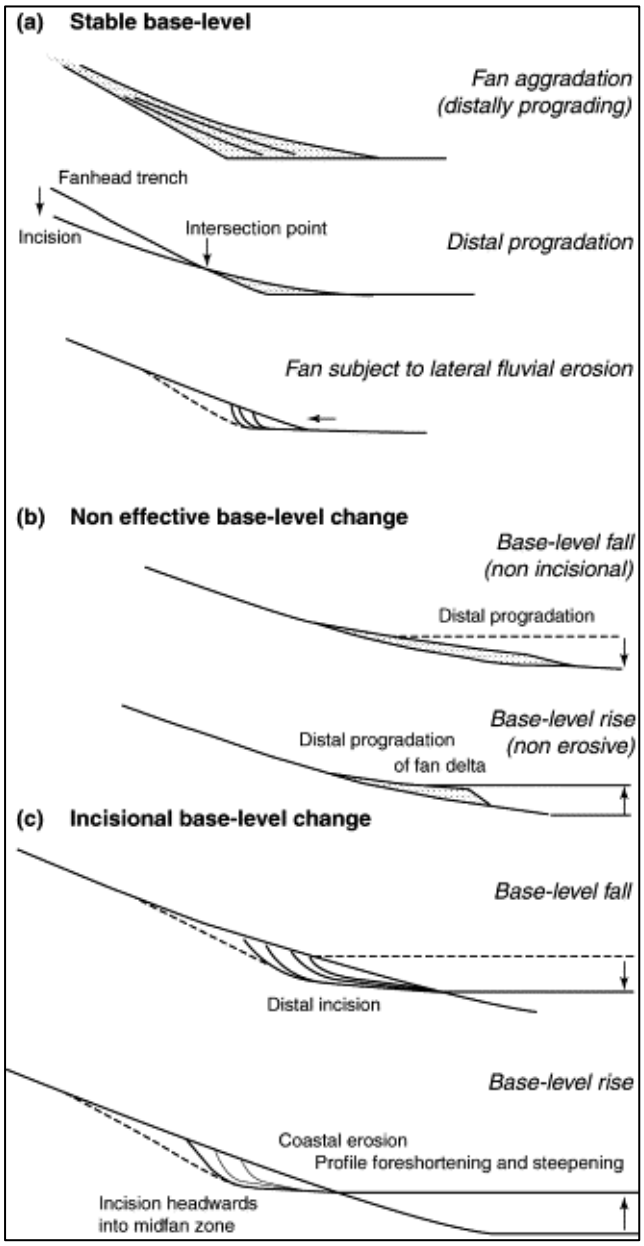


Figure 2.5 Schematic profile of relationships on alluvial fans under a range of base-level conditions (Harvey, 2002, p70).

Studies have also identified the influence of exposed, resistant dolerite dykes and sills on river behaviour. Tooth *et al.* (2002; 2004) showed that rock barriers play a significant role in driving local base level fall along river channels and long-term shifts in floodplain and hillslope sedimentation and erosion (Figure 2.6). In the first stage of the model, rivers incise vertically

into relatively soft sedimentary rock and become superimposed on more resistant dolerite sills and dykes (Figure 2.6a). These rock barriers (dykes and sills) determine the local base level as the erosion rates of these barriers are less than the upstream sedimentary rocks. As a result enhanced lateral migration results in valley widening, floodplain development and lower channel gradients (Figure 2.6b). During this stage floodplains and hillslopes remain stable. With the partial or complete breaching of the rock barriers downstream, knickpoints migrate upstream, leading to channel incision, channel straightening and floodplain abandonment. The local base level is lowered as an increased drop in height between the river channel bed and the adjacent hillslopes or floodplain is created. Extensive dendritic gully networks erode headward, upslope from the steepened river channel banks (Figure 2.6c) This process of dissection and gully formation continues until a river is superimposed onto another rock barrier (Tooth *et al*., 2004).

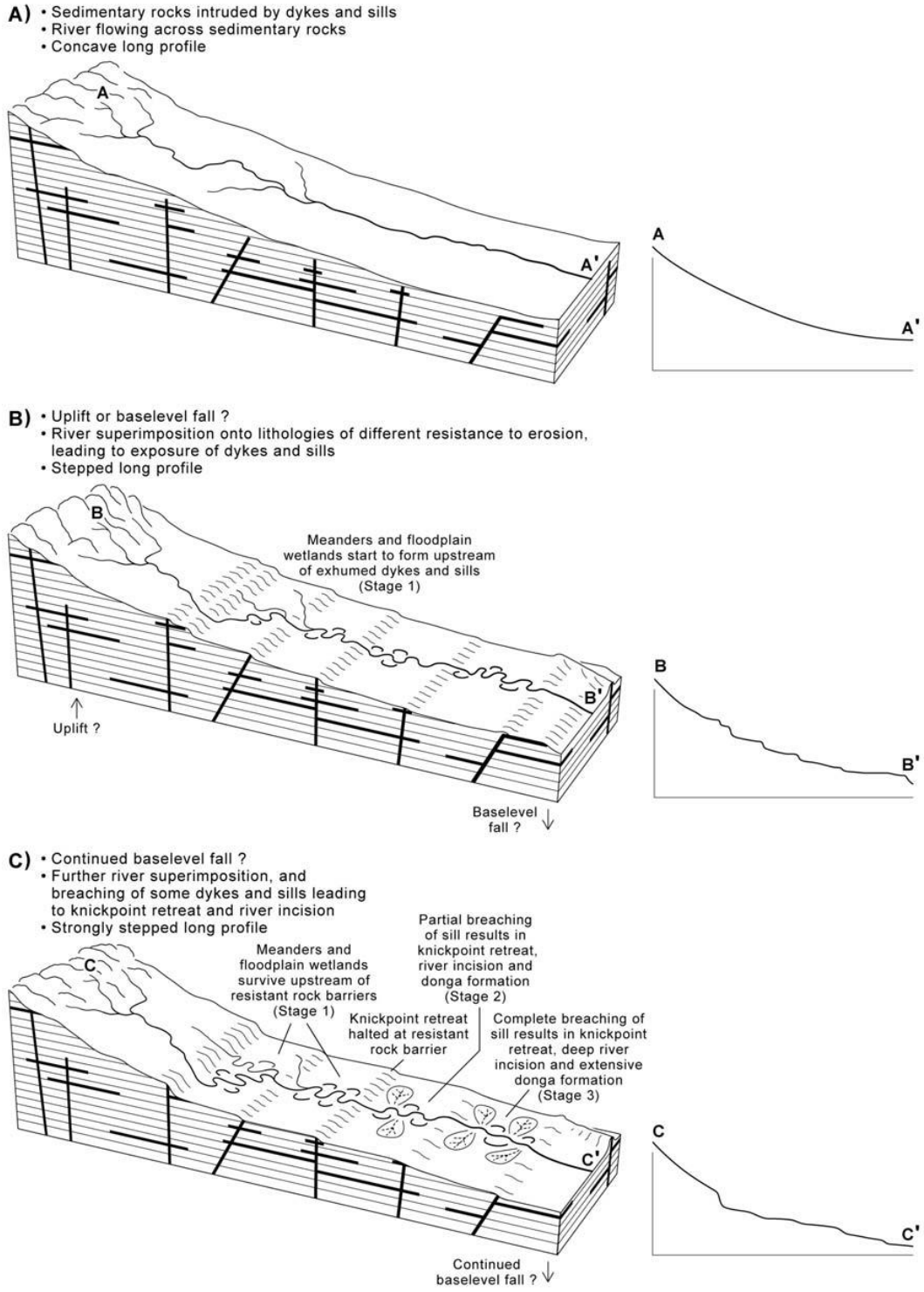


Figure 2.6 Model of a geologically controlled river and hillslope development (Tooth *et al*., 2004).

As gullies are an ideal location for exposing the underlying stratigraphy, it is possible to reconstruct the deposition environment of the sedimentary

sequences. Critical to an environmental reconstruction is establishing the absolute ages of the sedimentary deposits and in late-Quaternary sediments this can be achieved through radiocarbon (^{14}C) or optically stimulated luminescence (OSL) dating techniques, amongst others.

2.4 DATING OF FLUVIAL SEDIMENTS

Radiocarbon (^{14}C) and optically stimulated luminescence (OSL) dating have contributed greatly to the understanding of late Quaternary environments, specifically to the understanding of alluvial fan and debris cone evolution as well as to investigations of other depositional environments. The application of radiocarbon dating requires the deposition and preservation of organic matter within the stratigraphy; whereas, OSL dating determines the time when sediments were buried after sufficient exposure to daylight to reset the luminescence clock.

Radiocarbon dating is often the preferred geochronological tool for dating soils. However, it is not widely applicable for dating sediment found in fluvial environments because of the lack of carbon content and its limited age range (<50 ka). Also, measured ^{14}C ages of soils or its fractions are usually younger than the true ages of soils because of the continuous addition of organic matter into the soil. Different ^{14}C signatures of organic matter for soils of the same age are the result of differences in soil carbon dynamics due to the effect of climate and soil depth (Wang *et al*., 1996).

Therefore, the deviation of the measured ^{14}C age from the true age of oil formation could differ significantly between soils or soil horizons. Therefore OSL is used increasingly to constrain the timing of depositional events. However the problem associated with dating fluvial sediment relates to the incomplete bleaching of the OSL signal prior to deposition (Murray *et al*., 1995; Olley *et al*., 1998; Wallinga, 2002) as sediment found in fluvial environments is most likely to have experienced limited exposure to sunlight prior to deposition. This may be a result of turbidity of the water or reworking of the sediment itself (Duller, 2008). As a result there would be a broad distribution of the equivalent dose (D_e) (which is the total radiation dose received by the quartz grains) in small aliquot measurements for these sediments, as shown by Olley *et al*. (1999) and Rodnight *et al*. (2006).

Olley *et al*., (1999), working with recent fluvial sediments from Australia, showed that for two of the samples, small aliquot measurements overestimated the known age of the sample. However, Rodnight *et al*. (2006), working with fluvial sedimnet from South Africa, suggested that they could obtain ages consistent with geomorphological relationships if they applied the finite mixture model to the small aliquot measurements. For both these studies, the overestimation of the D_e appears to be that only a small number of the grains were well bleached, and while the Australian samples were very bright, the South African samples were less so (Duller, 2008).

Thomsen *et al*. (2007) applied OSL to fluvial sediments in Namibia in environments of high insolation and found there were significant overestimates of the ages if the dose of the small aliquots were averaged out. The ages of three samples were determined by OSL and compared to the ages of the pottery found in the sediment and the effect of averaging the data was that the resulting dose distribution gave no indication of incomplete bleaching, even though single-grain analysis revealed relatively poor bleaching at deposition.

Fluvial sediments were also dated in Australia in the Lake Burragorang catchment near Sydney by Rustomji and Pietsch (2007) and on Gilmore Creek in New South Wales by Page *et al*., (2007). The study by Rustomji and Pietsch (2007) was to assess the impact of European settlement on the catchment area and obtained ages of within the past 150 years. They demonstrated that the potential for incomplete bleaching in younger sediments is large. Similarly the study by Page *et al*., (2007) also demonstrated that incomplete bleaching of the grains was significant. However the ages they obtained using the minimum age model was consistent with historical data from the area.

Jain *et al* (2004) suggested that fluvial samples are generally sufficiently well bleached that the type of small aliquot or single grain methods are only necessary for young samples less than 1000 years old. However, Jacobs (2004) suggests that it is not the actual measurement of the single

aliquot or single grain that is significant, but rather the testing of the measurement procedures and the analysis of the data that is important. It has been shown that the single aliquot regenerative (SAR) protocol may not be appropriate for the measurement of all samples and that individual grains do not all behave in an identical manner.

CHAPTER 3: RESEARCH LOCALITY AND DESCRIPTION

3.1 RESEARCH LOCALITY

The research site is located on the game farm Heelbo (S28°28' 2.3"; E27° 49' 3.5") approximately 5 km south east of the town of Senekal on the eastern margins of the Free State Province (Figure 3.1).

The farm Spionkop 932, on which the Heelbo site is located (Figure 3.2), comprises a number of fenced-off areas for game farming. The research area is not stocked with game because of the dangers posed by the numerous deep, steep-sided gullies. However, during the hunting season (April to August) game are allowed to roam freely in the area. The land is also not used for agriculture as the slopes are too steep and the soil is not considered fertile enough for crop farming, although some agriculture takes place on the southern, more gentle slopes of the mesa (Figure 3.2) (Nel Human, *pers comm*.).

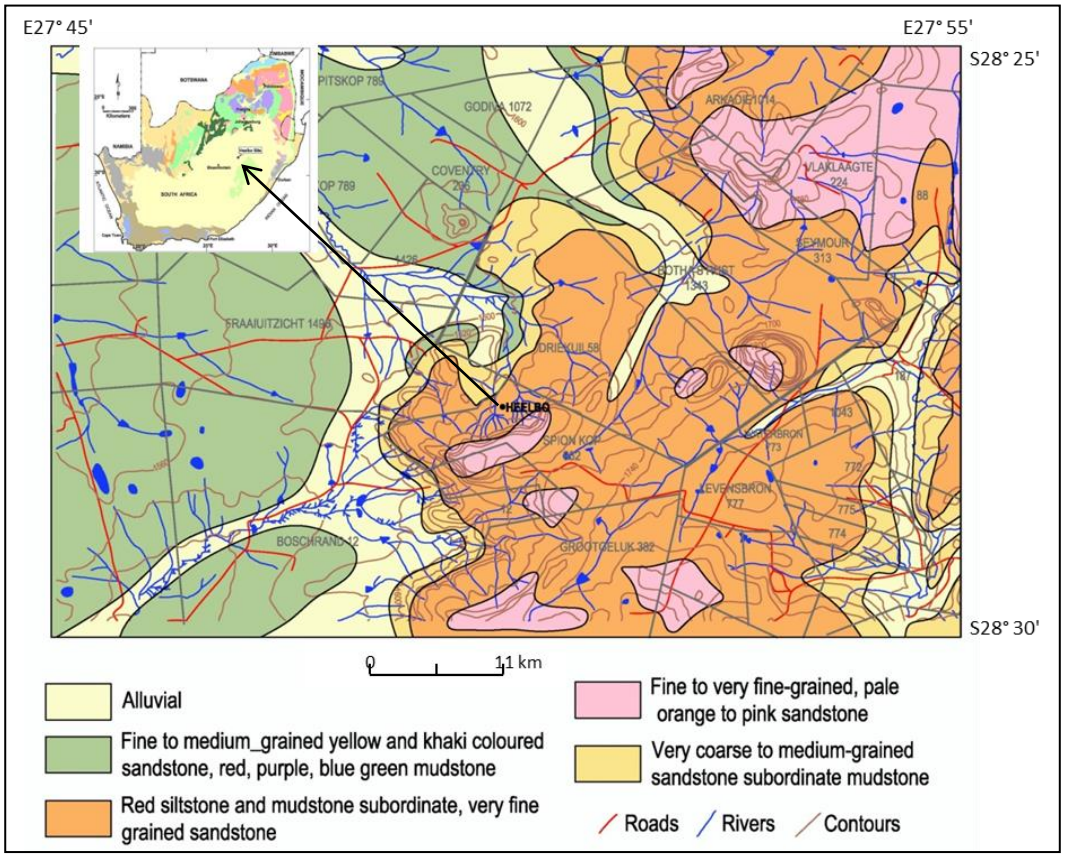


Figure 3.1 Location of the Heelbo game farm which is situated within exposed Elliot Formation of the Karoo Supergroup. (Inset: map of South Africa).

The Heelbo hillslope deposit has formed on the mountain front of a Karoo mesa. There are two deposits separated by a high-lying, basement rise. The two deposits are referred to as Area 1 and Area 2 (Figure 3.2) and the exposed bone bed identified towards the base of the slope, north of Area 1 was also investigated and referred to as the Bone Bed section.

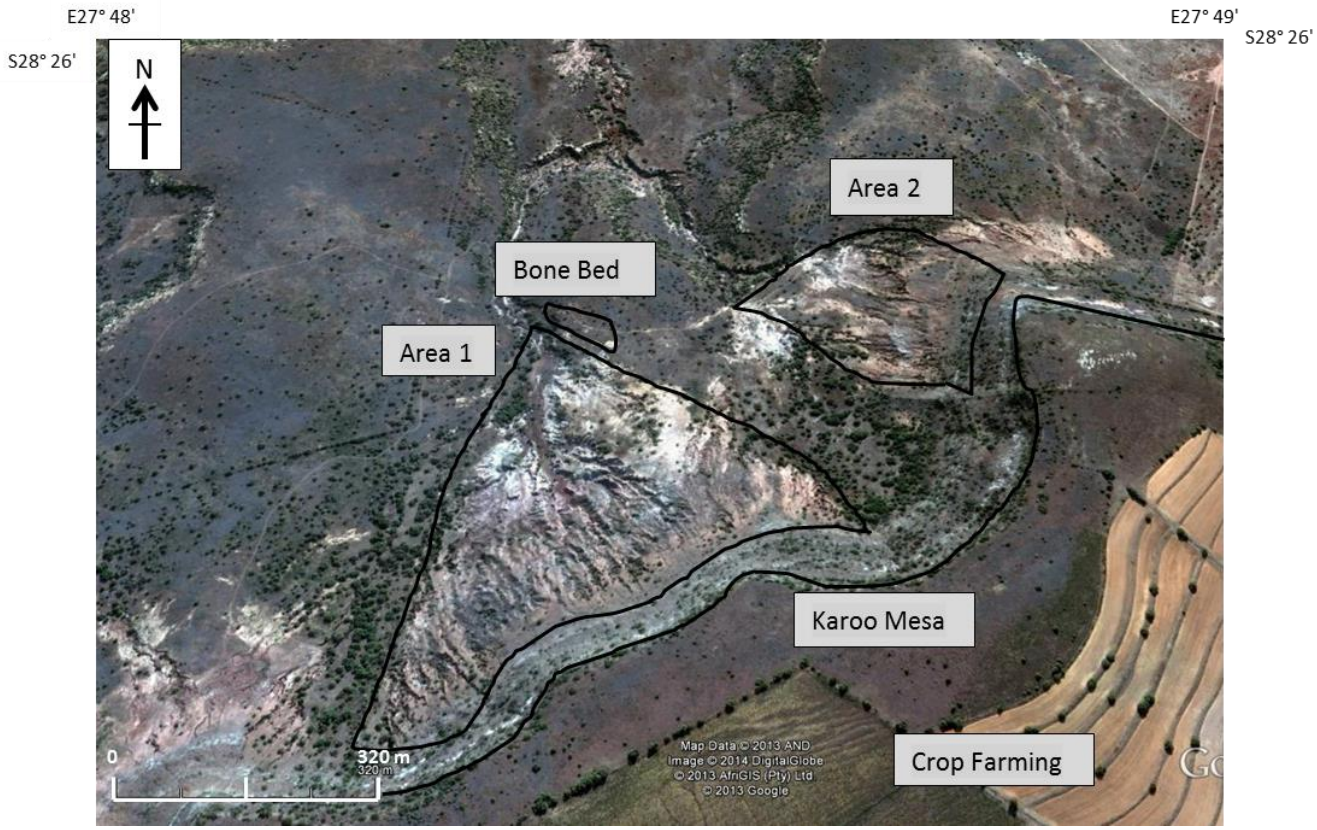


Figure 3.2 Google Earth image of the Heelbo research site, showing the location of the deposit, the Karoo Mesa and the farming areas on the southern slopes of the mesa. The dark lines represent the approximate outlines of the 2 Areas, the bone bed and the crest of the Karoo mesa.

The top of the Heelbo mesa extends about 1450 m from north-west to south east and rises about 90 m above the valley floor (Figure 3.3) with a summit of ~1760 m.a.s.l. The head of the hillslope deposit commences at about 30 m below the crest of the mesa at ~1730 m.a.s.l. and the sediment extends north-westward across the valley floor for about ~475 m (Figure 3.3). The deposit is not extensive and the sediment source for the deposit appears to be the weathered sand and silt derived from the bedrock and the rock face of the mesa as it moves downslope under the influence of gravity. The deposit is slightly concave in longitudinal profile

from the head to the foot slope, and convex in transverse cross-section parallel to the mesa crest.

There are some defined stream channels on the hillslope. The water flows as sheetwash down slope, then collects in and flows through the gullies. Confined channels form in the low-lying distal reaches and flows north-westwards before joining Sandsloot. Sandsloot flows for approximately 30 km into Sandrivier which flows to the north of Senekal (see APPENDIX A).

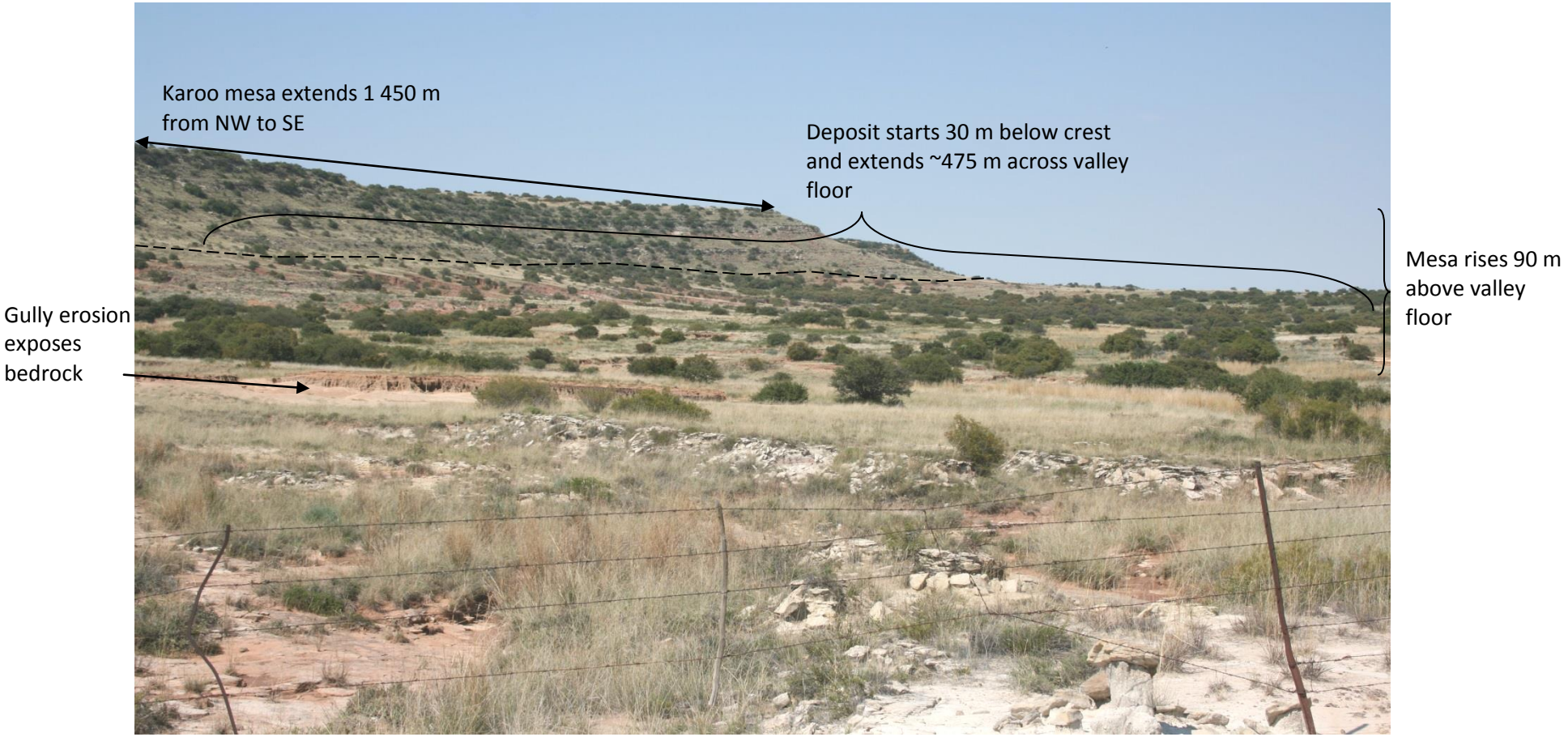


Figure 3.3 Photograph facing southwards towards the Heelbo ridge showing the relief of the hillslope deposit of Area 1. Dimensions of the deposit are shown. Exposed bedrock of Area 2 is shown in the foreground. The dashed line marks the start of the deposit.

3.2 REGIONAL GEOLOGY

The research site is a sedimentary deposit situated on the mountain front of a Karoo mesa. The deposit lies unconformably on the exposed Elliot Formation (Figure 3.4) within the retro-arc foreland basin sediments of the Karoo Supergroup (Johnson *et al*., 2006). The Karoo Supergroup sequence begins with the tillites of the Dwyka Formation which form the basal member of the Karoo Sequence, and following glaciation, the Karoo Basin was filled with sediments of the Ecca and Beaufort Groups and the Molteno, Elliot and Clarens Formations (South African Committee for Stratigraphy, 1980; King, 1982; Johnson *et al*., 2006).

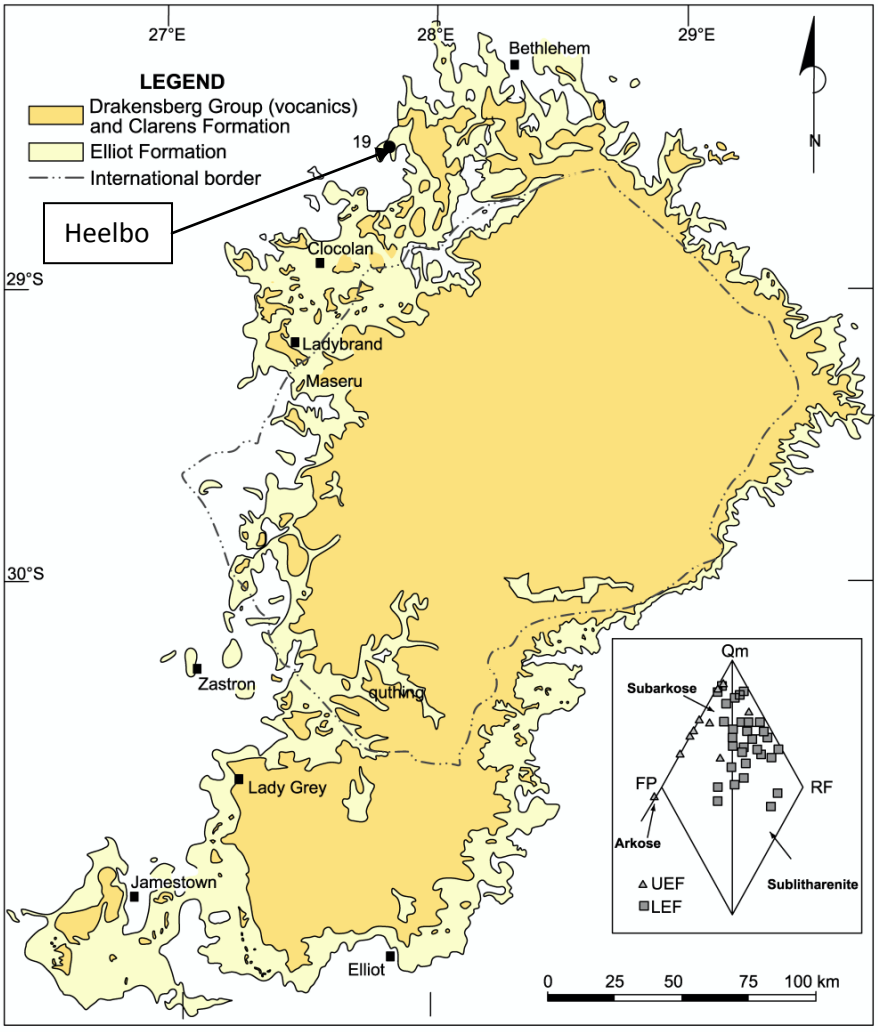


Figure 3.4 Outcropping area of Elliot Formation in South Africa and Lesotho with the sandstone classification for the Upper and Lower Elliot inset; with approximate location of Heelbo shown (modified after Bordy *et al*., 2004a, p348).

The Elliot Formation, together with the Molteno and Clarens Formations comprise the informal “Stormberg Group” and are considered to have formed in the distal sectors of the Karoo Basin during the final unloading phase of the Cape Fold Belt (Catuneanu *et al*., 1998; Bordy *et al*., 2004a; b). The Elliot Formation extends across the interior of South Africa and

Lesotho (Figure 3.4). The Elliot Formation, which has a thickness ranging from a maximum of 460 m in the south to less than 70 m in the north, has a relatively sharp lower contact with the Molteno Formation and a gradational upper contact with the Clarens Formation (Lucas and Hancox, 2001).

It was generally accepted that the Molteno/Elliot alluvial wedge resulted from three episodes of fan progradation into the foreland in response to three uplift events in the Cape Fold Belt Mountains (Smith and Kitching, 1997). Bordy *et al.* (2004b) however, disputed this previous three-part division of the Elliot Formation and suggested that two units – a Lower Elliot Formation (LEF) and an Upper Elliot Formation (UEF) – exist. The differences between the two units are defined in terms of their bed thickness and grain size. The variability in grain size is extreme in the LEF but more constant in the UEF. The basinal south to north grain size decrease occurs in the LEF but not the UEF and the slight vertical grain size increase in the UEF is not present in the LEF. The coarse- versus fine -grained sediment ratio in the LEF decreases sharply from south to north but not in the UEF (Bordy *et al.*, 2004b).

An increasingly arid palaeo-environment is described in the Elliot Formation reconstruction (Visser and Botha, 1980; Eriksson, 1985; Smith and Kitching, 1997). Bordy *et al.* (2004a) described the Lower Elliot Formation as asymmetrical, isolated channel sandstones and thick

mudstones, interpreted as a perennial meandering system. The UEF consists of sheet-like laterally continuous sandstones and interbedded mudstones interpreted as an ephemeral flash-flood dominated fluvial system. The stratigraphy and lithology for the Elliot Formation closest to Heelbo is described by Bordy *et al.*, (2004b) and shown in Figure 3.5. The sequence indicated the occurrence of fossils, seemingly characteristic of the Karoo sedimentary basin, and Butler (2004) noted that the UEF of South Africa and Lesotho hosts the world's most diverse fossil record, with medium to large dinosaur fossils found in the LEF and smaller, light-limbed forms found in the UEF.

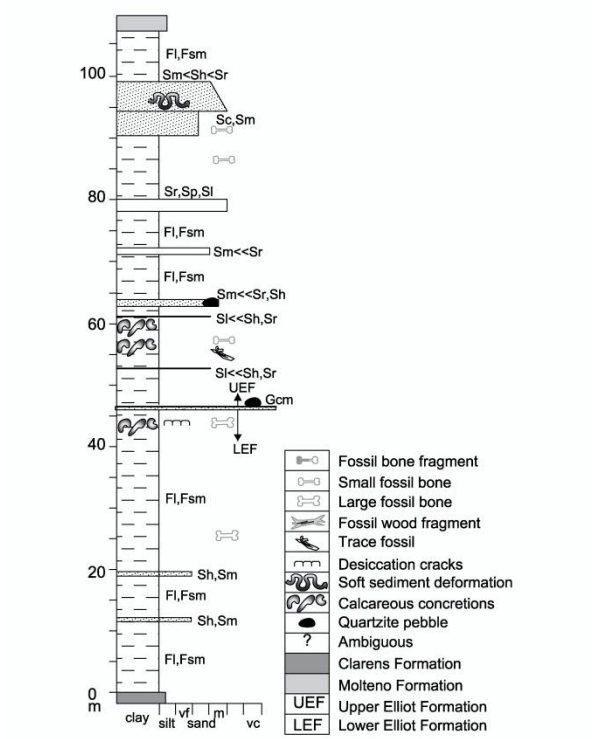


Figure 3.5 Stratigraphy and lithology of the Elliot Formation section closest to Heelbo (see location 19 on Figure 3.4) (modified after Bordy *et al.*, 2004b).

Sedimentation in the Karoo Basin terminated abruptly when basaltic lava flowed through the ruptured crust and covered almost all of southern Africa, forming the volcanic layer known as the Drakensberg Group (King, 1982; Lurie, 1994; Holmes and Barker, 2006). The associated dolerite sills protected the underlying sediments from erosion and produced the flat-topped hills characteristic of the contemporary Karoo landscape (South African Committee for Stratigraphy, 1980; King, 1982). Since then the interior of southern Africa has been dominated by erosion (Partridge and Maud, 2000; Holmes and Barker, 2006).

The rugged topography found in the Free State after scarp retreat and post-Cretaceous weathering is a reflection of the contrast in erosion resistance which exists within and between geological structures and between rock types. Such contrasts account for the varied topography of the eastern Free State region surrounding the Heelbo site.

3.3 REGIONAL CLIMATE

The South African interior rainfall is strongly influenced by the tropical northerly airflow, which is enhanced by the periodic coupling with temperate troughs. Summer heating establishes a persistent low pressure circulation over Zaire, which draws moisture from the Indian Ocean into the continental interior, from which it is advected southwards over South Africa (Partridge *et al*., 1998; Tyson and Preston-Whyte, 2000).

The Free State Province lies almost uniformly at about 1 300 m above sea level and experiences a typical interior plateau climate with summer rainfall and cold, dry winters with snowfall in the eastern mountain regions. The temperature and rainfall are lowest from May to September. The average maximum temperature is about 33 °C in summer with January being the hottest month with a temperature between of 15 °C - 33°C. June is the coldest month with a temperature between of 1 °C – 17 °C and the average minimum temperature for winter is about 13 °C (Figure 3.6).

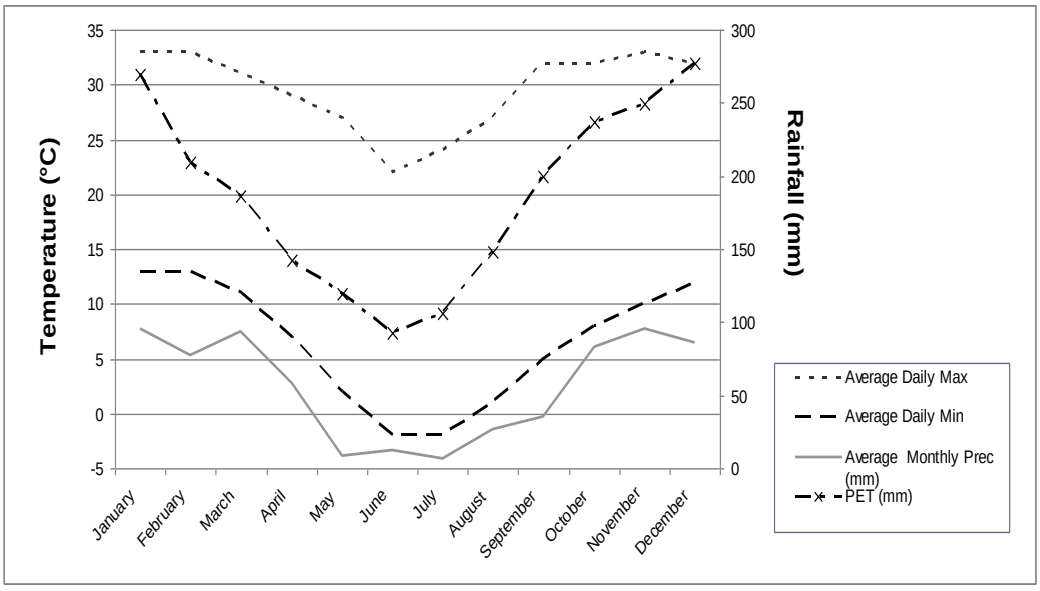


Figure 3.6 The average monthly temperature, precipitation and potential evapo-transpiration of Bethlehem - the closest weather station to Heelbo (modified from data from www.weathersa.co.za; Shultz, 1997).

The region receives its highest rainfall during the summer months and has an annual precipitation of ~680 mm/year. Most parts of the eastern Free State Province experiences rainy season duration of between 181 to 200 days (Figure 3.7). The far eastern margins along the provincial border

with Lesotho have long rain season duration in excess of 200 days Moeletsi *et al*., 2011).

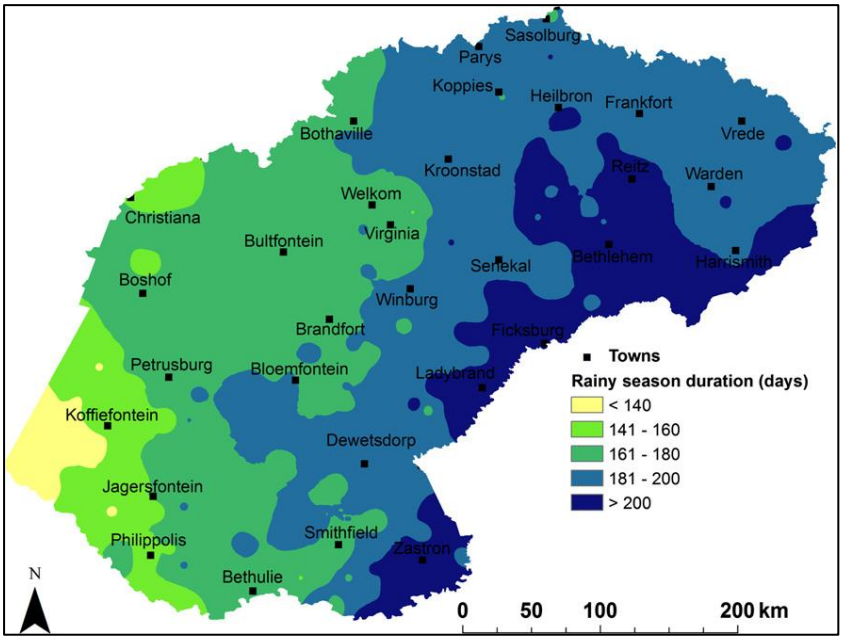


Figure 3.7 Mean rain-season duration over the Free State Province (Moeletsi *et al*., 2011).

In late winter and spring, the region is characterised by strong northerly winds (Figure 3.8) associated with steep pressure gradients which are, in turn, associated with the passage of frontal systems across the Cape region (Holmes *et al*., 2012). October is usually the windiest month.

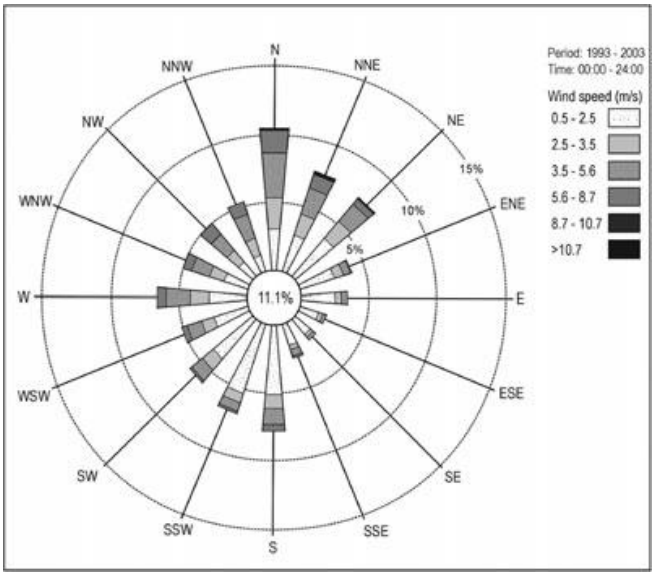


Figure 3.8 Annual wind rose for Bloemfontein (~175 km from Heelbo) (after South African Weather Services, 2003; in Holmes *et al.*, 2012).

3.4 SITE DESCRIPTIONS AND CHARACTERISTICS

The sedimentary mantle on the Heelbo mountain front is composed of weathered bedrock and saprolite transported down the hillslope onto the low lying pediment. The deposit occurs over a broad front rather than from a point-source river and sediment transport is not spatially confined in river channels, but instead spreads out across the mountain front as a series of wedges. Two separate areas were identified that formed on the apron of the same mesa, but are separated by the high-lying bedrock between them (Figure 3.9). The bedrock serves as a watershed dividing the two drainage areas.

At Area 1 the sediment deposit is thickest in the proximal reaches but becomes very thin and undefined towards the base of the structure. The deposit at Area 2 has been mostly eroded away, with some remnants of the stratigraphy still visible. As a result, most of the analytical work is centred on Area 1 with some descriptions and OSL ages derived for Area 2. The Bone Bed section is small, with much of the deposit eroded away. However, this section appears to be a separate lobe of deposition on the hillslope, in which a mass mammal death site is found.

Sample points were identified along the most undissected and continuous section of the slope at Area 1 (see green markers in Figure 3.9) and an average gradient was measured from the crest of the mesa to the distal reach of the deposit along these sample points. The average gradient from the crest of the mesa to the start of the deposit is 20.13°; and from the start of the deposit to the end is 10.20° (Figure 3.10). This average is based on the ideal scenario of the hillslope being rectilinear. However as it is a curved surface, the individual sections along the deposit will be discussed in Chapter 5.

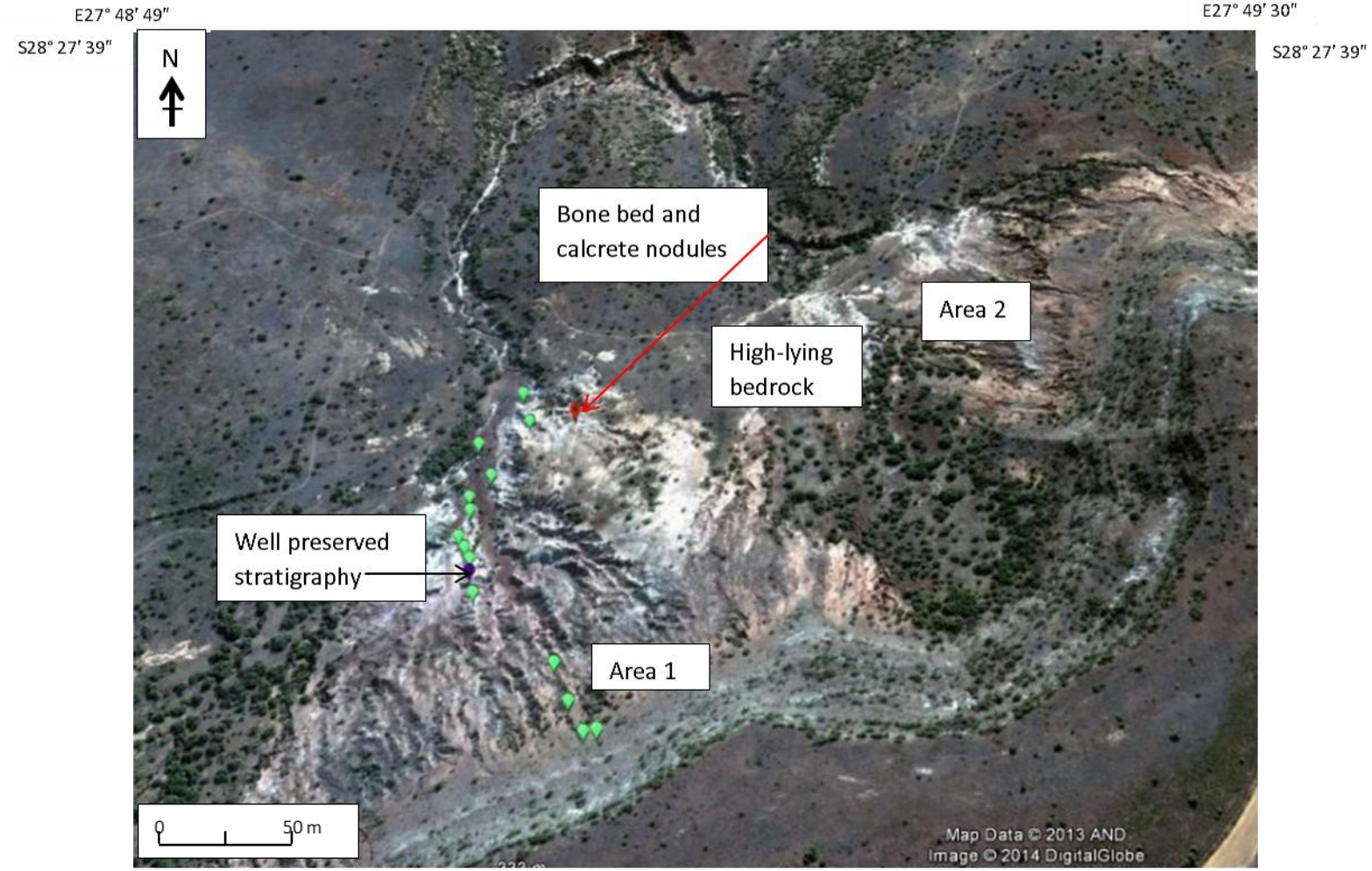


Figure 3.9 Google Earth (2013) image of the location of the sample points for the hillslope gradient (Figure 3.10), the preserved stratigraphy (Figure 3.13) and the bone bed and calcrete nodules (Figures 3.14 and 3.15). The green dots mark the location of the sample points.

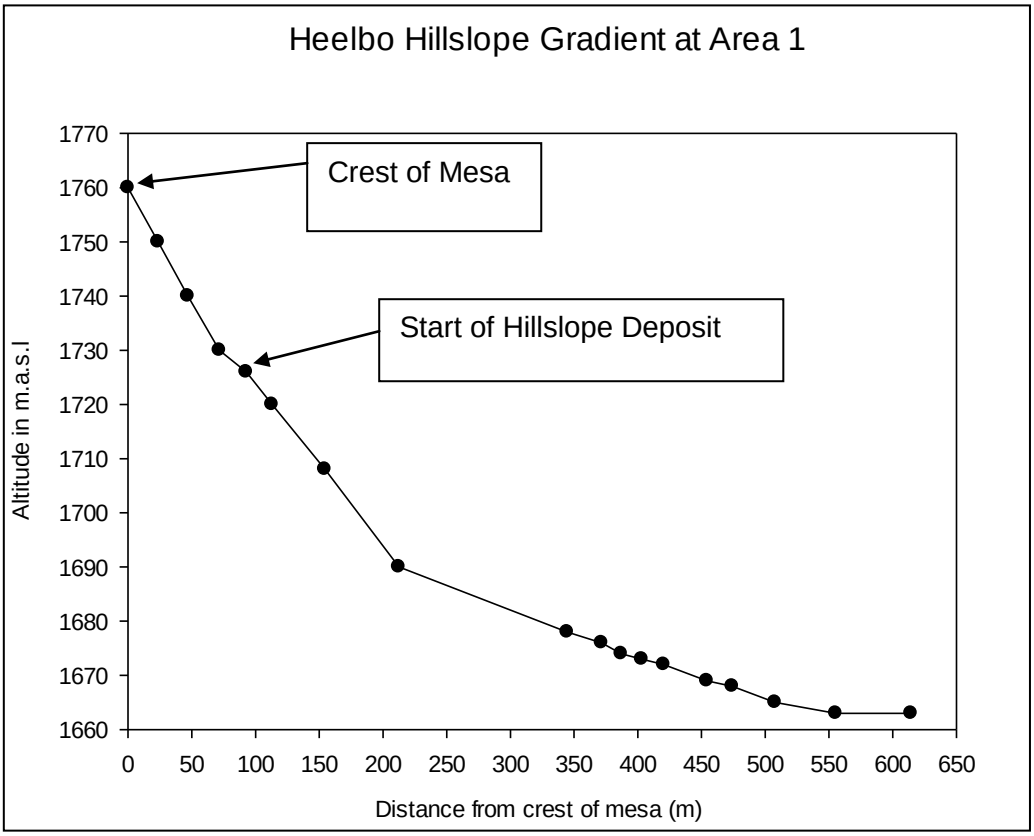


Figure 3.10 Gradient of the hillslope measured downslope perpendicular to the scarp face (vertical exaggeration = 5 times).

3.4.1 Gully Erosion

A network of gullies has formed within the deposit, with depths ranging from a few centimetres to up to six metres, at Area1. The gullies range from shallow, steep-sided, with V-shaped cross-sections in the proximal portion of the deposit, to deeper, steep-sided U-shaped profiles, in the medial and distal sections (Figure 3.11), before merging into channels which drain into the Sandsloot tributary. Continuous gullying has removed most of the deposit at Area 2. Transects and detailed descriptions of the gully morphology are presented in Chapter 5. A consequence of gully

erosion, as it cross-cuts the deposit, is to create isolated stacks in which the stratigraphy is well preserved.

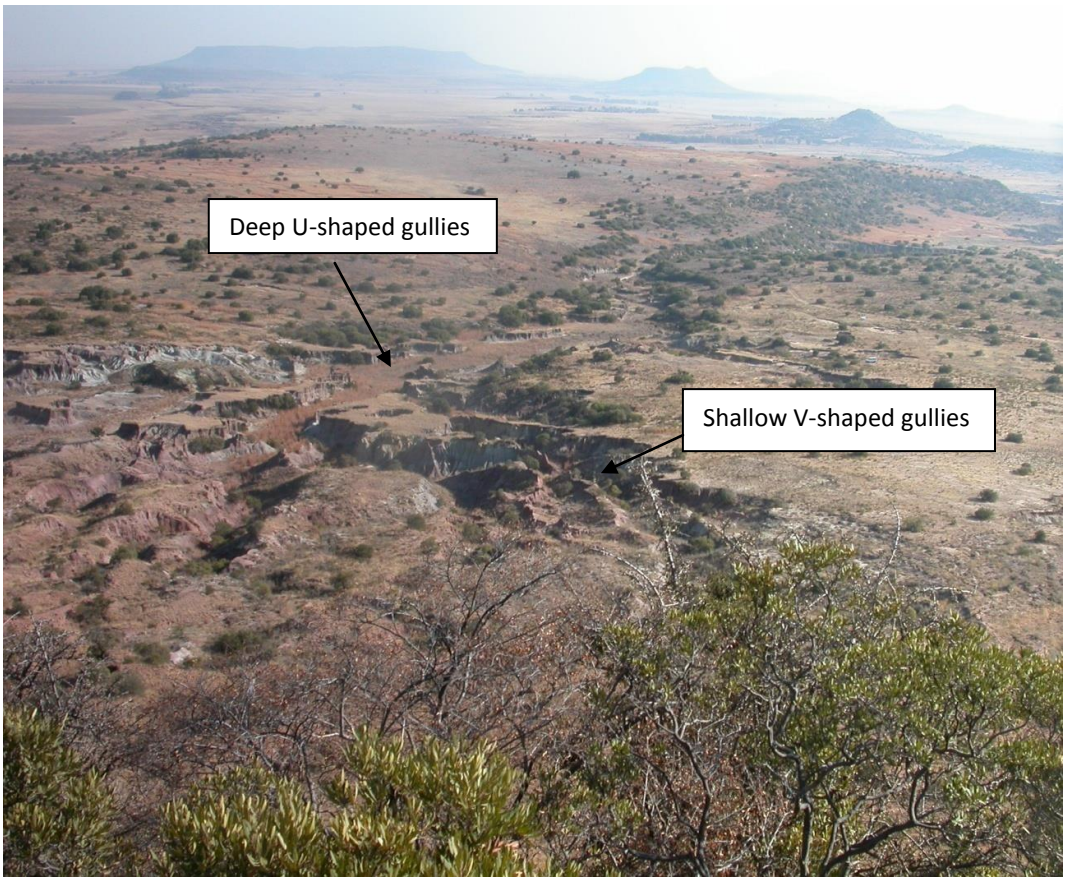


Figure 3.11 A view from the top of the ridge facing north at Area 1, showing the network of gullies in the hillslope deposit. Note the shallow steep V-shaped gullies in contrast to the U-shaped gullies in the medial / distal portions of the deposit.

The gully walls are fluted, and there appears to be an increase in the presence of piping towards the base of the hillslope deposits (Figure 3.12). Subsurface flow has also been observed within the deposit. The hillslope sediments display the physical characteristics of dispersive soils, because they are hard and impermeable, and deflocculate easily in water. The

sodicity of the soil could be one of the root causes of the extensive gullying and piping in the deposit.



Figure 3.12 Fluting along the gully walls at the head of the deposit in Area 1, is indicative of a highly dispersive soil profile. The soil is hard and impermeable and water flows through cracks, and subsurface piping is visible.

3.4.2 Stratigraphy

The gullies have exposed the underlying stratigraphy which consists of palaeosols interlayered with sediments (see Figure 5.3a). The buried soil and sediment layers were identified based primarily on colour-banding and supported by other pedogenic features such as cutans, fossil root traces, calcareous nodules, rhizocretions or slickensided ped surfaces (based on

Retallack, 2001). The stratigraphy exposed in the side-walls of the gullies reveals a number of sedimentary layers including some well-developed organic-rich palaeosols. These soils are easily recognised around the deposit and have been used as a stratigraphic marker in the interpretation of the deposit. As it is not easy to distinguish in the field if the sediment is a product of pedogenesis or diagenesis (Valentine and Dalrymple, 1976), the term “soil” is used in this research in the broad definition as described by Valentine and Dalrymple (1976, 210) to refer to “a natural body having formed in the surface materials of the earth under the influence of climate, biota, topography and time. It will have vertically differentiated layers due to the relative intensities of the biological, chemical and physical weathering and the translocation of products”.

Six distinct stratigraphic layers were identified along the slope and are referred to mostly by their colour. Overlying the Karoo Basement are two alternating brown (10R 7/4) sediments (B) and dark, organic-rich (BT) palaeosols (10R 4/3). As there are two of each unit, they are distinguished by the subscript 1 and 2 – with 1 being the older unit. The sequence is then followed by a red brown (10R 5/4) sediment horizon (RB) and a top sediment (5YR 4/6) horizon (TS) (see Figure 5.3a). For the purpose of description the black turf refers only to the colour and the organic content of the layer, rather than implying a specific palaeosol.

3.4.3 Bone Bed

Towards the distal reaches of the deposit (see the marker in Figure 3.9) at Area 1 is a dense and well-preserved fossil bone bed. The fossils are situated between horizons B_1 and B_2. The BT_1 horizon is not clearly visible at this point so it may have been eroded away or it is possible that the presence of the fossils obscures the BT_1 horizon. The bone bed extends over approximately 400 m^2 and is situated between 1 and 1.5 m below the modern land surface (Figure 3.13). The fossils appear to be in a hollow (possibly a water hole) that had formed at the foot slope of the deposit and have been undisturbed since burial as numerous articulated skeletons were excavated. No other fossils were found at Area 1 and no fossils were found at Area 2.

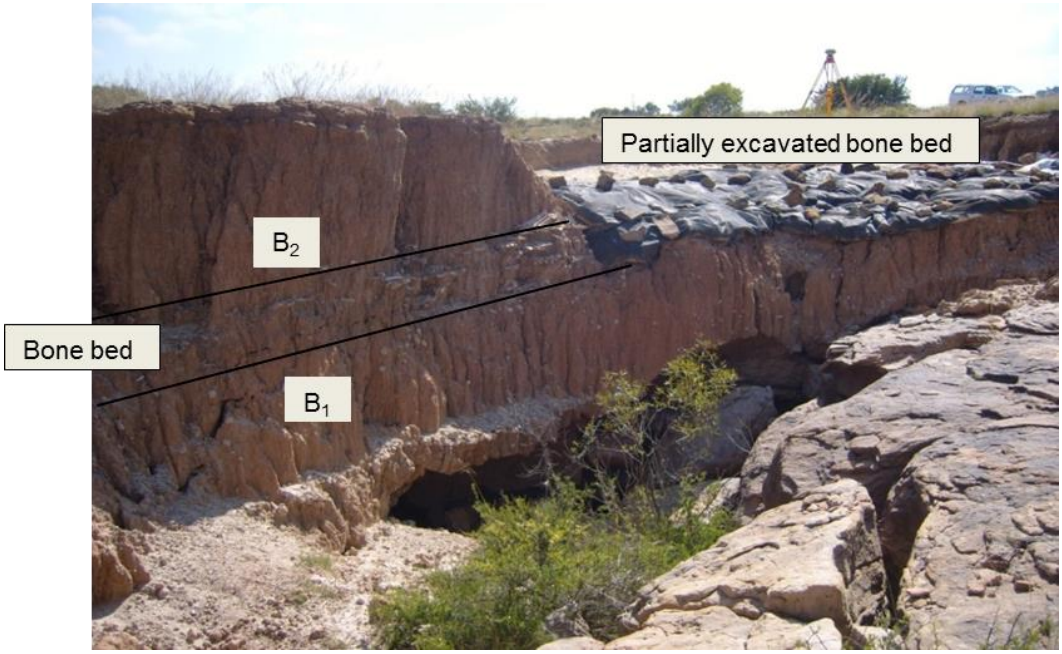


Figure 3.13 The well-preserved fossil bone bed located towards the distal reaches of the hillslope (see location in Figure 3.9).

3.4.4. Calcrete Nodules

A number of calcrete concretions have developed *in situ* in the lower layers (B_1) of the sedimentary deposit (Figure 3.14) at Area 1. The nodules range in size from a few millimetres to about 5 cm in diameter. No calcrete concretions have formed in the subsequent layers but there are detrital clasts found along the base of some layers in the package. The detrital material suggests that the clasts have been liberated during episodes of erosion and reworked within the deposit. The calcrete nodules appear to pre-date the bone layer. A few scattered and small calcrete nodules were found in B_1 at Area 2.

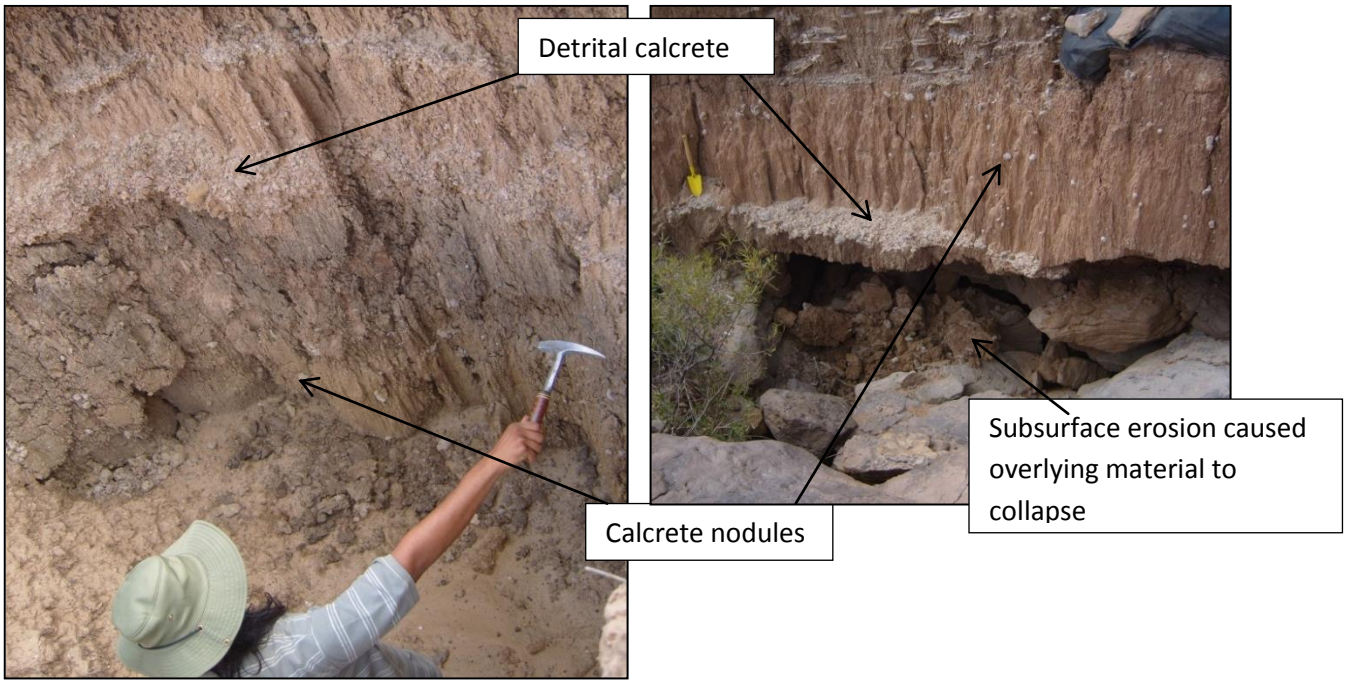


Figure 3.14 Calcrete occurs as *in situ* concretions and as detrital layers. Also visible in the main photograph is the collapse of overlying material as a result of subsurface erosion.

CHAPTER 4: METHODS AND MATERIALS

4.1 INTRODUCTION

The Heelbo hillslope mantle is a small-scale deposit which covers an area less than 1 km^2 and the deposit and the surrounding areas have not been previously described in the literature. To reconstruct the environmental history of the hillslope deposit it is important to fully understand the structure, morphology and stratigraphy of the deposit as well as to analyse the grain size and chemical properties of the different horizons and to provide high resolution ages for the deposit. Samples were collected for grain size analysis, to determine the sodium adsorption ratio (SAR_s), electrical conductivity (EC) and pH, for x-ray fluorescence (XRF) and x-ray diffraction (XRD) to determine major elemental concentrations and for luminescence (OSL) and radiocarbon (^{14}C) dating. As the abbreviation for sodium adsorption ratio is the same use to denote the single aliquot regenerative protocol, the subscript 's' is added to the sodium adsorption ratio (SAR_s) for clarity. Samples were also collected for thin-sections.

The research site was divided into two areas (Figure 3.2), separated by a high-lying basement rock watershed. Although both areas had been gullied extensively, the sedimentary deposit was better preserved in Area 1 than Area 2. Consequently, the bulk of the sampling and measurements were concentrated on Area 1.

4.2 MAPPING AND FIELD DESCRIPTIONS

The research site was fully described in terms of the sedimentary characteristics. The dimensions of the deposit were determined from the topographic maps, aerial photographs and Google Earth images. These images were also used to assess if the gullies have changed in recent time. The stratigraphic horizons were described in terms of their colour, using the Munsell colour chart. The location of sample sites was measured using a differential GPS but when it rained, or the sample location was beneath a tree, the handheld GPS was used. The cross-section topographic profiles of the proximal, medial and distal sections of the hillslope deposit were mapped in a roughly east – west orientation (Figure 4.1). However, as large tracts of the deposit were eroded to bedrock level the traverses were staggered in places to include the isolated stacks in the gullies. The cross-section profiles were drawn to show the changes in the gully morphology from upslope to down slope. These changes may reflect the maturity of the gully system. The influence of the basement highs and undulating ridges were taken into account in measuring and mapping the deposit.

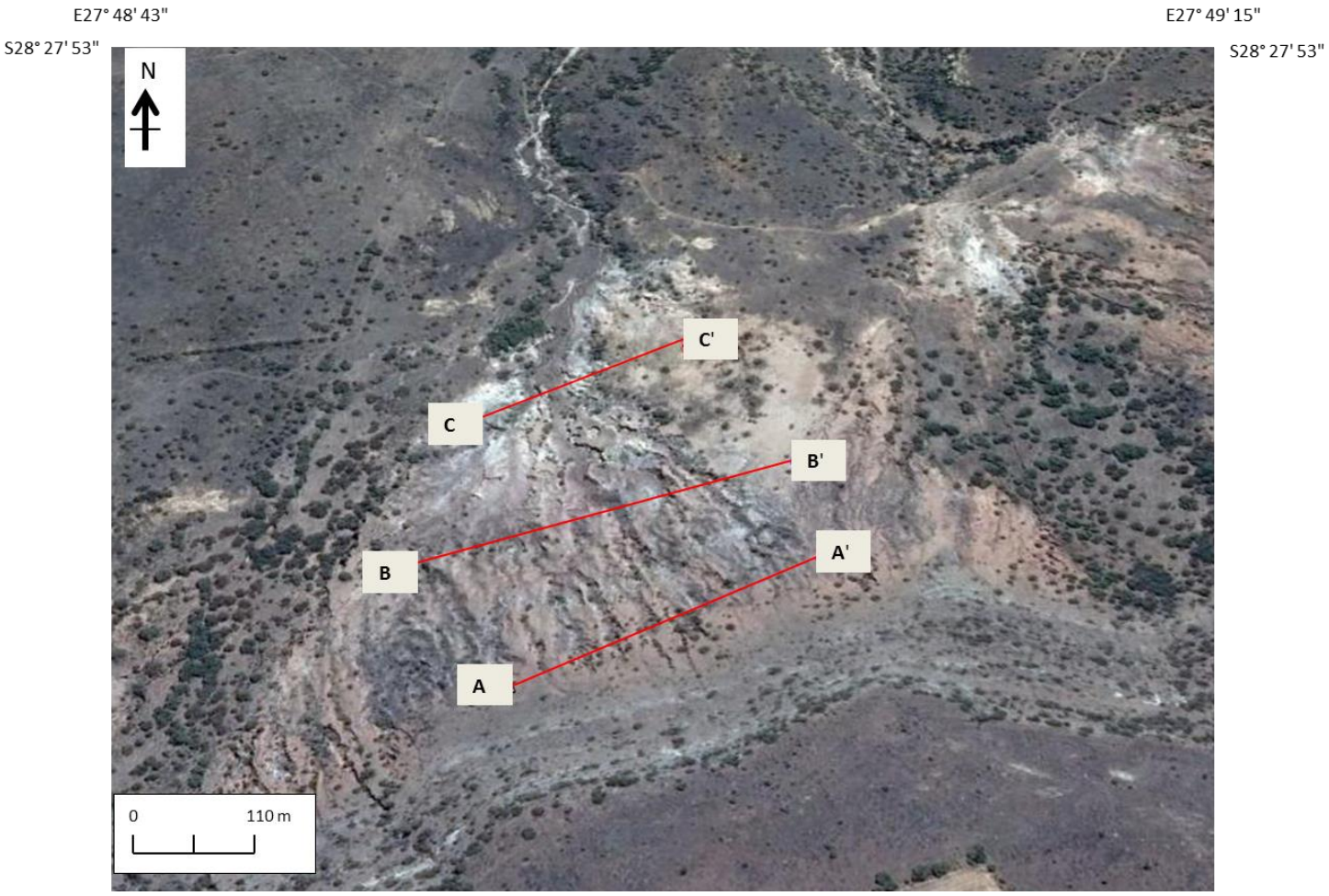


Figure 4.1 Google Earth image (2013) showing the position of the cross-sectional traverses that were mapped from the proximal (A-A'), medial (B-B') and distal (C-C') sections of the hillslope deposit.

4.3 GRAIN SIZE ANALYSIS

Grain size is considered a fundamental property of sediment particles which provides information on sediment provenance, transport history and depositional conditions (Blott and Pye, 2001). One of the focus points of this research is to characterise the landform of the hillslope deposit in terms of its morphology and structure. A distinguishing feature of hillslope

deposits such as alluvial fans is the downslope fining of sediment. The grain size distribution was compared between up and down slope, and between surface and subsurface samples; and these grain size characteristics were used to describe this landform. Samples were collected at Area 1 where the network of gullies and the undulating topography made it difficult to sample a continuous profile down the slope. Therefore, the most-continuous slope was selected for sampling using aerial photographs and Google Earth images (Figure 4.2a, b).

Samples were also collected to determine the grain size characteristics of the vertical profiles at Areas 1 and 2 where the fully stratigraphy was visible and at the bone bed section. The samples were taken at HB-15 of the bone bed horizons and at HB-18 for the stratigraphy of Area 1 (Figure 4.2a). At Area 2 samples were taken of the stratigraphic horizons from HB-19 and HB-20 (Figure 4.2b).

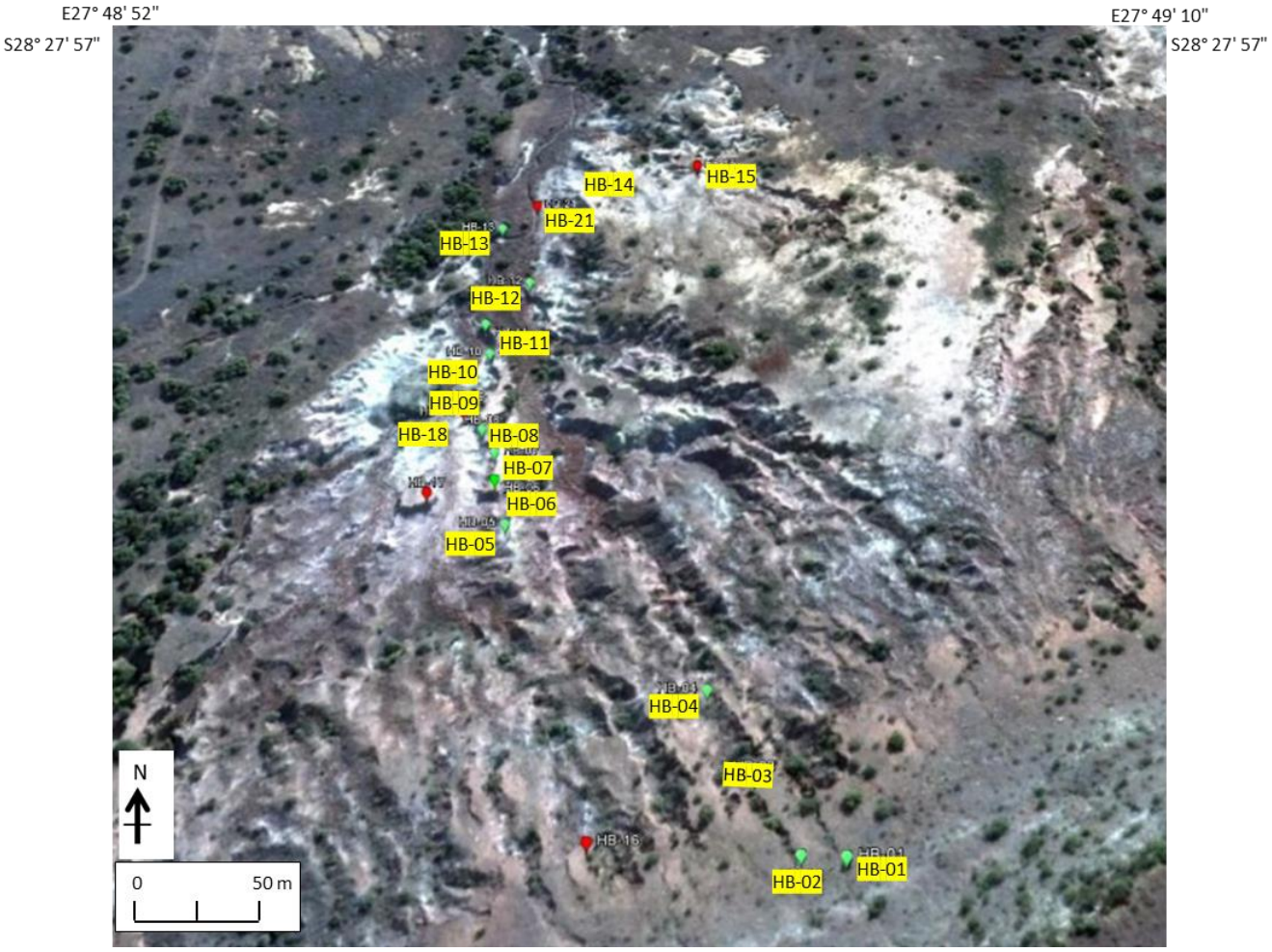


Figure 4.2(a) Google Earth (2013) image showing sample locations for grain size analysis at Area 1 and the bone bed. The green markers indicate the position of the TS and RB samples down slope and the red markers at HB-15 and HB-18 indicate additional samples taken for vertical profile analysis.

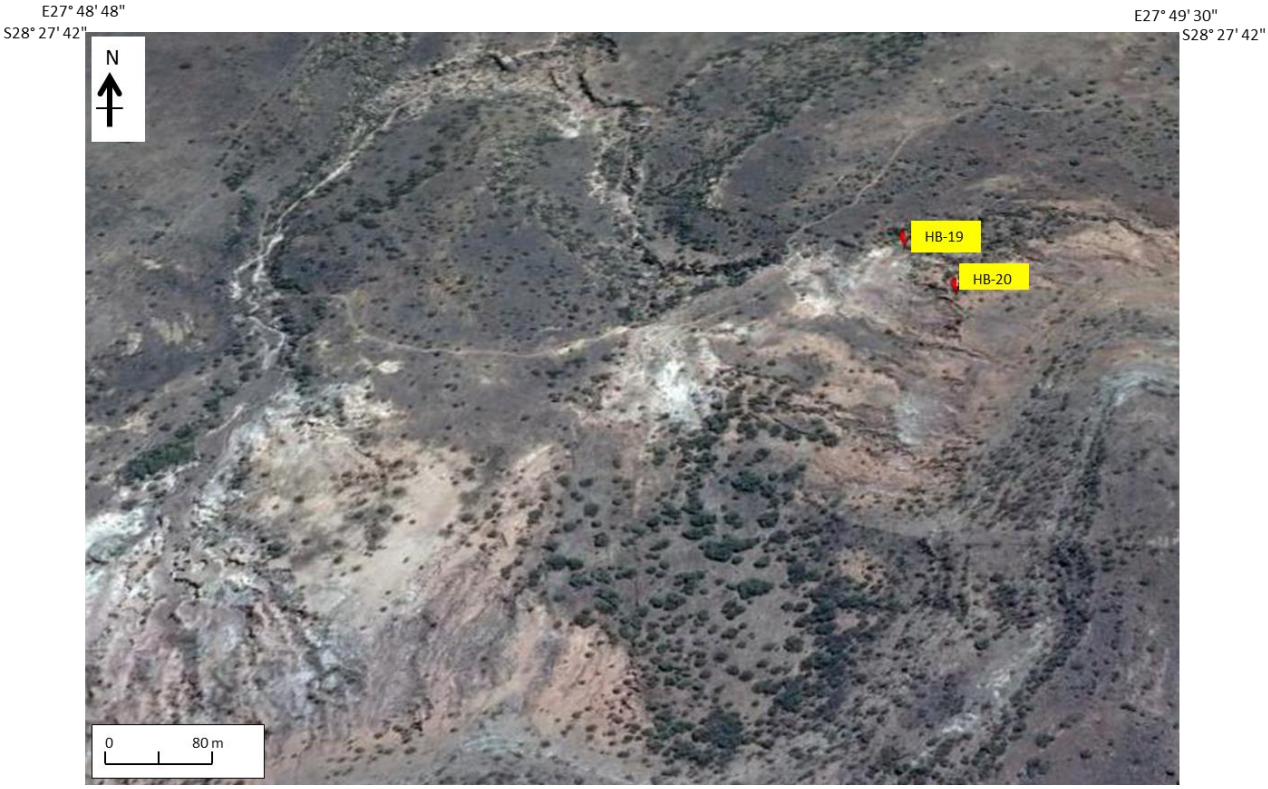


Figure 4.2 (b) Sample locations for grain size analysis at Area 2.

Two horizons were sampled for grain size analysis: the first profile selected was the Top Sediment horizon (TS), which represents the last depositional horizon and the present soil surface utilized by the dominant grasses of the area. The second profile sampled was the Red-Brown (RB) sediment which underlies the top sediment horizon and represents an older hillslope deposit (Figure 4.3).

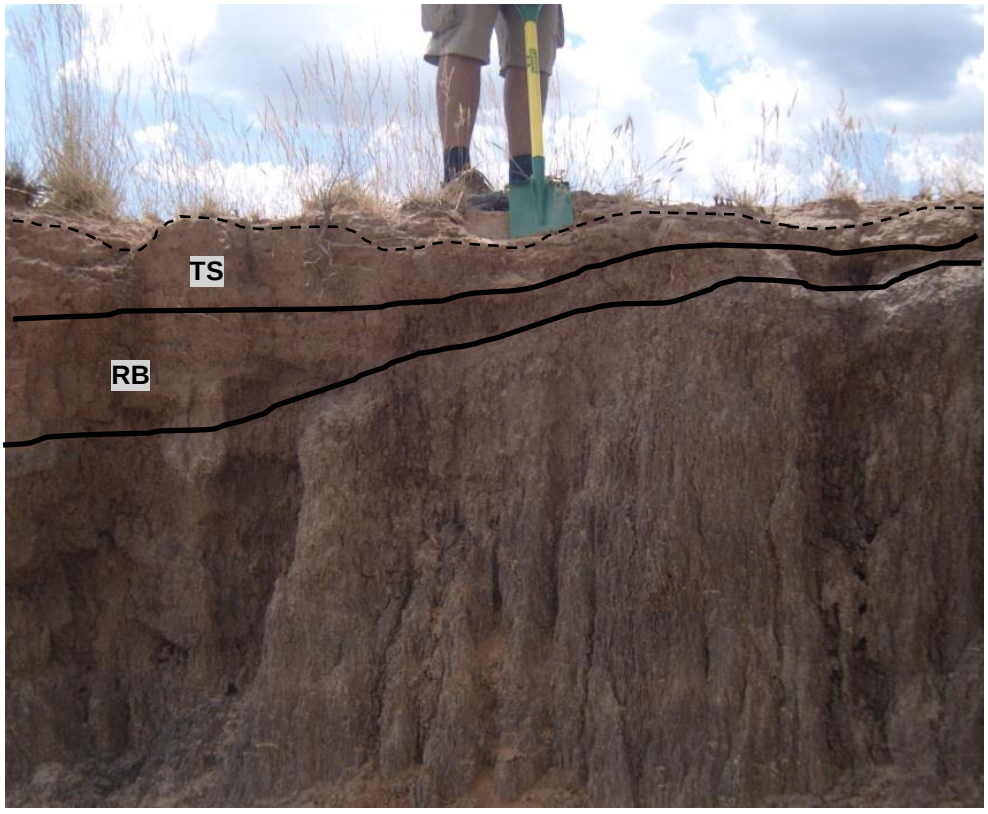


Figure 4.3 Top Sediment (TS) and Red Brown (RB) horizons sampled for grain size analysis at HB-09. See Figure 4.2 (a) for location of site.

A total of 43 samples were collected for grain size analysis. The samples collected down slope where taken approximately 20 m apart, starting at the head and ending at the foot slope of the deposit. The vertical samples were taken from the mid-point of each horizon. Approximately 500 g of sediment were collected at each site, and all samples were bagged and labelled for processing in the Sedimentology Laboratory at the University of the Witwatersrand.

All the techniques available for the determination of grain size distribution involve dividing the sample into size fractions and constructing the

distribution based on the weight percentage of sediment in each fraction (Blott and Pye, 2001). A measured sample of 200 g was used for the analysis. Thirty six of the samples consisted of unconsolidated, loose-grained material and these were air dried for a week before dry-sieving. The rest of the samples were clay-rich and clumping, and these were placed in a solution of sodium hexametaphosphate to deflocculate the clays. These samples were then wet-sieved. Dried samples were sieved using a sieve shaker for 45 minutes in multiple screens of 0.5 Φ intervals ranging from 0 Φ (1000 μm) to >4.0 Φ (32 μm) (Figure 4.4), and the sediment from each grain size fraction was weighed. The clay-rich samples required wet sieving which involved washing the samples through the same sequence of sieve screens. Each size fraction was dried and then weighed. The logistics of the wet sieving meant that the very fine fraction could not be reclaimed but was estimated based on the total amount of material used. Blott and Pye (2001) recommend that if the remaining fraction in the pan is <1% of the sample that it be excluded from the calculation. The TS samples at HB-01, HB-11, HB-13 and HB-14 were contaminated during the sieving process and were therefore discarded from the analyses.

The sieved size fractions were used to plot histograms and cumulative frequency distribution (CFD) curves using Sigma Plot for all samples. Statistical values were calculated to determine the grain size distribution of the sediments. These calculations included the mean, mode, median,

standard deviation, skewness and kurtosis and are based on the Folk and Ward (1957) method. The calculations were completed using GRADISTAT, an Excel-based program used to compute grain size statistics (Blott, 2010). The *mean* value represents the average of all grain sizes present, the *mode* is the most frequently occurring particle size, the *median* is the midpoint of the grain distribution by weight, *standard deviation* determines the spread or sorting of the grain sizes about the average, *skewness* describes the symmetry or preferential spread to one side of the average value and *kurtosis* is the degree of concentration of the grains relative to the average value (Folk, 1980; Blott and Pye, 2001). All the above statistical parameters were calculated by GRADISTAT using the method of moment, which gives a more rigorous treatment of the sediment characteristics (see Table 4.1 for equations and descriptions of statistical parameters). For a detail description of the GRADISTAT program and the equations used see Blott and Pye (2001).

The Folk and Ward statistics determined by GRADISTAT are reported logarithmically, as a log-normal distribution of ϕ sizes and geometrically, as a log-normal distribution of metric sizes. Each sample is then given a descriptive term based on a modified Udden-Wentworth grade scale. Blott and Pye (2001) recommend reporting results from the Folk and Ward graphical method as this method more accurately describes the general characteristics of the bulk sample. Therefore all statistical values quoted

in this thesis are calculated using the Folk and Ward approach and are reported in µm sizes.

Table 4.1 Calculations used to determine statistical parameters and scales for sorting, skewness and kurtosis as calculated by GRADISTAT using Folk and Ward (1957) graphical measures (from Blott and Pye, 2001).

(d) Logarithmic (Original) Folk and Ward (1957) Graphical Measures

Mean	Standard Deviation	Skewness	Kurtosis
$M_Z = \frac{\phi_{16} + \phi_{50} + \phi_{84}}{3}$	$\sigma_I = \frac{\phi_{84} - \phi_{16}}{4} + \frac{\phi_{95} - \phi_5}{6.6}$	$Sk_I = \frac{\phi_{16} + \phi_{84} - 2\phi_{50}}{2(\phi_{84} - \phi_{16})} + \frac{\phi_5 + \phi_{95} - 2\phi_{50}}{2(\phi_{95} - \phi_5)}$	$K_G = \frac{\phi_{95} - \phi_5}{2.44(\phi_{75} - \phi_{25})}$

Sorting (σ_I)		Skewness (Sk_I)		Kurtosis (K_G)	
Very well sorted	< 0.35	Very fine skewed	$^{+}0.3$ to $^{+}1.0$	Very platykurtic	< 0.67
Well sorted	0.35 – 0.50	Fine skewed	$^{+}0.1$ to $^{+}0.3$	Platykurtic	0.67 – 0.90
Moderately well sorted	0.50 – 0.70	Symmetrical	$^{+}0.1$ to $^{-}0.1$	Mesokurtic	0.90 – 1.11
Moderately sorted	0.70 – 1.00	Coarse skewed	$^{-}0.1$ to $^{-}0.3$	Leptokurtic	1.11 – 1.50
Poorly sorted	1.00 – 2.00	Very coarse skewed	$^{-}0.3$ to $^{-}1.0$	Very leptokurtic	1.50 – 3.00
Very poorly sorted	2.00 – 4.00			Extremely leptokurtic	> 3.00
Extremely poorly sorted	> 4.00				

(e) Geometric Folk and Ward (1957) Graphical Measures

Mean	Standard Deviation
$M_G = \exp\frac{\ln P_{16} + \ln P_{50} + \ln P_{84}}{3}$	$\sigma_G = \exp\left(\frac{\ln P_{16} - \ln P_{84}}{4} + \frac{\ln P_5 - \ln P_{95}}{6.6}\right)$

Skewness	Kurtosis
$Sk_G = \frac{\ln P_{16} + \ln P_{84} - 2(\ln P_{50})}{2(\ln P_{84} - \ln P_{16})} + \frac{\ln P_5 + \ln P_{95} - 2(\ln P_{50})}{2(\ln P_{95} - \ln P_5)}$	$K_G = \frac{\ln P_5 - \ln P_{95}}{2.44(\ln P_{25} - \ln P_{75})}$

Sorting (σ_G)		Skewness (Sk_G)		Kurtosis (K_G)	
Very well sorted	< 1.27	Very fine skewed	$^{-}0.3$ to $^{-}1.0$	Very platykurtic	< 0.67
Well sorted	1.27 – 1.41	Fine skewed	$^{-}0.1$ to $^{-}0.3$	Platykurtic	0.67 – 0.90
Moderately well sorted	1.41 – 1.62	Symmetrical	$^{-}0.1$ to $^{+}0.1$	Mesokurtic	0.90 – 1.11
Moderately sorted	1.62 – 2.00	Coarse skewed	$^{+}0.1$ to $^{+}0.3$	Leptokurtic	1.11 – 1.50
Poorly sorted	2.00 – 4.00	Very coarse skewed	$^{+}0.3$ to $^{+}1.0$	Very leptokurtic	1.50 – 3.00
Very poorly sorted	4.00 – 16.00			Extremely leptokurtic	> 3.00
Extremely poorly sorted	> 16.00				

Along with the Udden-Wentworth grade scale to describe the clast sizes, the samples were also analysed for colour (using the Munsell Colour Chart), sorting and roundness (Powers, 1957) (Figure 4.4).

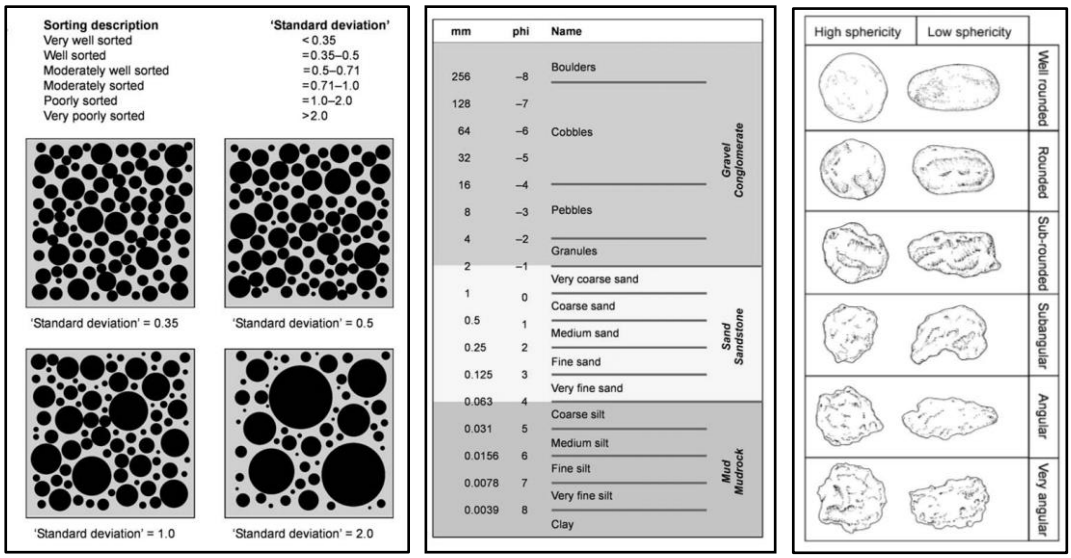


Figure 4.4 The Udden-Wentworth grain-size scale where the clast diameter in mm is used to define the different sizes on the scale, and the phi (Φ) values are $-\log_2$ of the grain diameter; the graphic illustration of sorting in clastic sediments; and the roundness and sphericity estimate comparison chart (in Nichols, 2009, 7, 24).

4.4 SOIL AND SEDIMENT ANALYSIS

The causes of gully formation and development are an integral part of this research and analysis of the geochemistry of the soil is central to establishing the possible causes of the gullies. Samples were collected from the RB horizon at the same sites as for the grain size analysis in Area 1 (see Figure 4.2a). The RB layer was selected for sampling as it was present and easily identifiable at all the sample points down the slope. Samples were also taken from a vertical section in the distal reaches of

the deposit (Figure 4.5) to determine the vertical changes in the deposit. The vertical section was sampled at the base of the slope just below HB-14 (Figure 4.2 a).

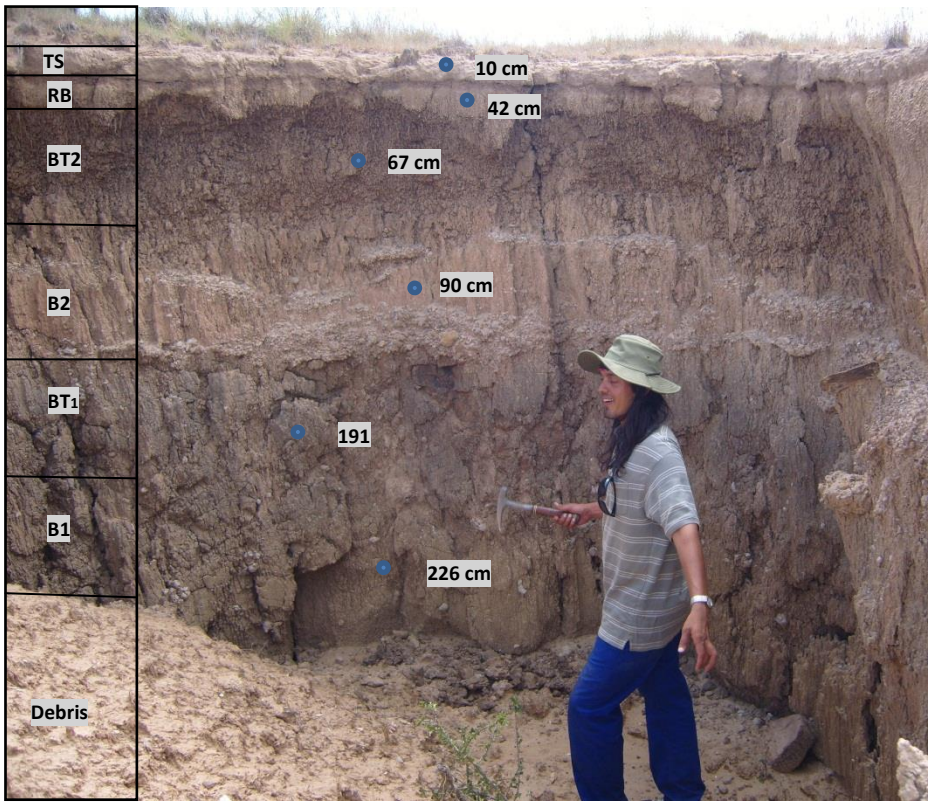


Figure 4.5 Vertical section sampled to determine vertical changes in the soil characteristics at the base of the slope. The stratigraphy of the section and the sample depths are shown.

4.4.1 Soil Dispersion Test

A simple dispersion test as described by Davies and Lacey (2009) was carried out on two samples taken from the proximal, medial and distal sections of the slope. Samples were taken of RB in the proximal (A, B), medial (C,D) and distal (E,F) sections of the hillslope at Area 1; and samples were taken from TS, RB, BT_2, B_2, BT_1, B_1 at Area 1 (G,H,K,L,M,N) and Area 2 (P,R,S,T,U,W) respectively. The samples were

placed in petri dishes (see Figure 5.25) and distilled water was added to each one without being mixed or agitated. Some of the aggregates crumbled after been placed in the water but Davies and Lacey (2009) cautioned that this should not always be mistaken for dispersion. The water around the edges of the soil aggregate was checked for cloudiness and milkiness which would indicate the presence of dispersed clay (Figure 4.6). The samples were checked at intervals of 0, 2, 5, 10, 20, 30 minutes and the results noted as per Figure 4.6. The soil was classified as sodic or non-sodic based on the soil dispersion test as shown in Table 4.2.

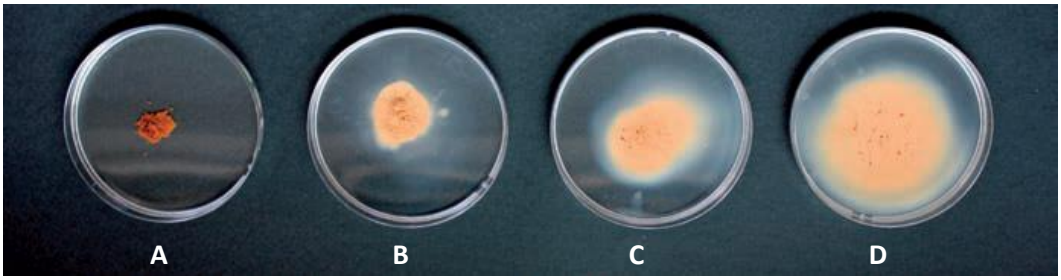


Figure 4.6 Degree of soil dispersion of a sample placed in distilled water A – sample crumbles when placed in water; B - water around edges of sample becomes milky and cloudy; C – dispersive soil after 10-30 minutes in water; D – dispersive soil after 2 hours in water (after Davies and Lacey, 2007).

Table 4.2 Soil classification based on soil dispersion test (after Davies and Lacey, 2009).

Rating	Soil Dispersion Test
Non-sodic	No dispersion evident after 24 hours. Aggregates slaked but not dispersed.
Slightly sodic	Dispersion (milky halo) evident after 24 hours. Soil aggregates slightly dispersed.
Moderately sodic	Dispersion evident after several hours. Soil aggregates partially dispersed.
Highly sodic	Dispersion evident in less than 30 minutes. Soil aggregates completely dispersed.

4.4.2 SAR_s, pH and EC Analysis

Approximately 200 grams of each sample was crushed to a fine powder in a swing mill for about 45 seconds. The crushing bowl was cleaned by crushing quartz chips for a minute in the bowl after every sample to avoid the cross-contamination of all the samples. The crushed samples were sent to the Agricultural Research Council's (ARC) laboratory for analysis where saturation extracts (a saturated paste of soil and water from which the solution is extracted) were prepared. From these extracts the calcium (Ca), magnesium (Mg) and the sodium (Na) concentrations, the sodium adsorption ratio (SAR_s), pH and electrical conductivity (EC) were measured.

The salinity or sodicity of a soil can determine its behaviour as dispersive, crusting or prone to swelling. Saline soils have a high concentration of dissolved salts in their soil water which can include NaCl, Ca^{2+}, Mg^{2+} and other compounds. The salinity of the water is referred to in terms of the total dissolved solids (TDS) but is usually approximated by measuring the EC (in dS/m) of water. The total dissolved solids (TDS) can be calculated as:

TDS (mg/l) = EC x 640 (Western Fertilizer Handbook, 1995).

Sodic soils have a high concentration of sodium (Na+) relative to the amount of calcium (Ca^{2+}) and magnesium (Mg^{2+}) in its soil water (Western Fertilizer Handbook, 1995; Davies *et al.,* 2007). The sodicity is expressed in terms of its sodium adsorption ratio (SAR_s) which was determined according to Rengasamy and Churchman (1999) as:

$$SAR_s \text{ (mmol/) l} = \frac{Na}{(Ca+Mg)^{\frac{1}{2}}}$$

4.5 X-RAY DIFFRACTION (XRD)

Thirty samples were taken for XRD at the sample sites (Table 4.3 and Figure 4.2 for the location), and were taken from the middle of each layer wherever possible. However if the middle was inaccessible the distance from the layer contact to the sample was recorded.

Table 4.3 The sample numbers, their location and altitude above sea level which were collected for XRD analysis.

Sample Number	Latitude	Longitude	Altitude (m.a.s.l)
HB-01	S28°28' 16.27"	E27° 49' 04.33"	1726
HB-02	S28°28' 15.82"	E27° 49' 30.70"	1720
HB-04	S28° 28' 12.86"	E27° 49' 02.52"	1690
HB-05	S28° 28' 09.55"	E27° 48' 59.40"	1678
HB-06	S28° 28' 08.69"	E27° 48' 59.23"	1676
HB-08	S28° 28' 07.67"	E27°48' 59.01"	1673
HB-09	S28° 28' 07.17"	E27° 48' 58.75"	1672
HB-10	S28° 28' 06.10"	E27° 48' 59.13"	1669
HB-12	S28° 28' 04.63"	E27° 48' 59.86"	1665
HB-13	S28° 28' 01.35"	E27° 48' 59.75"	1663

Clay mineral samples were prepared for XRD analysis according to the method described by Moore and Reynolds (1997). The samples were disaggregated by dispersion in water to increase the surface area of the grains. Approximately 100 g of the sample material was placed in a beaker and water was added to make up 500 ml. Sodium hexametaphosphate $(NaPO_3)_5$ was added to the mixture to deflocculate the clay minerals and the mixture was left to stand for 5 minutes where the standing time was determined by Table 4.6 (which plots the particle diameter against the temperature of the water). It was decided that the 5 minutes standing was preferable as a longer waiting time produced grain mounts with insufficient clay material for XRD analysis, even though the standing time at 25°C should have been between 6 minutes 48 seconds for 16 µm and 27 minutes 14 seconds for 8 µm (Table 4.4), The separation of the clay size fraction (all particles <2 µm) was achieved by removing the top 5 cm of liquid from the flask as soon as dispersion was achieved so as to prevent the dispersed clay minerals from flocculating

Table 4.4 Table showing the standing time for the grain size separation (modified after Day, 1965)

Diameter of Particle (mm)	< .625	< .031	**< .016**	**< .008**	< .004	< .002	< .0005
Depth of Withdrawal (cm)	10	10	10	10	5	5	3
Time of Withdrawal	seconds	min'/sec"	min'/sec"	min'/sec"	min'/sec"	hour:/min'	hour:/min'
Temperature (°C)							
25	25	1'42"	**6'48"**	**27'14"**	54'25"	3:38'	
26	25	1'40"	6'39"	26'38"	53'12"	3:33'	
27	24	1'38"	6'31"	26'02"	52'02"	3:28'	
28	24	1'35"	6'22"	25'28"	50'52"	3:24'	31:00'
29	23	1'33"	6'13"	24'53"	49'42"	3:10'	
30	23	1'31"	6'06"	24'22"	48'42"	3:05'	

Moore and Reynolds (1997) describe several ways to prepare an oriented clay mineral aggregate. The Millipore® Filter Transfer Method was selected because the clay surface is a true representation of the particle size composition of the sample without displaying particle-size segregation despite producing only a fair crystallite orientation. This method uses a vacuum filter apparatus with a funnel reservoir and a side-necked vacuum flask.

The filter was inserted, followed by the application of the vacuum, and then the addition of the suspension to the funnel. The suspension liquid in the funnel was stirred to prevent any particle-size segregation by overcoming the settling velocity of the grains, and to keep the suspension homogeneous. Stirring allows for an indefinite suction time, making it easier to achieve a thick enough layer of clay minerals on the filter. Once the clay mineral layer accumulated on the filter, the vacuum was removed and the flask returned to room pressure. Water was kept in the funnel when the vacuum was removed to ensure that no air was drawn into the filter paper. Air would prevent the proper adhesion of the clay minerals to the glass slide, thereby producing a slide with the texture of the filter paper, instead of a smooth surface. Once the filter was removed, a glass slide was placed on top of it, and allowed to dry in an oven at 50°C. The slide was then peeled off the filter, and sent to the laboratory for XRD analysis.

A second set of samples was prepared under ethylene-glycol-solvated conditions to ensure the correct identification of the clay minerals, and to identify mixed-layer smectites (Moore and Reynolds, 1997). Smectite is also called swelling clays owing to its unique ability to absorb water molecules into the interlayer space. It is this swelling ability that makes smectite minerals so useful in XRD analyses. Ethylene-glycol can occupy the interlayer space in place of water, thereby expanding the interlayer spacing by a known amount (usually to ~16.9Å), which allows for more accurate mineral identifications (Velde, 1992; Moore and Reynolds, 1997; Nesse, 2000).

Seven samples were selected as representative samples of the layers for both the distal and proximal environments. The proximal set comprised BT_2, B_1 and B_2 at site HB-06, whilst the distal set comprised BT_1 and BT_2 at site HB-09, and BT_1 and B_2 at sites HB-10 and HB-13, respectively. For these samples, the glass slide was prepared according to the Millipore® Filter Transfer Method. However, instead of air drying, the samples were allowed to dry overnight in a desiccator with ethylene-glycol. The samples were sent to the laboratory for analysis immediately, as the ethylene-glycol evaporates which affects the expansion of the clay minerals, and these samples were analysed within one hour of being mounted on glass slides (as suggested by Moore and Reynolds (1997)).

The XRD samples were run on a Bruker D2 Phaser at the School of Chemistry, University of the Witwatersrand. The data are returned as XRD patterns, which were analysed, using the Eva software programme. Air-dried mounts were scanned from 5° to 90°, and ethylene-glycol solvated samples from 5° to 55°. Minerals were assigned to the samples based on the fit of their peaks to the peaks of the data pattern. The analysed XRD patterns for the air-dried samples are included in APPENDIX B, together with the corresponding ethylene-glycol XRD patterns.

4.6 X-RAY FLUORESCENCE (XRF)

XRF is a widely used method for the determination of major and trace elemental compositions for a given sample (Rollinson, 1993). Four samples of the basement bedrock rock and eighteen samples of the deposit were collected for XRF analysis. The sample sites are shown in Figure 4.7, and the site descriptions are in Table 4.5. The XRF samples HLB4 and HLB5 were collected to determine the extent of leaching that may occur in the thickest layer sampled within the Heelbo deposit. Leaching is determined by comparing the accumulation of CaO between the layers, as CaO is sparingly soluble in water, and is likely to percolate to, and accumulate in, the lower horizons, if leaching is commonplace. HLB4 and HLB5 were sampled at approximately 30 cm and 102 cm from

the surface, respectively. The XRF analyses of major elements were processed at the Earth Laboratory at the University of the Witwatersrand.

Table 4.5 Site descriptions where samples were collected for XRF analysis

Sample Number	Site Description		Sample Number	Site Description
HLB21	Bedrock Area 1 (red)		HLB8	BT_1 (Area 1)
HLB22	Bedrock Area 1 (yellow)		HLB9	B_2 (Area 1)
HLB23	Bedrock Area 2 (red)		HLB10	BT_2 (Area 1)
HLB24	Bedrock Area 1 (yellow)		HLB11	RB (Area 1)
HLB1	RB in bone bed		HLB19	TS (Area 1)
HLB2	B_2 in bone bed		HLB16	B_1 (Area 2)
HLB3	B_1 in bone bed		HLB12	BT_1 (Area 2)
HLB4	RB start of deposit (30cm)		HLB13	B_2 (Area 2)
HLB5	RB start of deposit (102 cm)		HLB14	BT_2 (Area 2)
HLB6	B_1 isolated stack (Area 1)		HLB15	RB (Area 2)
HLB7	B_1 (Area 1)		HLB20	TS (Area 2)

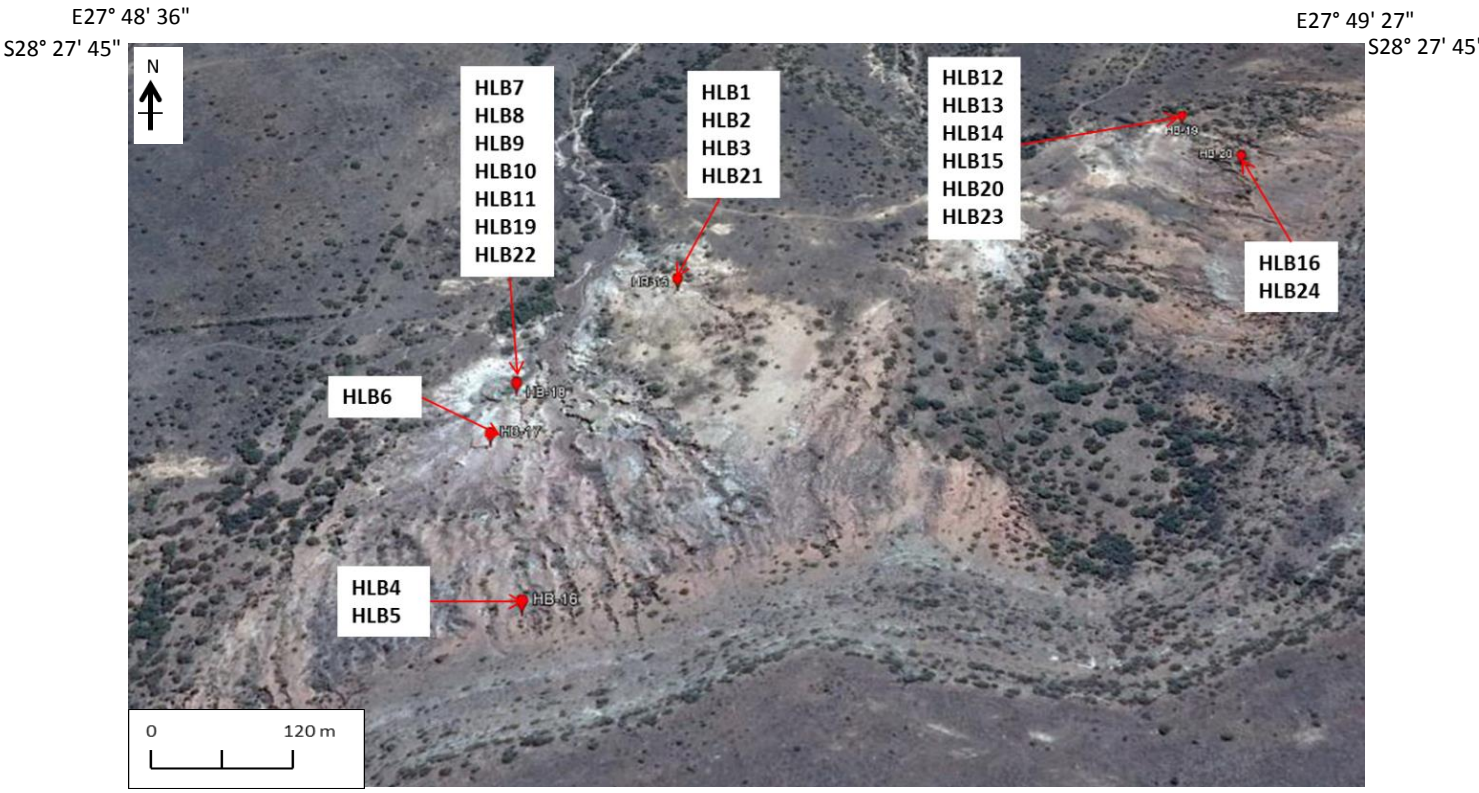


Figure 4.7 Site location for samples collected for XRF analysis.

All major elements were analysed on an infinitely-thick, fused disk. Samples were ignited at 1000 °C for 40 minutes and the loss on ignition (LOI) was calculated. The individual ignited samples were mixed with a commercially available pre-ignited flux (of composition $Li_2B_4O_7$ = 47%, Li_2CO_3 = 36.7%, La_2O_3 =16%) with a ratio of 1:5 and fired for 40 minutes at 1000 °C. This was then poured and pressed by a mechanical press into an infinitely-thick, fused disk.

All data collection was performed on a PANalytical PW2404 WD XRF, with a Rh tube set at 50kV and 50mA. The analysis time was 40 seconds per element, and 20 seconds per background. Background was measured for

Si, Al, Mg, Na and P. The elemental concentrations are obtained by comparison to 13 known standards. The standards used are: W2, GSP1, BHVO2, AGV2, G2, DTS1, PCC1, BCR2, NIM N, NIM P, NIM S, NIM D and NIM G. A synthetic internal standard was run after every 5 analyses to monitor, and compensate for, instrument drift. Table 4.6 summarises the specific element data.

Table 4.6 Major element calibration instrument parameters

Element	Analysis Line	Crystal	Collimator	Detector
Ti	Ka	LiF200	150 µm	Flow
Ca	Ka	LiF200	150 µm	Flow
K	Ka	PE 002-C	550 µm	Flow
Si	Ka	PE 002-C	550 µm	Flow
Al	Ka	PE 002-C	550 µm	Flow
Mg	Ka	PX1	550 µm	Flow
Na	Ka	PX1	550 µm	Flow
P	Ka	Ge 111-C	550 µm	Flow
Ni	Ka	LiF 220	150 µm	Duplex
Fe	Kb	LiF 220	150 µm	Flow
Mn	Ka	LiF 220	150 µm	Duplex
Cr	Ka	LiF 220	150 µm	Duplex

All trace elements were analysed for on an infinitely-thick pressed pellet. Approximately 6 g of sample was mixed with three drops of commercially purchased Moviol (polyvinyl alcohol), and ground with a mortar and pestle to remove any clumps. The mixture was then pressed under 10 ton pressure into an Al cup, using a 40 ton press. The pressed pellet was allowed to dry for 24 hours prior to analysis.

Data were collected on a PANalytical PW2404 WD XRF with an Rh tube set at 50 kV and 50 mA. The instrument parameters for some elements

are set according to the Protrace recommendation. PANalytical software Protrace was used to process the raw data, and the standards used for the calibration were the Protrace standards, supplied by PANalytical. Protrace drift standards were run after every five analyses to compensate for instrument drift, and internal checks were performed by analysing known standards as unknowns, and comparing these to reported concentrations. The known standards used were AGV2, BHVO2, GSP2, NIM D and NIM S.

The intensity and duration of weathering in sediment can be evaluated by determining the relationship between alkali and alkaline earth elements (Nesbitt and Young, 1982, 1996). Feldspars are the most abundant of the reactive minerals; therefore the dominant process during chemical weathering is the alteration of feldspars to form clay minerals. During weathering, calcium, sodium and potassium are removed from feldspars, and the amount of the elements remaining is a quantitative index of the intensity of weathering (Nesbitt *et al.,* 1980). The calculation of the chemical index of alteration (CIA) is a measure of the degree of chemical weathering. The more weathered the material, the larger the CIA becomes. Bauxite, which is the ultimate end product of weathering, has a CIA of 100. The CIA is determined using the molecular proportions described by Nesbitt and Young (1982) and Hamer *et al*. (2007):

$$CIA = (Al_2O_3 / (Al_2O_3+CaO+Na_2O+K_2O)) \times 100$$

CaO is affected by calcite precipitation in the sediment, so CIA can be calculated without CaO as:

$$CIA = (Al_2O_3 / (Al_2O_3 + Na_2O + K_2O)) \times 100$$

Another good method of quantifying the degree of chemical weathering is by calculating the plagioclase index of alteration (PIA), which is determined using the molecular proportions:

$$PIA = ((Al_2O_3 - K_2O) / (Al_2O_3 + CaO + Na_2O - K_2O)) \times 100$$

4.7 THIN SECTION PREPARATION

Samples of the bedrock at Area 1 and Area 2, and the stratigraphic horizons at both areas, and the bone bed were collected for thin section analyses. The oriented samples were wrapped in cotton wool to prevent them from breaking apart in transit. The thin sections were prepared in the Rock Cutting Laboratory, at the University of the Witwatersrand. The samples were friable, and needed to be impregnated with resin before thin sections could be cut. The resin prevented the disturbance of the material within the sample during the cutting process, which could have rendered the thin-section unusable for palaeo-environmental reconstruction (Francus and Asikainen, 2001). It was important that the sample retained its sedimentary/pedogenic texture as these soil structures provide

important clues about the conditions during the time of soil formation. Retallack (2001) asserts that palaeosol thin sections should be cut thinner than those prepared from normal rocks, to ensure that the soil matrix can be penetrated by sufficient light, since it is characteristically more opaque than typical mineral grains.

The thin sections were cut from the samples in such a way that the cut-face was perpendicular to the palaeosol horizons, as observed in the field. They were viewed and photographed under the microscope. Lithic fragments were identified based on their matrix colour and grain images for the estimation of particle roundness (see Figure 4.4).

4.8 OPTICALLY STIMULATED LUMINESCENCE DATING

Establishing the timing of deposition of the sedimentary horizons, the cut-and-fill sequences of the gullies, and pedogenesis is essential for the palaeo-environmental reconstruction of the hillslope deposit and this can be achieved through luminescence dating.

Optically stimulated luminescence dating is a well-established dating technique. It falls within the category of radiation dosimetric dating techniques which are based on the time-dependent accumulation of radiation damage in minerals (Aitken, 1998; Murray and Wintle, 2000; Vandenberghe, 2004), which is the result of exposure to natural low-levels

of ionising radiation. The intensity of the radiation damage is a measure of the total dose or the total amount of energy absorbed from the ionising radiation by the mineral over a certain period of time. In luminescence dating the intensity of the radiation damage is detected as a small amount of light called luminescence. This latent luminescence signal can be removed or "zeroed" by exposure to heat or light. Thus for sediment dating the zeroing event or "bleaching" is the exposure to daylight during erosion, transport and deposition of the mineral grains. Once the sediments are buried again and no longer exposed to sunlight, the luminescence signal can start to build up again (Duller, 2004; 2008). The latent luminescence signal can also be released under laboratory conditions using heat (thermoluminescence) or light (optically stimulated luminescence), and this signal can be recorded. This luminescence signal is related to the dose the mineral has received since the last zeroing event (or last exposure to sunlight); and if the rate is determined at which the dose was absorbed, it is possible to determine an age for the sediment. However, this age refers to the time that has elapsed between the moment the sediment was deposited and the moment of sampling for analysis (Figure 4.8). The OSL signal acquired during the previous burial period is reset by sunlight during sediment transport prior to deposition (Figure 4.8). Quartz or feldspar minerals are commonly used for OSL dating of sediments, but, quartz is the preferred dosimeter as the physical basis of OSL production in quartz is better understood; and feldspar may be

subject to phenomena such as anomalous fading (e.g. Bøtter-Jensen *et al.*, 2003a; b).

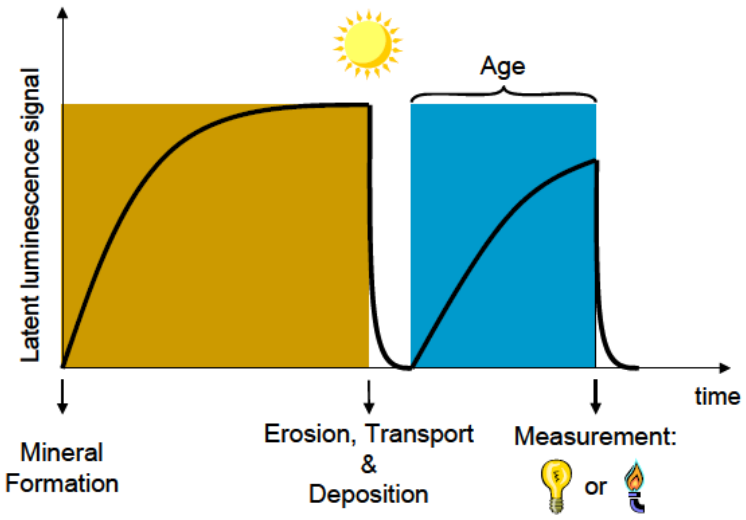
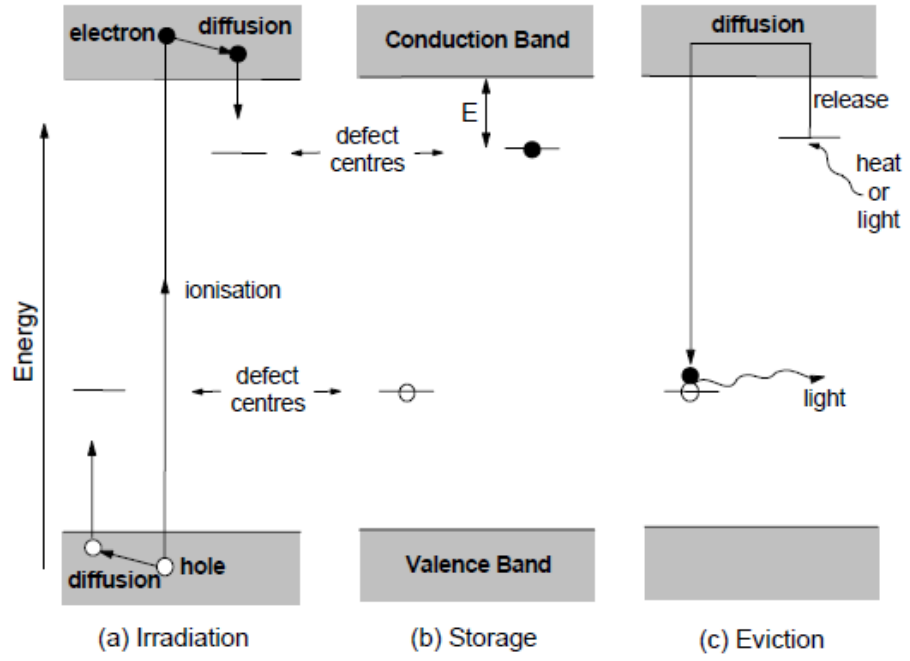


Figure 4.8 Schematic representation of the event that is being dated in the luminescence dating of sediments where minerals are continuously exposed to a low-level of natural radioactivity, through which they can acquire a latent luminescence signal. During erosion, transport and deposition, the minerals are exposed to sunlight and all the previously accumulated luminescence is removed. Once shielded from the sunlight, the signal starts to build up again, until the moment of measurement in the laboratory. The age that is being determined is consequently the time that has elapsed between these two zeroing events (Vandenberghe, 2004)

The main process causing luminescence can be described in terms of the energy level diagram for non-conducting ionic crystalline materials (Figure 4.9). Aitken (1998) indicated that electrons are associated with discrete ranges of energy called "bands"; where the lowest energy band is the valence band, and the highest energy band is the conduction band. The gap between the two is referred to as the "forbidden zone" which in an ideal crystal, no electron will occupy a position in this zone. However, in a

natural crystal, defects such as impurities or missing atoms are present and disturb the ordered crystalline structure, which give rise to the presence of energy levels in the forbidden zone. The conduction and valence bands extend throughout the crystal, but the defect states are associated with the defect itself and are referred to as localised energy levels which are significant to the luminescence phenomenon, as they carry the memory of exposure to nuclear radiation. Therefore luminescence requires the existence of lattice defects within the crystal structure (Aitken, 1998).



○ hole

● - electron

Figure 4.9 Energy level representation of the luminescence process (modified after Aitken, 1998, in Vandenberghe, 2004).

In nature, low-level radiation can raise an electron from the valence band into the conduction band, through its ionising effect (Figure 4.9 (a)). For every electron created, an electron vacancy (hole) is left behind, and both the electron and the hole are free to move through the crystal. In this way, the energy of nuclear radiation is taken up. This energy can be released again by recombination, and most charges do recombine easily. However, the electron and the hole may be trapped at defect centres. In this instance, the nuclear energy is stored temporarily in the crystal lattice, and the system is said to be in a metastable state (Figure 4.9 (b)). Energy is required to remove the electrons out of the traps, and return the system to a stable situation, where more energy is required to empty deeper traps. By exposing the crystal to heat or light, the trapped electrons may absorb enough energy to bridge the barrier to the conduction bands (Figure 4.9 (c)), where, once excited they can be trapped again, or can recombine with holes in recombination centres (Wintle *et al.*, 1993; Duller, 2004; Rodnight, 2006).

Recombination can result in either the emission of heat or light, and the defect sites, where radiative (light) recombination occurs,is called *luminescence centres,* and the resulting light is called TL (if heat is used to release the electrons from the traps), or OSL (if light is used). The amount of light emitted is proportional to the amount of electrons stored in defects, therefore the amount of energy received from irradiation. Since the energy is absorbed at a certain rate, the intensity is related to the time of

accumulation, i.e. the longer the material is exposed, the more signal is acquired (Aitken, 1998; Vandenberghe, 2004). The process of stimulation and eviction of the electrons is termed signal bleaching, with stimulation by heat or light resulting in a TL or OSL signal, respectively. If the grain is stimulated sufficiently to evict all the trapped electrons, it is described as being fully bleached. Whilst the TL glow curve contains contributions from traps of various depths, the main source of the OSL signal is thought to be the traps associated with the readily bleachable 325°C TL trap (Aitken, 1998). As OSL is generally very much more rapidly reset than TL (Godfrey-Smith *et al.*, 1988), it is more suitable for dating sediments, where the bleaching occurs by exposure to light rather than to heat.

The radiation to which a grain is exposed during burial derives from a number of different sources, and consists of alpha and beta particles, and gamma rays. Quartz grains contain very little internal radioactivity, so the majority of the radiation they receive is derived from uranium, thorium, and potassium, contained within the surrounding sediment, as well as a small level of cosmic radiation. The radiation flux at a sampling location is termed the environmental dose-rate, and can be obtained, either by field, or by laboratory measurements. The amount of radiation that a grain has received during burial can be determined by measuring the OSL signal from the natural dose (i.e. that received during burial), and the OSL signals from a series of laboratory irradiations of known dose. The laboratory measurements are used to calibrate the OSL signal derived

from the natural dose, and thus determine the laboratory dose that is equivalent to the dose received by the grains in nature. This is termed the equivalent dose (D_e), with the unit of measurement in Grays (Gy) (Wintle *et al.*, 1993). Since the OSL signal is bleached on exposure to light during sediment transport, the D_e normally represents the amount of radiation received following deposition and burial after the last transport event. By deriving the burial dose (D_e) of a sample, and the environmental dose-rate at the sampling location, the age of a sample can be calculated using the equation:

$$Age(yr) = \frac{EquivalentDose(Gy)}{DoseRate(Gy/ka)}$$

Equivalent dose (in Grays) is the laboratory radiation dose that produces the signal, equivalent to the natural luminescence signal for the grains being measured (Duller, 2004; 2008). The dose rate (in Grays per thousand years) is the annual dose received by those grains in their depositional environment (Wintle *et al*, 1993; Duller, 2004; Schaetzl and Anderson, 2005). Ideally, the OSL signal is derived from a single type of mineral grain such as quartz or potassium feldspar mineral separates (Rodnight, 2006). The dating technique can be applied to the age range from present to approximately 300 000 years ago and precision varies from ~3-10% of age for heated materials and ~5-20% for sediments (Wintle *et al*., 1993).

4.8.1 Sample Collection

Eighteen samples were collected for OSL dating from the two areas at Heelbo and four of the BT palaeosol samples were used for ^{14}C dating. The location of each of the sites is shown in Figure 4. 10, and descriptions of each of the samples are provided in Table 4.7. Samples were collected from the bone bed to establish the timing of deposition of the units above and below the fossils. The ages of the fossils were determined independently of this project (Lucinda Backwell, *pers comm*). Two samples were taken from the RB unit at the head of the deposit to determine the averaged sedimentation rate of the unit. Samples were taken of the stratigraphic profiles at Area 1 and Area 2. The TS unit was not sampled as this was too thin to be viable, but the relative ages of these units can be estimated. Two samples were taken from the channel fill at Area 1 to constrain the timing of sedimentation in the channel.

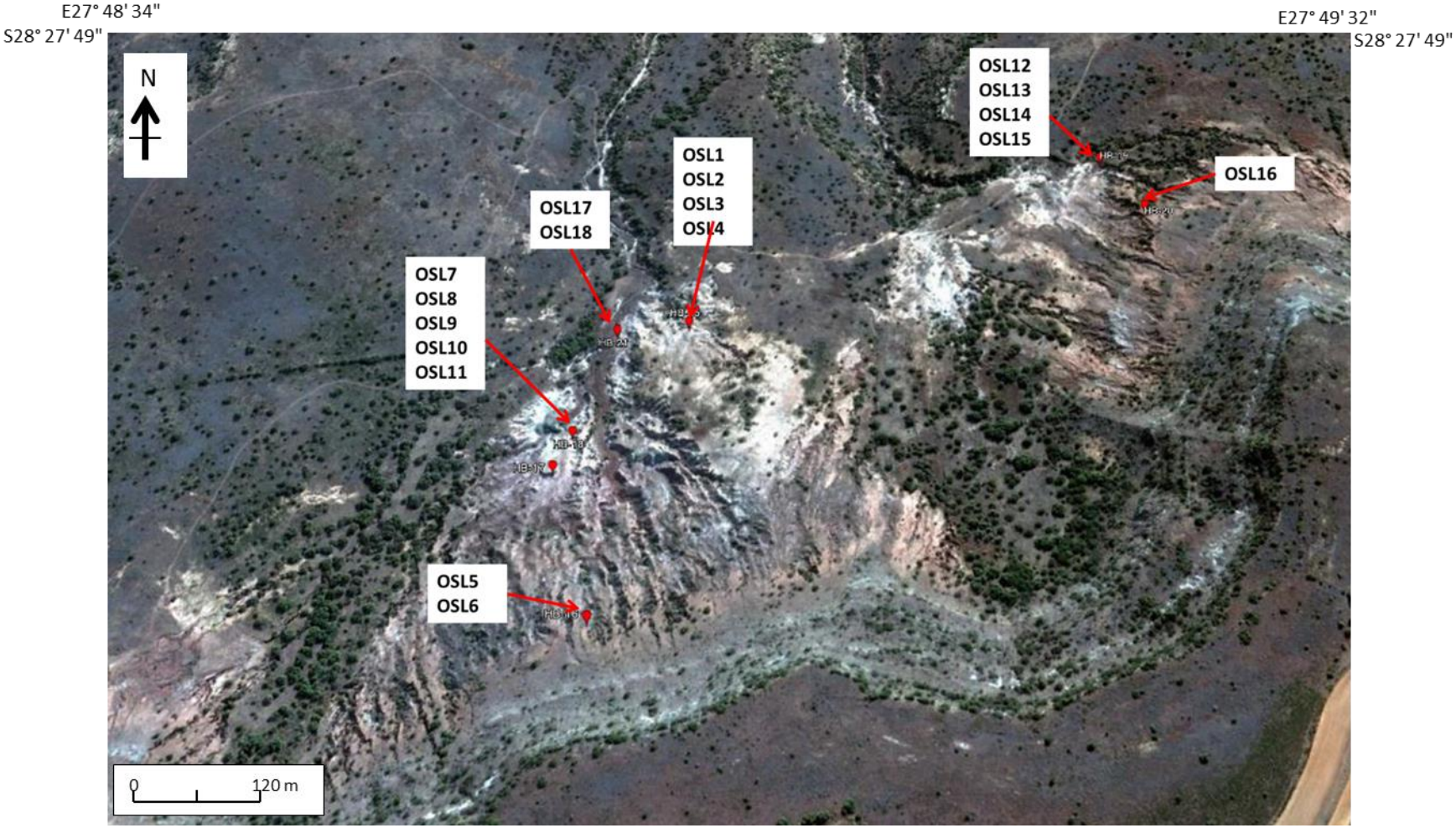


Figure 4.10 Location of the sample sites for OSL dating. Samples OSL7, OSL8, OSL10, OSL13 and OSL15 were also collected for ^{14}C dating.

Table 4.7 Sample location and description for OSL and ^{14}C dating

Sample	Latitude	Longitude	Altitude (m)	Depth (cm)	Comment		
OSL 1	S 28° 28' 2.3"	E27° 49' 3.2"	1669	25	RB	Bone bed	
OSL 2	S 28° 28' 2.3"	E27° 49' 3.2"	1669	56	BT_2	"	
OSL 3	S 28° 28' 2.3"	E27° 49' 3.2"	1669	82	B_2	"	
OSL 4	S 28° 28' 2.3"	E27° 49' 3.2"	1669	183	B_1 with calcrete nodules	"	Fossils lie between B_1 and B_2 showing that BT_1 has been eroded
OSL 5	S 28°28' 14.9"	E 27° 49' 0.6"	1705	102	B_1 at start of gully	Start of gully Area 1	37 cm to contact with bedrock
OSL 6	S 28°28' 14.9"	E 27° 49' 0.6"	1705	30	"	"	
OSL 7	S 28° 28' 7.3"	E 27° 48' 58.1"	1662	33	RB	Stratigraphic sequence at Area 1	^{14}C dating
OSL 8	S 28° 28' 7.3"	E 27° 48' 58.1"	1662	42	BT_2	"	^{14}C dating
OSL 9	S 28° 28' 7.3"	E 27° 48' 58.1"	1662	70	B_2	"	
OSL 10	S 28° 28' 7.3"	E 27° 48' 58.1"	1662	102	BT_1	"	^{14}C dating
OSL 11	S 28° 28' 8.8"	E 27° 48' 58.1"	1663	135	B_1 - 30 cm from contact with bedrock		
OSL 12	S 28°27' 53.8"	E 27° 48' 58.7"	1663	24	RB	Stratigraphic sequence at Area 2	
OSL 13	S 28° 28' 7.3"	E 27° 48' 58.7"	1662	70	BT_2	"	^{14}C dating
OSL 14	S 28°27' 53.8"	E 27° 48' 58.7"	1663	83	B_2	"	
OSL 15	S 28°27' 53.8"	E 27° 49' 21.9"	1663	134	BT_1	"	^{14}C dating
OSL 16	S 28°27' 56.3"	E27° 49' 23.8"	1671	500	B_1	" - very thick overhang	
OSL 17	S 28° 28' 2.7"	E 27° 49' 00"	1655	74		Channel fill in Area 1 - 74 cm from surface	
OSL 18	S 28° 28' 2.7"	E 27° 49' 00"	1655	30		Channel fill in Area 1 - 30 cm from surface	

The OSL samples were collected according to strict protocols in that they were not exposed to sunlight or white light at any time during the collection, or preparation process. As the layers were not very thick, the samples were taken roughly in the middle of each layer, ensuring the maximum distance from the nearest stratigraphic units. The depth of the overburden, the co-ordinates and the altitude of the sampling sites were recorded (Table 4.9). Where the sediment was not too compacted, steel tubes where hammered into the sedimentary unit (Figure 4.11 shows the equipment used during sampling), and when removed, any spaces in the tube were filled with plastic to ensure that there was no mixing of the sample in the tube, during transit. A cap was placed over the end of the tube that was extracted, and sealed at both ends with light-proof tape. The tubes were wrapped in light-proof plastic, labelled and placed in a light-proof container.



Figure 4.11 Equipment used for OSL sampling. From left to right: black tape to cover the ends of the tube; the hammer and sample tube; the former, which is placed at the end of the tube, to form a solid surface for the hammer to strike; the trowel to collect sediment from the sampling hole for radionuclide analysis; and bubble-wrap plastic to fill the tube so that the sediment does not move around during transportation. The plastic tube was replaced with steel as the soil was too compacted, and the plastic tube could not penetrate it.

The OSL samples were removed from the steel tubes under subdued red-light conditions which did not affect the OSL signal of the quartz grains. The sediment at both ends of the tubes were removed to a depth of 5 cm at each end and set aside for water content measurements and for radionuclide analysis. The outer rind of the one sample that was collected as a block was removed so that the unexposed centre could be analysed.

About 400 g of material for each sample was placed in beakers and labelled for the standard treatment used in the University of the Witwatersrand's Geo-luminescence laboratory (as per Aitken, 1998). It was not possible to do field gamma spectrometry measurements at the time of sampling, as the calibration of the instrument was unreliable; therefore additional material at each sample site was collected to measure the environmental dose rate.

4.8.2 Sample Preparation

All luminescence measurements were conducted on quartz grains in the size fractions 90–106 µm or 180–212 µm. As the sediment was dispersive in water, there was no need to deflocculate the samples, other than to fill the beakers with distilled water and leave overnight. The distilled water was carefully decanted, and 33% hydrochloric acid (HCl) was added to the samples to remove any carbonates in the sediment, and any reactions were noted. The mixture was stirred regularly, and when all reaction ceased, the samples were rinsed with distilled water.

To remove the organic matter from the sample, a weak concentration (20%) of hydrogen peroxide (H_2O_2) was added to the samples. The B_2 and all the BT samples were highly reactive, indicating high organic matter content. The samples were stirred periodically, and additional H_2O_2 was added until all reaction had ceased. When no further reaction was

observed, the samples were rinsed thoroughly with distilled water and dried.

Each sample was then dry-sieved through a set of four sieves (90, 106, 180, 212 µm), using an automatic sieve shaker, for 45 minutes. The grains retained in the size fractions 90-106 µm and 180-212 µm were used in the subsequent steps. The unused material was bagged and labelled and set aside in storage.

The quartz grains were isolated in two separation processes. The first process involved magnetic separation of magnetic grains from the non-magnetic crystalline grains, which according to Porat (2006) is a highly effective and simple process. The dried samples were placed in the *Frantz Magnetic Barrier Laboratory Separator* to remove any metals that were present in the samples. The size fractions were processed separately and the settings on the Franz were based on Porat (2006), with the optimal setting for fine sand (74-180 µm): slope of 25°, tilt of 17°; current = 1.4-1.5 Amp on the magnet; and the sample flow rate = 2-3 g/min. The samples were run through the Frantz magnetic separator twice, and small adjustments were made to the current and sediment flow rate as the instrument required.

The resulting non-magnetic fraction was a mixture of quartz, feldspars and heavy minerals, and in the second separation process these were

separated from each other by suspension in heavy liquid, with densities that are higher or lower than quartz (Wintle, 1997). A solution of sodium polytungstate (Na_6 ($H_2W_{12}O_{40}$).H_2O) and distilled water was prepared, first with a density of 2.62 g/cm^3, and then with a density of 2.70 g/cm^3. These were used to remove feldspars (ρ <2.62 g/cm^3) and heavy minerals (ρ >2.70 g/cm^3) respectively. The remaining grains (2.62 g/cm^3 < ρ < 2.70 g/cm^3) were retained for further processing.

In the final preparation stage, to remove any remaining feldspar contamination from the quartz grains, and to etch the alpha irradiated cover of the quartz grains, the grains were placed in 40% hydrofluoric acid (HF) for 45 minutes. The feldspars are chemically less resistant to the HF than the quartz and are partly or completely dissolved in the solution. During this process, the outer rind of the quartz grains was also removed, which reduced the external alpha particle contribution to a negligible level. The HF was deactivated with concentrated HCl to remove any fluoride precipitates, and then rinsed off in a secure container for approved methods of disposal. The sample was then rinsed thoroughly in distilled water, and dried overnight at 50 °C.

Each sample was sieved again, as the etching process reduces the size of the grains, and the size fraction 90-106 µm and the 180-212 µm were selected and stored in marked vials to be used for OSL measurements.

4.8.3 Instrumentation for Measuring D_e

All luminescence measurements were performed on a Risø TL/OSL Reader Model -DA-15 (Figure 4.12).

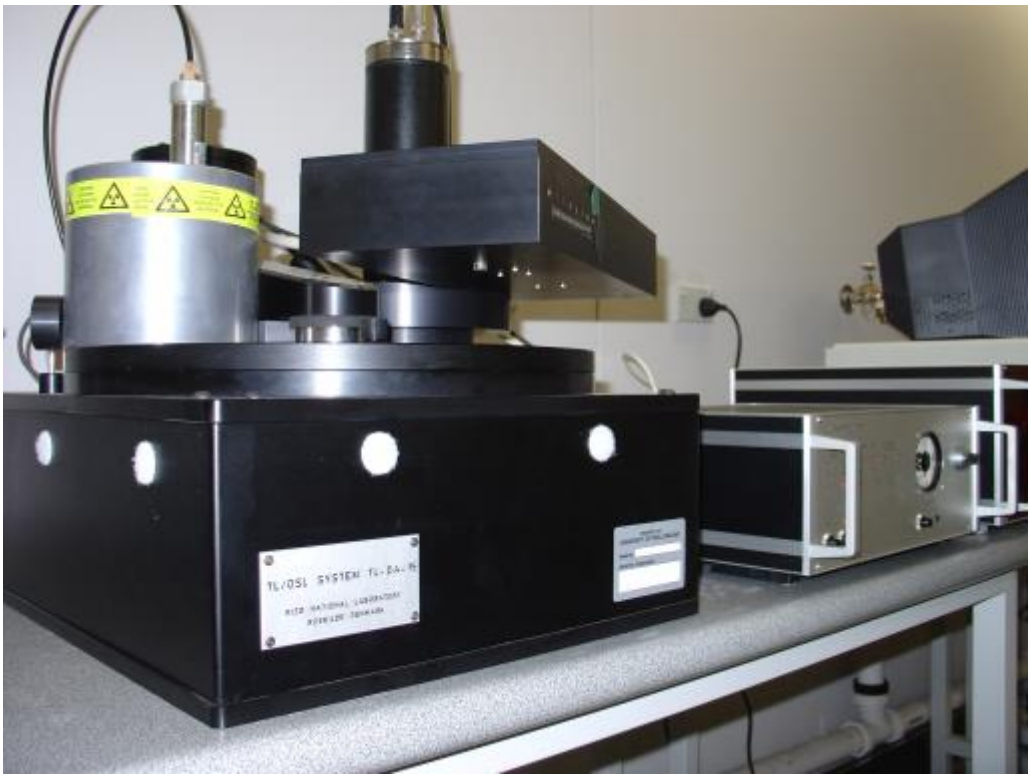


Figure 4.12 The Risø TL/OSL Reader Model -DA-15 (photo: G. Susino).

The Risø TL/OSL Reader Model-DA-15 automatic measurement system enables measurement of both thermoluminescence and optically stimulated luminescence of quartz, feldspar and poly-minerals. The characteristics of the reader are provided by the operating manuals (Risø National Laboratories, Denmark). The system allows up to 48 samples to be individually heated to any temperature between room temperature and

700 °C, individually irradiated by radioactive beta or alpha ($^{90}Sr/^{90}Y$) source, and optically stimulated using various light sources. The emitted luminescence is measured by a light detection system comprising a photomultiplier tube and suitable detection filters. The sample is placed in a light tight sample chamber which can be programmed to be evacuated (vacuum), or have a nitrogen atmosphere maintained by a nitrogen flow. The standard photomultiplier tube (PMT) in the RisøTL/OSL luminescence reader is bi-alkali EMI 9235QA PMT, which has maximum detection efficiency at approximately 400 nm. The distance between the PMT cathode and the sample is 55 mm, giving a detection solid angle of approximately 0.4 steradians. A 7.5 mm Hoya U-340 detection filter, with a peak transmission around 340 nm is fitted to prevent scattered stimulation light from reaching the PMT.

Thermal stimulation is achieved using the heating element located directly underneath the PMT. The heating element heats the sample and lifts the sample into the measurement position. The heater strip is made of Kanthal (a high resistance alloy) and heating is accomplished by feeding a controlled current through the heating element, where the heating system is able to heat samples to 700 °C at linear heating rates from 0.1 to 30 K/s. The heating strip is cooled by a nitrogen flow, which also protects the heating system from oxidation at high temperatures.

Optical stimulation is achieved using an array of light emitting diodes (LEDs), which are arranged in 7 clusters, each containing 7 LEDs (i.e. a total of 49 LEDs). The distance between the diodes and the sample is approximately 20 mm. The Risø TL/OSL luminescence reader is equipped with two stimulation sources: 1) Infrared (IR) LEDs emitting at 875 nm arranged in three clusters, each containing seven individual LEDs. The maximum power from the 21 IR LEDs is approximately 135 mW/cm^2 at the sample position; and 2) Blue LEDs emitting at 470 nm arranged in four clusters each containing seven individual LEDs. The total power at the sample position from the 28 LEDs is ~40 mW/cm^2. A green long pass filter (GG-420) is incorporated in front of each blue LED cluster, to minimise the amount of directly scattered blue light reaching the detector system.

A detachable beta irradiator is located above the sample carousel. The irradiator normally accommodates a 1.48 GBq (40 mCi ^{90}Sr/^{90}Y) beta source, which emits beta particles with a maximum energy of 2.27 MeV. The source is mounted into a rotating, stainless steel wheel, which is pneumatically activated. The distance between the source and the sample is 5 mm. A 0.125 mm beryllium window is located between the irradiator and the measurement chamber.

The reader is programmed through a sequence protocol written on *Sequence Editor (*Risø National Laboratory), which is directed through the

MINI-SYS computer attached to the reader. The reader then carries out the measurements in a fully automated way. The measurements are saved in a BIN file which can be processed through the ANALYST programme (authored by G.A.T Duller, Aberystwyth University) and exported to Microsoft Excel for further analysis.

4.8.4 Calibration of the Beta Source

As the Risø reader had been transported and relocated to the laboratory, the $^{90}Sr/^{90}Y$ beta source was calibrated using gamma-irradiated calibration quartz (180 – 212 µm) (provided by Risø National Laboratory, Denmark). Six aliquots of the calibration quartz were measured using the standard SAR measurement sequence (see section *4.8.6*) and the resulting equivalent dose was used to calculate the beta dose rate. Subsequently a second reader was purchased and installed and the beta source was calibrated in the same way. The dose rate in quartz at the sample position was approximately 0.158 Gy/s or 9.48 Gy/min for Reader A (the first instrument) and 0.135 Gy/s or 8.10 Gy/min for Reader B (the second instrument).

As the half-life of the $^{90}Sr/^{90}Y$ beta source is 28.79 years (Chu *et al.*, 1999; Jacobs, 2004), there will be a small decrease in the dose rate over the period of measurements. The expected dose rate at the time of the sample measurement based on the calibration can be calculated as:

$$N(t) = N_0 e^{-\lambda t}$$

Where N_0 is the dose rate at time (t) = 0 and λ is the decay constant and $\lambda = \frac{1}{\tau} = 0.693/\tau_{1/2}$ (Aitken, 1985; Jacobs, 2004). The dose rates were calculated and modified according to the date when the measurements were made.

4.8.5 Testing the Appropriateness of the SAR Protocol

Multiple-grain aliquots of the 200 µm fraction were made up on 9.7 mm diameter stainless steel discs, where a mask of 2 mm was placed over the disc and the exposed area of the disc was sprayed with a silicone based, adhesive spray). Each disc was placed spray-side down in a small pile of the quartz grains to allow the grains to adhere to the disc, which was tapped lightly to remove any loose grains and to ensure only a monolayer of quartz grains was retained for analysis. The distance that exists between the beta irradiation source and the disc results in the outer region of the disc receiving a smaller dose than the centre of the disc. This means that the sample was limited to the central area of the disc only. Another consideration in preparing the sample was that the effect of build-up and attenuation strongly influences the dose that the grains receive (Aitken, 1985); therefore it is essential that only a single layer (monolayer)

of grains is placed on the disc. This was checked under the microscope once the aliquots were prepared.

Prior to determining the D_e estimates of the samples essential for age determination, it was necessary to test the purity of the quartz grains. This was to determine that all the feldspars had been adequately removed, as well as to validate the sample preparation technique of the laboratory. Wintle and Murray (2006) also recommend three further tests to evaluate whether a particular SAR protocol is appropriate for D_e determination using a particular sample – the recycling ratio test, the recuperation test and the dose recovery test.

4.8.5.1. Sample Purity

After the pre-treatment of the sample to isolate the quartz grains, six aliquots were prepared to test the purity of the quartz extract by testing for feldspar contamination in the samples. Any feldspar grains that were not eradicated in the pre-treatment could cause scatter in the equivalent dose measurements. This can result in an overestimation of the D_e values because of the potassium contribution to the internal dose rate, or it can result in an underestimation of the D_e if anomalous fading has taken place (Spooner 1994; Thomsen *et al*., 2007). The OSL-Infra-red (IR) depletion ratio test relies on the depletion of the OSL signal in feldspars under room temperature IR stimulation, where the quartz remains unaffected. Discs

with multiple-grain aliquots of 2 mm of each sample were prepared and the sequence to test for the feldspar contamination is shown in Table 4.8.

Table 4.8 Sequence to test for feldspar contamination in the quartz grains

Step	Treatment
1	Preheat to 260 °C for 10 s
2	OSL stimulation at 125 °C for 40 s at 90 % power
3	Give dose for 250 s (36 Gy)
4	Cut heat 220 °C
5	OSL stimulation at 125 °C for 40 s at 90 % power
6	OSL stimulation at 280 °C for 40 s at 90 % power
7	Repeat steps 1-6 with beta dose 500 s (73 Gy) for 3 more runs. Insert OSL 125 °C IR Diodes for 100 s before step 2 in the final run.

The ratio of the OSL signal over the signal arising from the initial recycling dose is the OSL-IR depletion ratio and should be consistent with unity if no feldspars are present (Duller, 2004; Rodnight, 2006). A depletion ratio of less than 10% would be considered acceptable. Any aliquots with an OSL-IR depletion ratio above this criterion would be assumed to contain feldspar and were returned to the sample preparation section for additional density separation and HF etching. This additional stage of density separation and etching can be problematic as it may lead to the attrition of the sample. Instead, the contribution of the feldspar to the OSL signal can be determined by using IR stimulation of the grains. Before the aliquot is expose to blue LED optical stimulation the sample is stimulated by IR to detect any infra-red stimulated luminescence (IRSL) arising from the feldspars. If any feldspar is present either as grains or as inclusions in the

quartz grains, the OSL signal following the IR stimulation will be depleted. The ratio of the OSL signal to the signal arising from the initial recycling dose is referred to as the IR-OSL depletion ratio, and should be consistent with unity if no feldspars are present on the disk (Duller, 2003).

4.8.5.2 Recycling Ratio Test

The recycling ratio test is used to assess reproducibility within the SAR measurement cycle and if SAR is successfully correcting for the sensitivity changes. The sequence for the recycling ratio test involves giving the smallest dose first, then increasing each dose up to a value that is greater than the expected natural dose. A measurement is taken when no dose is given, and then one of the dose points is repeated. The repeated dose point is usually the one given after the natural was taken (i.e. the lowest dose) as the sensitivity changes are usually progressive. The ratio of the two sensitivity corrected data points is the recycling ratio. If the SAR is successfully correcting for sensitivity changes then the value for the recycling ratio is close to unity (Wintle and Murray, 2006). For real data sets Murray and Wintle (2000) suggest a range of acceptability from 0.90 to 1.10 for this ratio.

4.8.5.3 Recuperation Test

The measurement of a zero dose point should give zero signals. However the transfer of charge may cause the signal to be above zero.

Recuperation, or ‘charge transfer’, is the trapping of electrons in the OSL-related traps when they are ejected from non-OSL traps as a result of the previous irradiation, optical stimulation and heat treatment (preheating). This phenomenon can result in unacceptable variability in D_e values (Murray and Wintle, 2003; Wintle and Murray, 2006). Recuperation was tested by expressing the ratio between an additional zero dose OSL signal and the natural OSL signal as a percentage of the natural equivalent dose. All values greater than 5% were rejected as suggested by Murray and Wintle (2000).

4.8.5.4 Dose Recovery Test / Preheat Plateau

The dose recovery test is probably one of the most important tests as it determines the ability of the grains to recover the laboratory dose that it was given. The dose recovery test is also used to determine if the instrumental uncertainty estimates are reliable and appropriate (Jacobs, 2004). If the SAR protocol is applied to grains that are artificially irradiated with a known dose, and that dose cannot be recovered again, there is a high probability the D_e will be inaccurate (Murray and Wintle, 2003). For the dose recovery test, a SAR protocol is applied to an aliquot that has been given a known laboratory dose, following optical bleaching of the grains. The ratio of the measured dose to the given dose should be unity. This ratio provides a more stringent test than that of the recycling ratio as

the known dose is applied before any thermal treatment, therefore mimics the natural dose (Murray and Wintle, 2003).

The initial tests as well as problems with the mechanics of the reader resulting in repeated test measurements meant that large amounts of the sample was used, therefore a conservative number of 24 discs with multiple grain aliquots of 2 mm were used to determine the D_e for all samples.

4.8.6 Determining the Equivalent Dose (D_e) with SAR

The single aliquot regenerative (SAR) protocol was applied to determine the D_e of the samples (as described in Murray and Wintle, 2000). The Heelbo samples met the requirements of all the initial tests and it was decided that a D_e could be determined using the SAR protocol. In a standard SAR protocol (Steps 1-7 in Table 4.11), the natural OSL signal and the laboratory generated signal are both corrected for sensitivity prior to being compared with one another. In a conventional SAR sequence the natural dose (L_N) is measured (Step 3 in Table 4.11); and thereafter progressively larger doses are used to irradiate the sample to produce the stimulation value (L_x) (repeat of Step 3). A fixed test dose is given after each OSL measurement (Step 4) to correct for sensitivity changes in the quartz grains (Armitage *et al*., 2000); after which T_x is then measured (Step 7). The growth curve for the sample can then be plotted using the

L_x/T_x values onto which L_N can be interpolated. The preheat (Step 1) is used to empty the 110 °C TL trap prior to the measurement of the OSL signal; and the cutheat (Step 5) which serves the same purpose as the preheat can be any temperature between 160 °C and 300 °C but it is generally held at 160 °C in order to minimise sensitivity change (Armitage *et al*., 2000).

However any uncertainties in the behaviour of the quartz grains were addressed by the modification to the SAR protocol as suggested by Murray and Wintle (2003). To reduce the effect of one measurement cycle on the next, Murray and Wintle (2003) suggested a modification to the SAR protocol which involves an additional optical stimulation (Step 8), directly after the measurement of every test dose (T_x) to evict any optically sensitive charge that had not been reset by the 40 s optical stimulation at 125 ºC that forms part of the conventional SAR procedure. The modification involved adding a 40 s optical stimulation with blue LED at 280 ºC at the end of each measurement cycle. The modification would also resolve problems of an inability to recover a known dose, the pre-heat temperature dependence of the dose response curves, and the problem of thermal transfer of charge between measurement cycles (Murray and Wintle, 2003).

A conservative number of 24-36 discs with multiple grain aliquots of 2 mm were used to determine the D_e for all samples. The measurement sequence based on the SAR protocol is shown in Table 4.11.

Table 4.9 Sequence to determine the D_e for all samples, based on the SAR protocol.

Step	Treatment
	Natural
1	Preheat to 200 °C for 5 s
2	OSL stimulation at 175 °C IR Diodes for 40 s at 90 % power
3	OSL stimulation at 125 °C for 40 s at 90 % power (Lx)
4	Test dose Beta radiation 50 s
5	Cut heat 160 °C
6	OSL stimulation at 175 °C IR Diodes for 40 s at 90 % power
7	OSL stimulation at 125 °C for 40 s at 90 % power (Tx)
8	OSL stimulation at 280 °C for 40 s at 90 % power
	Dose Response Curve
	Repeat steps 1-8 with a beta dose of 35, 75, 50, 100, 0, 35 s and test dose 35 s

The dose response curve is plotted as an exponential and is generated from the integration of channels 1-5 and background from channels 200-250.

4.8.7 Sample Preparation for Dose Rate Acquisition

The samples were split into a palaeodose and a dose rate samples under safe light conditions. The "wet" dose rate samples were measured and dried at 50 °C until all moisture was removed. The "dry" samples were measured and the water content was calculated.

To determine the dose rates, 100 g of each sample was sent to iThemba LABS, Gauteng for radionuclide measurements of ^{238}U and ^{232}Th and ^{40}K. The elemental concentrations of uranium, thorium and potassium were converted into dose rates using the method o utlined by Adamiec and Aitken (1998).

The annual dose rate is derived from the measurement of the radionuclide concentration (or activity) by means of a conversion factor. These conversion factors (see Adamiec and Aitken, 1998) are based on the nuclear data tables known as the Evaluated Nuclear Structure Data File (ENSDF) and the dosimetry- orientated formulation is known as the Medical Internal Radiation Dose (MIRD). The emission values are converted to dose-rate based on the infinite matrix assumption that the dose rate is equal to the rate of energy emission per unit mass, and implying that there is homogeneity in the radioactive content and in the absorption co-efficient (Adamiec and Aitken, 1998). The “full-series” conversion table is used as the radionuclides are assumed to be in radioactive equilibrium, i.e. the rate of disintegration of each daughter is equal to that of the parent. The dose rate for U, Th and K were determined using the conversion tables in Table C.1 and Table C.2 in APPENDIX C.

4.8.7.1 Environmental Dose Rate

The source of the environmental dose rate to a buried grain of sand comes

from the internal radionuclides (which is negligible in quartz), from the external radionuclides (alpha, beta and gamma radiation) and the cosmic radiation (see Prescott and Hutton, 1994). The dose rate (given in Gy/ka) is made up of the components $D_\alpha + D_\beta + D_\gamma + D_{c,}$ where D_α is the alpha dose rate which has a short penetration range, D_β is the beta dose rate with a longer range, D_γ is the gamma dose rate which is penetrating (Figure 4.13) and D_c is the contribution made by the cosmic dose rate which consists of a mixture of light and heavy particles and photons (Aitken, 1985; Guérin *et al*., 2012). The different penetrating powers of the alpha, beta and gamma radiation is important to OSL dating. Alpha and beta particles have a short penetrating range of 10^{-2} and 10^{0} mm respectively and are therefore limited in terms of their radiation contribution to the sample. Gamma rays however, have a greater radiation penetrating range of ~30-50 cm, and therefore a larger volume of sediment will provide a larger gamma dose to the sample; which means that the surrounding environment is significant to the dose rate of the sample.

The different penetrating powers can influence the grain size used for analysis for example: fine-grained techniques use minerals with a grain size 4 – 11 µm. These grains are small enough to ensure complete penetration of all three types of radiation; however in coarse-grained techniques the grain size 100-200 µm is used. The outer layer of the grain can be etched away and the contribution of the alpha radiation will be removed, and only the contribution from the gamma rays and from the partly attenuated beta

particles remains (Figure 4.13). The quartz grains themselves are assumed to be free of radioactivity (Vandenberghe, 2004)

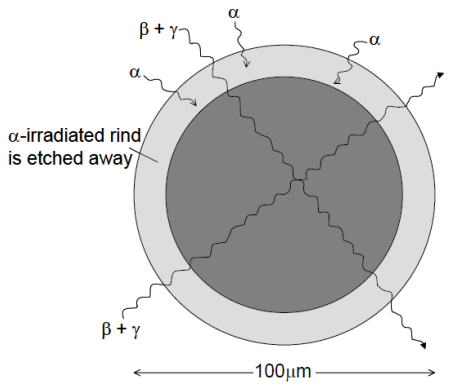


Figure 4.13 The effect of radiation on a 100 μm coarse grain of quartz where the quartz is assumed to be free of radioactivity. The alpha particles deliver their dose to only the outer layer of the grain, which is removed during etching with HF. The dose measured from these grains results from their exposure to beta and gamma radiation, and cosmic rays (Vandenberghe, 2004).

The dose rate can be measured through types of integral measurements (where the number of disintegrations per unit time is measured) such as alpha counting, beta counting or field gamma counting. However, as no information is provided about radionuclide disequilibrium, assumptions about dose rate stability cannot be tested. Alternatively the dose rate can be measured through radionuclide concentrations (where the amount of each constituent is quantified), for example high resolution gamma spectroscopy, thermal ionisation mass spectrometry (TIMS), inductively coupled plasma mass spectrometry (ICP-MS) or neutron activation analysis (NAA). These methods determine the individual concentrations of the ^{238}U, ^{232}Th chains and ^{40}K directly and therefore assumptions about dose rate stability can be tested, and the effects of water content can be predicted.

The luminescence age equation is based on the assumption that the annual dose has remained constant over the time period that is being dated, and that the dose rate is derived from the ionising radiation from radionuclides in the uranium, thorium and potassium decay series. This assumption depends on the sample being located in a closed system with no radionuclides being added or removed, i.e. the U and Th decay chains have reached a state of radioactive equilibrium (Olley *et al*., 1996; Vandenberghe, 2004). The decay of these radionuclides ^{232}Th, ^{238}U and ^{235}U and their daughters and ^{40}K and ^{87}Rb is attended with the emission of alpha particles, beta particles and/or gamma rays, as shown in the decay series for ^{235}U (Figure C.1), ^{238}U (Figure C.2), ^{232}Th (Figure C.3), and ^{40}K and ^{87}Rb (Figure C.4) in APPENDIX C. The activity of each daughter (number of disintegrations per unit time) is the same and equal to the parent activity. All the daughters from the U and Th decay chains will then contribute to the dose rate that remains effectively constant through time because of the long half-life of the parent (Vandenberghe, 2004).

The equilibrium of the radionuclides can be disturbed by adding or removing a daughter (Prescott and Hutton, 1995; Olley *et al*., 1996); or more commonly in the ^{238}U decay series as ^{222}Rn, with a half-life of 3.82 days, escapes as it diffuses through the sediment. The half-lives of the radionuclides in ^{232}Th decay have a tendency to be mobile and short lived, thus the radioactive disequilibrium is considered negligible. Disequilibrium in ^{235}U is also considered insignificant due to its low abundances and low

contribution to the total dose rate. Olley *et al*. (1996) discussed the effects of disequilibria in the U and Th decay chains on burial dose rates in fluvial sediments and found that the dose rate is comparable with other luminescence dating uncertainties of ±5 – 10 %. Therefore in OSL dating, certain assumptions regarding the equilibrium of the radionuclides are made: that the decay chain was always in equilibrium or that the dose-rate measured has prevailed over the burial time of the sample, and for the purposes of this research the radionuclides are considered to be in secular equilibria.

The concept of the infinite matrix assumption is used to evaluate the rate at which energy is being deposited in the soil and the sedimentary grains. The infinite matrix assumption assumes that the rate of energy absorption is equal to the rate of energy emission per unit mass, if the radiation is uniform within the matrix and the absorption coefficients of the constituents are uniform. The sample should be homogeneous over a distance of at least 3-4 mm for beta radiation and 0.3 m for gamma radiation (Adamiec and Aitken, 1998). The infinite matrix allows the radioisotopic concentrations in the sample to be converted to corresponding alpha and beta dose rates using conversion factors (see Adamiec and Aitken, 1998). The infinite matrix assumption is also the basis for calculating attenuation factors and for taking the effect of the water content of the sediment into account.

The degree of attenuation within the grain is dependent on a range of diameter of quartz grains as well as the water content of the sediment. The appropriate values for the grain size of quartz used in the OSL analysis can be used to calculate the attenuation. The HF etching for coarse grain sediment will have a higher absorption fraction than the centre of the grain (Mejdahl, 1979).

4.8.7.2 The effect of water content

The effect of water content on the dose rate is firstly to dilute the radio-elements (radio-isotopic content per unit mass) and secondly that water absorbs a significant amount of radiation that would have reached the mineral grains (Aitken, 1998; Vandenberghe, 2004). Water is not usually radioactive and in comparing the absorption coefficients per unit mass, water is 50% higher than sediment for alpha particles, 25 % higher for beta particles, and 14 % higher for gamma radiation (Zimmerman, 1971; Vandenberghe, 2004). Therefore the dose rate in moist sediment is less than in dry sediment, which means that the moisture content of the sediment, over the time of its burial, needs to be considered when determining the annual dose rate. The moisture content may fluctuate due to seasonal or climatic changes and these changes need to be corrected for to avoid an underestimation of the age.

The porosity of the sample determines the upper limit to the effect of water

content in the sediment. The porosity (W) can be calculated as the ratio of the mass of water that the sample can hold at full saturation to the mass of the dry sample. The saturation level for sediment ranges from 20 to 40 % (Vandenberghe, 2004) and it is important to consider how near to the saturation limit the sample has been on the average over the entire burial period. If the dose rates are obtained, the correction for the water content can be obtained by introducing the appropriate attenuation factors (see Aitken and Xie, 1990):

$$D\alpha = \frac{D\alpha, dry}{1 + 1.50xWxF}$$

$$D\beta = \frac{D\beta, dry}{1 + 1.25xWxF}$$

$$D\gamma = \frac{D\alpha, dry}{1 + 1.14xWxF}$$

4.8.7.3 Cosmic radiation

Cosmic radiation is primarily derived from outer space and consists mainly of protons and alpha particles. The contribution of cosmic rays is included in the estimates of the external dose rate, despite being a small contribution (Aitken, 1985). Cosmic radiation consists of two types of components: the 'soft' component (electrons and photons) which is absorbed by the top 150 g/cm^3 (~0.6 m) of sediment; and the hard electron component, which consists mainly of muons (Aitken, 1998; Vanderberghe, 2004; Kim, 2009).

The cosmic dose rate is not measured directly but is derived from expressions to calculate cosmic dose rates at any depth below ground level (see Prescott and Hutton, 1994; 1995) and at any altitude up to 5 km and at any geomagnetic latitude (see Prescott and Stephan, 1992). The penetration of cosmic radiation is dependent on the bulk density of the sample, therefore the cosmic ray dose can be estimated from the depth of the sample for any given overburden density (Kim, 2009). The geographic location and altitude may also affect the cosmic radiation, and Prescott and Hutton (1994) estimate the circulation of the cosmic dose rate to be associated with a 50% uncertainty without allowances being made for corrections in altitude and latitude.

4.9 RADIOCARBON (^{14}C) DATING

Radiocarbon dating is a well-established dating technique, and is used to constrain the ages of the palaeosols in the Heelbo deposit, as well as provide an independent age control on the luminescence ages. Carbon has three isotopes: ^{12}C, ^{13}C and ^{14}C, of which ^{12}C is the most abundant comprising 98.9% of all naturally occurring carbon and ^{13}C forming about 1.1%, with ^{14}C making up less than 1 part per billion of all natural occurring carbon (Walker, 2005; Hua, 2009). The isotopes ^{12}C and ^{13}C are both stable, but ^{14}C decays to a stable form of nitrogen (^{14}N), through the emission of beta particles (Walker, 2005). The radioactivity is derived from the beta particles released from the nucleus of every atom of ^{14}C that

decays. ^{14}C is produced by cosmic rays in the stratosphere and upper troposphere, and is distributed throughout the atmosphere, oceans and lithosphere in different forms (Walker, 2005; Kumari and Kumar, 2009).

Radiocarbon, in organic matter, can be measured by means of decay counting or through accelerator mass spectrometry (AMS). The ^{14}C content is measured directly, relative to ^{12}C and ^{13}C present in the sample. The samples were prepared and analysed according to the laboratory procedures of Lund University Radiocarbon Dating Facility (goran.skog@c14lab.lu.se).

4.9.1 Sample Preparation

Samples of 500 g were collected for ^{14}C dating from the organic-rich layers that appeared to have a high carbon content. These samples were sieved to break up any clumps and to remove any roots and grasses. The samples were labelled and packaged and, as mentioned before, sent to University of Lund in Sweden for radiocarbon dating (^{14}C) analysis.

The methods reported here were described by the Lund University Radiocarbon Dating Facility. Samples were slurried and wet sieved into coarse and fine fractions. The coarse fraction was archived as reference material and the fine fraction was used for analysis. Organic contaminates, such as humic acids and modern organic material like roots

and leaf litter in the sample, may adversely affect the ^{14}C age of the sample. The roots and leaves were thus, either, sieved or hand-picked out of the sample. Humic acids are mobile, decay products from recently dead plants which leach down through site profiles, and are adsorbed by certain receptive substances. Humic acids were removed through treatment with a base solution of sodium hydroxide (NaOH).

The samples were then treated with dilute (10 %) HCl to remove adsorbed carbonates particularly from percolating groundwater. The HCl was added to the sample, and the beaker placed on a hot plate and heated slowly to boiling point. After ~1 hour, the beaker was removed, and the sample placed in a Büchner funnel, which uses the pressure of flowing water to create a vacuum. A glass filter was place at the bottom of the funnel and dampened with distilled water. The sample was later placed on top of the filter paper and distilled water poured in, and drawn through the sample by the vacuum effect. The aim is to reduce the pH levels of the sample to a neutral pH by continual rinsing and checking with litmus. Once the required pH level was reached, two fractions remained: an acid soluble fraction which contained carbonate contaminants, and was not used for dating, and an acid insoluble fraction which contained no carbonates, and was placed in a petri dish and dried in the oven.

The radiocarbon sample was then analysed using accelerated mass spectrometry (AMS), which is a preferred method owing to the smaller

sample size required, and the faster, more efficient processing time (Hua, 2009). AMS directly measures the ^{14}C isotope relative to the stable ^{12}C and ^{13}C isotopes within the sample.

4.9.2 Radiocarbon Conventional Ages

Radiocarbon ages are reported as years before present which is defined as AD 1950. In the age calculation the atmospheric ^{14}C concentration in 1950 is a hypothetical value, and is conventionally set at 100 % Modern Carbon (pMC), or 1 fraction modern carbon (f) (Stuiver and Polach, 1977; Hua, 2009). Measured ^{14}C concentrations must be corrected for isotopic fractionation using $\delta^{13}C$. To simplify the calculation, atmospheric ^{14}C concentration is assumed to be constant through time, with the implication that all living terrestrial matter have an initial ^{14}C concentration of f=1. The conventional radiocarbon age of a sample is then defined as:

$$t = -\frac{T_{1/2}}{ln2} \ln(fs)$$

or

$$t = -8033 \ln(fs)$$

where f_s is the ^{14}C concentration in sample S in fraction modern carbon after correction to $\delta^{13}C$ = 25 ‰ PDB (Hua, 2009). This value is determined by measuring sample S against ^{14}C standard reference materials such as oxalic acid I oxalic acid II or ANU-sucrose (Hua, 2009). $T_{1/2}$ is the Libby half-life of radiocarbon of 5568 years. This half-life is approximately 3 %

shorter than the correct half-life of 5730± 40 years (Godwin, 1962; Hua, 2009). The discrepancy between the two half-lives is corrected during the radiocarbon calibration process. Ages up to about 50 000 years (~9 to 10 half-lives of ^{14}C) can be determined by radiocarbon dating.

4.9.3 Calibration of ^{14}C Ages

Variations in the rate of carbon production in the atmosphere as a result of changes in the Earth's magnetic field, variability in solar activity and changes in the carbon cycle, have resulted in the ^{14}C concentration of the atmosphere not being constant in the past (Taylor, 1987; Reimer *et al*., 2004). Changes in the Earth's magnetic field causes long-term (10^3–10^4 years) fluctuations in atmospheric ^{14}C, and short- and medium-term (10^1–10^2 years) variations in atmospheric ^{14}C are mainly due to variability in solar activity. Additionally, centennial-scale variability may also be a result of variations in geomagnetic field intensity (St-Onge *et al*., 2003). As a result, radiocarbon and calendar ages are not identical, and radiocarbon ages need to be converted to calendar ages using a calibration curve. The calibration curve describes the atmospheric ^{14}C concentration in the past, measured in precisely and independently dated materials. The most recent internationally-ratified calibration curve is IntCal13 (see Reimer *et al*., 2013 for details relating to this calibration curve). The calibration of ^{14}C ages is usually derived using a number of computer programmes which are available online, such as Calib 7.1 which was used in this thesis (http://calib.qub.ac.uk/calib/calib.html).

CHAPTER 5: RESULTS

5.1 INTRODUCTION

The Heelbo landscape is described in this chapter. The description includes the field observations and measurements of the hillslope deposit and the gully networks. The sedimentary succession at Heelbo consists of unconsolidated sediments interlayered with palaeosols which have been exposed in the gully side-walls. The horizons are referred to in terms of their principal colour, although colour changes within certain horizons have been noted. Further distinguishing characteristics of each horizon are described at both a macro- and microscopic level. Although there are two areas on the deposit that were worked on, the main descriptions are made at Area 1, with supporting information from Area 2, as most of the deposit at Area 2 has been eroded, and from the bone bed. The grain size analysis is presented in this chapter as well the results of the major and trace elements, clay mineral analysis, pH, EC and SAR_s of the horizons. The burial ages of the sediment were determined using OSL dating and ^{14}C on selected horizons and these results will be presented in the next chapter.

5.2 HILLSLOPE MORPHOLOGY

The Heelbo occurrence is a small-scale sedimentary deposit which has accumulated on the hillslope of a Karoo mesa. The deposit rises 60 m above the valley floor and extends across the mountain front for approximately 1450 m, and spreads out across the valley floor for a distance of 475 m (Figure 5.1). The estimated volume of original sediment that would have made up the deposit is approximately 0.02 km^3; although much of this original sediment has been removed by later erosion. An analysis of archive photos shows that the hillslope deposit has not changed in shape and has increased only slightly in size (Figure 5.2). The photographs also indicate that erosion at Area 2 has increased as less of the deposit is visible in the 2004 photograph. This lack of difference between the two photographs over more than 74 years is significant in that it suggests that the current rates of erosion and deposition on the hillslope are slow.

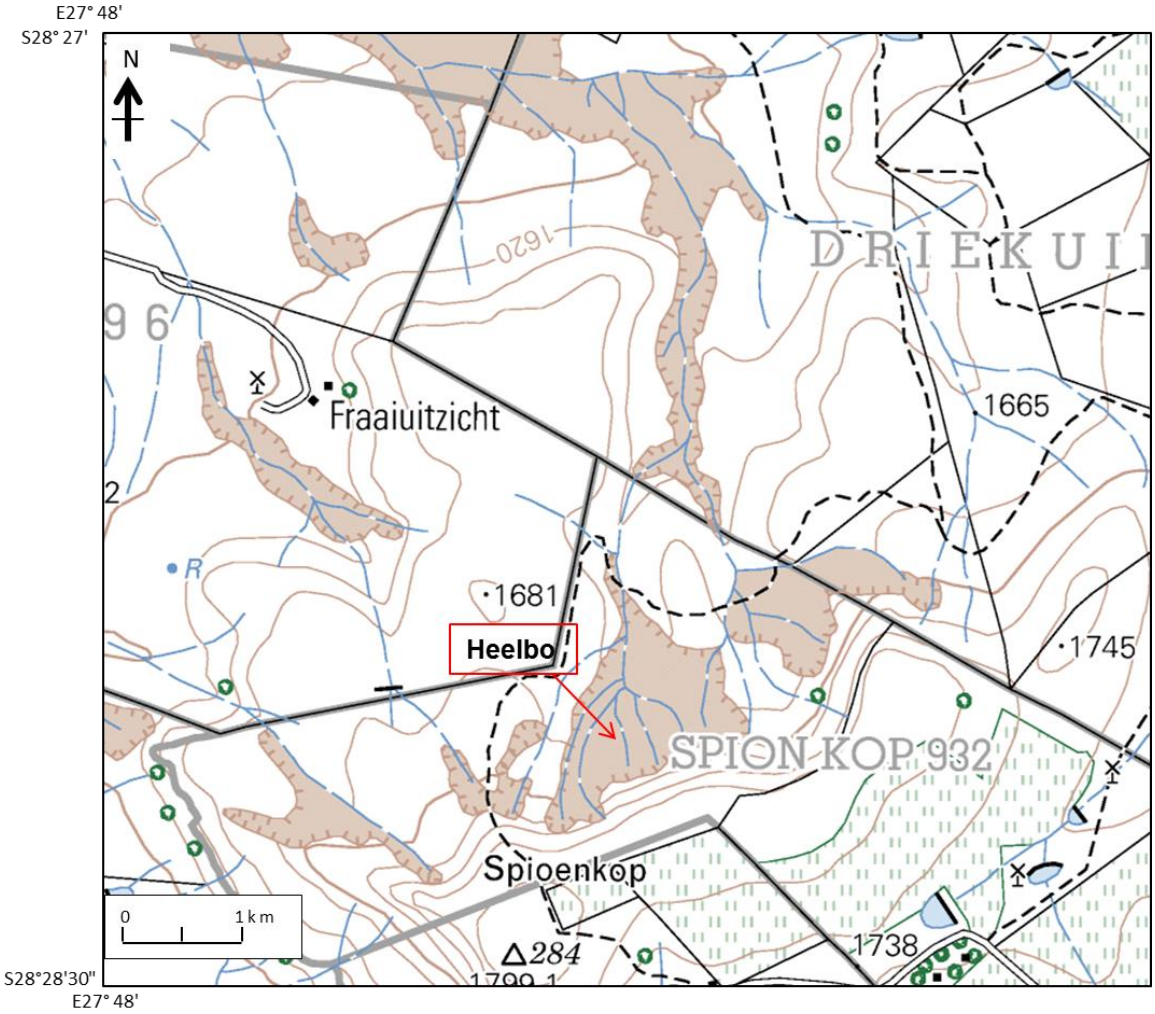


Figure 5.1 South west section of the 1: 50 000 topographic map of the Heelbo hillslope deposit. The full map with key is provided in APPENDIX A. (National Geospatial Information, 2014).

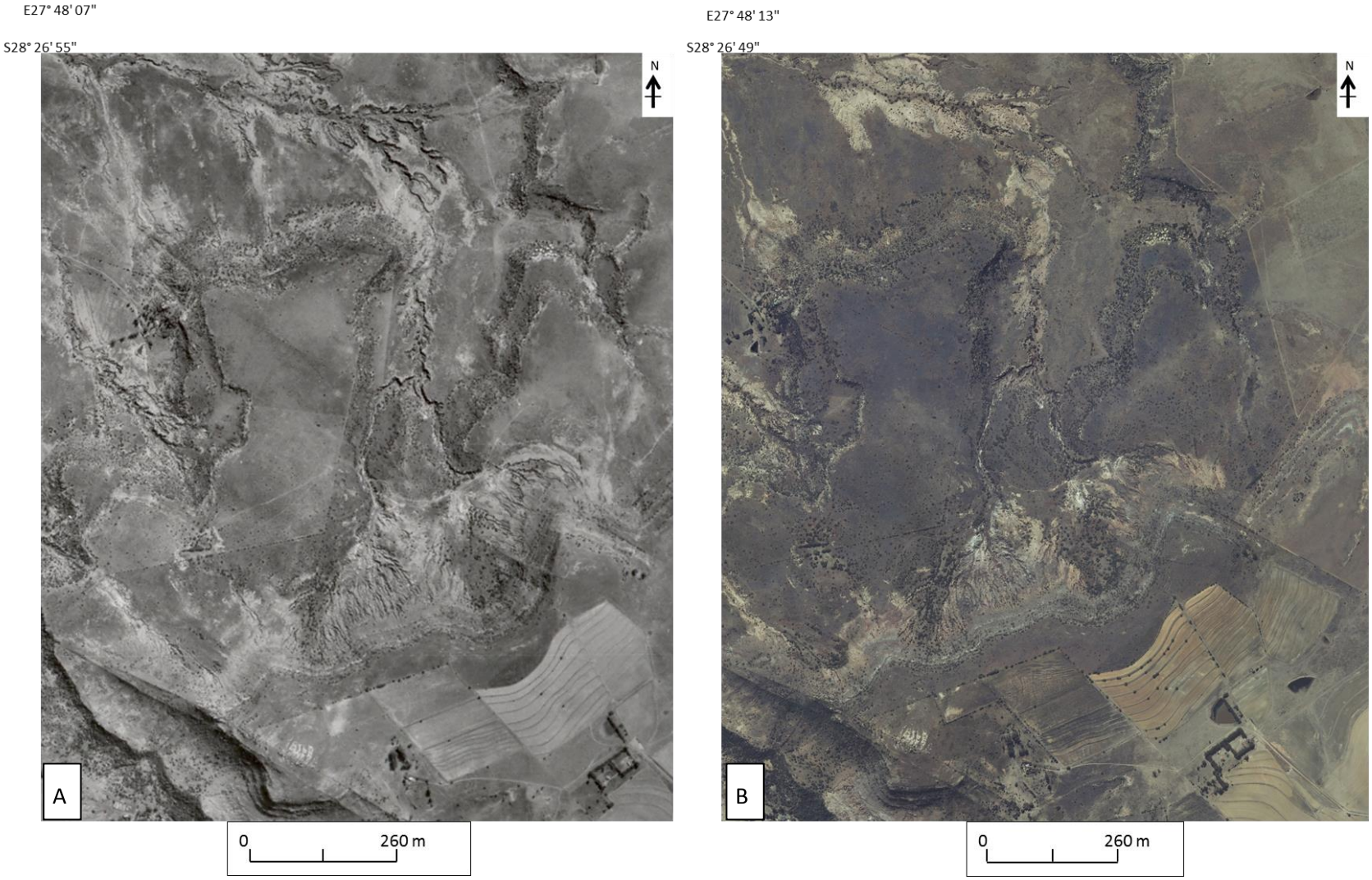


Figure 5.2 Aerial photographs of the Heelbo deposit from 1940s (A) (exact year not given) and in 2004 (B). Photos courtesy of National Geo-spatial Information (NGI).

A slope profile of the deposit at Area 1, measured by dGPS, shows a concave profile (Figure 5.3). The gradient between each point was determined with the average gradient of the deposit being 10.20°. The gradient of the scarp face of the mesa is 22.7° (Figure 5.3).

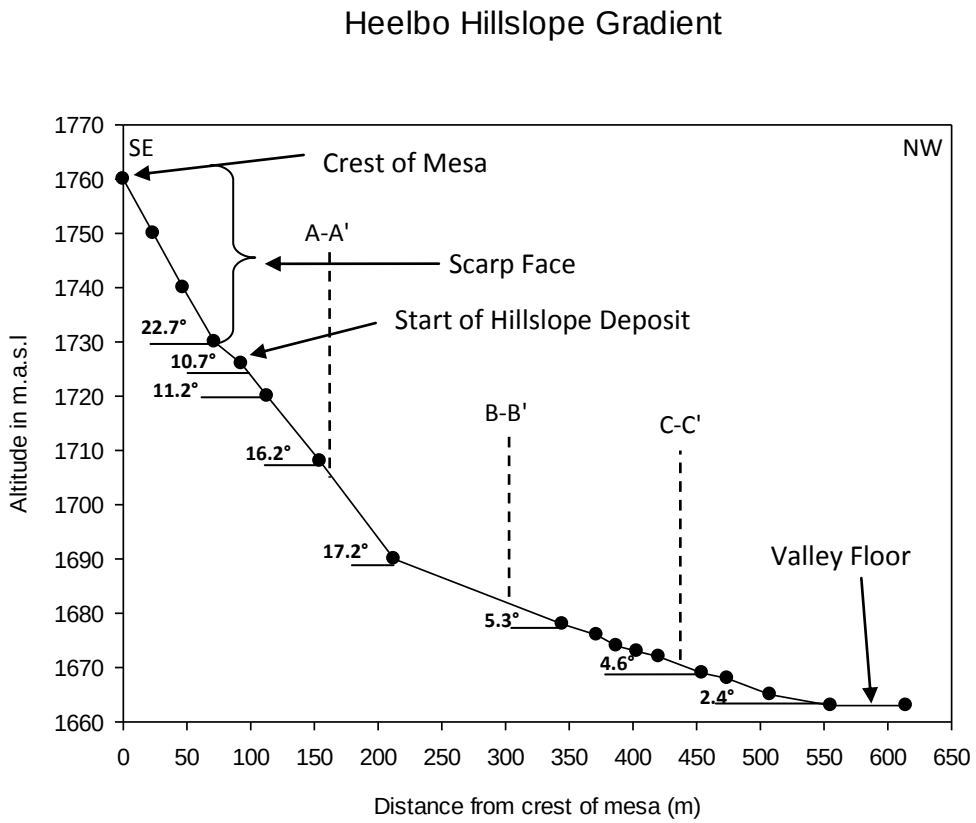


Figure 5.3 The gradient of the mesa slope is steep at 22.7°. The hillslope deposit indicates a concave shape with a steep gradient upslope of the deposit becoming gentler towards the valley floor. The positions of the cross-section profiles along the slope are shown. See Figure 4.2 (a) for location of measured points. (Vertical exaggeration = 5 times)

Cross-sectional topographic profiles of the deposit were constructed across the gullies (Figure 5.4), in a roughly east – west orientation, in the proximal (A-A'), medial (B-B') and distal (C-C') sections of the slope (see position of traverses in Figure 5.3) and the location of the traverses is

shown in Figure 4.1. The section A-A' shows the high-lying rise between two drainage systems which acts as a watershed between them. This rise is eroded away towards the medial and distal sections as the drainage systems merge into a network of channels (Figure 3. 9). The gullies in the proximal section are shallow and V-shaped as at this point the gullies have only cut into the top layers of the hillslope sediment and the bedrock is not visible. Lower down the slope, the gullies become increasingly deeper and wider, forming U-shaped gullies as they merge towards the base of the slope. The stratigraphic relationships in the gullies are presented later in this thesis.

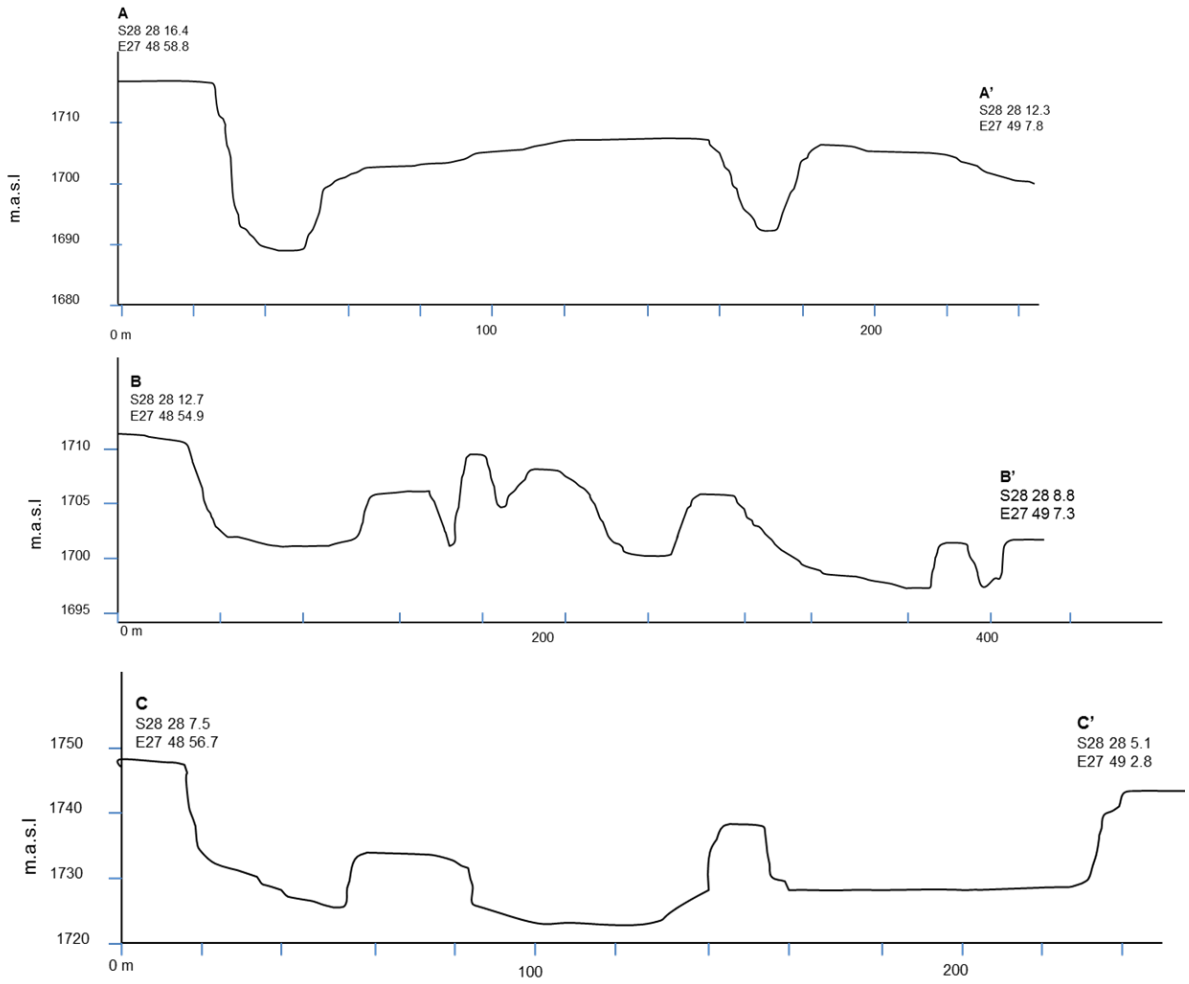


Figure 5.4 Topographic cross-sections through the proximal (A-A'), medial (B-B') and distal (C-C') sections of the hillslope deposit (view is upslope). The orientation of all three profiles is SW to NE. The change from narrow V-shaped gullies to wider, deeper U-shaped gullies is clearly shown. More of the stratigraphy is preserved in the medial to distal sections and are exposed through the valley incisions. Towards the medial portion a combination of V- and U-shaped gullies are visible, which become increasingly deeper downslope. The bedrock is visible and the stream channels begin to merge and widen downslope of the deposit.

5.3 STRATIGRAPHY

The stratigraphic records on hillslopes can potentially provide information on climate controls on sedimentation. Sedimentary sequences for Areas 1 and 2 and the bone bed are presented in Figure 5.5 (a) and (b) respectively. The stratigraphy at the bone bed is similar to that of Area 1 and 2, but the BT_1 horizon has been incorporated into the bone bed (Figure 5.5b). This horizon has been greatly disturbed and the sediment is well mixed. Photographs with associated stratigraphic profiles and lithologies for some of the sample sites are given in Figure 5.6. The stratigraphic relationship downslope at Area 1 is shown in Figure 5.7. The locations of the sample sites are in Figure 4.2a. The sedimentary analysis of the bedrock and the deposit is supported by petrographic analysis using thin sections produced of each stratigraphic unit.

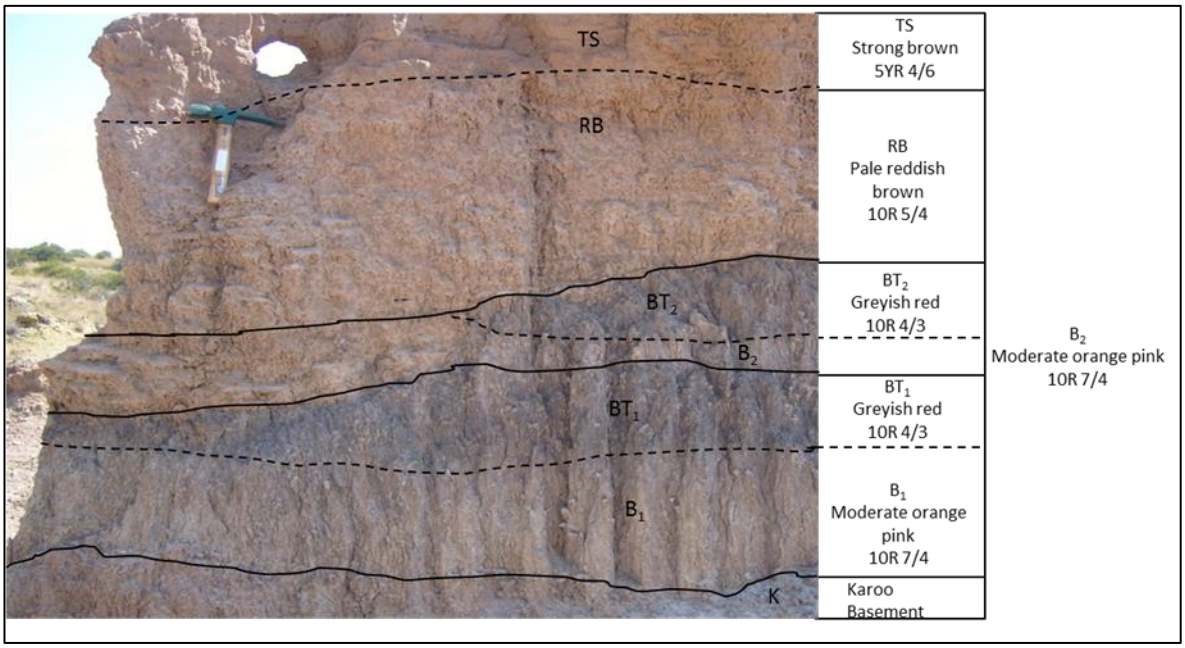


Figure 5.5a An example of the typical sedimentary package seen in the Heelbo stratigraphy at sample site HB-06 in Area 1. The remnants of a palaeo-channel can also be seen on the photograph between RB and BT_2 units. K is the Karoo basement, B_1 and B_2 are the two units of brown sediment; BT_1 and BT_2 are the two organic-rich palaeosols; RB is the red-brown horizon and TS is the top sediment horizon. The dashed lines in the photograph and the column indicate gradational contacts, whereas the solid lines are sharp erosional contacts. The colour and Munsell reference for each horizon is also indicated. The length of the hammer is 30 cm.

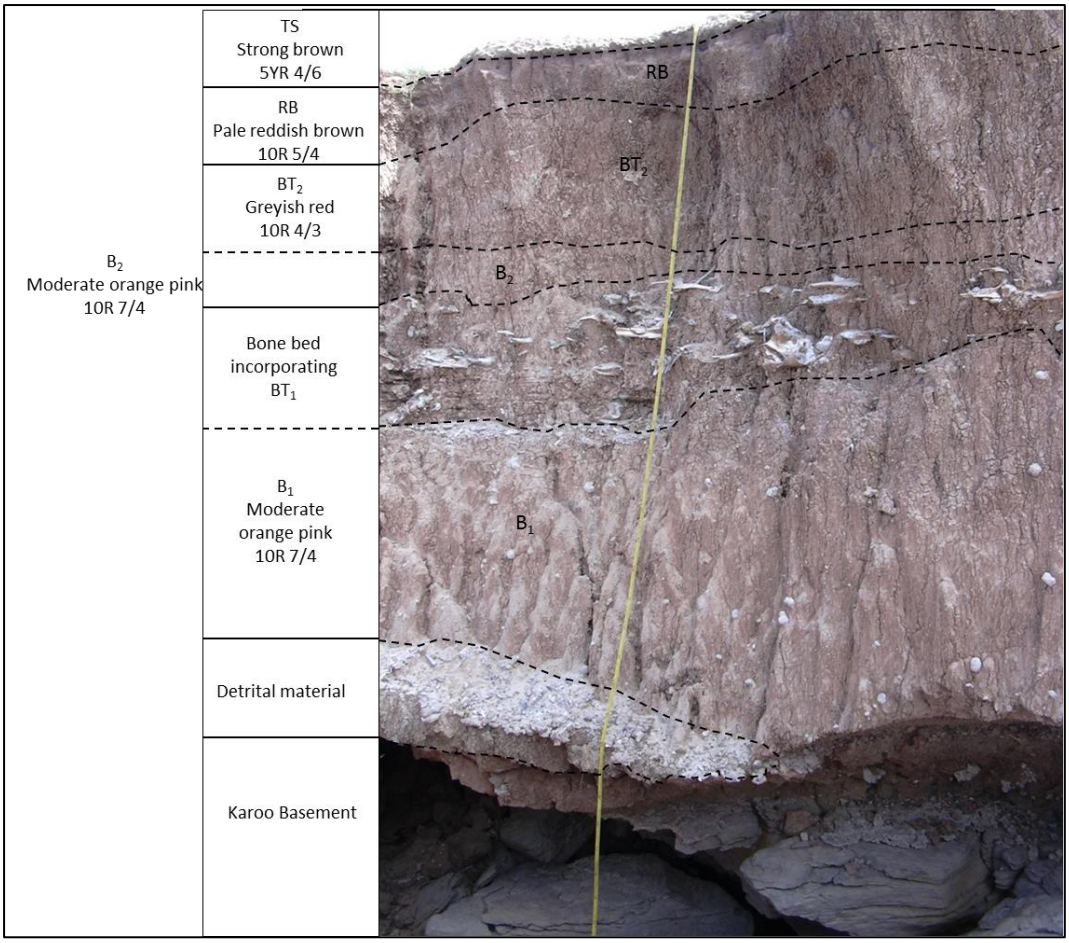
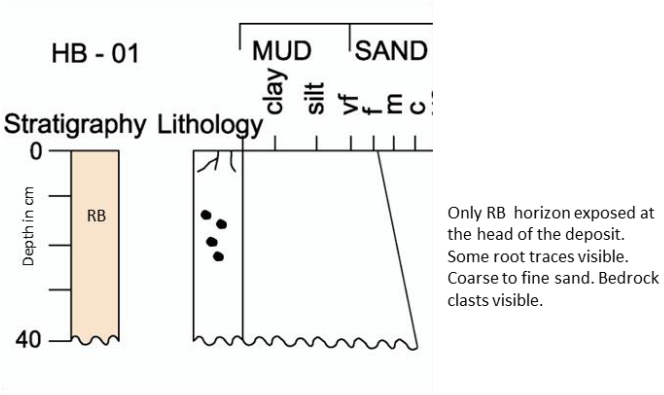


Figure 5.5b .The stratigraphy at the bone bed is similar to that at Area 1 and therefore the same symbols are used (Figure 5.5a). BT_1 appears to have been incorporated into the bone bed.

a) HB-01





b) HB-02



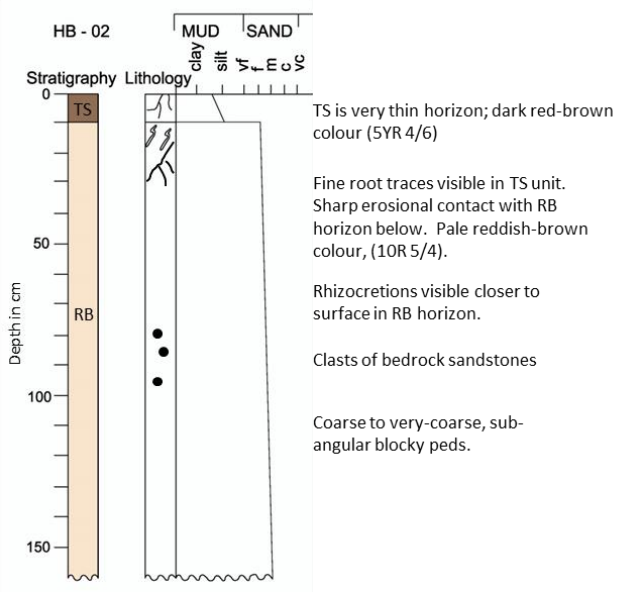
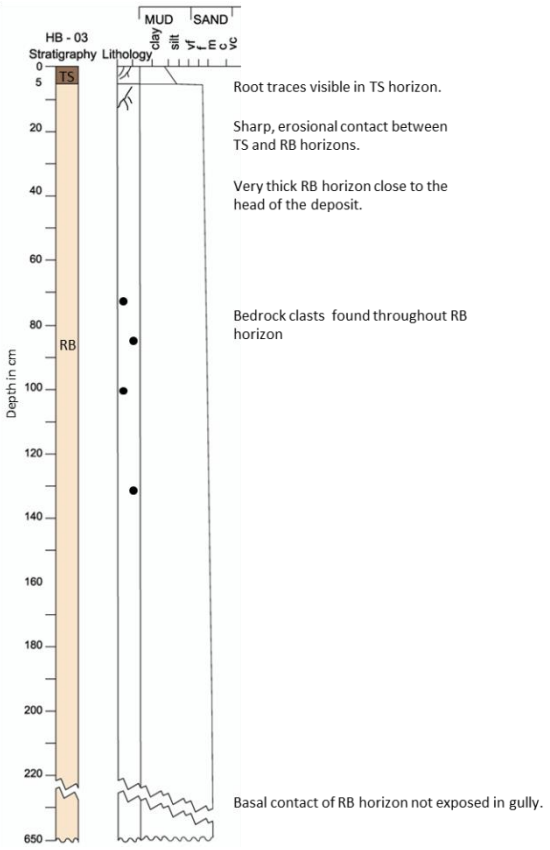


Figure 5.6 Photographs, stratigraphy and lithology of a) HB-01 and b) HB-02. Key for stratigraphy and lithology are provided at the end of the profiles.

c) HB-03





d) HB-04



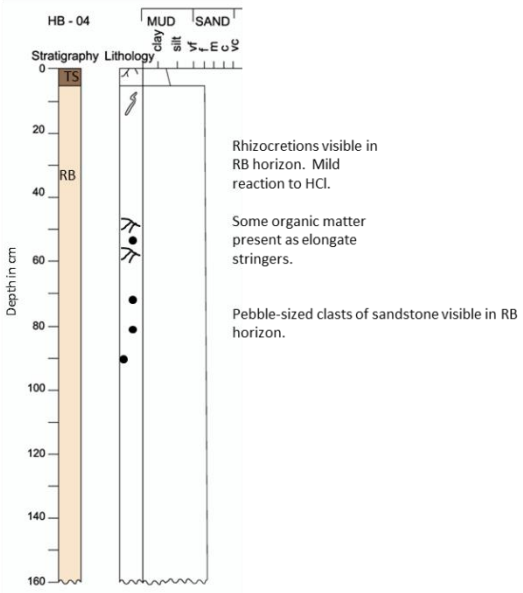
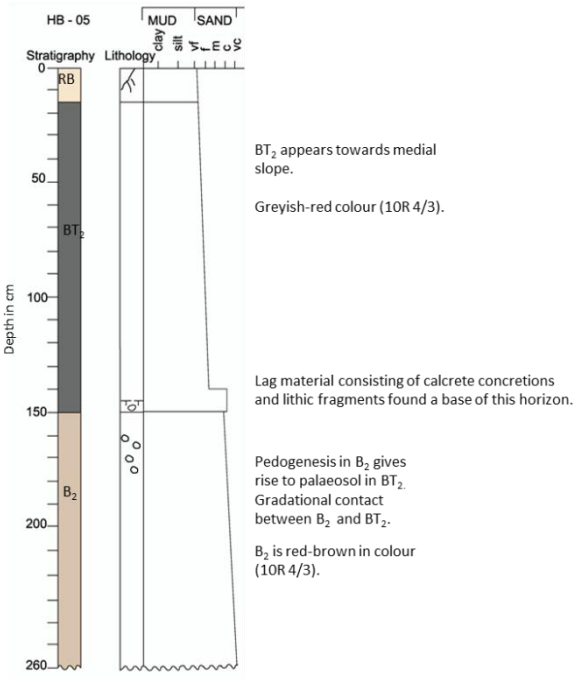


Figure 5.6 (continued) Photographs, stratigraphy and lithology of c) HB-03 and d) HB-04. Key for stratigraphy and lithology are provided at the end of the profiles.

e) HB-05





f) HB-06



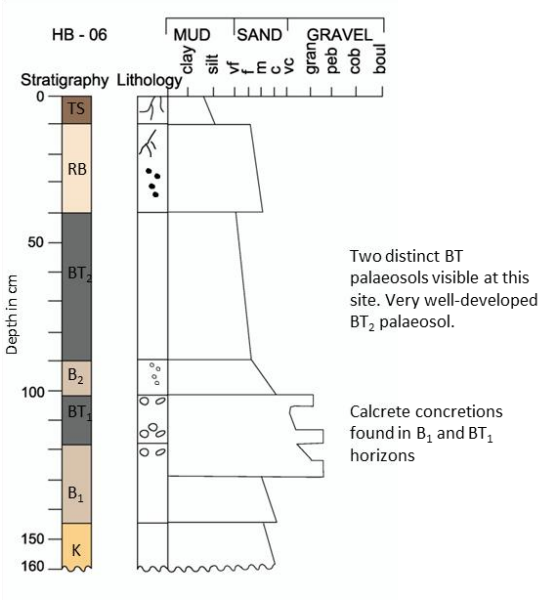
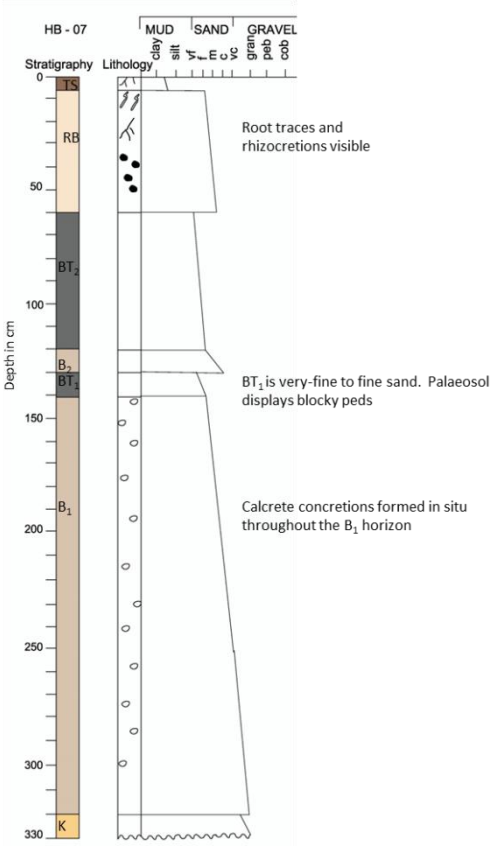


Figure 5.6 (continued) Photographs, stratigraphy and lithology of e) HB-05 and f) HB-06. Key for stratigraphy and lithology are provided at the end of the profiles.

g) HB-07





h) HB-08



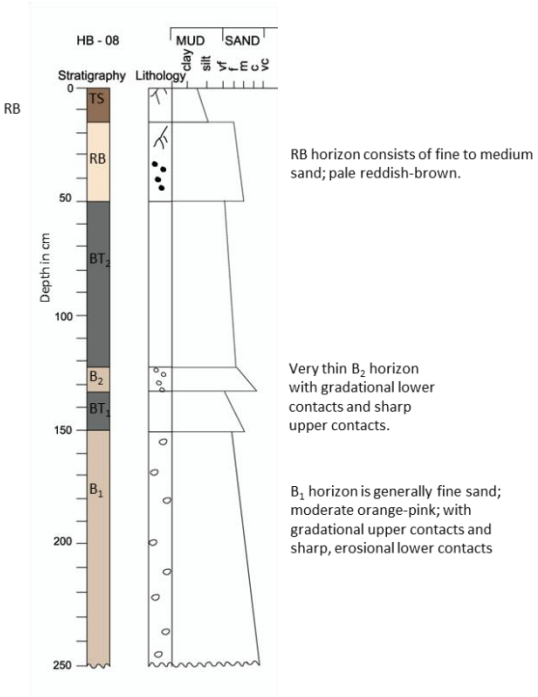
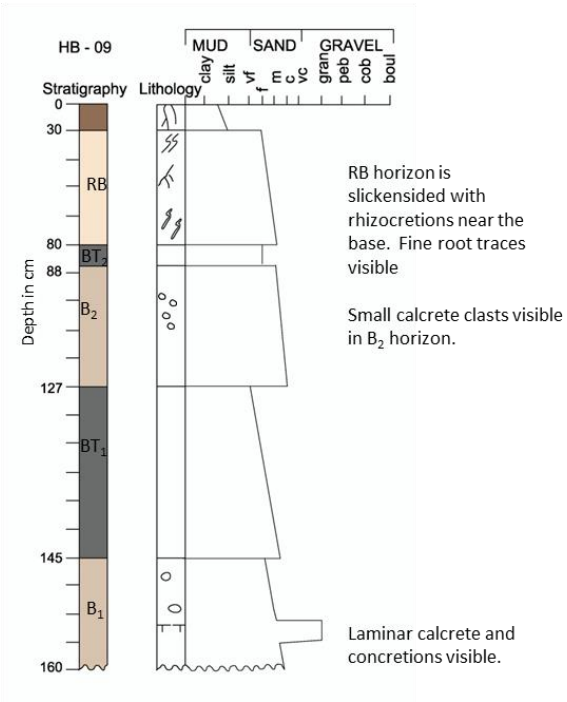


Figure 5.6 (continued) Photographs, stratigraphy and lithology of g) HB-07 and h) HB-08. Key for stratigraphy and lithology are provided at the end of the profiles.

i) HB-09





j) HB-10



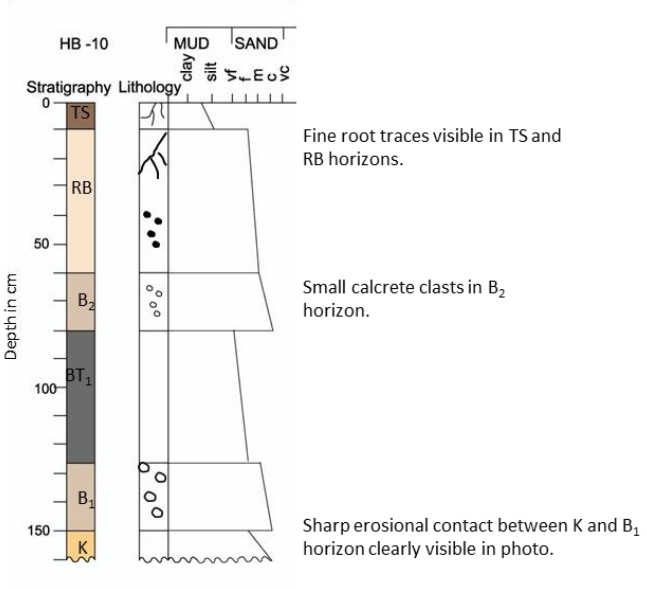
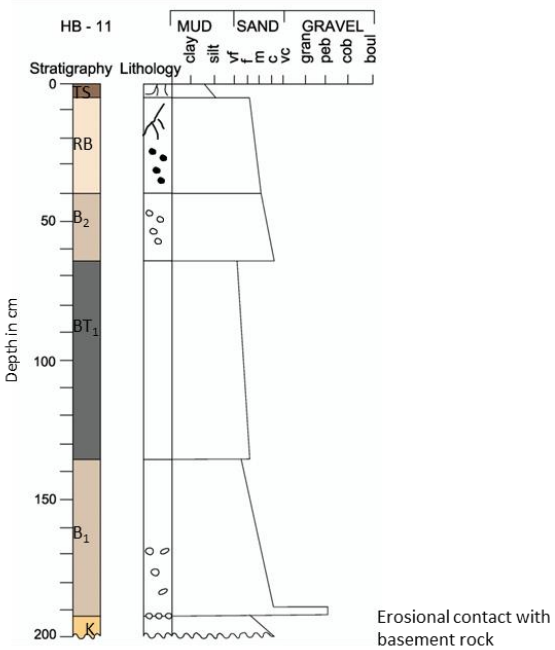


Figure 5.6 (continued) Photographs, stratigraphy and lithology of i) HB-09 and j) HB-10. Key for stratigraphy and lithology are provided at the end of the profiles.

k) HB-11





l) HB-12



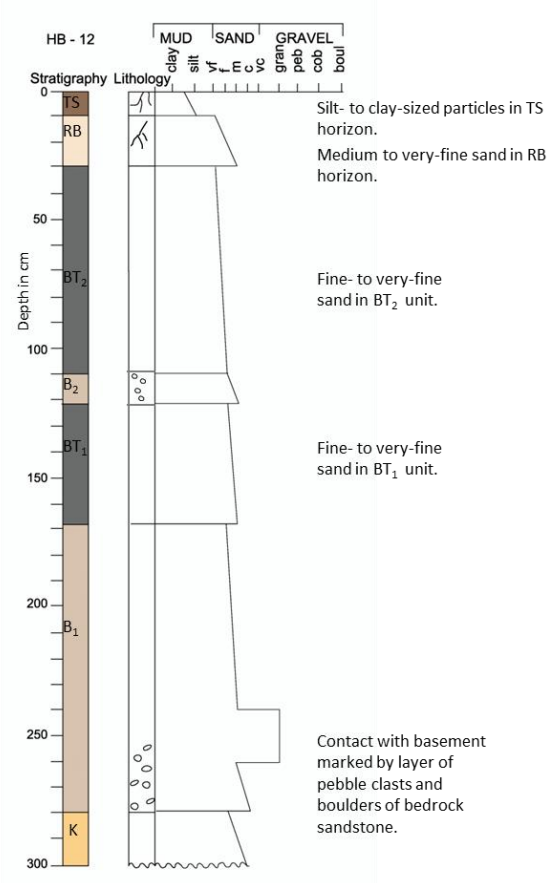
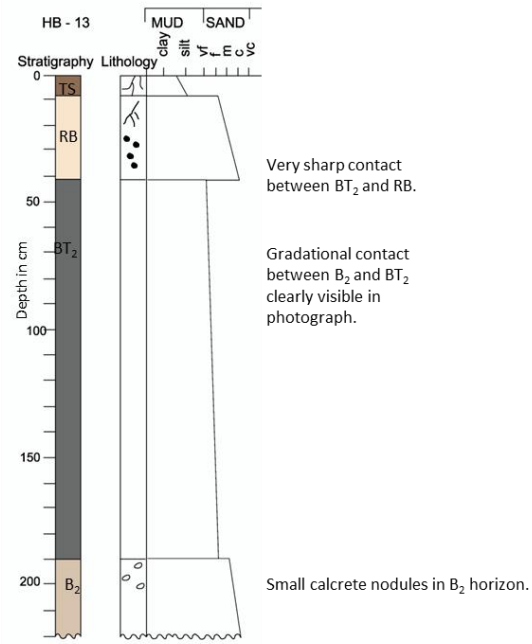


Figure 5.6 (continued) Photographs, stratigraphy and lithology of k) HB-11 and l) HB-12. Key for stratigraphy and lithology are provided at the end of the profiles.

m) HB-13





n) HB-14



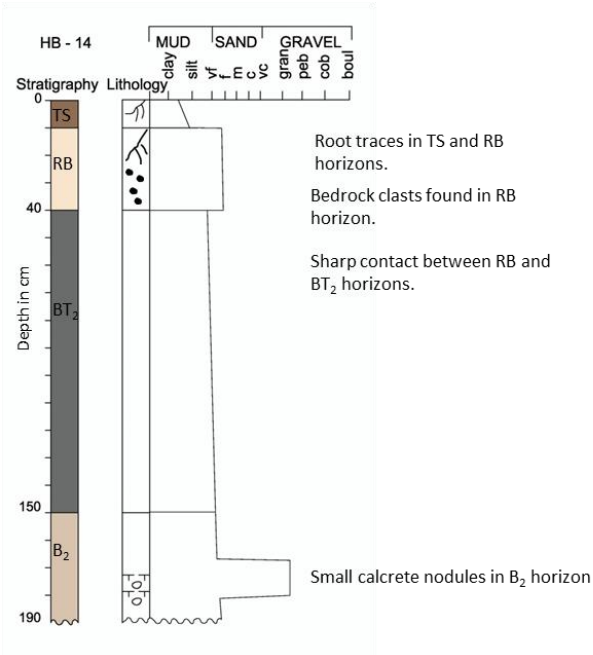


Figure 5.6 (continued) Photographs, stratigraphy and lithology of m) HB-13 and n) HB-14. Key for stratigraphy and lithology are provided at the end of the profiles.

o) HB-15, 16, 17



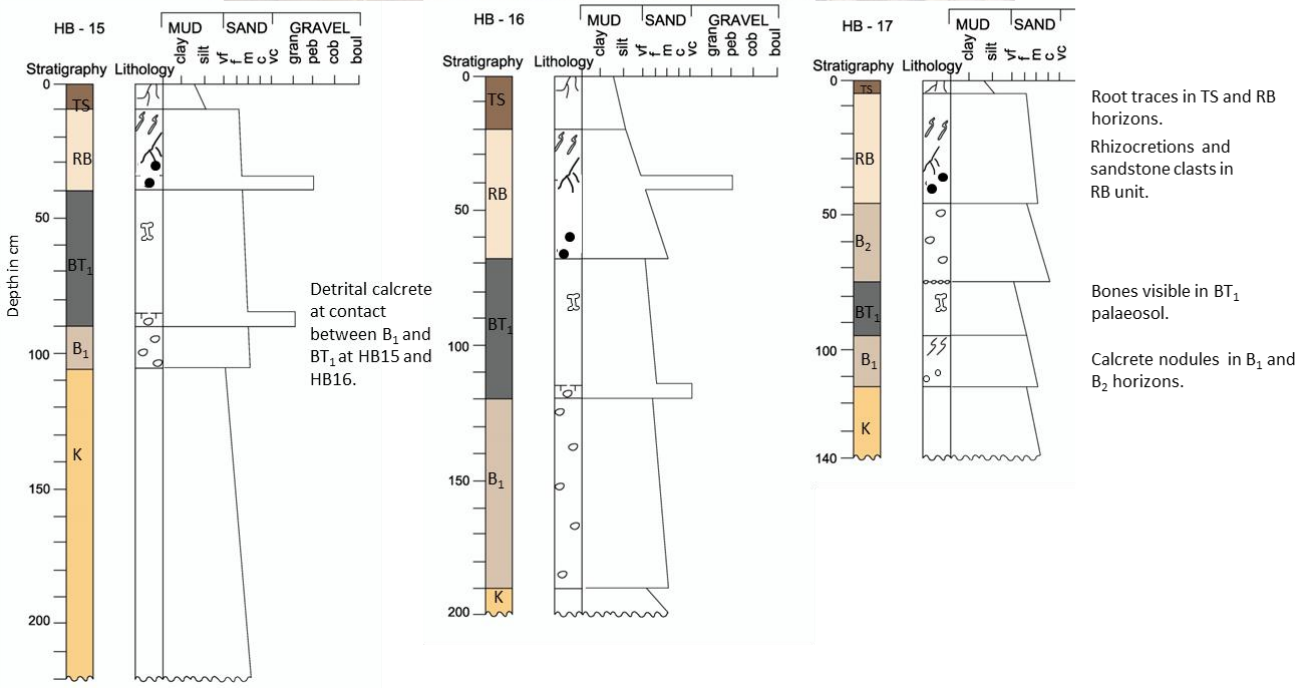
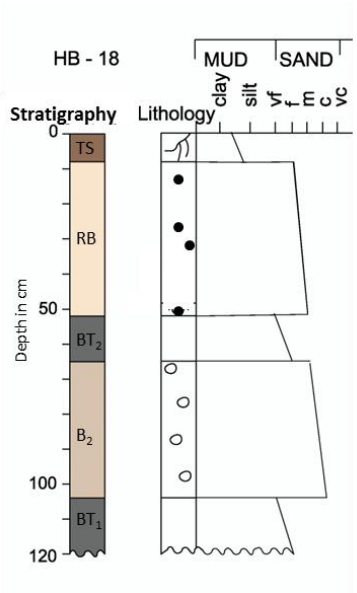


Figure 5.6 (continued) Photographs, stratigraphy and lithology of 0) HB-15, HB-16, and HB-17. The sections were taken at the base of the hillslope at the bone bed section. The three sites are next to each other along the profile, however part of the section had been excavated before the photograph was taken. Key for stratigraphy and lithology are provided at the end of the profiles.

p) HB-18





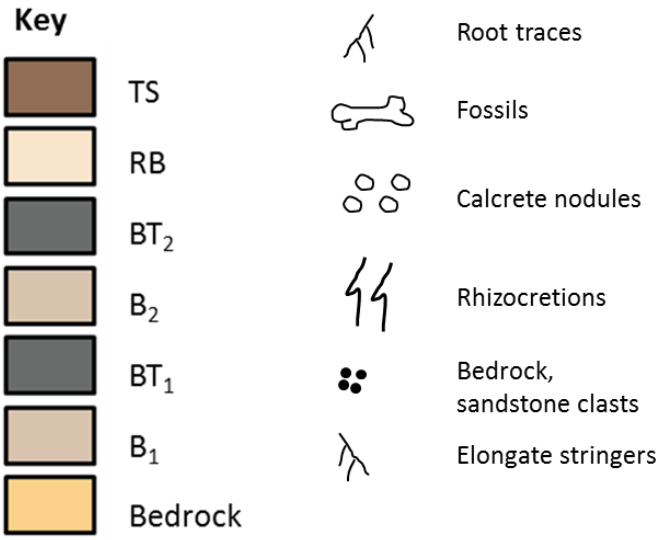


Figure 5.6 (continued) Photographs, stratigraphy and lithology of selected sample sites at Area 1, 2 and the bone bed. Key for stratigraphy and lithology is provided. Depth on all stratigraphic profile is in cm from the surface. Detailed descriptions of the horizons are provided in the text.

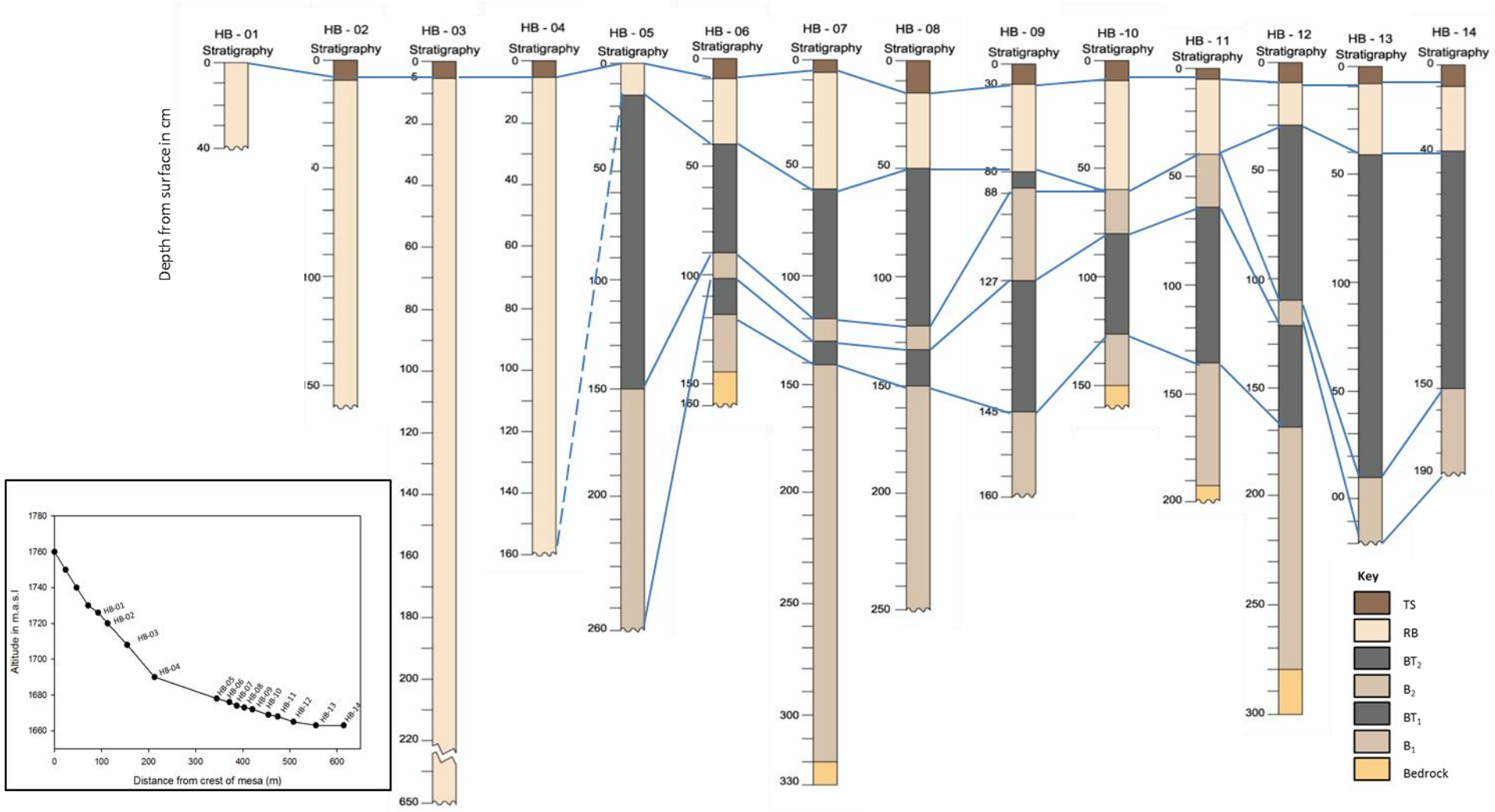


Figure 5.7 A summary of the depositional and erosional sequences of the Heelbo hillslope. Not drawn to scale but shows the stratigraphic relationships of each unit. (Inset: position of stratigraphic profiles relative to the slope). Bedrock is not exposed at all sites.

5.3.1 Karoo Basement

The Karoo basement material is the heavily weathered sandstone and siltstone of the Elliot Formation, as described by Bordy *et al*. (2004a; b). The Karoo basement lies unconformably beneath the sedimentary deposit and the contact is always a sharp, undulating erosional contact, which was expected due to the younger age of the sedimentary package. The surface profile of the deposit is sub-parallel to the bedrock profile (Figure 5.8).

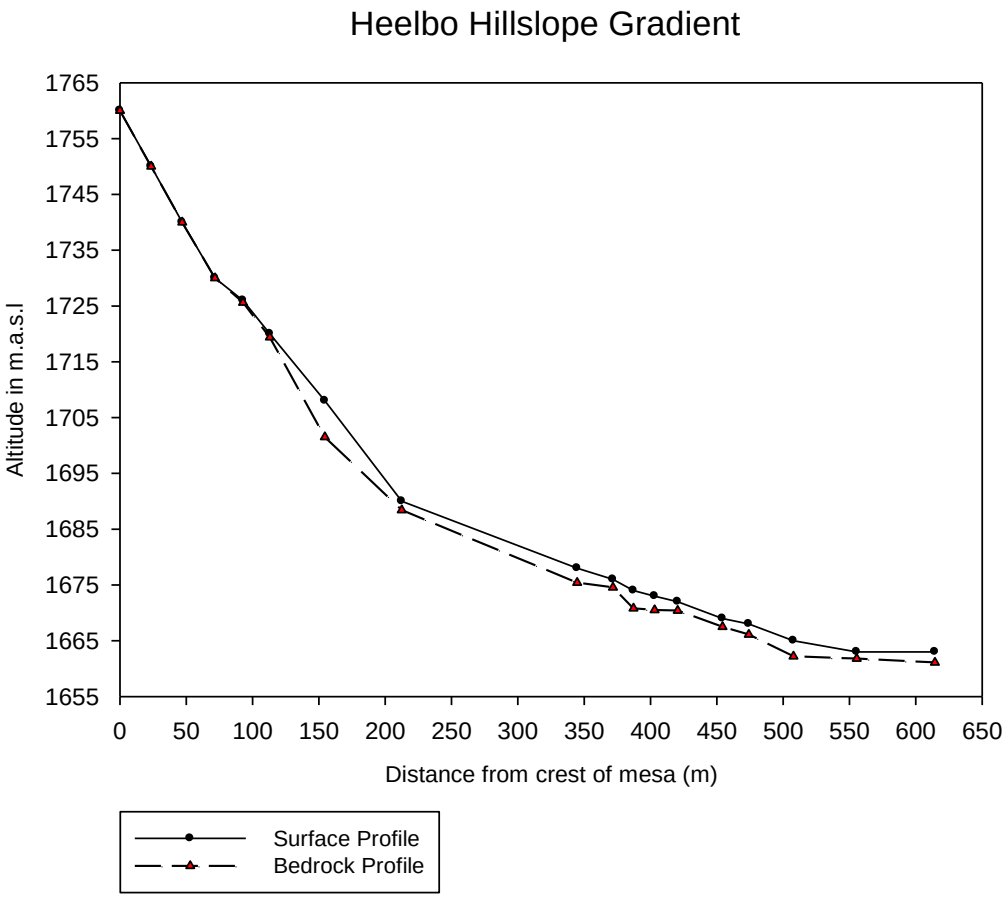


Figure 5.8 Relative altitudes of the surface of the deposit and the underlying bedrock.

At site HB-12 (towards the base of the slope), the contact is marked by a layer of pebbles, cobbles and boulders up to 68 cm in diameter, of the weathered material from the upper Karoo stratigraphy that accumulated at the base of the slope after weathering and erosion. There are clasts of Karoo rocks incorporated in higher sedimentary units (discussed in the relevant stratigraphic unit). These clasts range in size from microscopic lithic fragments (~0.2 cm) (which were confirmed in thin section) to over 5 cm in diameter. The underlying bedrock was found in undulating highs and lows throughout the deposit (Figure 5.8), and this may have had some initial effect on the morphology of the sedimentary system. There are two distinct colours of basement rock namely reddish brown (5R 4/2) and yellowish (10YR 7/4) and lithic fragments of these can be seen in Figure 5.9.

At a microscopic level the basement rock at both Area 1 and Area 2 reveals a mature siltstone / sandstone that comprise mostly quartz grains that are sub-angular to sub-rounded and well-sorted, as seen in thin-section (Figure 5.9). Calcite needles and feldspars in the form of plagioclase are also visible. The grains are supported with carbonate cement that has a moderate reaction to dilute HCl. There are few to no cavities or pores spaces between the grains and there are traces of hematite staining on the grains.

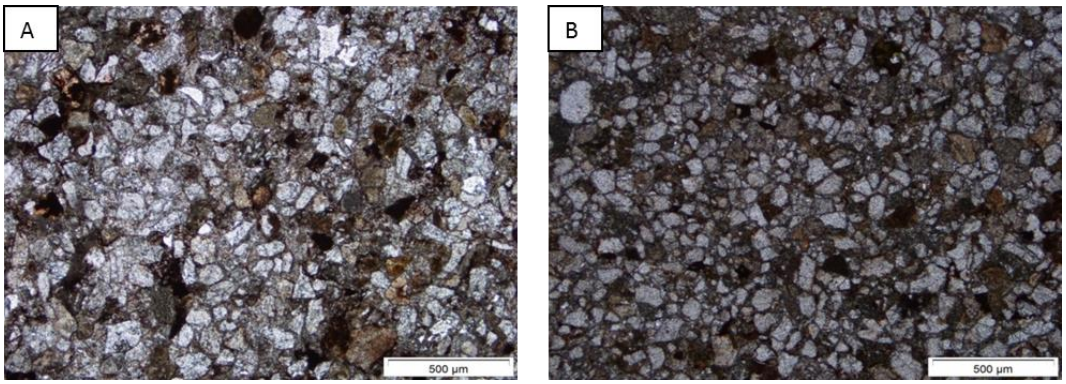


Figure 5.9 Photomicrograph showing the bedrock material at Area 1 (A) and Area 2 (B). Closely packed, matrix supported grains are visible with some hematite staining.

5.3.2 Brown Sediment Horizon (B_1)

The Brown Sediment horizon (B_1) is the oldest of the sedimentary horizons within the hillslope deposit. The first brown, sandy, sediment layer (B_1) comprises generally fine sand but does display some variation in grain size. It also displays variation in colour from a brown, general Munsell Reference of 10R 7/4 (moderate orange pink) to a more reddish colour 10R 5/4 (pale reddish brown). The red tinge is ascribed to weathering of the surface of the horizon. The horizon ranges in thickness from about 15 cm to over 1 m, with the thickest exposure found in the medial section (see HB-07 in Figure 5.7) of the deposit. The upper contacts are all gradational with the overlying BT_1 palaeosol whereas the lower contacts are all sharp, erosional contacts as the layer overlies the Karoo basement unconformably, with a distinct pebble-bed or conglomeratic basal contact between the two.

Root traces and burrows are present in the B_1 horizon and grey reduction haloes formed, probably due to the decay of the roots. Calcrete nodules (very hard calcite-cemented carbonate deposit) approximately 2 cm in length, are common within this horizon and many have been partially eroded and protrude from the weathered surface. The calcrete nodules appear to have formed *in situ* and may reflect environmental conditions prevalent at their formation (as calcrete nodules form in dry conditions where evaporation exceeds precipitation). The reaction to 10 % HCl of the B_1 horizon is weak but becomes stronger close to the calcrete nodules. Elsewhere in the deposit these calcrete nodules can be found as a detrital layer which has been washed in – suggesting that some of these nodules have been liberated from the B_1 horizon and reworked into the later strata of the deposit. There are no distinguishable depositional features such as layering or bedding within the horizon.

In thin section, pale yellow (5Y 7/4) lithic fragments (1 mm) identified in B_1 at both Area 1 and Area 2 are generally sub-angular with a low sphericity (Figure 5.10). The quartz grains are sub-angular to sub-rounded similar to the bedrock material, but are matrix-supported. At site HB-05 the B_1 sediment contains dark red lithic fragments (Figure 5.10) whereas at HB-08 and HB-12 hosts both the dark red and yellow-brown fragments. These lithic fragments are Karoo siltstone and mudstone. The samples also display a variable matrix colouring probably due to very-fine- grained authigenic minerals which are too small to identify individually, with HB-12-

B_1 tending towards a greyish-yellow hue. Calcite is also visible in thin-section.

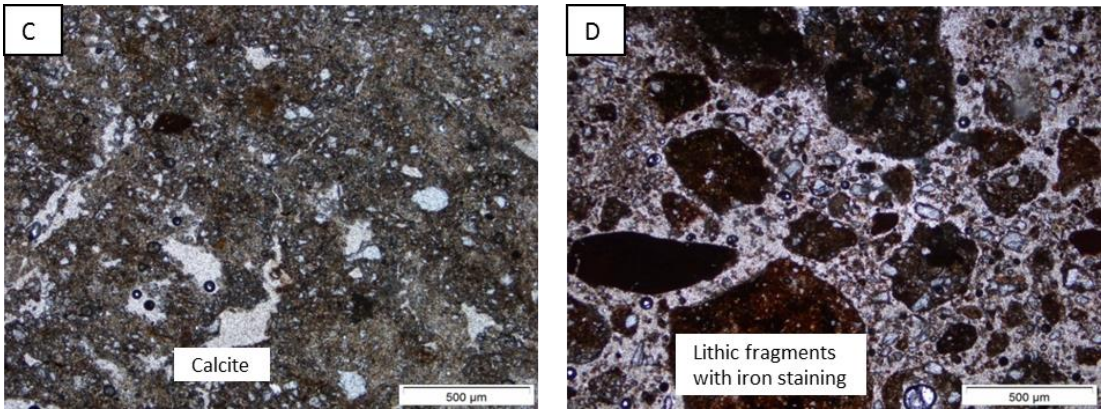


Figure 5.10 Photomicrograph showing B_1 at Area 1 (C) and Area 2 (D).

5.3.3 Black Turf (BT_1) Palaeosol

The BT layers are considered to be true soil and represent the A-horizon of a palaeosol. The BT_1 horizon is a dark, humus-enriched, vertisol and the dark colour is an indication of the presence of high organic matter content or a combination of organic matter and clay minerals (Samadi *et al*., 2005). The BT_1 palaeosol is not present in the proximal section of the deposit but makes its first appearance on surface some distance down the slope (and in the stratigraphic logs (Figure 5.7)) at HB-05. The thickness of the horizon is an indication of how well suited the original ground was to soil formation. The colour of the BT_1 unit is greyish red (10R 4/3) and the soils formed from the underlying B_1 unit.

The BT_1 horizon is very-fine to fine sand and ranges between 15 cm and 150 cm in thickness (Figure 5.7). Root traces are common and there are burrows that have been filled in by coarse-grained sediments. The infill becomes lighter in colour with depth, which may be due to the leaching and redeposition of calcium carbonate. The upper contacts of the layer are generally sharp erosional contacts whereas the observable lower contacts are gradational. The palaeosol displays generally blocky peds. Small (< 3 mm) calcrete nodule clasts are common near the upper part of the BT_1 palaeosol and the reaction to HCl is stronger nearer to these clasts, than lower down in the horizon where there is virtually no effervescence. The small size of these calcrete clasts compared to those in the B_1 horizon and their position at the upper contact of the palaeosol indicates that the clasts were eroded from the B_1 horizon and deposited in the BT_1 horizon.

The stratigraphic horizons for Area 1 and Area 2 are similar to those of the bone bed site, except for the BT_1 horizon (Figure 5.5b). The bone bed overlies the B_1 horizon and has incorporated the BT_1 unit. The BT_1 horizon at the bone bed section lacks the sedimentary structures of the same horizon at the other two areas. The fossils are located in what is thought to be a depression (L. Backwell, *pers comm*.), which created a water-hole where the animals could drink. As local lake or pool development would inhibit vertisol formation, the bone-bed is equivalent to the BT_1 horizon, but the actual BT lithofacies is absent here. The BT horizon is greatly

disturbed through the trampling and struggling of the animals found here. This mixing of the sediment makes it difficult to date using the OSL method (see Chapter 6). The fossils have been buried in the BT_1 horizon, which is located between 28 cm and 1.5 m below the surface and is between 20 cm to 1 m thick. The BT_1 horizon at the bone bed also contains detrital calcrete which was liberated from the underlying B_1 horizon, similar to that found at Area 1.

Thin sections prepared from the lower palaeosol (BT_1) (Figure 5.11) show many similarities to the B_1 horizon. The unit consists of quartz and feldspar grains with some lithic fragments. There are numerous pore spaces and cavities, some as much as 2 mm in length, which are possibly root-holes or burrows.

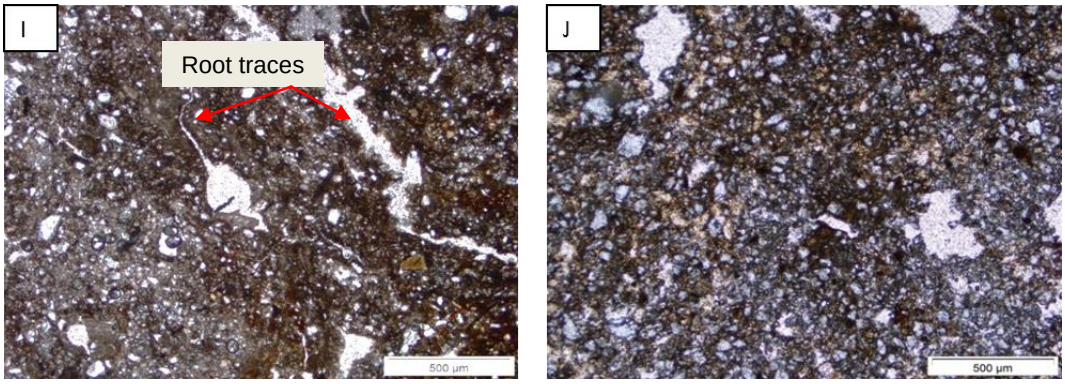


Figure 5.11 Photomicrograph showing BT_1 at Area 1(I) and Area 2 (J) (HLB 8, 12). Photomicrographs were taken under plane polarised light (PPL).

The same red and yellow lithic fragments as described previously are present with organic coatings. Within the matrix there are very small red lithic fragments composed of the original matrix material and small quartz

and feldspar grains. There is evidence of micro-horizons (Figure 5.12) where the groundmass alternates between yellow-brown and grey-black layers. A black groundmass is commonly due to the presence of organic matter whilst a grey groundmass indicates less organic matter or is produced by the presence of, or weathering of, clays, feldspars and carbonates (Aguilar *et al*., 2002). Furthermore, the cavities are concentrated within the darker layers and thus may be related to decomposition or bioturbation processes.

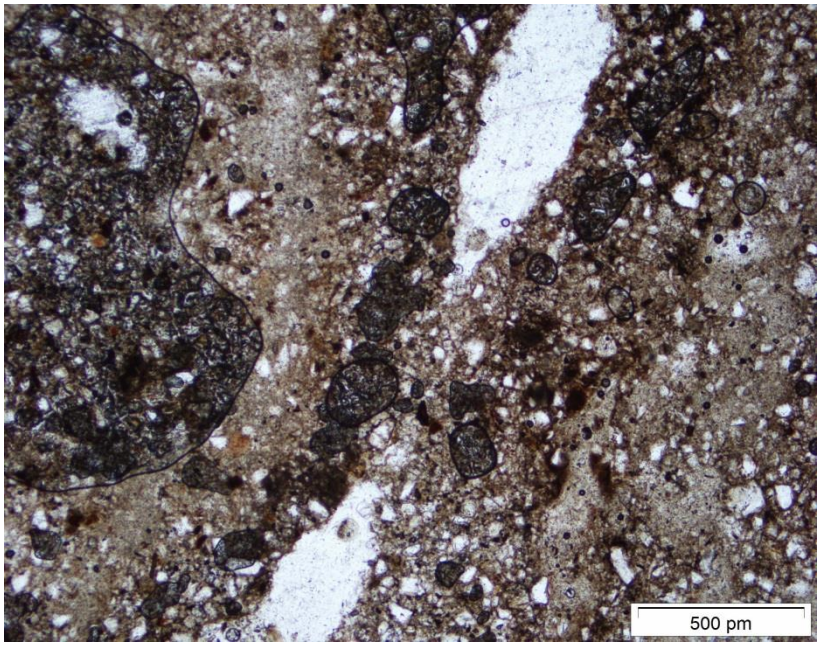


Figure 5.12 Thin section photomicrograph of BT_1 horizon at HB-10, with porosity in the form of cavities that have not been infilled. The orientation of the layers is near-horizontal.

5.3.4 Brown Sediment Horizon (B_2)

The second brown, sandy, sediment (B_2 horizon) shows variation in grain size from fine to coarse sand and a thickness from 12 cm to 115 cm (Figure 5.7). There is a discernible change in colour from red-brown (10R 4/3) to a lighter yellow-brown (5R 4/2) upwards through the unit (Figure 5.13).

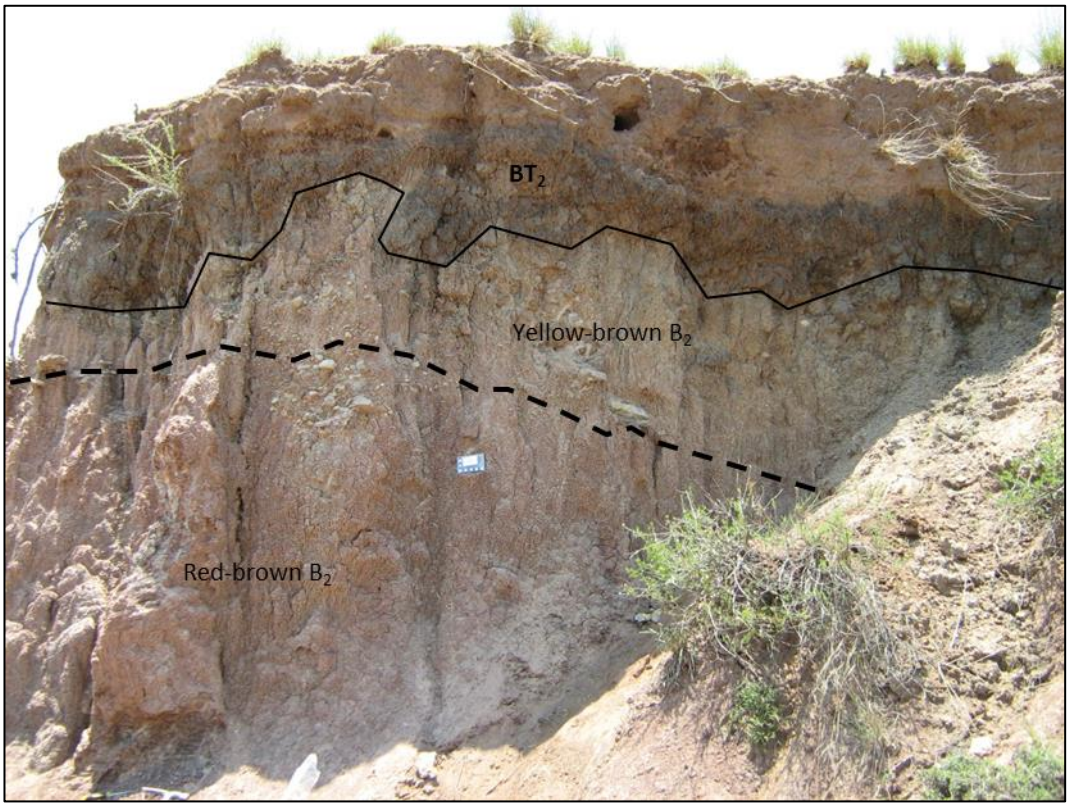


Figure 5.13 Colour changes from red-brown (10R 4/3) to yellow-brown (5R 4/2) in B_2 horizon at site HB-06.

The B_2 horizon hosts numerous calcrete and sandstone pebbles and clasts at the point where the change in colour and grain size occur. A

possible explanation may be that the top of the layer represents B_2 whilst the finer-grained, lower portion is actually the B_1 horizon, with the intervening BT_1 palaeosol having been eroded away; however, this cannot be proved conclusively. The lower contacts with the underlying BT_1 are generally sharp, but the upper contact with BT_2 is gradational. The B_2 horizon displays a large proportion of root traces together with numerous small (< 1cm) calcrete clasts not usually observable on the weathered face, and weak to moderate effervescence with 10% concentration of HCl. Very fine laminations are present in this horizon. As these are less than 2 mm in thickness they are easily overlooked.

Towards the distal reaches of the deposit the B_2 sandy sediment occurs as a thin (~20 cm) lens as it pinches out of the sequence. It still maintains sharp lower and gradational upper contacts with the BT palaeosols.

Thin sections were prepared from the B_2 horizon. The quartz grains are sub-angular to sub-rounded. In addition to the small quartz grains, the heavily altered feldspars that are breaking down to form the clay minerals are observable as grey aggregates (Figure 5.14). These are visible in both sections.

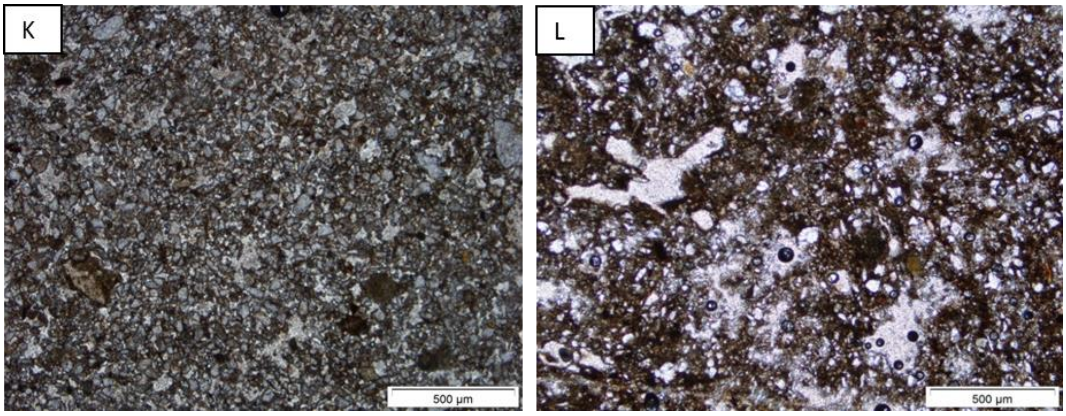


Figure 5.14 Photomicrograph of B_2 horizon at Area 1(K) and Area 2 (L), taken under plane polarised light (PPL).

The lithic fragments visible towards the top of the horizon are the typical dark red-brown and yellow-brown varieties mentioned above, whilst the base of the horizons hosts only the former (Figure 5.15). B_2 at HB-12 contains fragments that are so dark red in colour that they appear black. Lithic fragments together with altered feldspars have been fractured by burrows and root traces in all three samples (Figure 5.15)

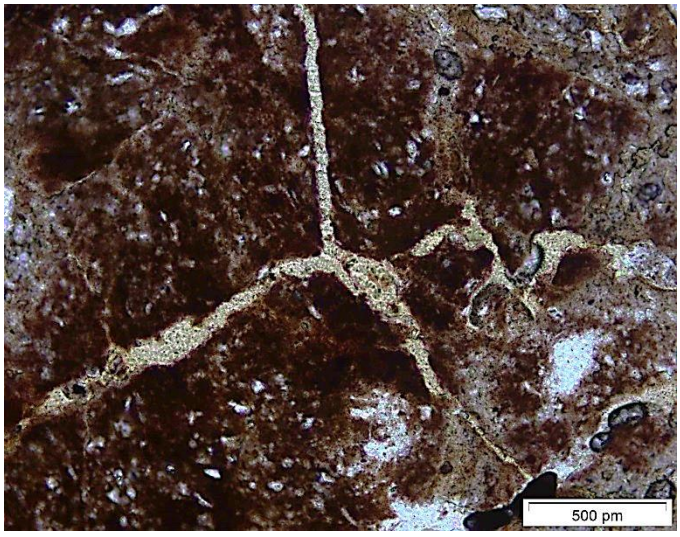


Figure 5.15 Photomicrograph of a lithic fragment that has been fractured by roots in B_2. Photograph taken under plane polarised light (PPL).

Furthermore, the matrix of all three samples is variable in colour with grey, yellow and brown hues. The B_2 (top) sample, at HB-06, hosts carbonate veins large enough to be clearly observable, in the form of calcite, within the yellow lithic fragments (Figure 5.16).

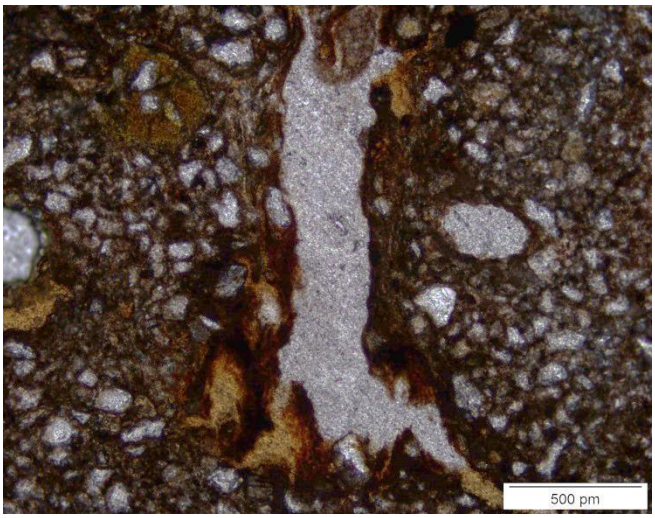


Figure 5.16. Photomicrograph of the thin section showing a calcite veinlet cross-cutting a lithic fragment in B_2 at HB-06, taken under plane polarised light.

5.3.5 Black Turf (BT_2) Palaeosol

The upper palaeosol (BT_2) is similar in characteristics to the BT_1 palaeosol as it is organic-rich and grey-red in colour (10R 4/3). It has a gradational contact with the underlying B_2 horizon but a sharp contact with the overlying RB horizon. It comprises very-fine to fine grained sand and is generally between 11 cm and 150 cm thick (Figure 5.7). It is characterised by a large number of root traces and displays a moderate reaction to 10% concentration of HCl. The peds are generally sub-angular, blocky and

relatively well-defined although some of the peds observed display a more columnar appearance in relation to the other sites. The two black turf palaeosols are not always visible together in the deposit. However, at site HB-09 the two horizons are clearly visible as two distinct units (Figure 5.17).

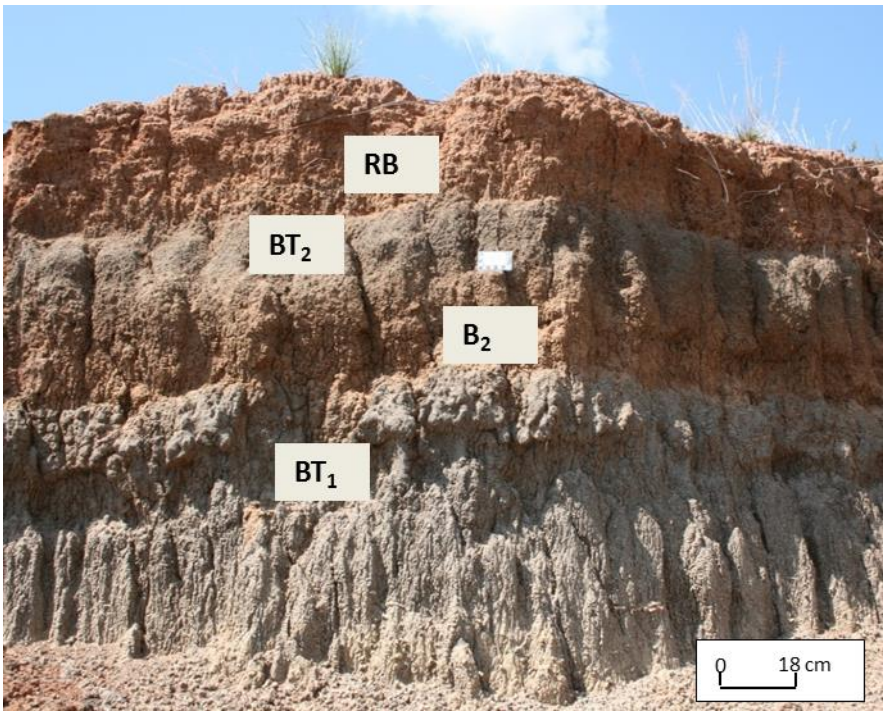


Figure 5.17 Two distinct black turf palaeosols can be seen at site HB-09.

The thin sections of BT_2 prepared from sites HB-06 and HB-13 (Figure 5.18) both show a well-developed soil texture with small sub-angular grains hosted in a fine-grained matrix. However the grains at HB-13 are larger and more angular with pore spaces that are more uniformly sized and spaced. At HB-06 dark red lithic fragments are present in a yellowish-brown groundmass most likely due to the Fe-hydroxide goethite. HB-13 has a much more prominent yellowish-hue to the groundmass, with

numerous yellow and very few dark red lithic fragments. The yellow lithic fragments are found at HB-13 and are generally sub-angular with a low sphericity (Figure 5.18). Detrital calcite is found at this level and there are also numerous cavities within the palaeosol.

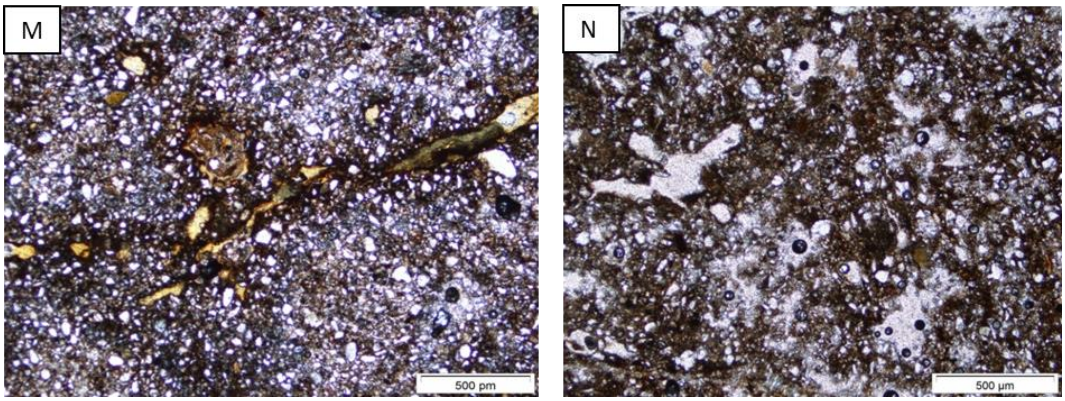


Figure 5.18 Photomicrograph of BT_2 at Area 1 (M) and Area 2 (N), taken under plane polarised light. Cavities and yellow lithic fragments are visible.

Many of the fragments in both slides are surrounded by black oxide coatings (Figure 5.19). In the HB-13 thin section there is a distinctive burrow feature which possibly represents infilled pore spaces.

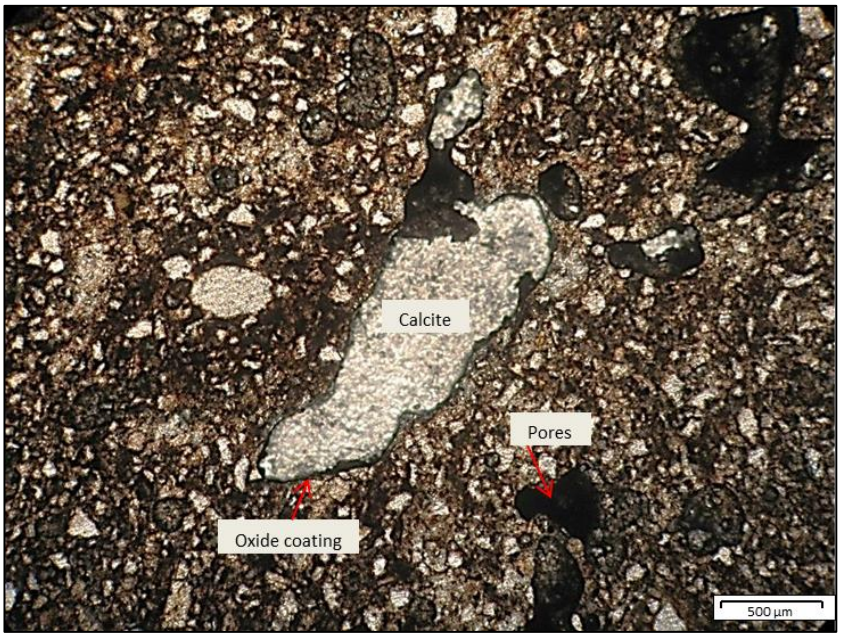


Figure 5.19. The black oxide coating found on lithic fragments and quartz grains is noticeable in the photomicrograph of BT_2 at HB-06, taken under plane polarised light (PPL). A calcite fragment is also visible with an oxide coating.

Downslope from site HB-09 the first and second cycle BT palaeosols merge to form a very thick, single, BT layer which was sampled as a single layer at site HB-10. The palaeosols then separate again further downslope into two distinct layers which were sampled at site HB-12 (see Figure 5.7).

5.3.6 Red Brown (RB) Horizon

The red brown (RB) sedimentary horizon overlies the BT_2 palaeosol. The RB horizon varies greatly in thickness from about 20 cm to over 6 m (Figure 5.7) and consists of a fine to medium sand with a pale, reddish-brown (10R 5/4) colour. The red colour indicates a significant quantity of

oxidised iron in the soil (Samadi *et al*., 2005). The thickest part of the deposit is found in the proximal reaches of the hillslope where the layer directly overlies the basement.

The RB horizon contains calcrete rhizocretions and displays a moderate reaction to 10% concentration of HCl. The presence of these sparse rhizocretions and matrix carbonates suggests that the sediment has undergone some diagenesis. The RB unit contains organic material in the form of sparsely distributed angular to elongate stringers up to 5 cm in length. Pebble-sized clasts of bedrock sandstones are present and distributed throughout the unit. The pebble clasts are between 1 cm and 15 cm in length, and are interpreted as clasts deposited during high energy flow events. Coarse to very-coarse, sub-angular blocky peds without cutans are found at HB-02 and at HB-03 (Figure 5.6). At HB-04 the peds are still medium – to – coarse, sub-angular and blocky but become slightly more columnar in appearance than at HB-02 and HB-03. The presence of these peds suggests that RB is possibly either an oxidised palaeosol that is poor in organic matter or a poorly-developed immature soil (see discussion in Chapter 7). Downslope of site HB-04 the contact between the RB horizon and the Karoo basement is observable. The basement rocks in the area undulate and so it is possible for entire depositional horizons to be missing over the basement highs.

The thin sections from the RB horizon show the quartz grains to be sub-angular within a dark red matrix (Figure 5.20). This degree of roundness

of the grains suggests short transport distances and little reworking of the grains. It is also possible that the particle roundness reflects the hardness of the source material rather than the nature of the transport processes. The lithic fragments are sub-angular to sub-rounded and highly spherical and as such, the possibility of wind-blown sediment as a source for the deposit is discounted. There are numerous pore spaces and cavities that have not been infilled. However, there is calcite cement that has formed around the edges of the pore spaces (Figure 5.20). Red lithic fragments were identified which are smaller than 4 mm in length and show fine grains of quartz surrounded by reddish-brown to dark-red cement, which is most likely hematite, with textural differences based on the amount of cement present. The groundmass has a variable colour, likely due to very-fine grained authigenic minerals which are too small to identify individually.

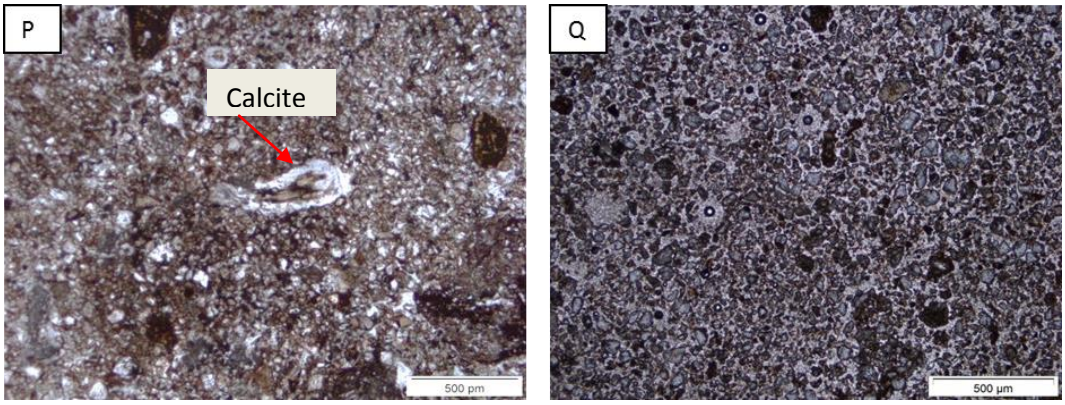


Figure 5.20 Photomicrograph of RB at Area 1(P) and Area 2 (Q) showing carbonate needles around the edge of a cavity. The photograph was taken under cross-polarised light (XPL).

5.3.7 Top Sediment Horizon (TS)

The top sedimentary layer represents the youngest depositional event of the sedimentary package. The layer is dark red-brown with a Munsell Reference 5YR4/6. The layer is relatively thin, with a thickness ranging between 14 cm and 62 cm, and the sediment comprises generally fine to medium silt with a sharp lower contact with the underlying RB. The unit contains a large amount of organic material such as plant roots, leaves (humus), seeds and numerous root traces and burrow structures. The TS horizon appears heavily weathered and the reddish colour suggests high iron content in the horizon; iron-staining is clearly visible on the surface of the deposit.

The thin sections indicate numerous quartz grains within a medium- to coarse-textured matrix. The red lithic fragments have been incorporated into the coarse matrix and the hematite staining is clearly visible on their surfaces. Rhizocretions have formed around a fine root structure (Figure 5.21). The horizon contains a large amount of organic matter such as roots and plants. This horizon supports most of the vegetation growing on the hillslope.

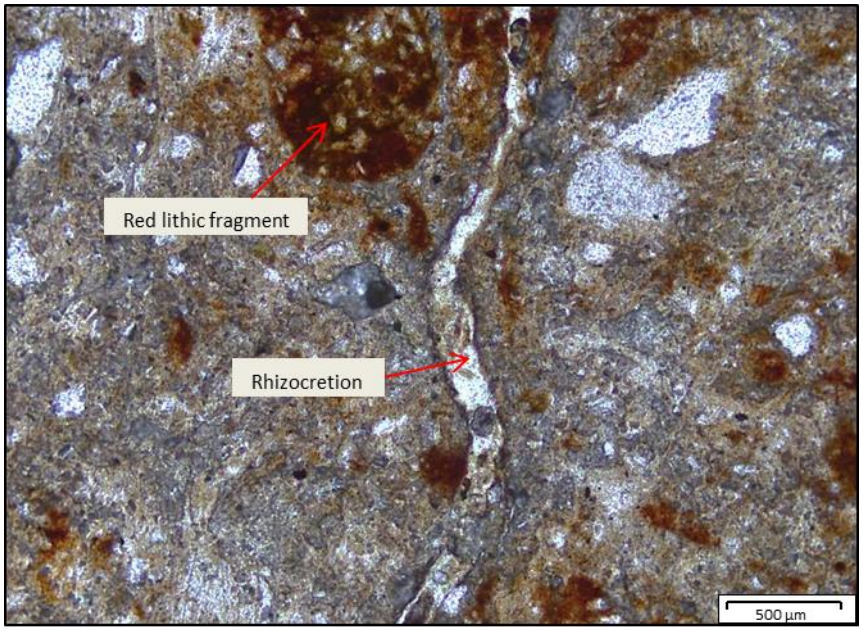


Figure 5.21. Photomicrograph of rhizocretions within a coarse matrix of the TS.

5.3.8 The Bone Bed Section

The bone bed section represents a remarkably dense and well-preserved fossil bone bed that extends approximately 400 m^2 and is situated about 1.5 m below the modern land surface, with the fossils exposed in a gully wall. The stratigraphy of the bone bed section is similar to that of the Areas 1 and 2 (Figure 5.5b). The detrital material left behind after the previous erosional cycle is exposed at the base of the sequence. B_1 was deposited on this pre-existing layer. There are numerous calcrete nodules visible in this horizon, ranging in size from microscopic to ~5 cm in diameter. The overlying BT_1 horizon is obscured by the presence of the bone bed. Preliminary investigations show that most of the faunal remains belong to the black wildebeest (*Connochaetes gnou*), with a single

hartebeest mandible located thus far. An estimated 70 animals were excavated (by Dr. L. Backwell from the University of the Witwatersrand) from the site and countless more may have been eroded away over time. The matrix is heavily calcretised. Fossils recovered were mostly complete, of mixed age-distribution, showed little damage caused by weathering, and no surface modifications (L. Backwell, *pers. comm., 2013*).

Several articulated limbs and vertebral series were found and one rib recorded pathology; there was also no distinct orientation in the long bones. A large fire place with abundant ash, charcoal, burnt, percussed and spirally fractured long bones indicated human activity at the site. A stone core and microlithic flake were found in the ash layer associated with the fire place, but their association with the fauna is unknown. A selection of LSA lithics have been collected from around the site, including a single flake from the middle of the bone bed in the donga wall. Radiocarbon ages of fossils found at the top and base of the section were 3610 +-110 BP and 4610 +-30 BP respectively (L. Backwell, *pers. comm*., 2013). Phytolith samples show an abundance of C_3 and short-cell phytolith morphotypes indicating drier and cooler conditions than at present (J. Brink, *pers comm*., 2013).

After a period of erosion the cycle of deposition and pedogenesis is repeated in the B_2 horizon and the BT_2 palaeosol, which overlies the bone

bed. Rhizocretions are recorded in the RB horizon, similar to that found in Area 1, and a thin layer of TS is preserved at the surface.

5.4 GRAIN SIZE ANALYSIS

As sediment moves down the slope either under the influence of gravity or through fluvial action there may be some sorting of the grain sizes, and this was investigated by means of a grain size analysis down the slope. Samples were collected from two units, the Top Sediment (TS) and the Red Brown (RB) horizon at Area 1 because these units are present over most of the deposit. The similarities in the stratigraphic horizons and palaeosols between Areas 1 and 2 and the bone bed were further supported by an analysis of the grain size distribution of these units. Therefore, further samples were collected from the vertical profiles at Area 1 and Area 2 and at the Bone Bed.

5.4.1 The Top Sediment Horizon

Histograms provide a graphical representation of the grain size distribution for each sample, where the weight percentage is plotted against the grain size (in µm) (Figure 5.22). In the proximal sections (HB-02 to HB-04) the higher micron units are in abundance. However, downslope of HB-04 the proportion of finer grained particles increases downslope.

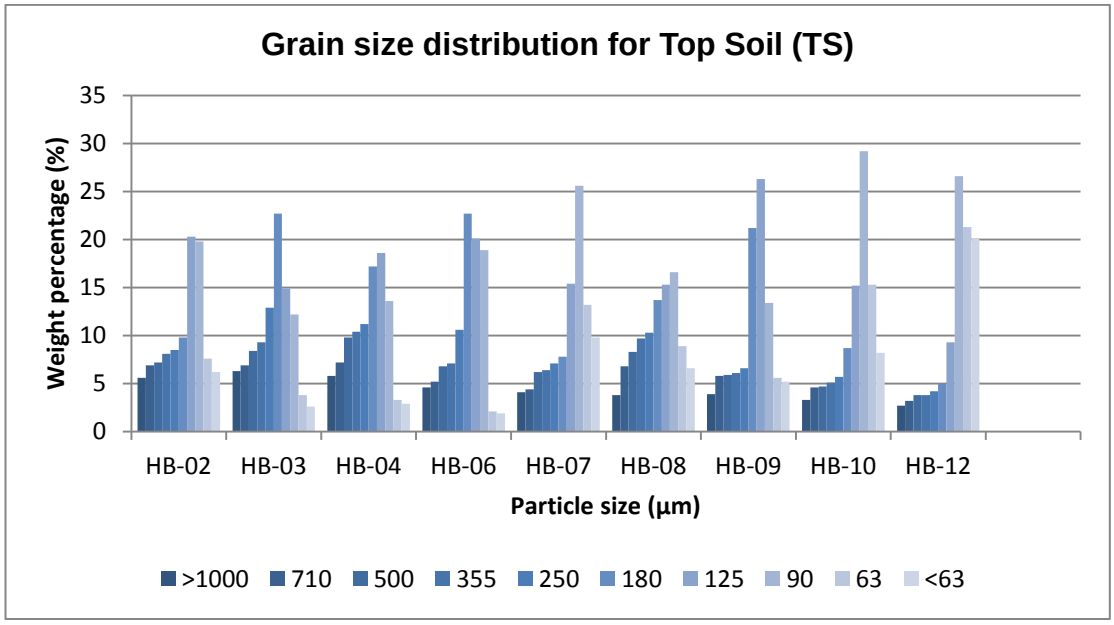


Figure 5.22 Histogram showing grain size distributions for the TS samples.

The grain size data was analysed using GRADISTAT to produce statistical values for the mean, median, mode, standard deviation, skewness and kurtosis (Table 5.1). For the proximal reaches (HB-02 - HB-04) the mean grain size is 240.3 µm, which is described as fine sand. The average sorting is 2.34, which is poorly sorted. However, in the distal reaches the mean grain size decreases to 180.4 µm, which indicates a slight fining of material; but the average sorting is 2.34, which is also poorly sorted.

The samples reflect an asymmetrical population where the skewness could be either fine (positive) or coarse (negative), indicating the dominant grain size fraction to be either fine-grained or coarse-grained respectively (Blott and Pye, 2001). The skewness values show 44% of the TS samples to be very coarse skewed and 56% to be coarse skewed (Table 5.1). Both

subsets are negatively skewed, indicating the dominant grain size fraction to be coarse grained.

Skewness and kurtosis are a measure of how closely the grain size distribution is to a normal Gaussian distribution. A single-source sediment would feature a fairly normal distribution (symmetrical and mesokurtic), whilst multiple-source sediments show pronounced skewness and kurtosis (Folk, 1980). The kurtosis values show that 44% of the grain size distributions are mesokurtic, 23% are platykurtic or relatively flat and 33% are leptokurtic or strongly peaked.

Thin section examinations revealed that the average roundness for the TS (Table 5.1) is sub-angular to sub-rounded for most of the samples. Only HB-07 tends towards sub-angular/angular, whereas towards the distal section of the slope the particles are more sub-rounded.

Table 5.1. Graphical mean, standard deviation, sorting and roundness characteristics of the TS.

	Folk and Ward Method (µm)				Description				
Sample	**Graphical Mean (M_G)**	**Sorting (σ_G)**	**Skewness (Sk_G)**	**Kurtosis (K_G)**	**Mean**	**Sorting**	**Skewness**	**Kurtosis**	**Roundness**
HB-02	210.9	2.48	0.31	0.92	Fine Sand	Poor	Very Coarse Skewed	Mesokurtic	Sub-angular / sub-rounded
HB-03	256.2	2.27	0.19	0.97	Medium Sand	Poor	Coarse Skewed	Mesokurtic	Sub-angular
HB-04	253.7	2.28	0.20	0.87	Medium Sand	Poor	Coarse Skewed	Platykurtic	Sub-angular / angular
HB-06	225.0	2.10	0.29	1.01	Fine Sand	Poor	Coarse Skewed	Mesokurtic	Sub-angular / sub-rounded
HB-07	165.0	2.50	0.35	1.08	Fine Sand	Poor	Very Coarse Skewed	Mesokurtic	Sub-angular
HB-08	214.3	2.44	0.15	0.90	Fine Sand	Poor	Coarse Skewed	Platykurtic	Sub-angular / sub-rounded
HB-09	207.5	2.24	0.25	1.30	Fine Sand	Poor	Coarse Skewed	Leptokurtic	Sub-rounded
HB-10	153.9	2.35	0.40	1.26	Fine Sand	Poor	Very Coarse Skewed	Leptokurtic	Sub-rounded
HB-12	116.5	2.40	0.32	1.41	Very Fine Sand	Poor	Very Coarse Skewed	Leptokurtic	Sub-rounded

5.4.2 The Red Brown Horizon

The Red Brown (RB) horizon underlies the Top Sediment (TS) unit. The histograms for the RB unit (Figure 5.23) reflect similar characteristics to the TS unit. As with the TS, the proximal hillslope for the RB unit shows an abundance of the coarser material from HB-01 to HB-05. Below HB-05 there is a steady change towards finer material down slope.

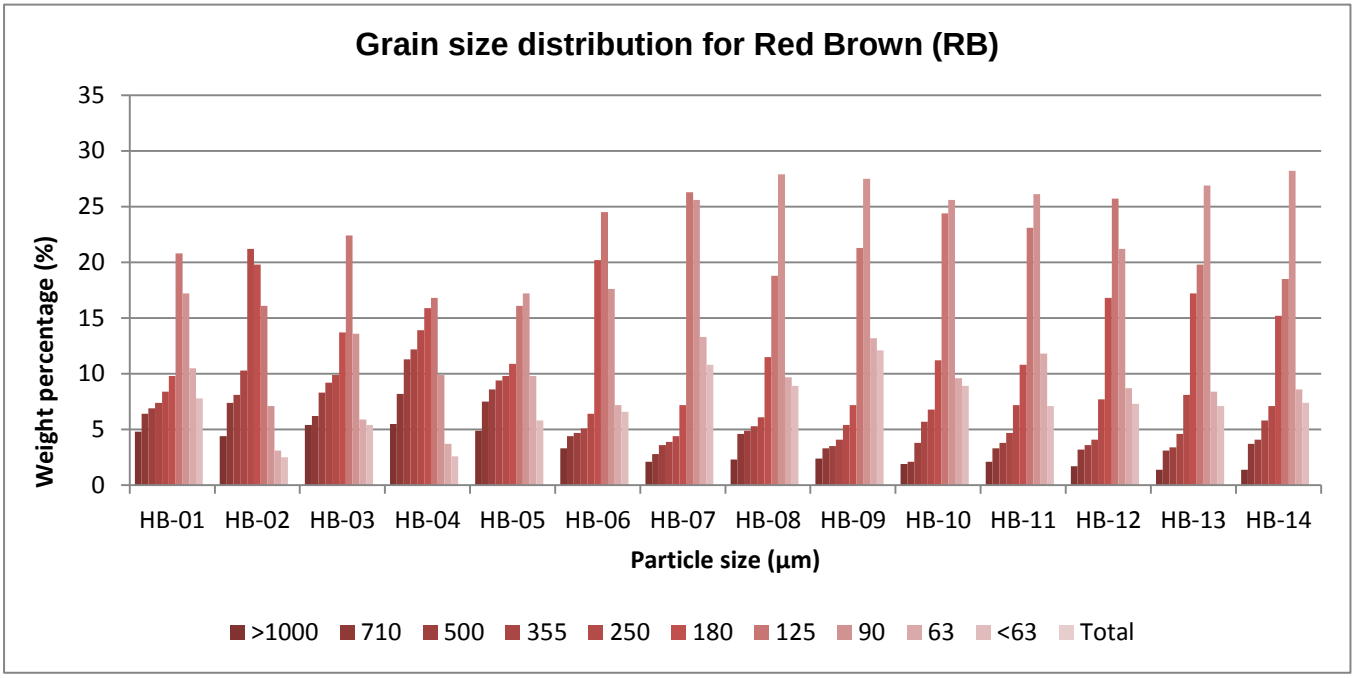


Figure 5.23. Histograms showing grain size distributions for the RB horizon which shows similar trends to TS.

As with TS, the grain size data for the RB horizon was analysed using GRADISTAT to produce statistical values for the mean, median, mode, standard deviation, skewness and kurtosis (Table 5.2). For the proximal reaches (HB-01 - HB-05) the mean grain size is 237.6 µm, which is

described as fine sand. The average sorting is 2.35, which is poorly sorted. However, in the distal reaches the mean grain size decreases to 171.1 µm, which indicates a slight fining of material; but the average sorting remains poor at 2.12.

The skewness values show that one sample, HB-08, is very-coarse skewed but all other samples are coarse skewed. All the samples are negatively skewed, indicating the dominant grain size fraction to be coarse grained.

The kurtosis values show that 22% of the grain size distributions are mesokurtic, 14% is platykurtic or relatively flat and 64% are leptokurtic or strongly leptokurtic. Where a sample curve is better sorted in the central part than in the tails it is considered to be excessively peaked or leptokurtic.

The average roundness for RB (Table 5.2) is described as sub-angular/ sub-rounded for most of the samples, with three samples described as sub-rounded and three as sub-angular.

Table 5.2. The graphical mean, standard deviation and sorting characteristics of the Red Brown horizon

	Folk and Ward Method (µm)				Description				
Sample	**Mean (M_G)**	**Sorting (σ_G)**	**Skewness (Sk_G)**	**Kurtosis (K_G)**	**Mean**	**Sorting**	**Skewness**	**Kurtosis**	**Roundness**
HB-01	195.4	2.53	0.26	0.97	Fine Sand	Poor	Coarse Skewed	Mesokurtic	Sub-rounded
HB-02	273.2	2.10	0.11	1.07	Medium Sand	Poor	Coarse Skewed	Mesokurtic	Sub-angular
HB-03	225.2	2.39	0.22	0.97	Fine Sand	Poor	Coarse Skewed	Mesokurtic	Sub-angular / sub-rounded
HB-04	276.3	2.24	0.11	0.88	Medium Sand	Poor	Coarse Skewed	Platykurtic	Sub-angular / sub-rounded
HB-05	217.9	2.49	0.21	0.84	Fine Sand	Poor	Coarse Skewed	Platykurtic	Sub-angular
HB-06	182.4	2.19	0.20	1.44	Fine Sand	Poor	Coarse Skewed	Leptokurtic	Sub-angular / angular
HB-07	134.3	2.11	0.19	1.70	Fine Sand	Poor	Coarse Skewed	Very Leptokurtic	Sub-angular
HB-08	161.0	2.27	0.31	1.31	Fine Sand	Poor	Very Coarse Skewed	Leptokurtic	Sub-angular / sub-rounded
HB-09	136.1	2.23	0.26	1.59	Fine Sand	Poor	Coarse Skewed	Very Leptokurtic	Sub-angular / sub-rounded
HB-10	151.7	2.08	0.21	1.35	Fine Sand	Poor	Coarse Skewed	Leptokurtic	Sub-rounded
HB-11	152.9	2.10	0.27	1.32	Fine Sand	Poor	Coarse Skewed	Leptokurtic	Sub-angular / sub-rounded
HB-12	160.1	2.02	0.17	1.36	Fine Sand	Poor	Coarse Skewed	Leptokurtic	Sub-angular / rounded
HB-13	158.4	2.00	0.22	1.28	Fine Sand	Poor	Coarse Skewed	Leptokurtic	Sub-angular / rounded
HB-14	162.1	2.08	0.28	1.27	Fine Sand	Poor	Coarse Skewed	Leptokurtic	Sub-rounded

5.4.3 Bone Site and Vertical Profiles at Area 1 and Area 2

The bone bed site is located near the foot of the hillslope deposit. The mean grain size for the three horizons at the bone bed site ranges between 94 and 102 µm, reflecting a much finer grain size distribution than the samples from RB and TS taken down the slope (Figure 5.24). The sediment is described as very-fine sand and two of the three horizons are moderately well-sorted. The B_1 horizon is poorly sorted and coarse-skewed. The units are described as leptokurtic, with RB very leptokurtic. There is agreement in the roundness of the particles in each horizon as it is described as sub-angular/sub-rounded (Table 5.3).

The grain size distribution for the stratigraphy at Area 1 is fairly consistent (Figure 5.24) showing a fining-upward sequence. The sediment particles are described as fine sand to very-fine sand with the mean grain size ranging between 80 and 225 µm (Table 5.3). The sorting for all the horizons is poor and all samples are coarse-skewed. All the samples are very leptokurtic, except for RB which is very platykurtic. There is agreement in the roundness of the particles in each horizon as it is described as sub-angular/sub-rounded.

At Area 2 the grain size distribution for the stratigraphic profiles ranges between 92 and 207 µm (Figure 5.24). However, most of the samples are in the 90 - 180 µm range, making these particles slightly coarser than at

Area 1. The RB and B_2 horizons are fine-skewed and symmetrical, respectively, and all the other profiles are coarse-skewed. There is no consistency in the kurtosis values, with TS and BT_1 being leptokurtic and very leptokurtic respectively, RB and BT_2 mesokurtic, and BT_2 and B_1 platykurtic. The particles range from sub-angular/sub-rounded to sub-rounded.

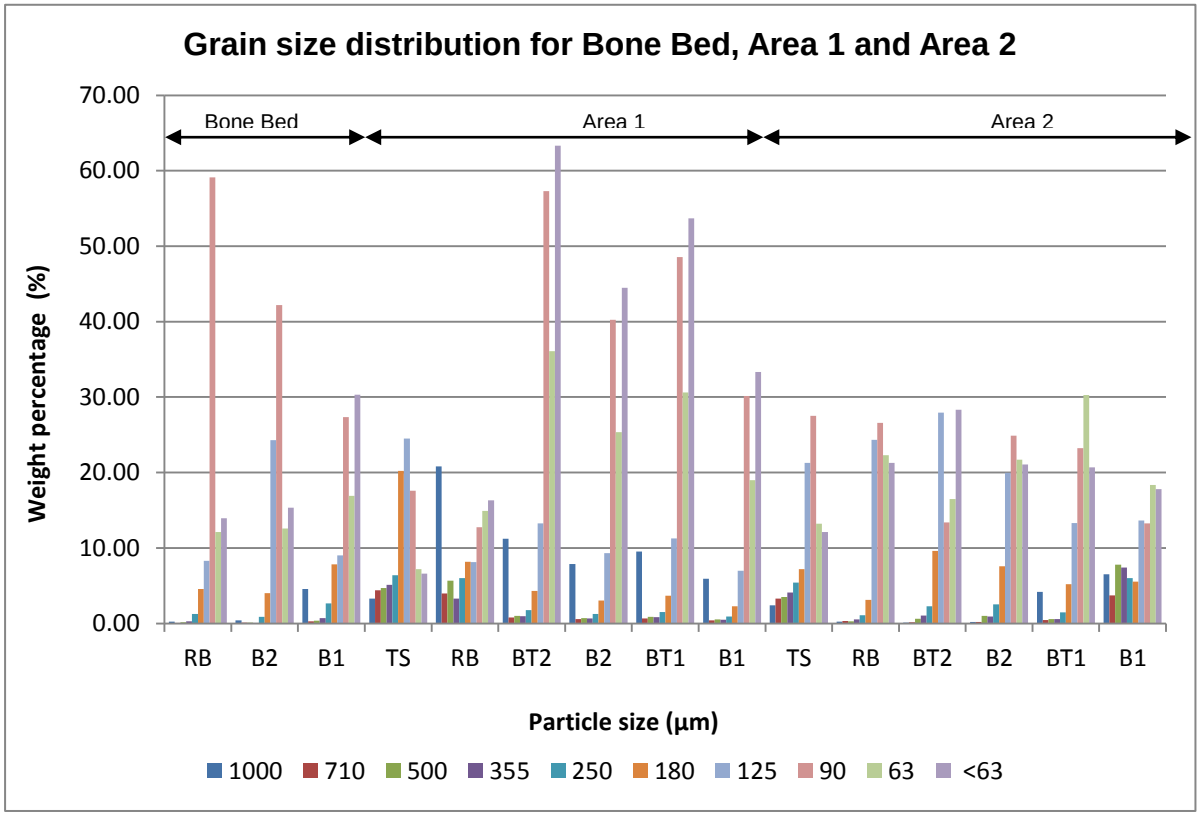


Figure 5.24. Histograms of the grain size distributions for the preserved stratigraphy at the Bone Bed site and a representative stratigraphy at Area 1 and Area 2.

Table 5.3 Graphical mean, standard deviation and sorting characteristics of the bone bed, Area 1 and Area 2 stratigraphy.

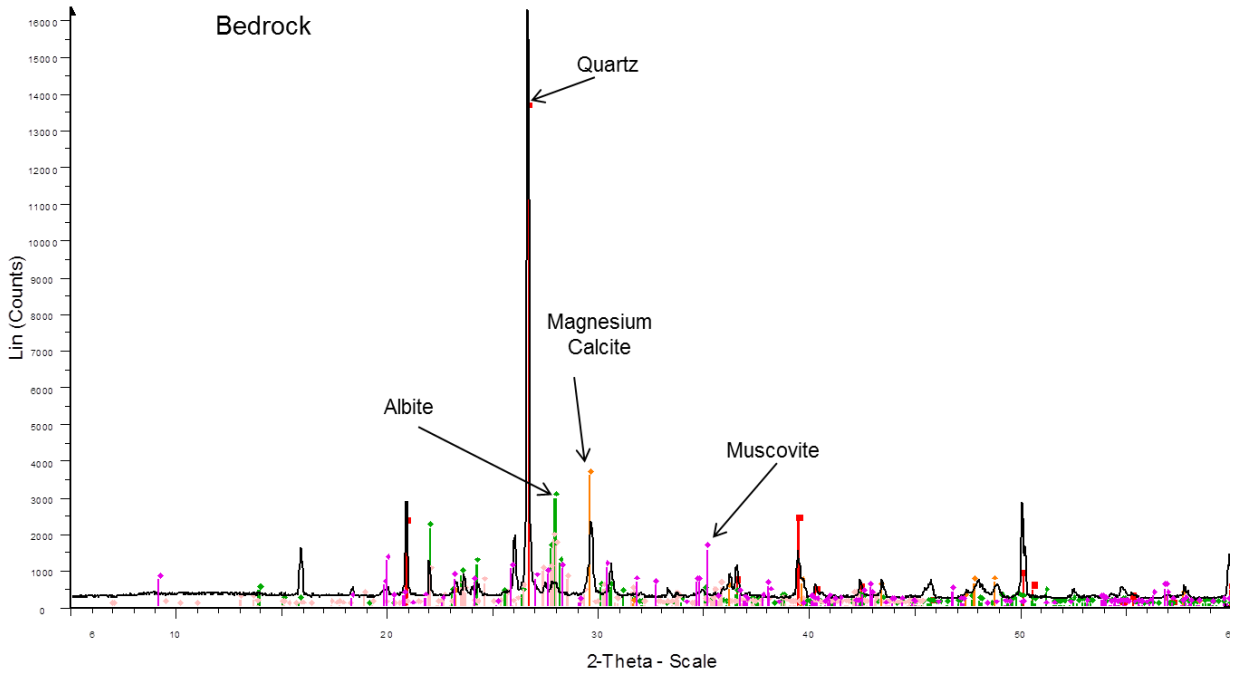
		Folk and Ward Method (μm)				Description				
Sample	**Horizon**	**Mean (M_G)**	**Sorting (σ_G)**	**Skewness (Sk_G)**	**Kurtosis (K_G)**	**Mean**	**Sorting**	**Skewness**	**Kurtosis**	**Roundness**
Bone Bed	RB	94.9	1.49	-0.27	2.16	Very Fine Sand	Moderately Well Sorted	Fine Skewed	Very Leptokurtic	Sub-angular / sub-rounded
	B_2	101.8	1.58	-0.22	1.32	Very Fine Sand	Moderately Well Sorted	Fine Skewed	Leptokurtic	Sub-angular / sub-rounded
	B_1	97.9	2.17	0.15	1.41	Very Fine Sand	Poor	Coarse Skewed	Leptokurtic	Sub-angular / sub-rounded
Area 1	TS	225.0	2.10	0.29	1.01	Fine Sand	Poor	Coarse Skewed	Mesokurtic	Sub-angular / sub-rounded
	RB	222.4	3.47	0.25	0.65	Fine Sand	Poor	Coarse Skewed	Very Platykurtic	Sub-angular / sub-rounded
	BT_2	80.3	2.21	0.14	1.79	Very Fine Sand	Poor	Coarse Skewed	Very Leptokurtic	Sub-rounded
	B_2	80.4	2.21	0.14	1.79	Very Fine Sand	Poor	Coarse Skewed	Very Leptokurtic	Sub-rounded
	BT_1	80.3	2.22	0.14	1.80	Very Fine Sand	Poor	Coarse Skewed	Very Leptokurtic	Sub-angular / sub-rounded
	B_1	80.3	2.21	0.14	1.79	Very Fine Sand	Poor	Coarse Skewed	Very Leptokurtic	Sub-rounded
Area 2	TS	207.5	2.24	0.25	1.30	Fine Sand	Poor	Coarse Skewed	Leptokurtic	Sub-rounded
	RB	92.8	1.67	-0.16	0.95	Very Fine Sand	Moderately Sorted	Fine Skewed	Mesokurtic	Sub-angular / sub-rounded
	BT_2	94.4	1.86	-0.14	0.79	Very Fine Sand	Moderately Sorted	Coarse Skewed	Platykurtic	Sub-angular / rounded
	B_2	96.3	1.77	-0.05	1.02	Very Fine Sand	Moderately Sorted	Symmetrical	Mesokurtic	Sub-angular / rounded
	BT_1	92.3	1.99	0.23	1.70	Very Fine Sand	Moderately Sorted	Coarse Skewed	Very Leptokurtic	Sub-rounded
	B_1	159.9	2.89	0.29	0.85	Fine Sand	Poor	Coarse Skewed	Platykurtic	Sub-rounded

5.5. MINERALOGY AND MAJOR ELEMENT ANALYSIS

The palaeo-environmental reconstruction of the stratigraphic sequence at Heelbo is supported by an analysis of the clay minerals and major elements in the soils. Clay minerals can be useful indicators of past climatic regimes and, while they do not produce indicators of climatic parameters, they provide integrated records of overall climate impact (Singer, 1984) and can also be linked to bedrock.

5.5.1 Mineral Concentrations by XRD and XRF

The X-ray diffraction patterns were analysed to determine the clay and non-clay minerals present in the samples (Figure 5.25). The analysis identified very similar mineral assemblages for all the sampled horizons at Area 1 and Area 2. The mineral assemblages are quartz, muscovite, feldspar, calcite and dolomite as the non-clay minerals. The basement material indicated similar non-clay minerals as quartz, feldspar, dolomite and muscovite (Figure 5.25). In both the basement material and the hillslope samples the main clay mineral identified is montmorillonite and a chlorite/smectite mixed layer mineral which was not easily classified. Additional XRD patterns are presented in APPENDIX B, which also show similar mineral assemblages as the RB horizon (Figure 5.25).



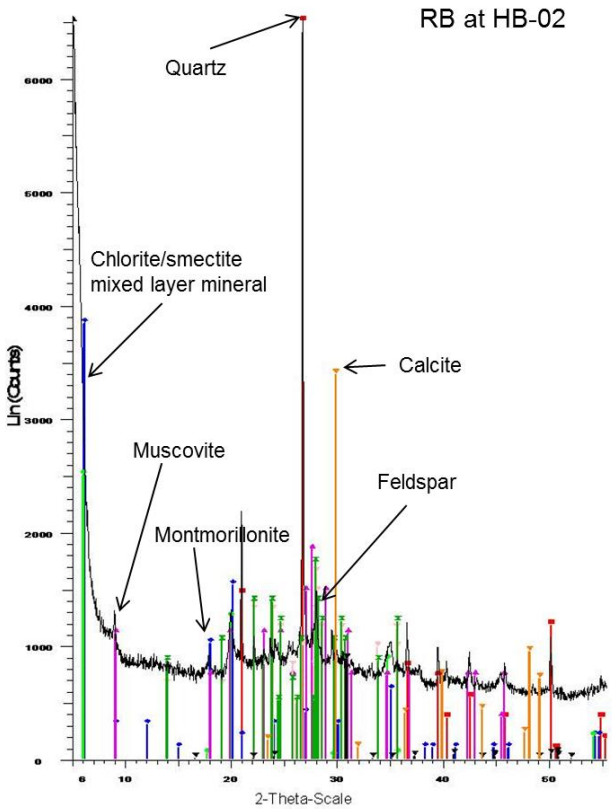


Figure 5.25 XRD patterns for mineral identification for the bedrock material, and RB horizon, at HB-02, respectively. The dominant mineral is quartz; with montmorillonite and muscovite.

The major element concentrations in weight percentages were determined for selected samples and representative bedrock samples by XRF (Table 5.4). The chemical differences between the bedrock and the hillslope deposit are shown in Figure 5.25. The abundance of quartz and feldspar in the horizons is indicated by the large amounts of SiO_2 and Al_2O_3. In the hillslope deposit the average SiO_2 content is ~ 80 wt%. This concurs with the XRD analysis that quartz is the most abundant mineral in both the bedrock and hillslope material.

Al_2O_3 is a major component of feldspar, and sandstone usually contains very little of this mineral ~5-8%, although this may increase to 15% in the presence of secondary clay minerals (Etemad-Saeed *et al*., 2011). The Al_2O_3 concentrations represent the presence of feldspar in both the bedrock and hillslope deposit, although there may be a great deal of variability in the average concentrations. The concentration of Al_2O_3 in the bedrock is high for sandstone with an average of 8.92 wt% at Area 1 and 13.38 wt% at Area 2, which is close to the upper limit of 15% (as suggested by Etemad-Saeed *et al*., 2011). The average concentration of Al_2O_3 at Area 1 is 9.92 wt%, which is is higher than average for the bedrock material, implying an enrichment of feldspar at Area 1. At Area 2, the higher Al_2O_3 in the bedrock suggests that there is no further enrichment of feldspar in the deposit at Area 2, which is to be expected as the bedrock is the only source material identified for the deposit at Area 2.

Table 5.4 Major element concentrations as determined by XRF

	Site Description	SiO_2 (%)	Al_2O_3 (%)	Fe_2O_3 (%)	MnO (%)	MgO (%)	CaO (%)	Na_2O (%)	K_2O (%)	TiO_2 (%)	P_2O_5 (%)	Cr_2O_3 (%)	NiO (%)	TOTAL (%)	LOI
HLB21	Bedrock Area 1 (red)	81.71	8.23	0.57	0.23	0.69	2.8	1.54	1.34	0.3784	0.05	0.0008	0.0024	99.72	4.79
HLB22	Bedrock Area 1 (yellow)	82.05	9.61	0.45	0.19	0.53	1.03	2.11	1.7	0.4807	0.04	0.0028	0.0008	99.92	3.44
HLB23	Bedrock Area 2 (red)	70.23	13.3	0.78	0.07	0.78	6.98	1.32	2.35	0.7758	0.04	0.0096	0.0019	99.56	10.13
HLB24	Bedrock Area 2 (yellow)	75.89	13.45	0.55	0.04	0.75	2.61	1.33	2.4	0.8066	0.04	0.0128	0.0031	99.93	7.01
HLB1	RB in bone bed	84.11	8.63	0.35	0.03	0.42	0.59	1.56	1.95	0.5171	0.04	0.0039	0.001	99.52	3.87
HLB2	B_2 in bone bed	83.85	8.58	0.34	0.03	0.44	0.79	1.69	2.04	0.4083	0.03	0.0217	0.0128	99.51	3.06
HLB3	B_1 in bone bed	80.11	9.73	0.49	0.06	0.62	2.56	1.46	2.09	0.5315	0.07	0.0057	0.001	99.58	5.96
HLB4	RB start of deposit (30cm)	78.89	10.91	0.51	0.07	0.72	1.81	1.58	2.39	0.5618	0.06	0.0089	0.0021	99.46	5.58
HLB5	RB start of deposit (102 cm)	78.31	11.72	0.59	0.08	0.78	1.16	1.84	2.49	0.5884	0.05	0.0055	0.0003	99.9	4.91
HLB6	B_1 isolated stack	80.33	10.06	0.46	0.07	0.56	1.75	1.87	2.12	0.5855	0.04	0.0035	0.0009	99.57	4.77
HLB7	B_1 at Area 1	80.52	10.37	0.48	0.03	0.55	1.54	1.91	2.09	0.5939	0.04	0.0052	0.0029	99.92	4.4
HLB8	BT1	77.03	11.89	0.56	0.07	0.82	1.92	2.05	2.56	0.6629	0.04	0.0055	0.0017	99.71	7.3
HLB9	B_2	83.5	8.81	0.34	0.07	0.41	1.1	1.98	1.97	0.5083	0.03	0.0046	0.0055	100.05	3.28
HLB10	BT_2	79.17	11.55	0.53	0.08	0.72	0.84	1.97	2.48	0.6605	0.05	0.0095	0.0008	100.06	6.07
HLB11	RB	78.93	10.24	0.55	0.07	0.57	3.55	1.39	2	0.5888	0.05	0.0076	0.0006	100.02	6.79
HLB19	TS	86.79	6.88	0.27	0.03	0.27	0.55	1.35	1.69	0.5642	0.04	0.0025	0.0001	99.45	2.73
HLB16	B_1 at Area 2	76.26	13.27	0.72	0.04	0.85	0.77	1.58	2.72	0.6765	0.1	0.0082	0.0004	99.73	5.33
HLB12	BT_1	82.61	9.42	0.43	0.03	0.52	1.42	1.57	2	0.6116	0.03	0.0118	0.001	100.3	4.91
HLB13	B_2	80.16	11.02	0.53	0.04	0.67	0.58	1.68	2.27	0.5707	0.04	0.007	-0.0003	99.57	5.11
HLB14	BT_2	79.03	11.86	0.61	0.05	0.76	0.8	1.66	2.5	0.6081	0.05	0.0045	0.0004	100.2	7.29
HLB15	RB	82.68	9.35	0.42	0.05	0.5	0.61	1.72	1.96	0.4936	0.03	0.0033	0.0002	99.4	3.64
HLB20	TS	87.67	6.41	0.22	0.02	0.18	0.37	1.47	1.67	0.5364	0.04	0.0047	0.0013	99.43	1.64

There is more K_2O than Na_2O in all samples, with an average of 2.17 wt% and 1.69 wt%, respectively, for the deposit material, and 1.95 wt% and 1.58 wt%, respectively for the bedrock material. Na can be explained by the presence of plagioclase and muscovite, and K by the presence of muscovite, potassium feldpar and biotite. The presence of K^+ is necessary for the formation of smectite, in combination with suitable temperature, available time and permeability (Moore and Reynolds, 1997).

There is a greater concentration of CaO in the bedrock at Area 2 (~average 4.80 wt%) than Area 1 (~average 1.92 wt%). This suggests there may have been calcite and dolomite precipitation during weathering. However, there is marginally more Na_2O in the bedrock at Area 1 than at Area 2 (Figure 5.26). The CaO and Na_2O would have been added from groundwater, or an increase in concentration due to evaporation of the groundwater (Etemad-Saeed *et al*., 2011). CaO is reflected in the calcrete nodules in the B_1 horizon, with concentrations of 2.56 wt% in the bone bed, 1.54 wt% at Area 1 and 0.77 wt% at Area 2. The calcite precipitated out to form the nodules during periods of low rainfall.

Leaching is indicated by the accumulation of CaO in the lower BT_1 palaeosol as it increases vertically through the profile, from 0.84 wt% at the top of the BT_2 horizon to 1.92 wt% at the base of the BT_1 palaeosol. Leaching through the entire stratigraphic succession occurs as water percolates through the open pore spaces, seen in the thin sections.

Further evidence of leaching and capillary action occurring as minor processes is seen in the difference between the Na_2O and K_2O values at the top and bottom of the RB horizon at the start of the deposit, with the Na_2O and K_2O values higher at the top of the horizon.

The major elemental compositions of the bedrock are compared to the hillslope deposit in Figure 5.26. The relative concentrations of Na_2O and K_2O (Figure 5.26 A) indicates that leaching has occurred in both the bedrock and hillslope deposit. The ratios of Na_2 / K_2O, Al_2O_3 / SiO_2, CaO / LOI and TiO_2 / Al_2O_3 of the Heelbo deposit follow similar trends to that of the bedrock, even though the values do not always concur. As the sediment is washed downslope, and weathering occurs, the concentrations in the mineral composition between the bedrock and the deposit differs The SiO_2 / Al_2O_3 ratio is a measure of clay or silica enrichment and Figure 5.26 B shows that there is a decrease in SiO_2 with an increase in Al_2O_3 in both the bedrock and the deposit. This increase in Al_2O_3 with a decrease in SiO_2 is related to a decrease in grain size or to a lower textural maturity of the soil.

The Al_2O_3 / TiO_2 ratio is a good indicator of sediment provenance and a good measure of sediment alteration (Hamer *et al*., 2007). The titanium (TiO_2) concentration is fairly constant at an average of 0.56 wt%, with the exception of the bedrock at Area 2, which averages 0.79 wt%. The molar Ti/Al ratio can be used to determine the uniformity of the source rocks due

to the elements' relatively immobile nature during weathering (Hamer *et al.*, 2007). Since a source rock will display a set ratio, a large variation in this ratio implies that the sedimentary horizons have been sourced from multiple parent rocks. This large variation in Ti/Al ratio between source rock and the sedimentary horizons does not apply at Heelbo (Figure 5.26 D), as the only source material for the deposit is the weathered Karoo bedrock.

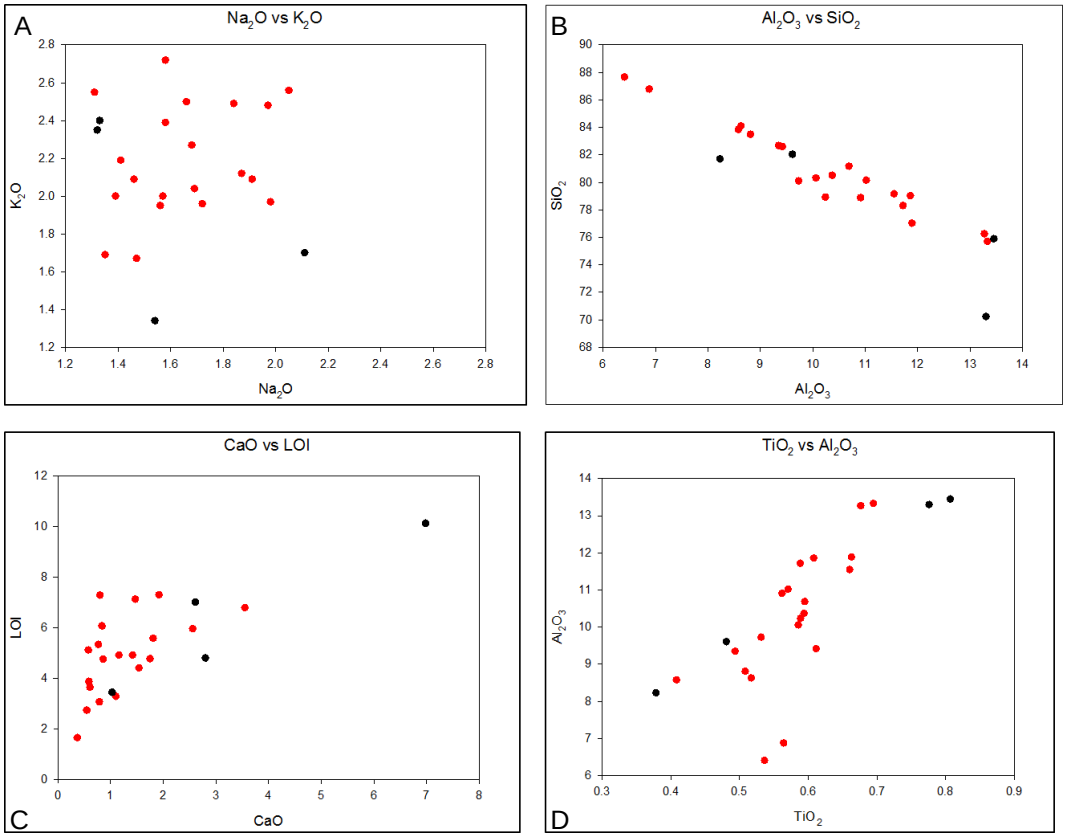


Figure 5.26 Chemical differences between the bedrock material and hillslope deposit. The bedrock samples are shown as black dots and the red dots represent the hillslope deposit samples.

The chemical index of alteration (CIA) and plagioclase index of alteration (PIA) of the bedrock, and each of the stratigraphic units, at both Area 1 and Area 2, were calculated (Table 5.6). CIA is interpreted as a measure of the extent of conversion of feldspars to clays, and has been used in numerous palaeosol studies (Nesbitt and Young, 1996); whereas PIA is an alternative index used where plagioclase is in abundance in silicate rocks (Etemad-Saeed *et al*., 2011). PIA is used when plagioclase weathering needs to be monitored. Low (~50%) CIA or PIA values would indicate low weathering conditions and may reflect cool and/or arid climate conditions, whereas high CIA or PIA (~80%) would indicate intense weathering (Etemad-Saeed *et al*., 2011).

The lowest CIA is calculated for the RB horizon at Area 1 (59.6%) and suggests rapid deposition and burial of this unit followed by pedogenic weathering (Nesbitt and Young, 1996). Low CIA values were expected in the TS unit as this is the uppermost and youngest unit in the sequence, and this would reflect the immaturity of the weathering profile (see the geochronology reults in Chapter 6). However, the CIA is comparable to the lower units, suggesting a change in climate conditions from dry conditions to that favouring chemical weathering. The depositional environments are the same for Areas 1 and 2 and therefore the degree of weathering is similar. This is reflected in the comparable degrees of weathering between the units at both sites (Table 5.5).

The difference in average CIA between the bedrock (62.84%) and the hillslope deposit (64.53%) is very small at Area 1, and only slightly larger (61.75% for bedrock and 68.71% for deposit) at Area 2. The low variation in CIA values is interpreted in terms of the textural and compositional homogeneity between the bedrock and the hillslope deposit. As there is homogeneity in the mineralogical composition of the sediments, large variations do not occur in major elements concentrations, which in turn result in similar CIA values. High CIA values reflect the removal of labile cations (such as Ca^{2+}, Na^{2+}, and K^{1+}) relative to the stable residual constituents (Al^{3+}, Ti^{2+}) during the weathering and may reflect hot and humid conditions. Conversely, low CIA values indicate the near absence of chemical alteration and consequently may reflect cool and/or arid conditions (Nesbitt and Young, 1996). The Heelbo results indicate a moderate degree of weathering in both the bedrock and the sediment horizons. This suggests a possible shift from low weathering conditions and cool arid conditions to warmer and wetter conditions more conducive to chemical weathering.

Table 5.5 Chemical index of alteration (CIA) and plagioclase index of alteration (PIA) of the bedrock at both Areas and of selected samples from each sedimentary unit at each Area.

	Area Description	CIA (%)	PIA (%)	CIA without CaO (%)
HLB21	Bedrock Area 1 (red)	59.17	61.35	74.08
HLB22	Bedrock Area 1 (yellow)	66.51	71.58	71.61
HLB23	Bedrock Area 2 (red)	55.53	56.88	78.37
HLB24	Bedrock Area 1 (yellow)	67.96	73.72	78.29
HLB1	RB in bone bed	67.79	75.65	71.09
HLB2	B_2 in bone bed	65.50	72.51	69.70
HLB3	B_1 in bone bed	61.43	65.52	73.27
HLB4	RB start of deposit (30 cm)	65.37	71.54	73.32
HLB5	RB start of deposit (102 cm)	68.10	75.47	73.02
HLB6	B_1 isolated stack	63.67	68.69	71.60
HLB7	B_1 at Area 1	65.18	70.59	72.16
HLB8	BT_1	64.55	70.15	72.06
HLB9	B_2	63.56	68.95	69.04
HLB10	BT_2	68.59	76.35	72.19
HLB11	RB	59.60	62.52	75.13
HLB19	TS	65.71	73.20	69.35
HLB16	B1 at Area 2	72.36	81.78	75.53
HLB12	BT_1	65.37	71.28	72.52
HLB13	B_2	70.87	79.47	73.61
HLB14	BT_2	70.51	79.19	74.03
HLB15	RB	68.55	76.03	71.76
HLB20	TS	64.62	72.04	67.12

5.5.2 Classification of the Sedimentary Horizons

Numerous sand and sandstone classification schemes exist, but in most schemes the fundamental parameters for classifying sands or sandstones are quartz (Q), feldspar (F), rock or lithic fragments (R or L) and matrix (M). Quartz may include chert as well as single-crystal grains of quartz and feldspar refers to single-crystal grains of alkali feldspars as well as

plagioclase (Herron, 1988). Matrix includes most silt-and clay-sized particles (Herron, 1988). These characteristics are usually determined by point-counting the relative abundance of the quartz, feldspar and lithic fragments in the thin sections. This method can prove problematic when the grains are stained by hematite or covered by organic matter as with some of the Heelbo samples, or where the identification of the components of the matrix and lithic fragments is difficult.

An alternate classification system referred to as the *SandClass* system was suggested by Herron (1988) and shows the relationship between chemical composition and sandstone type (Figure 5.27). This classification system uses the SiO_2/Al_2O_3 and Fe_2O_3/K_2O ratios. The use of the SiO_2/Al_2O_3 ratio allows the distinction between quartz-rich, high-ratio sandstones and clay-rich, low-ratio shales (Pettijohn *et al*., 1972). The ratio of total iron (Fe_2O_3) to K_2O is effective in distinguishing lithic fragments from feldspars (Herron, 1988) and can be used as an indicator of mineralogical stability. Herron (1988) suggests as a general rule that stable mineral assemblages have low Fe_2O_3/K_2O ratios and less stable mineral assemblages located close to the sediment source have high Fe_2O_3/K_2O ratios.

The ratios for the Heelbo samples (Figure 5.27) show that all the samples are arkose, except for two which are subarkose. The basement samples also plot as arkose which confirms the bedrock material as the source of

the sediment for the hillslope deposit. Bordy *et al*. (2004a) described the Elliot Formation sandstones as mostly lithic arkose (Figure 3.4), which further supports the argument that the Elliot Formation is the source material for the deposit.

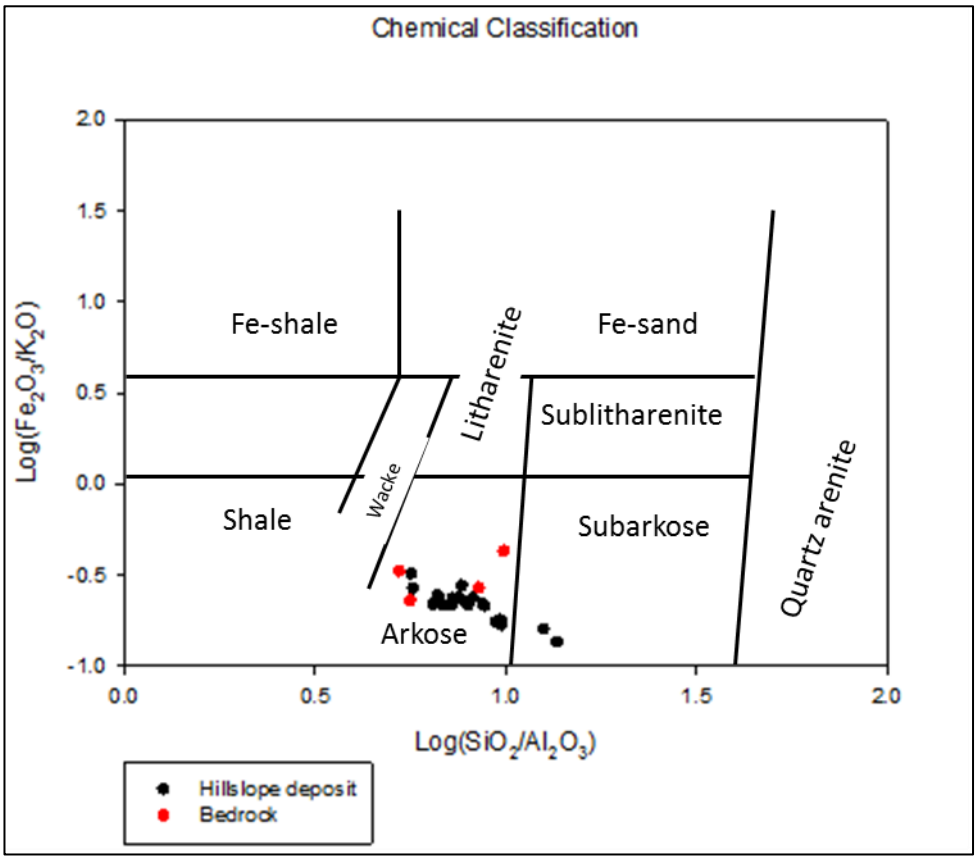


Figure 5.27 Geochemical classification using $log(SiO_2/Al_2O_3)$-$log(FeO_3/K_2O)$ (after Herron, 1988). Most of the Heelbo samples plot as arkose, with two samples plotting as subarkose. The bedrock samples (red dots) plot as arkose.

The samples can also be classified according to the Ca content within the *SandClass* system described by Herron (1988). Calcite and dolomite are important diagenetic components of sandstones. The samples can be divided into non-calcareous (Ca < 4%), calcareous (4% < Ca < 15%) and carbonate (Ca > 15%). Carbonate cementation is important for sediment

properties such as porosity and permeability. For some sands the Ca concentration of above 1% strongly indicates some carbonate cementation, but for others the source of Ca may be non-carbonate minerals including plagioclase. All the Heelbo samples have Ca between 1-4% and can, therefore, be classified as non-calcareous, although carbonate cementation is visible in thin section. The presence of plagioclase as identified by XRD, also contributes to the concentration of Ca in the samples.

5.5.3 Sodium Adsorption Ratio (SAR_s), pH and Electrical Conductivity

Several field indicators of dispersive soils, as described by Davies and Lacey (2007), appear to apply to the Heelbo sediments: 1) the soil became marsh-like when wet because of its structural instability; 2) after a rainstorm ponds of milky coloured water appeared on the soil surface; 3) the water infiltrated slowly into the ground; 4) the soils were prone to erosion; 5) the soils were hard-setting and formed a surface crust when dry; 6) and cracks appeared as the soil shrunk on drying. Prior to the analysis selective samples were placed in distilled water to measure the degree of dispersion based on Davies and Lacey's (2009) classification (see Table 4.2). Samples were taken of RB horizon in the proximal (A, B), medial (C,D) and distal (E,F) sections of the hillslope at Area 1; and samples were taken from TS, RB, BT_2, B_2, BT_1, B_1 at Area 1 (G,H,K,L,M,N) and Area 2 (P,R,S,T,U,W) respectively (Figure 5.28). The samples were checked at intervals of 0 (as the distilled water was added),

2, 5, 10, 20, 30 minutes. At 0 minutes the particles started dispersing and by 5 minutes most of the material had dispersed and some of the samples (B, C, N, U) displayed the milky halo described by Davies and Lacey (2009). Within 30 minutes all the material had dispersed for all samples, suggesting that the material displayed a high dispersion tendency.

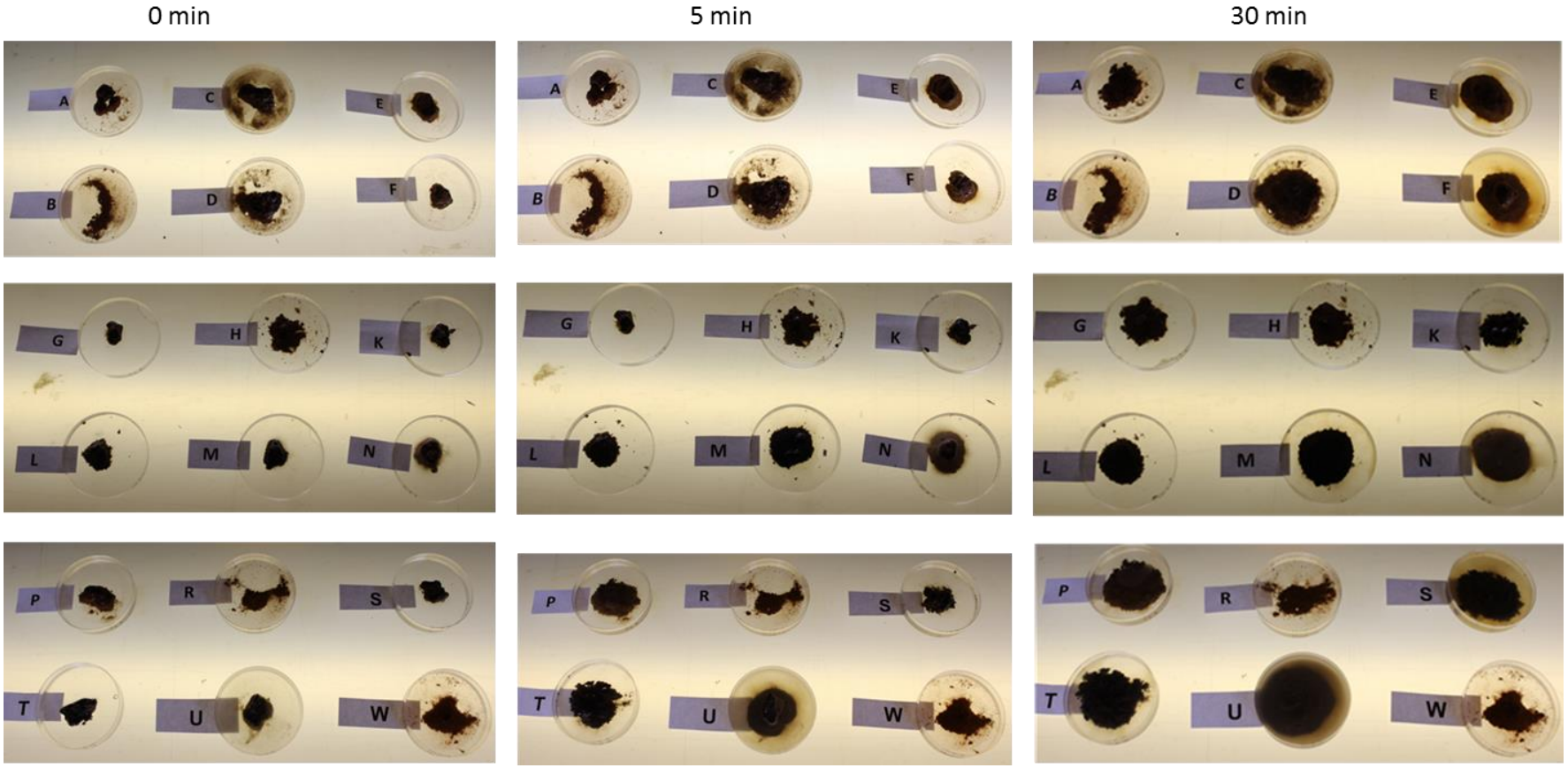


Figure 5.28 Dispersion tests with samples placed in distilled water for 0, 5 and 30 minutes respectively. Samples were taken of RB horizon in the proximal (A, B), medial (C,D) and distal (E,F) sections of the hillslope at Area 1; and samples were taken from TS, RB, BT_2, B_2, BT_1, B_1 at Area 1 (G,H,K,L,M,N) and Area 2 (P,R,S,T,U,W) respectively.

5.5.3.1 Variation in SAR_s down the slope profile

The SAR_s is used as a measure of the dispersivity of a soil or sediment horizon and is the ratio of the amount of positive charge that is contributed to a soil by the sodium cation relative to that of the magnesium and calcium cations (Davies, *et al.,* 2007). The soil salinity or sodicity and the risk of dispersion were determined according to the criteria presented in Table 5.6. The risk of dispersion, swelling and crusting applies to soils with more than 30% clay, such as clay-loam, silty-clay-loam or silty clay textural classes (Western Fertilizer Handbook, 1995). The higher the risk of dispersion, crusting and swelling of the soil, the greater the risk of gullies forming.

Table 5.6 Guidelines to determine risk of dispersion, crusting and swelling of soils which are more than 30% swelling clay (after Western Fertilizer Handbook, 1995).

SAR_s	EC (dS/m)	TDS (mg/l)	Risk of soil dispersion, crusting, swelling
0 – 3	<0.2	<128	Very High
	0.2 - 0.7	128 – 428	Moderate
	>0.7	>428	Low
3 - 6	<0.3	<192	Very High
	0.3 – 1.2	192 – 768	Moderate
	>1.2	>768	Low
6 - 12	<0.5	<320	Very High
	0.5 – 1.9	320 – 1216	Moderate
	>1.9	>1216	Low
12-20	<1.3	<832	Very High
	1.3 – 2.9	832 – 1856	Moderate
	>2.9	832 – 1856	Moderate
20-40	<2.9	<1856	Very High
	2.9 -5.0	1856 – 3200	Moderate
	>5.0	>3200	Low

To characterize the soil as saline or sodic, the SAR_s and EC can be compared as in Table 5.7.

Table 5.7 Salinity or sodicity of soil based on SAR_s values (Rengasamy and Churchman).

Classification	SAR_s (mmol/l)	EC (dS/m)
Sodic	>3	<0.8
Saline	<3	>0.8

The cation concentrations of Ca, Mg and Na used to calculate the sodium adsorption ratios (SAR_s) for each sample down the slope are presented in Table 5.8.

Table 5.8 Cation (Ca, Mg, Na) concentration of the soil samples taken down the slope from the RB horizon, given in mg/ℓ and converted to mmol/ℓ.

Sample No.	Distance from Head (m)	Ca		Mg		Na	
		mg/ℓ	mmol(+)/l	mg/ℓ	mmol(+)/l	mg/ℓ	mmol(+)/l
HB-01	0	44.03	2.158	2.54	0.209	6.48	0.282
HB-03	61.7	26.72	1.310	1.90	0.156	20.12	0.875
HB-04	119.69	4.28	0.210	1.86	0.153	92.68	4.031
HB-05	251.95	25.88	1.269	4.18	0.344	142.53	6.200
HB-06	278.91	7.33	0.359	1.87	0.154	35.88	1.561
HB-07	294.34	5.06	0.248	3.55	0.292	48.51	2.110
HB-08	310.36	9.76	0.478	1.51	0.124	99.65	4.334
HB-09	327.65	8.01	0.393	1.01	0.083	38.03	1.654
HB-10	361.53	24.77	1.214	0.95	0.078	14.29	0.622
HB-11	381.32	13.93	0.683	1.37	0.113	59.23	2.576
HB-12	414.96	8.27	0.405	1.04	0.086	65.74	2.860
HB-13	462.62	24.65	1.208	2.30	0.189	56.19	2.444
HB-14	521.6	30.23	1.482	2.58	0.212	23.89	1.039

The calculated SAR_s (mg/l) and measured pH, EC and saturation percentage for each sample down the slope are shown in Table 5.9.

Table 5.9 The SAR_s, pH and EC determined for each sample down the hillslope.

Sample no.	Distance from Head (m)	SAR_s	pH	EC	Sat	Description
		mg/ℓ		dS/m	%	
HB-01	0	0.26	7.28	0.23	87.72	Clay
HB-03	21.6	1.02	7.58	0.22	83.28	Clay
HB-04	62.0	9.46	8.31	0.38	84.36	Clay
HB-05	118.2	6.90	7.47	0.59	86.83	Clay
HB-06	250.82	3.08	7.32	0.19	61.88	clay loam
HB-07	278.05	4.06	7.27	0.21	67.62	Clay
HB-08	294.37	7.90	7.62	0.45	68.31	Clay
HB-09	310.10	3.39	7.33	0.21	76.27	Clay
HB-10	327.11	0.77	7.44	0.2	93.68	Clay
HB-11	361.63	4.08	7.66	0.35	76.04	Clay
HB-12	381.45	5.77	7.65	0.3	76.44	Clay
HB-13	415.60	2.92	7.79	0.36	66.98	Clay
HB-14	516.63	1.13	7.43	0.26	73.77	Clay

The variation in the SAR_s, pH and EC down the hillslope deposit is shown in Figures 5.29, 5.30, and 5.31 respectively. There is no apparent trend in the SAR_s downslope and it does not appear that the sodium accumulates in the distal reaches of the slope, nor does it indicate an increase in sodium cations down slope (Figure 5.29). The r^2 values, that determines the correlation coefficient for the variables has been determined and confirms that there is no significant trend.

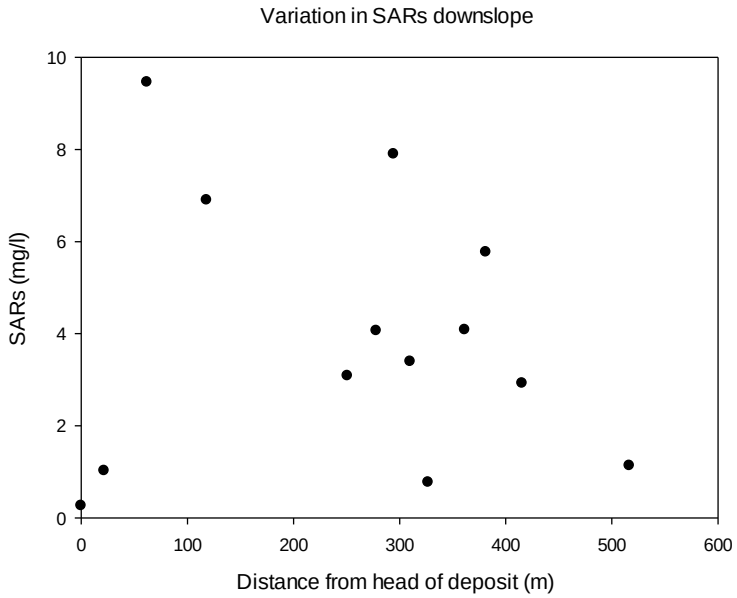


Figure 5.29 Change in sodium adsorption ratio (SAR_s) downslope shows no trend with r^2 = 1.2%

The pH of the samples ranges between 7.2 and 7.8, except for the outlier at HB-04 (Figure 5.30). The soil tends to be moderately alkaline but, again, no apparent trend is seen in the pH downslope.

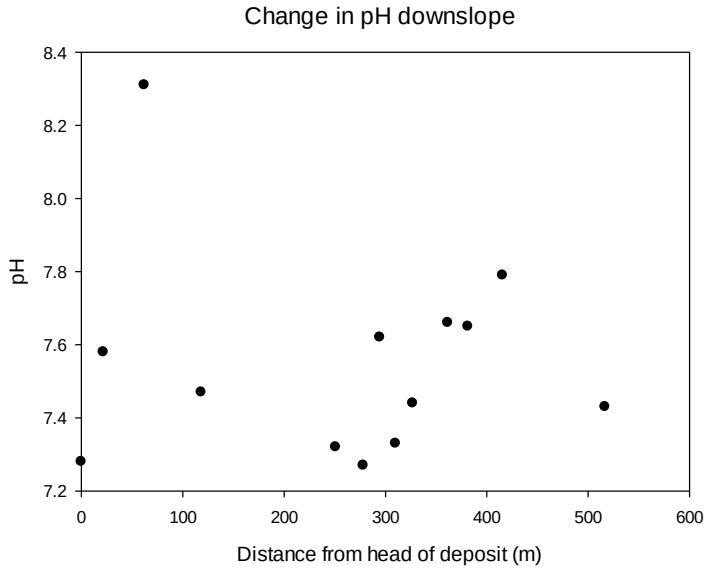


Figure 5.30 Variation in pH downslope indicates that most of the samples are slightly alkali but there is no trend downslope as indicated by r^2 = 1.5%

Electrical conductivity is also used to indicate the sodicity of the sample, and there is also no apparent trend seen in the EC down the Heelbo hillslope (Figure 5.31). The EC ranges between 0.2 and 0.4 dS/m, with HB-05 measuring the highest EC at 0.6 dS/m.

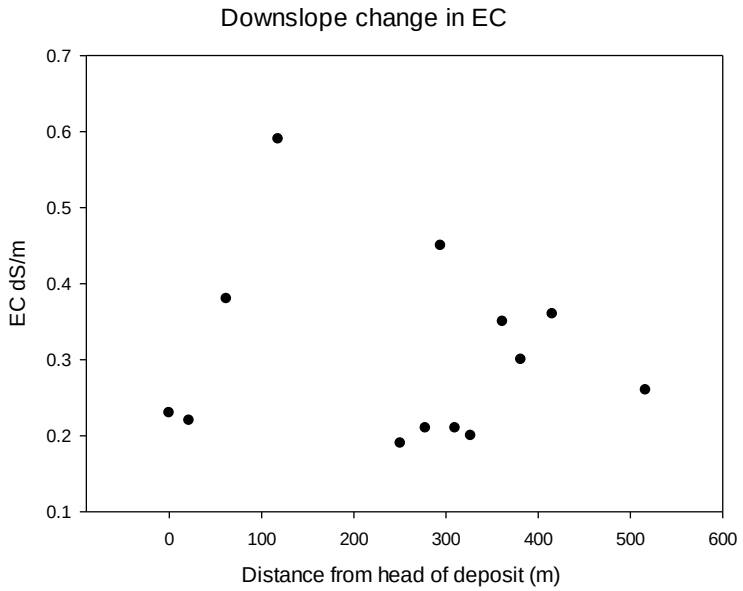


Figure 5.31 Change in electrical conductivity (EC) downslope indicates there is no trend downslope with r^2 = 0.9%.

To determine if the sedimentary unit was sodic, saline or sodic-saline, the SAR_s was calculated in mmol/l as described Rengasamy and Churchman (1999) (Table 5.10) who classified a soil that has a SAR_s > 3 mmol/l as sodic and a soil with a SAR_s < 3 mmol/l as saline. Five soil samples in the profile: HB-04, HB-05, HB-08, HB-12 and HB-15 can be described as sodic, and the rest are considered saline (Table 5.10).

Table 5.10 The SAR_S calculated in mmol/l based on calculations defined by Davies *et al*. (2007).

Sample	SAR_s (mmol/l)	pH	EC (dS/m)	Classification
HB-01	0.18	7.28	0.23	saline
HB-03	0.72	7.58	0.22	saline
HB-04	6.69	8.31	0.38	sodic
HB-05	4.88	7.47	0.59	sodic
HB-06	2.18	7.32	0.19	saline
HB-07	2.87	7.27	0.21	saline
HB-08	5.58	7.62	0.45	sodic
HB-09	2.40	7.33	0.21	saline
HB-10	0.55	7.44	0.2	saline
HB-11	2.89	7.66	0.35	saline
HB-12	4.08	7.65	0.3	sodic
HB-13	2.07	7.79	0.36	saline
HB-14	0.80	7.43	0.26	saline
HB-15	9.45	8.72	0.72	sodic

The pH value is also a determinant of the sodicity or salinity of a soil. The pH values of all the samples indicate that the soils are all saline, as they have a pH of <8.5; where a soil pH >8.4 usually indicates sodicity (Davies *et al*., 2007). The EC of a sodic sample is <4 dS/m (Davies *et al.*, 2007), which accounts for all the samples in the profile. However, the classification of a sample as saline or sodic is not necessarily important unless a medium for soil remediation is required (especially for agricultural soils). The debates over critical values to determine sodicity/salinity suggests that there is no accepted definition for sodic soils and that soils should be defined by their behaviour rather than their compositions.

A more important consideration for Heelbo is how the horizons behave in terms of their tendency to disperse or swell, which will lead to gully formation. The SAR_s, EC and TDS can be used to determine the risk of dispersion, swelling or crusting of the soil. All the samples reflected a moderate to very-high risk of dispersion, swelling and crusting (Table 5.11).

Table 5.11 The risk of dispersion, crusting and swelling of the Heelbo samples downslope, based on the SAR_s and EC or TDS of the samples (after Western Fertilizer Handbook, 1995).

Sample	SAR_s	EC	TDS	Risk of dispersion, swelling and crusting
	mg/ℓ	dS/m	mg/ℓ	
HB-01	0.26	0.23	147.2	Moderate
HB-03	1.02	0.22	140.8	Moderate
HB-04	9.46	0.38	243.2	Very high
HB-05	6.9	0.59	377.6	Moderate
HB-06	3.08	0.19	121.6	Very high
HB-07	4.06	0.21	134.4	Very high
HB-08	7.9	0.45	288	Very high
HB-09	3.39	0.21	134.4	Very high
HB-10	0.77	0.2	128	Moderate
HB-11	4.08	0.35	224	Moderate
HB-12	5.77	0.3	192	Moderate
HB-13	2.92	0.36	230.4	Moderate
HB-14	1.13	0.26	166.4	Moderate

5.5.3.2 Variation in SAR_s in the Vertical Section

Samples were taken from each of the sedimentary horizons which include the two palaeosols (BT_1 and BT_2) (see Figure 4.5). The cation concentrations are given in Table 5.12 and the SAR_s, pH and EC of the

horizons in the vertical section are given in Table 5.13. The change in the SAR_S, pH and EC properties of the horizons with depth are shown in Figures 5.32, 5.33, 5.34 respectively and the r^2 values have been determined to show the correlation coefficient of the variables.

Table 5.12 Measured cation (Ca, Mg, Na) concentrations of the samples taken through the vertical section (at the base of Area 1) in mg/l and the conversion to mmol/l.

Sample No	Depth in cm	Ca		Mg		Na	
		mg/ℓ	mmol(+)/l	mg/ℓ	mmol(+)/l	mg/ℓ	mmol(+)/l
TS HB-V1	10	7.37	0.361	5.02	0.413	65.77	2.861
RB HB-V2	42	27.07	1.327	4.30	0.354	281.65	12.251
BT_2 HB-V3	67	5.12	0.251	1.21	0.100	246.71	10.731
B_2 HB-V4	90	12.53	0.614	8.39	0.690	185.02	8.048
BT_1 HB-V5	191	5.49	0.269	4.81	0.396	161.51	7.025
B_1 HB-V6	226	5.46	0.268	3.19	0.262	175.58	7.637

Table 5.13 The SAR_S, pH and EC along the vertical section with the soil description and classification and the risk of dispersion, crusting and swelling of the vertical horizons, based on the SAR_S and EC or TDS of the samples (after Western Fertilizer Handbook, 1995).

Sample No		SAR_s	SAR_s	pH	EC	TDS	Risk of dispersion, swelling and crusting	Description	Sodic/Saline
	Depth in cm	mg/ℓ	mmol/ℓ		dS/m	mg/ℓ			
TS HB-V1	42	4.60	3.25	7.00	0.26	166.4	Very high	Clay	Sodic
RB HB-V2	67	13.36	9.45	8.80	1.03	659.2	Very high	Clay	Sodic
BT_2 HB-V3	90	25.63	18.13	8.95	1.01	646.4	Very high	Clay	Sodic
B_2 HB-V4	146	9.97	7.05	8.63	0.68	435.4	Moderate	Clay	Sodic
BT_1 HB-V5	191	12.18	8.62	8.87	0.63	403.2	Very high	Clay	Sodic
B_1 HB-V6	226	14.83	10.49	8.72	0.72	460.8	Very high	Clay	Sodic

If inferences are to be made about the environment of deposition, then the assumption must be that EC, SAR_s and pH are stable over time. The SAR_s does not vary systematically with depth (Figure 5.32).

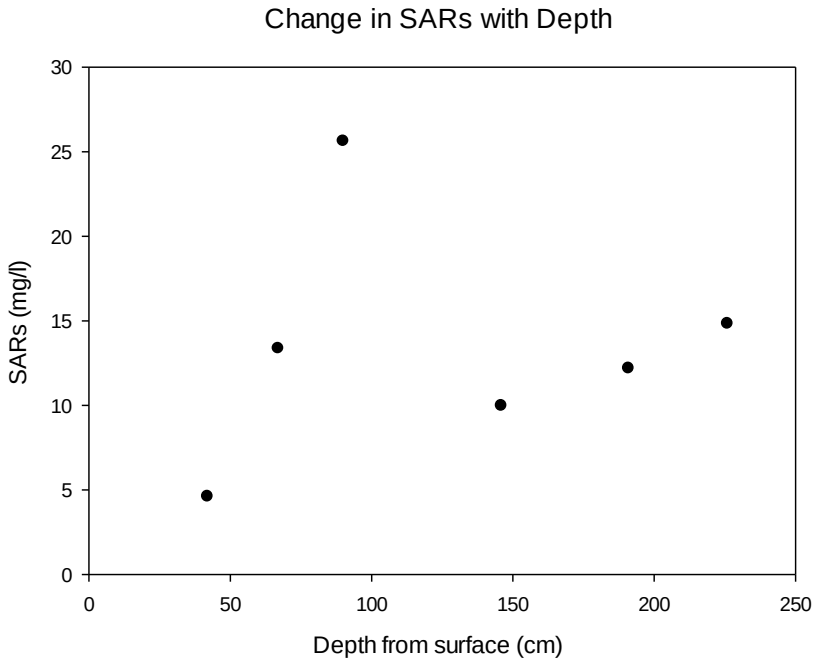


Figure 5.32 Change in sodium adsorption ratio (SAR_s) with depth indicates there is no trend in the change with depth as r^2 = 1.4%.

The pH levels of the horizons reflect an alkali environment with a trend of becoming more alkaline with depth (Figure 5.33). The slightly acidic pH closer to the surface, in the top 50-60 cm, can be attributed to acids from organic matter. Below 60 cm from the surface, the pH remains consistently alkaline.

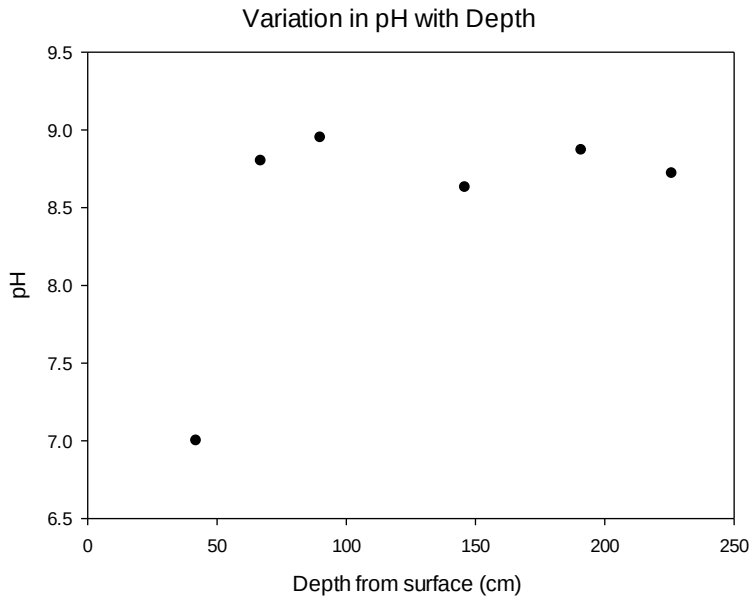


Figure 5.33 The pH of the Heelbo samples is slightly acidic near the surface, becoming more alkaline with depth. The r^2 =27.3% which suggests a small but insignificant correlation.

The electrical conductivity (EC) of the horizons, while indicating no obvious trend, shows a slight increase with depth at 50-60 cm before leveling off at between 0.6 and 0.8 dS/m at depth (Figure 5.34). The step created by the slight increase at 60 cm, then decrease below 100 cm, is a result of an exchange in the upper 1 m, caused by material being depleted near the surface, being elevated above deeper background at ~1 m depth.

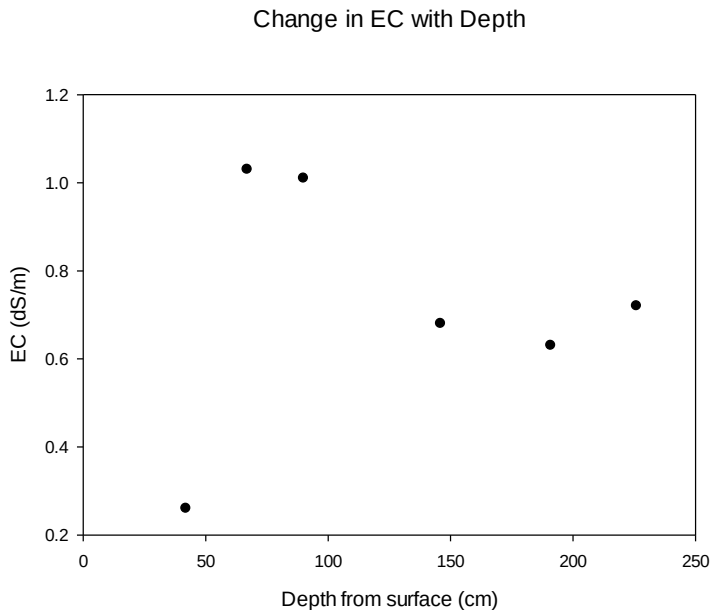


Figure 5.34 Change in electrical conductivity (EC) shows no trend with depth with a corelation coefficient, r^2 = 0.10%.

In summary, all the samples would be considered by Rengasamy and Churchman (1999) to be sodic as they all have SAR_s > 3 and an EC less than 0.8 dS/m. The samples were classified as arkosic implying that they are sandy, which is also supported by the grain size analysis. The samples though are poorly sorted and it is possibly the fine fraction (i.e., clays) that imparts the swelling properties. The behaviour of the samples all indicate a very high risk of dispersion, crusting and swelling (Table 5.12).

CHAPTER 6: GEOCHRONOLOGICAL RESULTS

6.1 INTRODUCTION

The rationale behind the sampling strategy for the geochronology and the methodology were presented in Chapter 4. Eighteen samples from the Heelbo deposit were collected for the geochronology. Five of the samples were sent for radiocarbon dating and the full eighteen samples were dated by the writer using optically stimulated luminescence (OSL) dating. The radiocarbon dating was carried out by the University of Lund, Sweden and thus only the final ^{14}C ages are presented here. The ^{14}C ages were to be used as independent age controls for the OSL ages. The OSL dating technique is an integral part of this research project and is therefore presented in greater detail. The initial test to determine the ideal temperature for measurement and the suitability of the SAR protocol for dating the samples are reported. The final equivalent dose (D_e) determinations are presented and the luminescence ages of all the samples are calculated.

6.2 RADIOCARBON AGES

Radiocarbon ages were determined for the two palaeosol horizons in Area 1 and Area 2 and RB in Area 1. The radiocarbon ages are given in Table 6.1. A bulk sample for each site was submitted to the Lund Laboratory,

they removed the carbonates during the pre-treatment, using HCl (Table 6.1) and the labile fraction using NaOH. As this is a standard bulk sediment analysis, the age represents the integral of all the remaining carbon in the sample. The ^{14}C ages (shown in Table 6.1) were calibrated using an online calibration programme (Calib 7.1). The calibration programme calculates the uncertainty in the age for both 1(68.3%) and 2 (95.4%) standard deviations (Table 6.2).

Table 6.1 Radiocarbon ages for the palaeosols at Area 1 and Area 2. (For sample details see Table 4.7)

Sample number	Location	Horizon	Lab number	^{14}C Age (BP)	mg C	Pre-treatment
OSL7	Stratigraphic sequence at Area 1	RB	LuS 8876	475 ± 45	1.0	HCl, NaOH
OSL8		BT_2	LuS 8879	2580 ± 50	5.3	HCl, NaOH
OSL10		BT_1	LuS 8880	4565 ± 50	2.6	HCl, NaOH
OSL15	Stratigraphic sequence at Area 2	BT_2	LuS 8878	1850 ± 50	4.0	HCl, NaOH
OSL13		BT_1	LuS 8877	2075 ± 50	1.2	HCl, NaOH

Table 6.2 Calibrated radiocarbon ages for the palaeosols for both 1σ and 2σ

Sample Number	^{14}C Age	Cal BP 1 σ (68.3%)	Cal BP 2 σ (95.4 %)	Median Probability
OSL 7	475±45	463 - 525	328 – 374 394 – 396 440 – 546	493
OSL 8	2580±50	2500 – 2593 2614 – 2635 2693 – 2745	2434 - 2757	2604
OSL 10	4565±50	5055 – 5187 5214 – 5224 5235 – 5244 5260 - 5302	4976 – 5016 5031 – 5319 5427 - 5431	5163
OSL 15	1850±50	1630 – 1644 1701 – 1756 1762 – 1822	1593 – 1838 1854 - 1867	1739
OSL 13	2075±50	1927 - 2053	1882 – 2112 2123 - 2147	1996

The ^{14}C dates were determined using bulk soil organic matter from the buried palaeosols and the weight of carbon available for analysis is given in mg C (Table 6.1). The age does not represent the date of the initiation of the sediment profile; instead the ^{14}C age is a weighted mean of the period of carbon accumulation based on the measurement of the average isotopic concentrations in the sediment (Botha, 1996). The incorporation of younger organic matter into the bulk sample may result in the ^{14}C date being low; thus, the uncertainties and errors that can be incurred through the limited sampling of sedimentary horizons and palaeosols need to be examined critically.

6.3 OPTICALLY STIMULATED LUMINESCENCE DATING (OSL)

Once the samples were prepared and the quartz grains extracted (as described in Chapter 4), it was necessary to test the appropriateness of the SAR procedure to determine the equivalent dose (D_e). These tests check that no unusual results arise and establish the suitable pre-heat temperature for each sample.

6.3.1. Infra-red (IR) Depletion Ratio

The pre-treatment of the sample to isolate the quartz grains is expected to eradicate all feldspars which may contaminate the sample and cause scatter in the equivalent dose measurements. The presence of feldspars

was noted in the SAR measurements (Figure 6.1). When feldspars are stimulated with IRSL they produce a luminescence signal similar to that of quartz, and this is recorded as a luminescence curve (Figure 6.1). When no feldspars are present only background noise will be recorded. The IRSL step was therefore included in the final SAR protocol which would deplete the effect of the spurious luminescence that would result from feldspar contamination, and in so doing not affect the luminescence signal from the quartz.

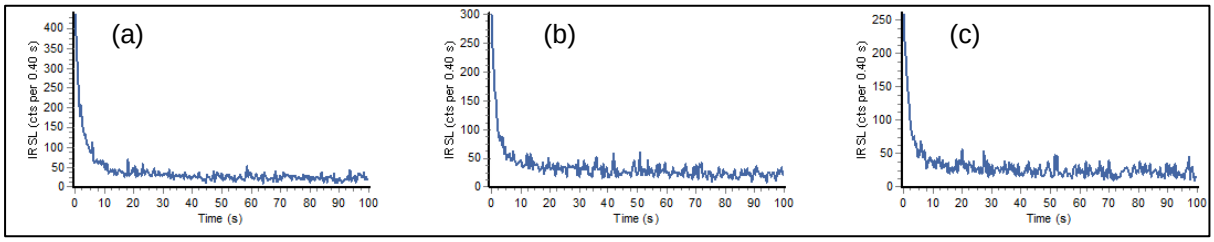


Figure 6.1. Luminescence signal after IR stimulation of feldspars in disks (a) 14, (b) 32 and (c) 47 respectively of sample OSL 3.

6.3.2 Preheat and Dose Recovery Test

The preheat and dose recovery tests were combined and run on the same sequence using 21 medium aliquots of quartz and a standard SAR protocol. The preheat temperature was determined where three aliquots were preheated for each of the given temperatures, which were increased at 20 °C intervals between 180 °C and 300 °C. The regeneration doses of 2, 5, 10, 0, 10 Gy were applied in this order to obtain measurements for the dose (L_x). The test dose applied was 5 Gy to obtain a measurement for the test dose (T_x). The measured D_e values were plotted against the

preheat temperatures (Figure 6.2) and no preheat plateau was identified, which implies that each sample probably has a different behaviour to thermal treatment.

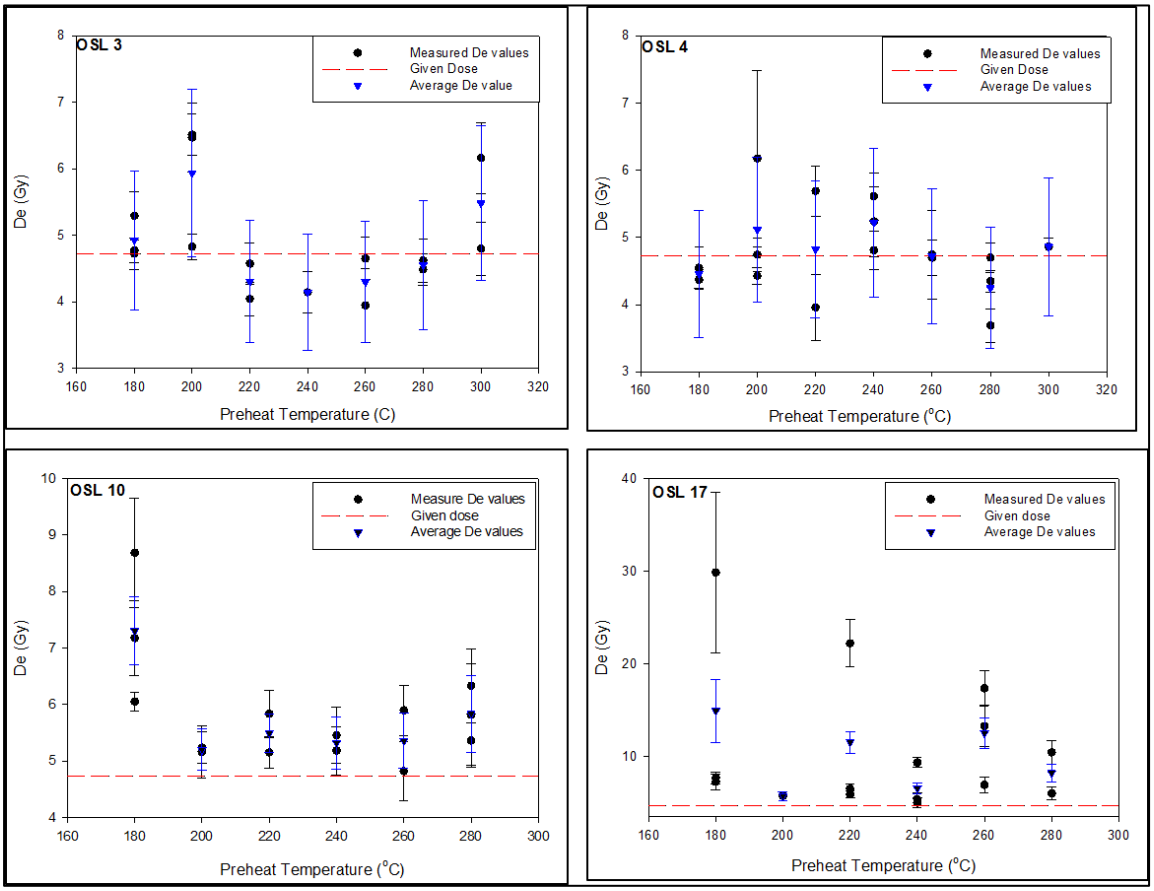


Figure 6.2 Equivalent dose measured at given preheat temperatures for samples OSL3, OSL4, OSL10 and OSL17. The dashed line represents the given dose of 4.73 Gy and the blue triangle represents the average D_e value at each temperature.

For the dose recovery test the natural signals from the grains are removed by optical bleaching, and the grains are then irradiated at room temperature in the lab. The irradiated lab dose is then regarded as an unknown dose and a D_e value is determined using a standard SAR

sequence. The ratio of the measured dose (interpolated from the growth curve) to the given dose (the known lab dose) should be consistent with unity if the SAR procedure is appropriate (Wintle and Murray, 2006). If the SAR protocol is applied to grains that are artificially irradiated with a known dose, and that dose cannot be recovered again, there is a high probability the D_e will be inaccurate (Murray and Wintle, 2003). Dose recovery tests were performed on the samples and they returned a dose recovery ratio within the acceptable ±10 % of unity for a given temperature, indicating that the instrument uncertainty levels were within acceptable limits for that temperature (Figure 6.3).

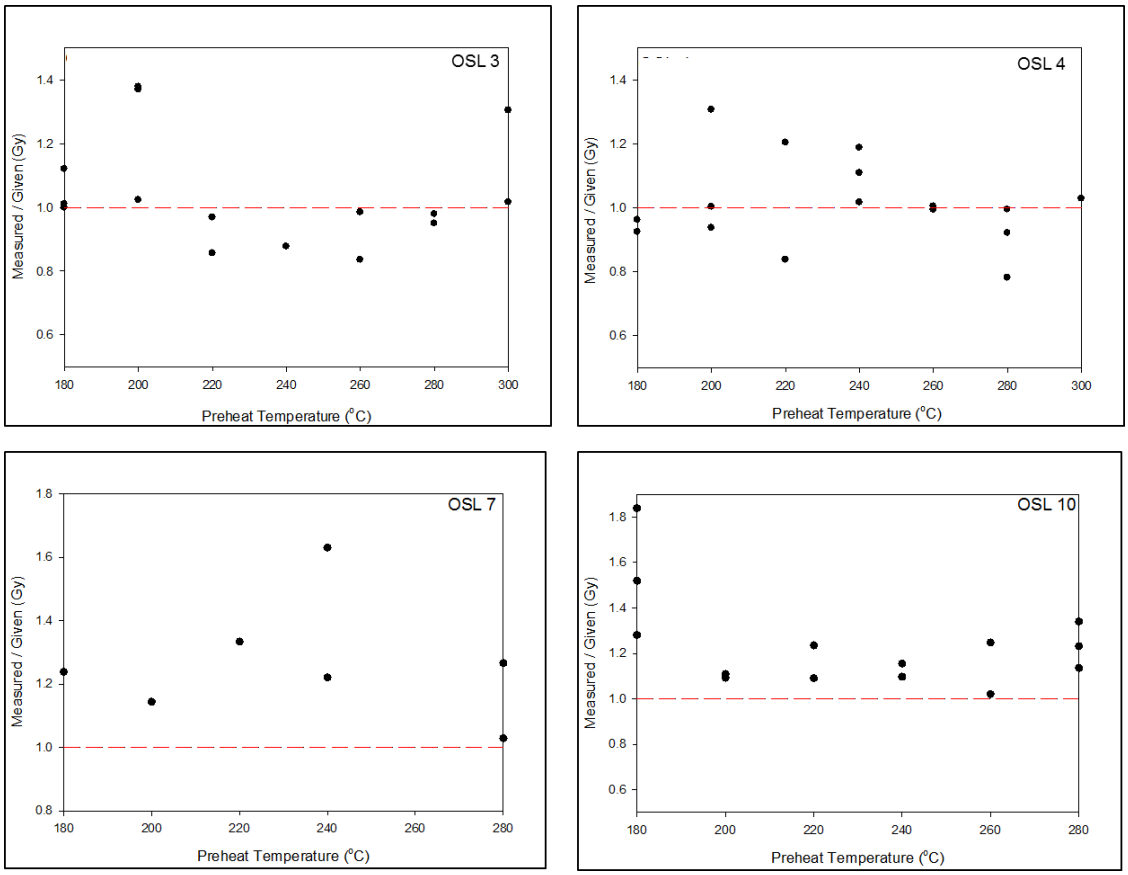


Figure 6.3 Dose recovery determined by dividing the measured dose by the given dose for different preheat temperatures for samples OSL3, OSL4, OSL7 and OSL10. The dotted line represents unity.

The results of the preheat plateau and the dose recovery tests indicate that, while no significant D_e dependence on preheat temperatures was evident, the preheat temperature of 200°C returned the best dose recovery (Figure 6.3). Therefore a preheat/cut-heat combination of 200°C / 180°C was selected for the SAR protocol to determine D_e. The exception to this was OSL3 where 180 °C returned a measured D_e closest to the given value (Figure 6.3).

6.3.3 Determining the Equivalent Dose (D_e)

The Heelbo samples met the requirements of the initial tests and the single aliquot regenerative (SAR) protocol was applied to determine D_e of the samples (as described in Murray and Wintle, 2000), with the addition of the IR stimulation for the IR-OSL depletion for feldspar contamination. Aliquots of 2 mm mask size were prepared, as Olley *et al* (1999) suggested that it is preferable to reduce the number of grains in an aliquot to detect heterogeneous bleaching. The reduced number of grains would make it easier to determine the differences in D_e values of different grains.

D_e is calculated by interpolation of the natural dose onto the dose response curve and each aliquot produces a single D_e value (Preusser *et al*., 2008). It is possible that an aliquot may not produce a D_e value, for the following reasons: a) no detectable OSL signal is present owing to the lack of light-emitting grains in the aliquot, b) neither an exponential nor exponential plus linear function can be fitted to the L_x/T_x points resulting in

the absence of a growth curve, c) failure of the recycling ratio test due to non-functioning sensitivity correction, d) failure of the OSL-IR depletion ratio test owing to feldspar contamination, and e) when the natural dose (L_n/T_n) does not intercept the dose response curve (Jacobs, 2004).

6.3.3.1 Rejection of data

For each sample a number of aliquots were prepared but not all of the measured aliquots were used to determine D_e, as some were rejected. The rejection of aliquots was processed by the Analyst programme and only the accepted aliquots are used to calculate the age of the sample. The rejection criteria used were the recycling ratio and the recuperation test, both of which were set at 10 %, which is a strict application of these criteria.

Recycling Ratio - The recycling ratio test is used to assess reproducibility within the SAR measurement cycle and if SAR is successfully correcting for the sensitivity changes. If the SAR is successfully correcting for sensitivity changes then the value for the recycling ratio is close to unity (Wintle and Murray, 2006). For real data, sets Murray and Wintle (2000) suggest a range of acceptability from 0.90 to 1.10 for this ratio. The recycling ratio and associated errors for the Heelbo samples are shown in Figure 6.4.

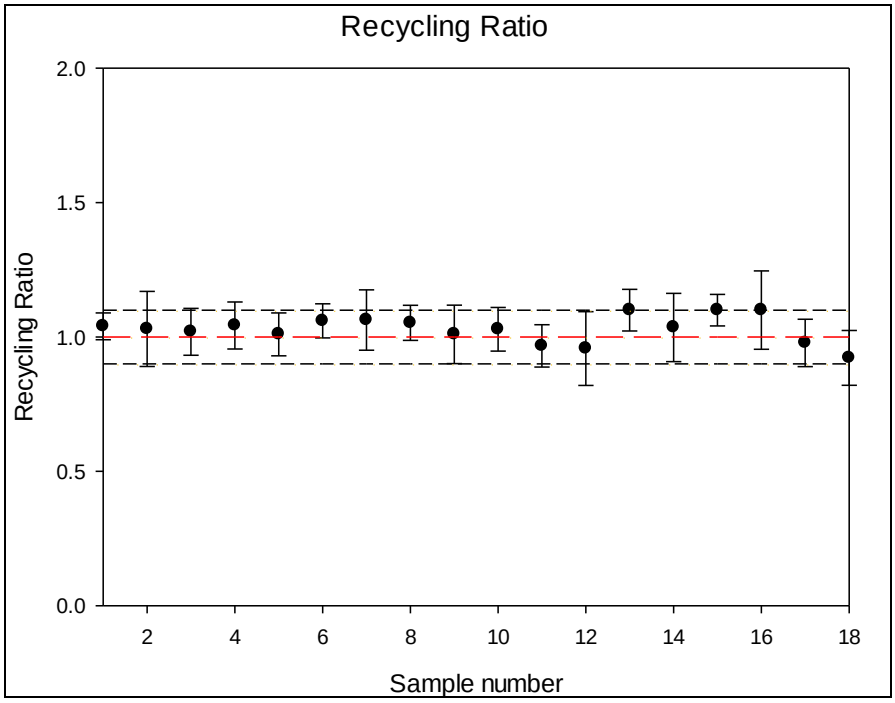


Figure 6.4 Recycling ratio and associated errors for the Heelbo OSL samples. All the samples fall within the acceptable recycling ratio limit of 0.9 to 1.1 (shown by the black dotted lines).

All the samples return a recycling ratio between the accepted limits shown by the dotted lines in Figure 6.4. Samples OSL 13, OSL 15 and OSL 16 are located at the limit of the rejection criteria, but these are still considered valid, as it is the measured value that is accepted, not the effect of the errors.

Recuperation Test - Measurement of a zero dose point should give zero signals, however the transfer of charge may cause the signal to be above zero. Recuperation is tested by expressing the ratio between an additional zero dose OSL signal and the natural OSL signal as a percentage of the natural equivalent dose. All values greater than 5%

were rejected, as suggested by Murray and Wintle (2000). The aliquots were rejected by the Analyst programme during data processing and did not form part of the D_e analysis.

The equivalent dose for each sample was measured using the standard SAR protocol with the corrections as discussed. The data were analysed on the Analyst programme from where the D_e was determined.

6.3.4 Graphical Display Methods

The graphical display of the data obtained for D_e measurements is important for the correct interpretation of the dose distributions and for deriving a D_e value appropriate for age calculations. The most common graphical displays for luminescence data are histograms, probability density plots and radial plots. The graphical display allows for the determination of coherent patterns in the data set and Murray *et al*. (1995) suggest that the form of the distribution can be used to identify heterogeneous bleaching and sedimentary processes such as bioturbation or pedoturbation (Bateman *et al*., 2003).

6.3.4.1 Histograms

The shape of the dose distribution of a sample is shown on a histogram, however, no indications of the errors associated with individual values are

shown. It is therefore impossible to differentiate between those D_e values that have low errors and those that have higher errors, therefore there is a large uncertainty associated with the values (Galbraith *et al*., 1999). As a result, it is not possible to determine whether an outlier is a true outlier or whether it falls within error of the main population (Rodnight, 2006). Figure 6.5 shows the histograms of the Heelbo samples where dose distributions indicate heterogeneous bleaching in OSL2, OSL7 and OSL8 for example, whereas OSL10, OSL13 and OSL15 display more homogenous populations. The value of the histograms is that it shows mixed populations in the sample group and therefore reflects incomplete bleaching of some of the grains in the sample. While the spread in D_e is obvious, it is not possible to tell the accuracy of the outliers without the associated errors.

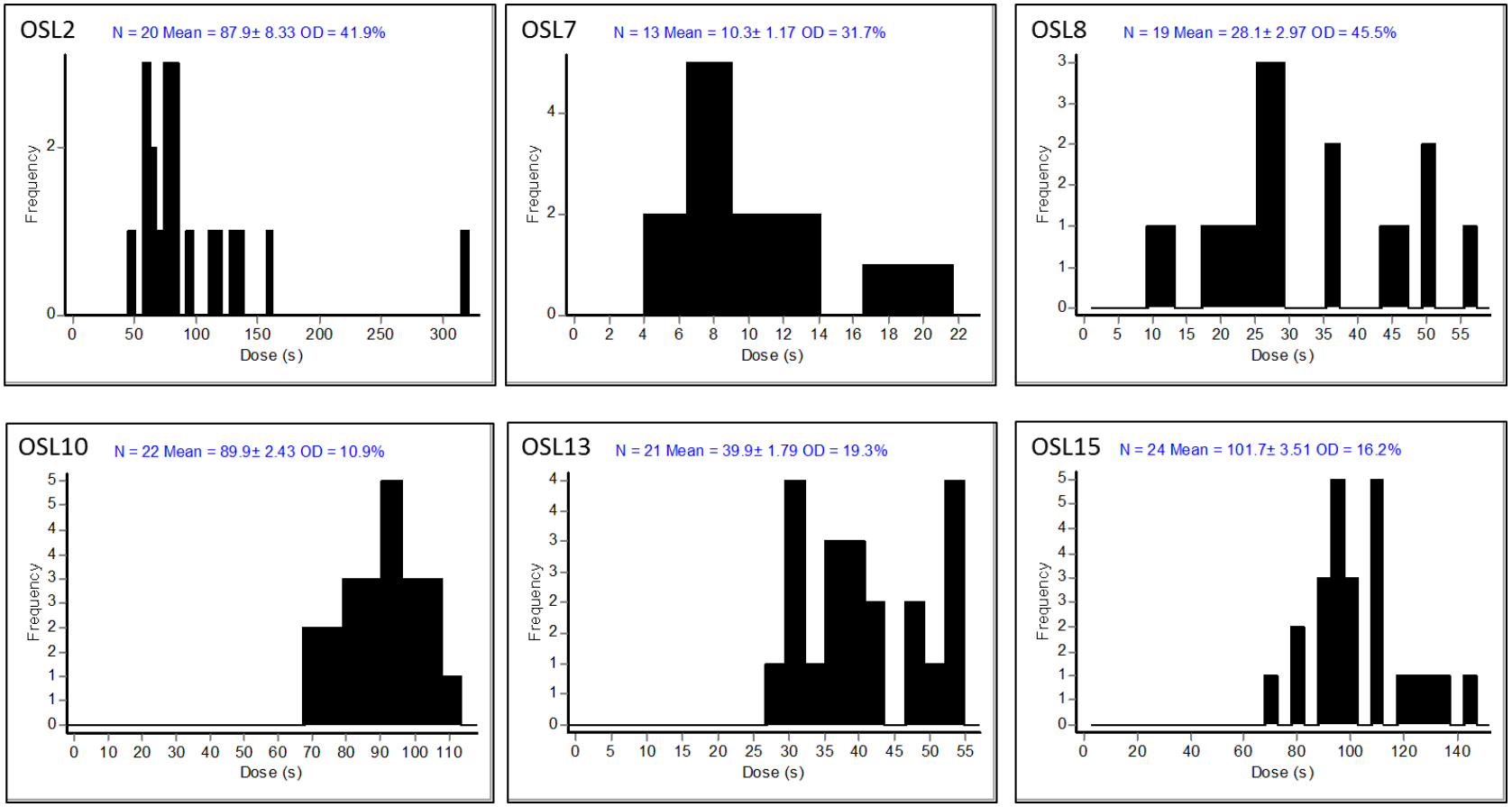


Figure 6.5 Histograms of weighted mean showing central age model D_e values.

6.3.4.2 Radial Plots

Radial plots were suggested by Galbraith (1988) and Galbraith *et al*. (1999) as a method to display individual data values that have highly variable errors associated with them, as in fission track dating or luminescence dating. The radial plot shows both the D_e estimate of a value and the error associated with it, where D_e is read off the right hand logarithmic scale, by extending a straight line from the origin of the left-hand y-axis through the selected data point. The percentage relative error for the given point is read off the top scale on the x-axis by dropping a vertical line from the point to the axis. The precision or reciprocal of the relative error can be read off the bottom x-axis (Galbraith *et al*., 1999; Rodnight, 2006). D_e values with relatively small errors and high precision fall to the right of the diagram, whereas less precise D_e estimates plot towards the left side. An appropriate error calculation is essential for plotting data values accurately in a radial plot to show the correct distribution of values. The radial plots for all the samples are shown in Figure 6.6. Where the aliquots plot within the 2σ band, it suggests complete rather than partial bleaching of the grains.

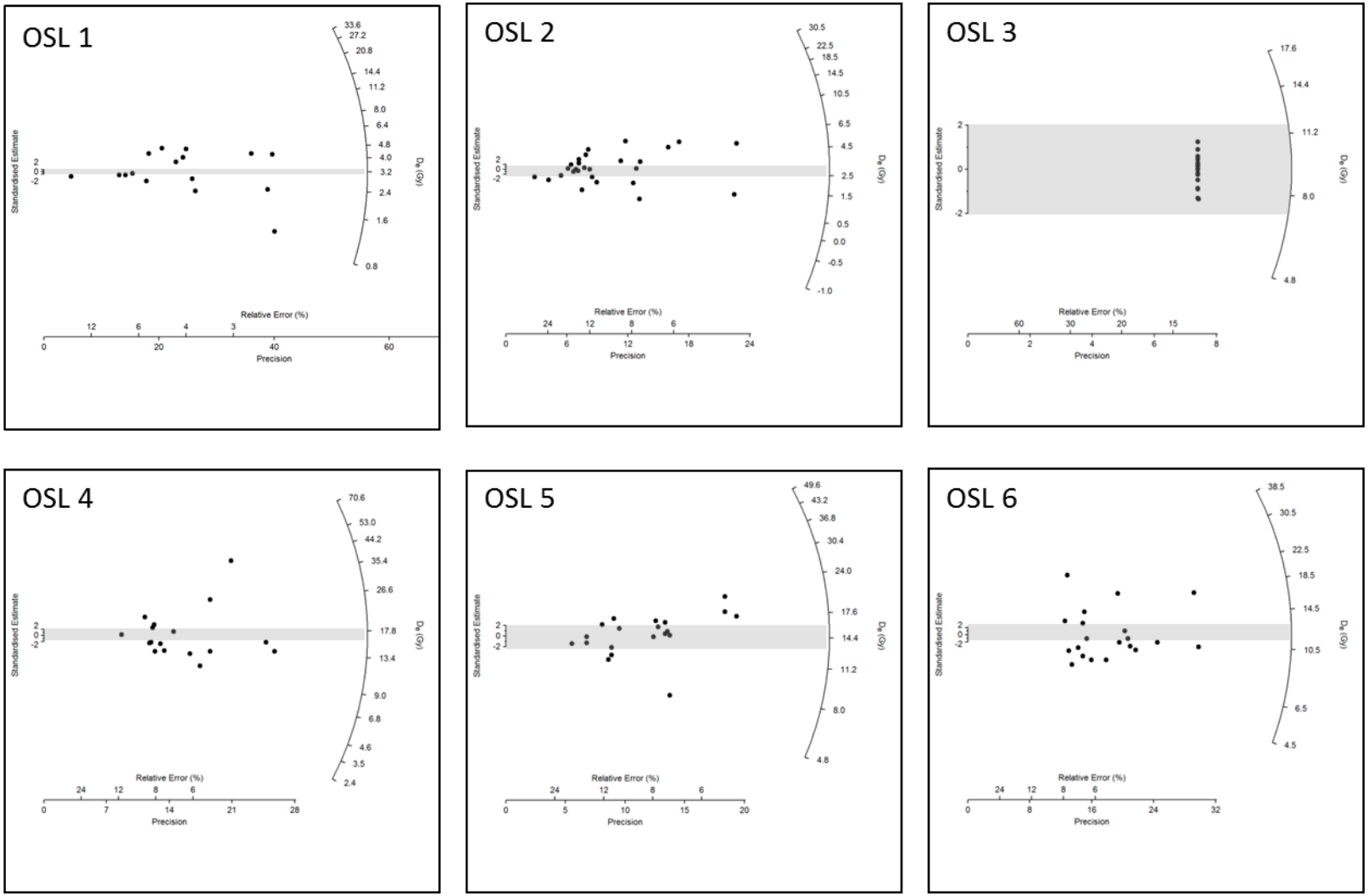


Figure 6.6 Radial plots for samples OSL 1-6 showing the equivalent dose distributions.

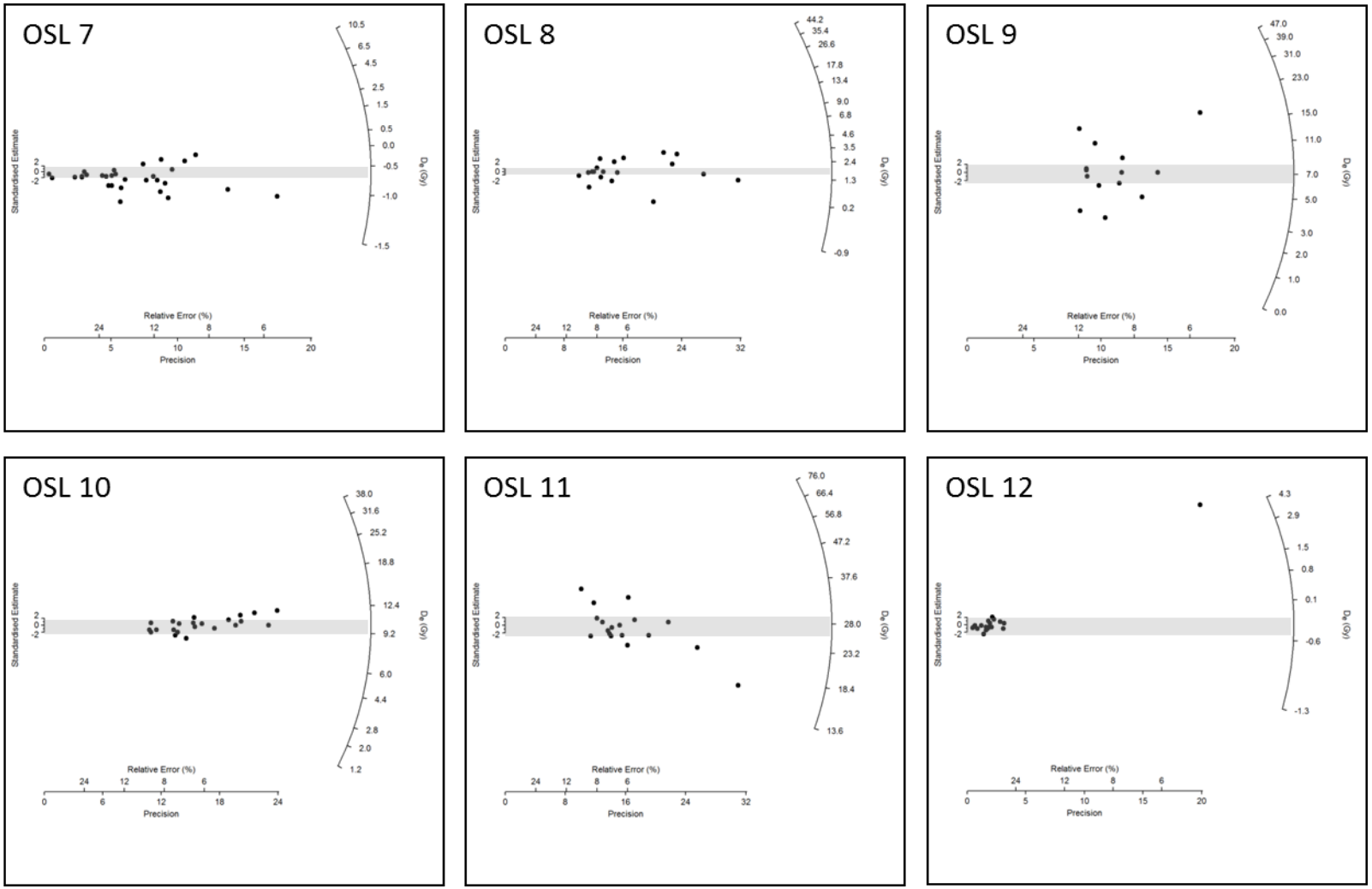


Figure 6.6 (continued) Radial plots for samples OSL 7 -12 showing the equivalent dose distributions.

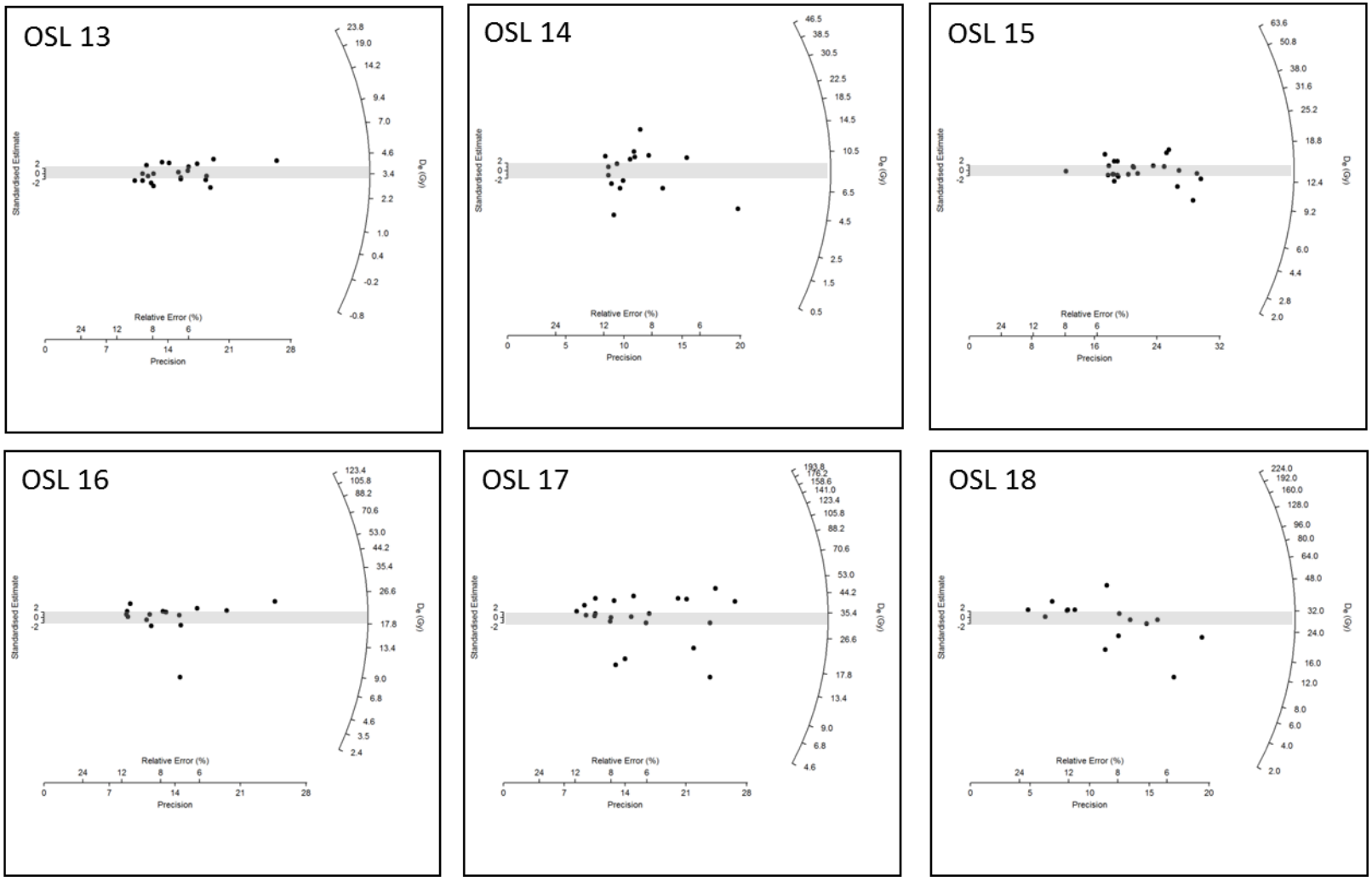


Figure 6.6 (continued) Radial plots for the samples OSL 13-18) showing the equivalent dose distribution. All plots are centred on the D_e derived from the central age model (CAM), with the 2σ standard deviation shaded.

Aliquots in OSL 3 record high precision with relatively low error and all the values are centred on the central age. This sample reflects a homogeneous sample population where all the grains are evenly bleached. Samples OSL 10, 13 and 15 also reflect a low degree of scatter in the population and the D_e values are centred on the mean. The rest of the samples reflect a great degree of scatter in the population. Sample OSL 12 has an extreme outlier, relative to the mean, which can negatively affect the age of the sample

6.3.5 Determination of the True Burial Dose (D_b)

To obtain a luminescence age, a meaningful true burial dose (D_b) has to be calculated from the numerous aliquot measurements, and therefore calculated from the multiple D_e values for each sample. As a result, the individual values for $D_e \pm 1\sigma$, (where σ is the standard error) have to be combined to obtain a single value for D_b (Rodnight, 2006). A common approach is to determine a simple mean or a weighted mean with the standard errors calculated as σ/n or $\sigma/\sqrt{n}$, respectively; where n is the number of independent estimates (Jacobs, 2004). However, a simple or weighted mean is often not appropriate, given the distribution of D_e values measured for each sample. It is possible to derive a representative D_b using more complex statistical models such as the central age model (CAM), finite mixture model (FMM) or the minimum age model (MAM) (Jacobs, 2004; Galbraith *et al*., 2005; Rodnight, 2006). However, multiple

D_e values may present with scatter in the datasets, which is expressed as overdispersion of the dataset.

The random variations in the dataset that cannot be explained by the measurement uncertainty are defined as overdispersion and this can be estimated using the statistical models (particularly the central age model) (Galbraith, 1994). Well-bleached quartz has shown overdispersion values of ≤20% where the aliquots have been heated prior to irradiation (Olley *et al*., 2004; Galbraith *et al.*, 2005; Thomsen *et al*., 2005). Therefore, an overdispersion of ~20% is used as a guide to determining the statistical model used to ascertain the true burial age. However, this is only a rough guide, as depositional environment and history also need to be considered, when deciding on the statistical model to be used to calculate D_b.

6.3.5.1 Central Age Model (CAM)

The central age model computes a statistic much like a weighted average but it assumes a natural distribution of values rather than one true value. The standard deviation of this distribution is called the overdispersion and represents a variation that cannot be accounted for statistically (Feathers, 2008). The CAM is based on the determination of two unknown parameters: the mean true logarithmic D_e (σ) and the standard deviation (σ), and it is assumed that $\sigma > 0$ (Galbraith *et al*., 1999). The CAM is

used when the overdispersion is below 20% and it is assumed that the samples have been uniformly bleached to the same extent (i.e. homogenous bleaching). The CAM D_b was obtained through a software programme add-on to Microsoft Excel provided by Geoff Duller (University of Aberystwyth, UK).

6.3.5.2 Minimum Age Model (MAM)

If incomplete bleaching is expected to be the reason for the skewed dose distribution, the minimum age model (MAM) is considered to be the most appropriate statistical model to determine only bleached grains at deposition (Rodnight, 2006). These samples would produce a large amount of scatter and a large overdispersion, greater than 20%. The MAM uses a truncated normal distribution and fits it to the individual D_e data points to determine the proportion of grains that were fully bleached before they were deposited (Galbraith and Laslett, 1993).

The MAM is used on partially bleached sediment from depositional environments such as archaeological material, deep-sea deposits, soils, and young, water-logged, sediments. In each case the grains would have been partially bleached prior to deposition and the MAM would apply to these sediments rather than those where the scatter is produced by post-depositional mixing (Olley *et al*., 2004). The MAM is calculated on a

programme written for the statistical package ‘R’ and was provided by Geoff Duller (University of Aberystwyth, UK).

6.3.5.3 Finite Mixture Model (FMM)

Galbraith and Green (1990) describe the finite mixture model (FMM) as appropriate for sediments containing grains of more than one discrete population, where each population (component) is well bleached and can be described by the central age model. With the FMM it is possible to estimate the number of dose components within a dose distribution, the corresponding D_e for each component and the relative proportion of each component (Galbraith and Green, 1990). For the FMM, the number of components (k) must be defined as well as the standard deviation (σ) of each component. The programme fits the components to the dataset, and for each component it gives the appropriate D_e and its error. In addition it generates two parameters: the log likelihood and the Bayesian Information Criterion (BIC). These parameters are used to assess the most appropriate number of components to fit to a dataset. The software can be run repeatedly on a dataset, steadily increasing the number of components (k). The BIC reduces to a minimum at the best fit, and then increases again. The number of dose components, starting with k=2, can be increased successively and the estimated maximum likelihood estimate can be used to choose the final k (Galbraith and Green, 1990). The finite mixture model can be applied to a heterogenously bleached sample. The

model selects populations based on D_e values that are consistent with one another and the appropriate D_e of the lowest population will be derived from a normal distribution of the lowest values. Therefore, if the dataset contains some D_e values measured from well-bleached grains, the appropriate D_e value can be determined from the lowest population for this sample. The estimate should decrease for an improved fit and then increase again when there are signs of parameter redundancy (Roberts *et al*., 2000; Jacobs, 2004). The FMM reduces to the central age model for k=1. The FMM is used for single-grain measurements and not for multi-grain aliquots that cannot randomly distinguish k>1. While the FMM was not used in determining the D_b for the Heelbo samples, it is described here for completeness.

The D_b values of the central and minimum age models and the overdispersion parameter for the Heelbo samples are presented in Table 6.3.

Table 6.3 The burial dose (D_b) for the central age model (CAM) and minimum age model (MAM) and associated errors calculated for the Heelbo samples with the overdispersion (OD) and associated errors.

Sample	CAM with error (Gy)	MAM with error (Gy)	Overdispersion (OD) with error (%)
OSL 1	3.24±0.49	1.29±0.07	60±2
OSL 2	4.89±0.54	2.21±0.31	56±2
OSL3	11.27±0.32	11.20±0.49	6±1
OSL4	19.67±2.12	14.43±2.34	42±2
OSL5	14.38±1.64	4.56±1.02	53±2
OSL 6	13.89±1.32	8.71±0.93	42±2
OSL 7	1.39±0.16	0.96±0.22	32±3
OSL 8	3.80±0.40	1.98±0.31	45±2
OSL 9	9.30±1.63	3.42±0.71	65±3
OSL 10	12.13±0.33	12.09±0.77	11±1
OSL 11	29.77±2.23	21.27±2.21	31±1
OSL 12	1.64±0.35	0.75±0.50	70±5
OSL 13	5.39±0.24	4.52±0.39	19±1
OSL 14	10.36±1.31	5.10±0.90	49±2
OSL 15	16.07±0.56	14.26±1.06	16±1
OSL 16	21.48±2.58	7.92±2.69	46±2
OSL 17	35.76±4.15	12.55±2.18	54±02
OSL 18	28.97±3.66	16.85±3.58	39±3

6.3.6 Determining the Annual Dose Rate

The annual dose rate is determined by the beta, gamma and cosmic dose rates. The beta and gamma dose rates are a function of the concentration of U_{nat} (the total U calculated from the measurement of the daughter products in the decay series), Th and K absorbed by the sample over the

burial period of that sample. These radionuclides were determined by high-resolution gamma-spectroscopy at iThemba LABS, Johannesburg, and the measured concentrations are given in Table 6.4, from which the total beta and gamma dose rates (in Gy/ka) were calculated using the conversion factors by Adamiec and Aitken (1998) to determine the dose rates contributed by each element.

Table 6.4 Concentration of U_{nat}, Th and K and the associated errors

Sample	Th	U_{nat}	K
	ppm	ppm	%
OSL1	8.87±0.08	1.49±0.14	1.82±0.01
OSL2	12.1±0.19	1.62±0.07	2.02±0.028
OSL3	9.66±0.24	2.69±0.04	1.64±0.028
OSL4	7.39±0.16	1.24±0.06	1.92±0.026
OSL5	11.82±0.28	2.98±0.05	2.19±0.037
OSL6	11.24±0.18	2.22±0.04	2.11±0.007
OSL7	11.58±0.18	2.4±0.04	2.13±0.025
OSL8	9.00±0.26	2.19±0.04	1.58±0.028
OSL9	12.95±0.19	2.29±0.08	1.75±0.024
OSL10	12.09±0.28	2.4±0.04	2.01±0.033
OSL11	10.93±0.2	2.07±0.08	1.85±0.026
OSL12	9.23±0.18	1.69±0.07	1.71±0.025
OSL13	12.53±0.21	1.88±0.08	2.26±0.032
OSL14	13.44±0.19	2.07±0.07	2.31±0.029
OSL15	12.88±0.2	2.47±0.08	1.85±0.027
OSL16	14.09±0.23	2.6±0.09	2.35±0.031
OSL17	14.7±0.2	2.6±0.08	2.26±0.026
OSL18	12.64±0.2	2.4±0.08	1.92±0.026

The concentrations reported by iThemba LABS are not that of the parent material. Instead the equivalent concentrations (i.e. daughter isotopes) are measured, that would have produced the gamma spectrum. Olley *et*

al., (1996) suggest that, for luminescence dating, two assumptions must be made regarding the radioactive history of the samples: 1) the decay chains are, and have always been, in equilibrium; and 2) the dose rate measured at the time of the sample collection has prevailed throughout the period of burial. However, this assumption does not necessarily imply secular equilibrium. The first assumption typically applies when parent nuclide concentrations are determined. The second assumption is made when the dose rates are deduced from thick-source alpha counting or gamma spectrometry (where gamma spectrometry measures nuclides in the lower half of the uranium and thorium decay chains) (Olley *et al*., 1996). Where the second assumption is made, that the dose rate has prevailed over the period of burial, then the disequilibrium in the decay chains will have a negligible effect on the results of the Heelbo samples. The concentrations were converted to a beta and gamma dose rate using the relevant conversion factors for U and Th (Table 6.5) and K (Table 6.6) from Adamiec and Aitken (1998).

Table 6.5 Dose rate conversion factors for the thorium and uranium series (Adamiec and Aitken, 1998, p.43)

	^{232}Th	^{238}U	^{235}U	U $_{nat.}$
1. Abundance by weight	100%	99.29%	0.71%	-
2. Half-life (Ga)	14.05	4.468	0.704	-
3. Parent Activity (Bq mg^{-1})	4.06	12.4	80	12.9
4. Activity Share in nat. U	-	95.6%	4.4%	-
Dose-rate (Gy ka-1) per ppm				
5. beta, full-series	0.0273	0.143	0.515	0.146
6. gamma, full series	0.0476	0.112	0.269	0.113
Dose-rate (Gy ka-1) per unit specific activity (Bq kg-1)				
7. Divide lines 5-10 by	4.06	12.4	80	12.9

Table 6.6 Dose rate data for potassium and rubidium (Adamiec and Aitken, 1998, p.44)

	^{40}K	^{87}Rb
1. Natural abundance (mg/g)	0.119	283
2. Half-life (Ga)	1.277	47.5
3. Average energy per disintegration (MeV)	β: 0.501 γ: 0.156	β: 0.082
4. Specific activity (Bq kg^{-1}) for concentration of 1% natural K and 50 ppm natural Rb	β: 270 γ: 32.5	β: 0.45.29
5. Dose-rate (Gy ka^{-1}) for concentrations of 1% natural K and 50 ppm natural Rb	β: 0.782 γ: 0.243	β: 0.019
6. As in 5 but for 1% K_2O and 50 ppm Rb_2O	β: 0.649 γ: 0.202	β: 0.017

The beta dose rate requires a correction for the attenuation of the beta particles within the quartz grain (Mejdahl, 1979; Aitken, 1985). The size of the grain and the energy of emission determine the degree of attenuation, and these differ for U, Th and K. As the 180 – 212 µm quartz fractions were used to determine the dose rate, the correction factors of Mejdahl (1979) are used (Table 6.7).

Table 6.7 Correction factors for beta attenuation of quartz grains in the 180-212 µm grain size (Mejdahl, 1979).

	Correction Factor
U_{nat}	0.80 ± 0.07
Th	0.733 ± 0.08
K	0.931 ± 0.06

Both the beta and gamma dose rates are corrected for the water content for reasons explained previously (see Chapter 4) and the moisture content was determined in the laboratory (Table 6.8). The Heelbo area, while being essentially a dry environment, does fall in a summer rainfall region and is prone to flash-flood events. Also, the high clay content in the soil suggests waterlogging for some period of time. Taking these factors into consideration, the measured moisture content is presumed to reflect the saturation history of the sample area over the life time of the deposit. Therefore, the measured moisture content with an error margin of 1% is assumed to cover the range of variability that might have occurred had the site been substantially wetter than the present, at a given time in the burial history of the deposit. The error on the water content is relatively low but, as the measured values are used in the calculation, any higher error would give a negative water content value. The water content measurement for each sample is shown in Table 6.8.

The variables were used to calculate the total environmental dose rate by determining the total attenuated beta, gamma and cosmic dose rates. An example of the calculation for sample OSL3 is presented in APPENDIX D.

6.3.7 THE LUMINESCENCE AGES

The luminescence ages (shown in Table 6.8) are calculated as the palaeodose (D_b) divided by the total dose rate. The ages for both CAM and MAM were determined. The luminescence age represents the burial date of the quartz grains after they had been exposed to light. Luminescence ages have no datum and are calculated in true calendar years. The date is reported relative to the calendar year of sampling (AD 2013) as it is assumed that a sample does not absorb radiation once it has been extracted (Jacobs, 2004).

Table 6.8 Palaeodose (D_b), dosimetry and total dose rates and luminescence ages calculated for CAM and MAM for the Heelbo samples.

Sample	Th	U_{nat}	K	Cosmic Dose Rate	Water Content	Total Dose Rate	Palaeodose CAM	Palaeodose MAM	Luminescence Age CAM	Luminescence Age MAM
	ppm	**ppm**	**%**	**Gy.ka^{-1}**	**%**	**Gy.ka^{-1}**	**Gy**	**Gy**	**a**	**a**
OSL1	8.87±0.08	1.49±0.14	1.82±0.01	0.31±0.02	1.25±1	3.06±0.15	3.24±0.49	1.29±0.07	1060±170	420±30
OSL2	12.1±0.19	1.62±0.07	2.02±0.028	0.29±0.02	1.40±1	3.49±0.17	4.89±0.54	2.21±0.31	1400±170	630±90
OSL3	9.66±0.24	2.69±0.04	1.64±0.028	0.34±0.02	1.29±1	3.20±0.16	11.27±0.32	11.20±0.49	3530±200	3500±180
OSL4	7.39±0.16	1.24±0.06	1.92±0.026	0.29±0.02	1.28±1	2.97±0.15	19.67±2.12	14.43±2.34	6620±790	4450±820
OSL5	11.82±0.28	2.98±0.05	2.19±0.037	0.34±0.02	2.28±1	2.44±0.11	14.38±1.64	4.56±1.02	5890±720	1870±430
OSL6	11.24±0.18	2.22±0.04	2.11±0.007	0.33±0.02	1.39±1	3.67±0.18	13.89±1.32	8.71±0.93	3790±410	2370±280
OSL7	11.58±0.18	2.4±0.04	2.13±0.025	0.30±0.02	2.55±1	2.43±0.11	1.39±0.16	0.96±0.22	570±70	400±90
OSL8	9.00±0.26	2.19±0.04	1.58±0.028	0.28±0.01	1.67±1	2.46±0.12	3.80±0.40	1.98±0.31	1560±180	810±130
OSL9	12.95±0.19	2.29±0.08	1.75±0.024	0.30±0.02	2.45±1	3.42±0.16	9.30±1.63	3.42±0.71	2720±490	1000±210
OSL10	12.09±0.28	2.4±0.04	2.01±0.033	0.27±0.02	2.32±1	2.40±0.11	12.13±0.33	12.09±0.77	5040±270	5030±400
OSL11	10.93±0.2	2.07±0.08	1.85±0.026	0.26±0.02	1.08±1	3.33±0.17	29.77±2.23	21.27±2.21	8940±810	6390±740
OSL12	9.23±0.18	1.69±0.07	1.71±0.025	0.34±0.02	1.78±1	2.98±0.15	1.64±0.35	0.75±0.50	550±120	250±170
OSL13	12.53±0.21	1.88±0.08	2.26±0.032	0.31±0.02	3.21±1	3.75±0.18	5.39±0.24	4.52±0.39	1440±100	1210±120
OSL14	13.44±0.19	2.07±0.07	2.31±0.029	0.29±0.02	2.00±1	3.94±0.20	10.36±1.31	5.10±0.90	2630±360	1300±240
OSL15	12.88±0.2	2.47±0.08	1.85±0.027	0.27±0.02	2.25±1	3.53±0.17	16.07±0.56	14.26±1.06	4550±280	4040±320
OSL16	14.09±0.23	2.6±0.09	2.35±0.031	0.21±0.02	2.01±1	4.07±0.21	21.48±2.58	7.92±2.69	5270±690	1940±670
OSL17	14.7±0.2	2.6±0.08	2.26±0.026	0.25±0.02	3.97±1	3.98±0.19	35.76±4.15	12.55±2.18	8980±1130	3150±570
OSL18	12.64±0.2	2.4±0.08	1.92±0.026	0.33±0.02	2.22±1	3.59±0.18	28.97±3.66	16.85±3.58	8070±1090	4690±1020

6.3.7.1 Factors affecting the OSL Ages

The calibration of the radiocarbon ages (see Section 6.2) suggests that, for the Heelbo samples, the calibrated ages are not reliable and cannot therefore, be used in the discussion of the reconstruction of the palaeo-environment of the hillslope deposit. Therefore, the OSL ages are critical and need a robust assessment of their validity.

Partial bleaching of the quartz grains is a significant problem with the Heelbo samples. It is the length of time since the quartz grains were last exposed to sunlight that is being measured, as it is the sunlight that resets the clock. Therefore, the amount of sunlight that the grains are exposed to is critical. Grains transported by water are commonly not sufficiently exposed to sunlight to reset the signal (Rittenour, 2008). This partial bleaching produces a great deal of scatter in the data and can result in an over-estimation of the age (Rittenour, 2008). Similarly, post-depositional mixing and reworking of the sediment can expose some grains to sunlight, while the rest carry the residual signal. This can lead to an under-estimation of the age. Ideally, where there is large scatter in the data, it would be useful to do single-grain measurements. However, single-grain measurements of the Heelbo samples were abandoned when less than 10% of the grains contributed to the luminescence signal, and the small aliquots and single grain measurements were found to be comparable. To generate the single D_e value from the D_e distribution the MAM was used,

which targets only the most fully bleached component of the samples (Galbraith *et al*., 1999).

The water content is another factor that may affect the validity of the ages. The Free State region is a very dry area presently (Botha, 1996). However, it is possible that a different, possibly wetter, climate regime may have prevailed. This is suggested by the presence of the palaeosols in the stratigraphic sequences. The measured water content, which was quite low, was used for the age calculation. Figure 6.7 shows the effect that an increase in the water content would have on the age of selected samples. In all cases, there is a slight increase in the ages (less than 1ka), and above 15 % the effect appears to stabilise. The error on the ages is also low, except for HLB16. This suggests that the water content does have a meaningful effect on the ages initially, but this then becomes negligible, even if the environment became much wetter in the past.

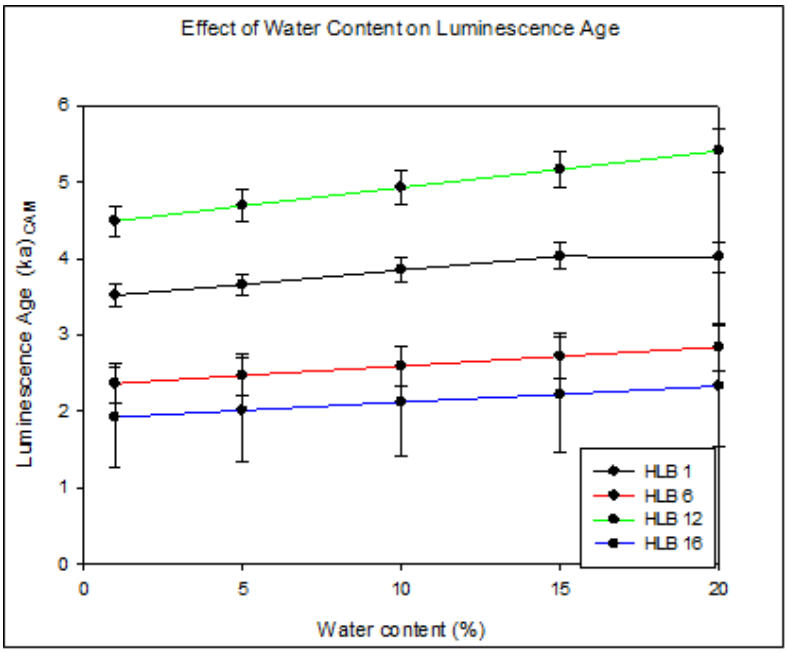


Figure 6.7 Effect of water content on luminescence ages of samples HLB1, 6, 12 and 16.

6.3.7.2 Luminescence Ages for Heelbo

The luminescence ages are presented in their stratigraphic contexts in Figure 6.8 for two B_1 samples at the head of the hillslope deposit; Figure 6.9 for the stratigraphic horizons at Area 1; Figure 6.10 for the units at Area 2; and Figure 6.11 for the bone bed units.

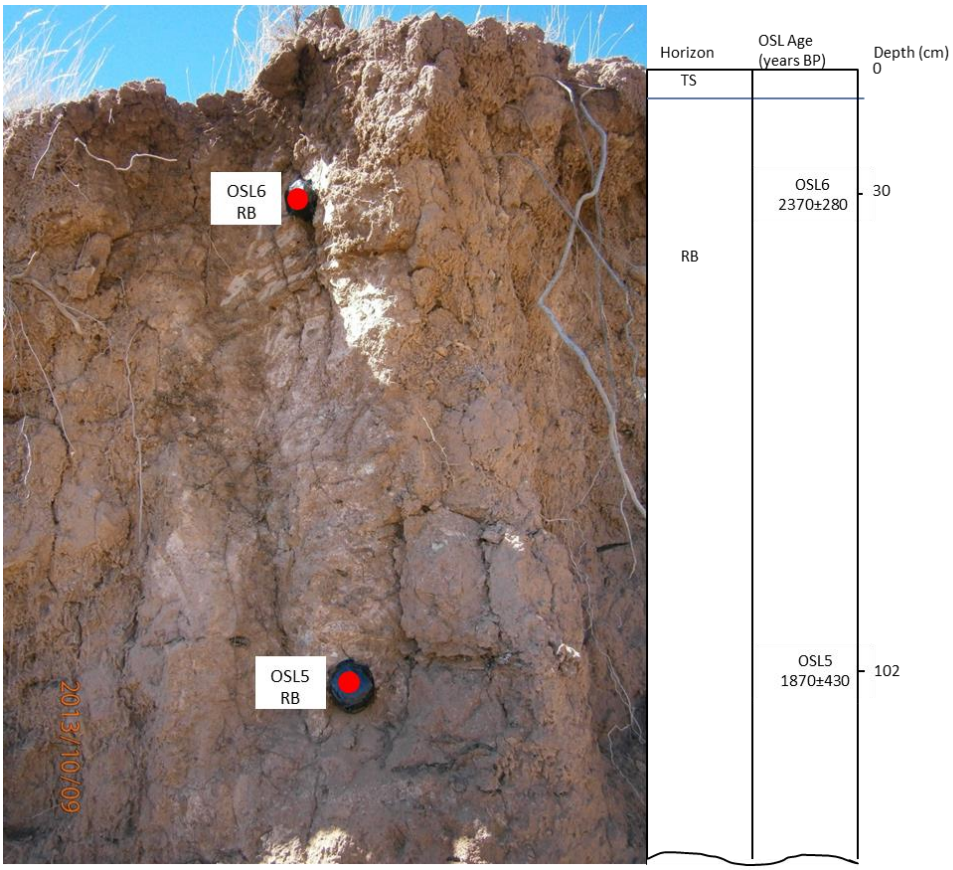


Figure 6.8 Luminescence ages (MAM) for two B_1 samples at the head of the hillslope deposit at Area 1, where the horizon was the thickest (see Figure 4.10 for location). The relative depths in cm are given and the red dots mark the sample positions on the photographs. The OSL age is given as years BP.

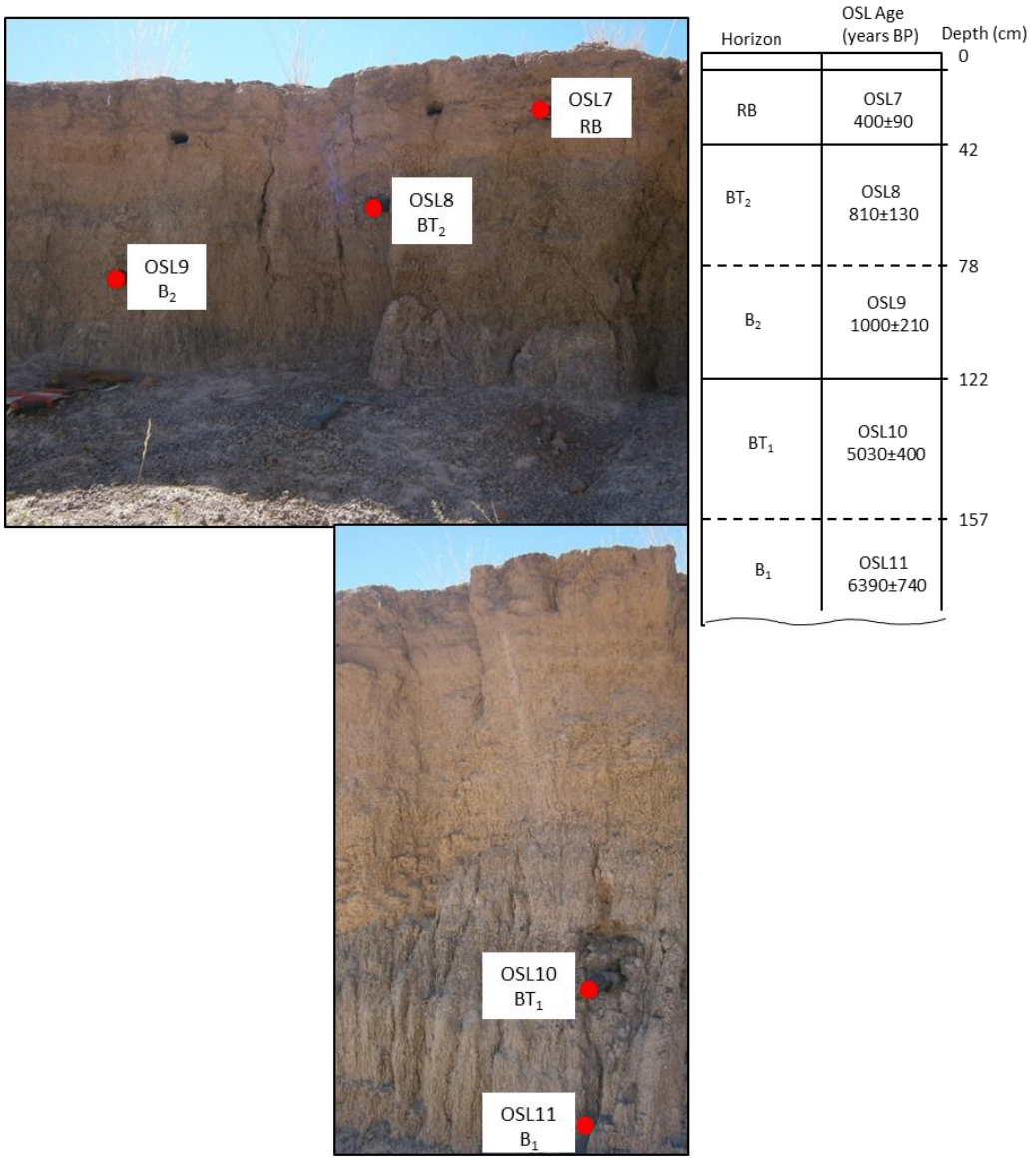


Figure 6.9 Luminescence ages and relative depths of the units of the horizons at Area 1. The red dots indicate the sample positions. Sample location shown in Figure 4.10.

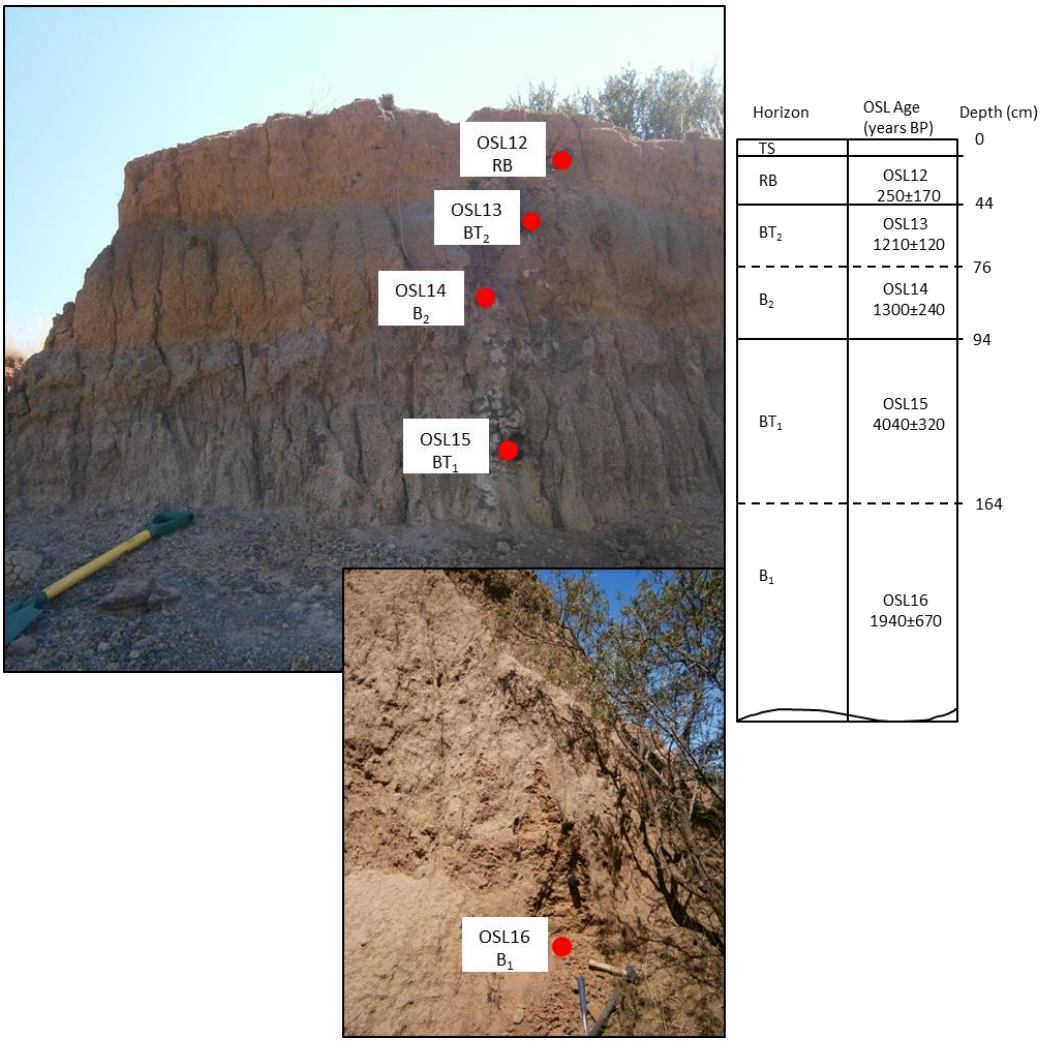


Figure 6.10 Luminescence ages for the stratigraphy at Area 2. As B_1 was not exposed where the other samples were taken, it was sampled to the right of the sequence. Sample location shown in Figure 4.10.

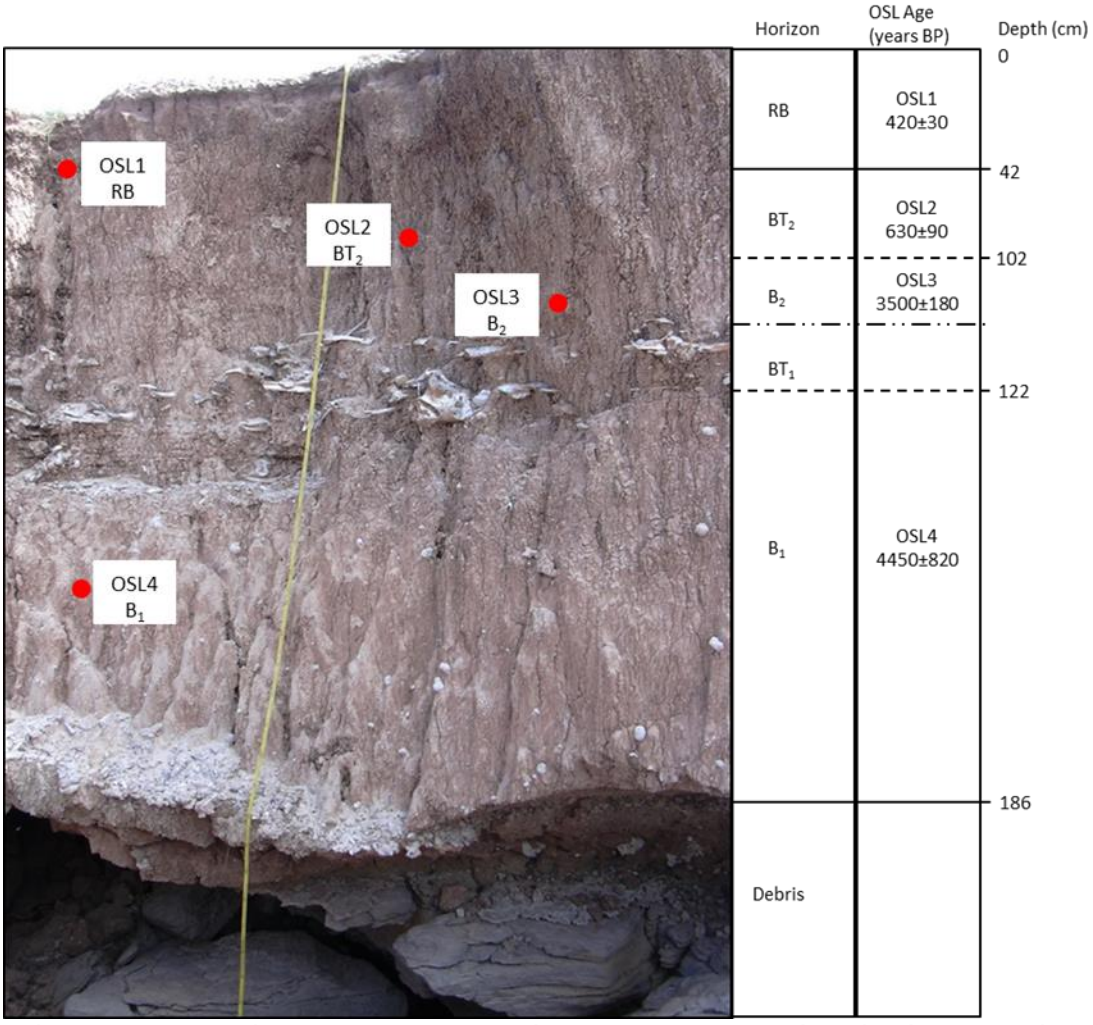


Figure 6.11 Luminescence ages of the RB, BT_2, B_2 and B_1 horizons at the bone bed at the base of the hillslope deposit.

At the base of the deposit, the B_1 horizon is thickest and it was possible to constrain the approximate timing of the first and last period of sediment deposition and attempt to calculate the sedimentation rates. The minimum age for the lowest unit of the B_1 horizon at the head of the deposit (Figure 6.8) is 1 870 ± 430 years BP. Although there is an age inversion recorded in the stratigraphy, with the oldest age found at the top, and the youngest age at the base, these are the same age, within error. This age inversion

occurs for the minimum age model (not the central age model) and implies that the lower unit may be contaminated by younger material. It is necessary to consider post-depositional mixing (bioturbation), which can result in sediment bleaching unrelated to sediment deposition and can potentially invalidate the ages. In this case single grain measurements were considered. However, the low return on luminescence signal (<10%) using single-grain measurements deemed the use of small aliquots comparable (Lyons *et al*., 2013). The age inversion also makes it difficult to calculate the sedimentation rates for this unit.

The minimum ages for Area 1 are consistent with stratigraphy (age increases with depth) and reflect young, late Holocene, sediments (Figure 6.9). The minimum ages for Area 2 are inconsistent with stratigraphy as B_1 is much younger that the overlying unit (Figure 6.10). This B_1 unit is consistent, within error, with the lower B_1 unit at the head of the slope (Figure 6.8). This suggests that post-depositional mixing may also have affected this unit and the mixed populations render this age as unreliable. The B_1 horizon at the bone bed site appears to have been deposited slightly later than at Area 1 at 4 450 ± 820 (Figure 6.11). There would have been a lag in time for the sediment to reach the foot of the slope and for the deposit to become established in this area of the hillslope.

A period of pedogenesis followed sedimentation on B_1, as indicated by the BT_1 palaeosol. This period of soil formation started around 5 030 ± 400

years BP at Area 1, and 4 040 ± 320 years BP at Area 2. Whilst these two episodes are offset by approximately 300 years, within error, the units are close enough, in age, to be comparable. The BT_1 horizon could not be dated at the bone bed and it appears that the B_2 horizon age more likely represents the BT_1 episode of pedogenesis at 3 500 ± 180 years BP, comparable to Area 1 and 2. The problem could possibly be related to the samples taken, as the boundary between BT_1 and B_2 at the bone bed was not always clearly visible, and it could be that the horizons were mistaken for each other.

The BT_1 episode of soil formation was followed by another period of sediment accumulation, $B_{2,}$ at 1 000 ± 210 years BP for Area 1, which is consistent with 1 300 ± 200 years BP at Area 2. This episode of sedimentation is a short one in both areas and implies a rapid, short-lived event before the second stage of pedogenesis (BT_2) began. The ages are consistent with the palaeosols forming in two pulsed depositional events of B_1 and $B_{2.}$

The RB horizon comprises very young sediments at 400 ± 90 years BP at Area 1, 250 ± 170 years BP at Area 2 and 420 ±30 years BP at the bone bed site. The error margin on RB at Area 2 is high relative to the age of the sample; this is consistent with the problems of dating very young samples with OSL.

Samples were also collected from one of the gullies at the foot of the hillslope and, as it is not part of a stratigraphic profile, the ages are shown in stratigraphic context (Figure 6.12). The assumption was made that, after the sedimentary horizons were deposited, there was a period of erosion and incision which would have resulted in the gullies forming. Over time and with a subsequent episode of deposition, the channels filled in, and this sediment should, thus be younger than the youngest dated hillslope horizon, RB. However, surprisingly, the luminescence ages for these samples are older than the hillslope horizons at 4 690 ± 1020 years BP at the top and 3150 ± 570 years BP at the base, and are contemporary with the B_1 horizon in Area 1. These ages are problematic in that they are also not consistent with stratigraphy and collectively are much older that the RB horizon. This suggests that these samples do not, in fact, represent channel-fill material, but are most likely remnants from earlier periods of deposition, possibly of another lobe of deposition on the hillslope.

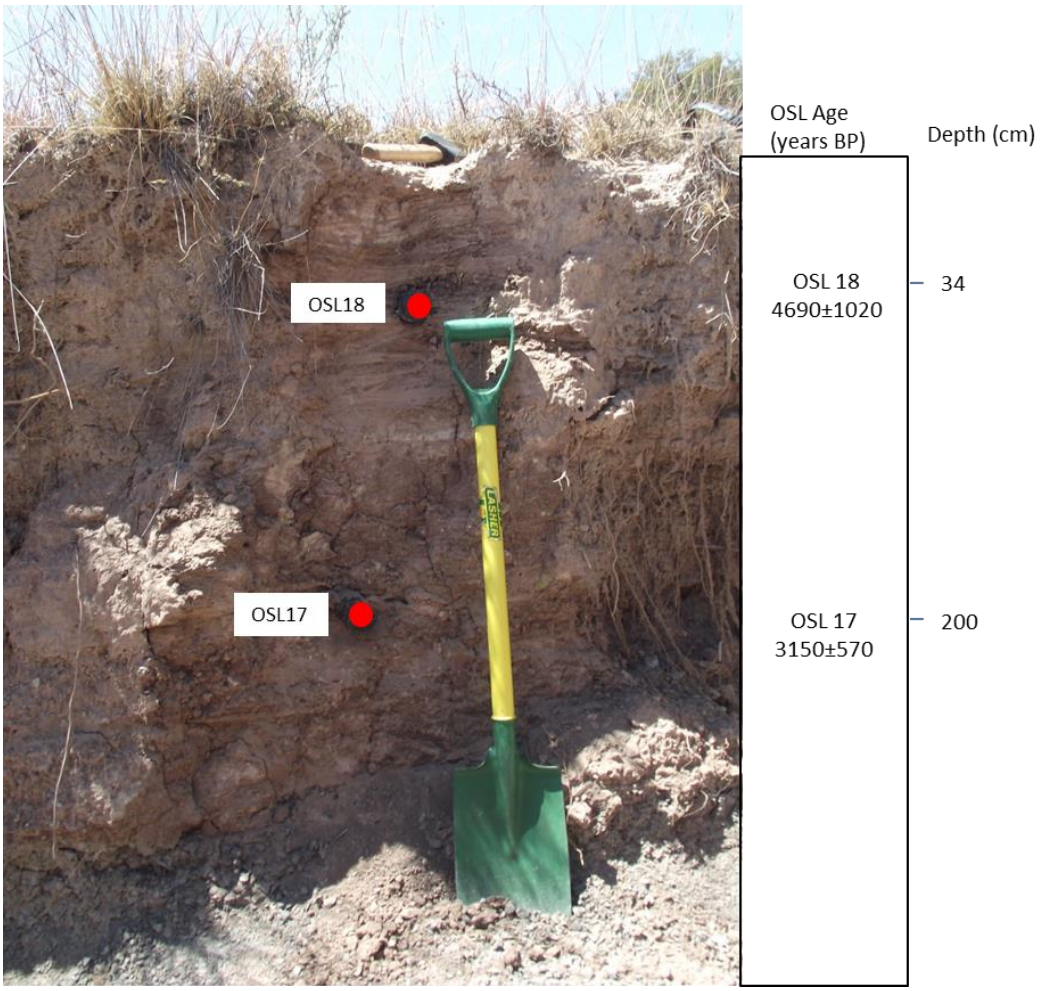


Figure 6.12 Luminescence ages of the channel-fill at the base of Area 1. See Figure 4.10 for location of the site.

The significance of the ages, the rates of sedimentation and the comparisons with the ^{14}C ages are discussed in Chapter 7.

CHAPTER 7 DISCUSSION
GEOLOGY AND SEDIMENTOLOGY OF THE HEELBO HILLSLOPE DEPOSIT

7.1 INTRODUCTION

The characteristics and significance of the Heelbo hillslope deposits are discussed in this chapter. The Heelbo hillslope was divided into three separate areas: Area 1, Area 2 and the bone bed section (Figure 3.9). The bulk of the analysis was carried out in Area 1. This is because unlike at Area 1 where the stratigraphic units are well-preserved, most of the hillslope deposit in Area 2 has been eroded away (Figure 3.3). Towards the base of the slope at Area 2, the units of the stratigraphy are exposed and were described as similar to that of Area 1(see Section 5.3). The bone bed section is not a complete hillslope deposit but also reflects a similar stratigraphy to that at Area 1 and makes up only a small section at the base of the deposit (Figure 5.5b).

Sedimentary mantles, accumulated on hillslopes, have been described as colluvial mantles (Botha, 1996), alluvial fans (De Chant *et al*., 1999), talus slopes (Sas and Krautblatter, 2007) or alluvial slopes (Smith, 2000), each with their own identifying characteristics. The Heelbo hillslope deposit is described in this project, as an alluvial slope deposit which has characteristics consistent with alluvial fans and colluvial mantles.

However, there are also characteristics in the deposit that distinguish it from these features, and these will be discussed in detail in this chapter.

The gullies (Figure 5.4) have exposed the underlying stratigraphy enabling a description of the history of aggradation, erosion and pedogenesis of the deposit. The formation and evolution of the Heelbo deposit and the associated gullies are presented in this chapter. The stratigraphy and sedimentology are also discussed before the history of erosion, sedimentation and pedogenesis are outlined.

7.2 ORIGINS OF THE HEELBO HILLSLOPE DEPOSIT

A fluvial system has formed on the hillslope deposit at Heelbo. The system of streams that flows through the gullies originated on the watershed of the Heelbo mesa and flows into the ephemeral Sandspruit, before joining the Sandrivier north of Senekal (see APPENDIX A). There are a number of similar mesas along the course of the Sandspruit with colluvial mantles on the foot slopes, but none of these have gully systems associated with them (see 1: 50 000 map of Paul Roux, APPENDIX A).

The Heelbo deposit originates midway down from the summit of Spionkop, and spreads out across the valley floor. The position of the deposit midway down from the summit indicates that the source of the sediment is the Spionkop mesa, and that it formed either through scarp retreat or

mass-wasting of the mesa. With scarp retreat or mass-wasting there would have been a mix of colluvial and fluvial material being transported downslope. The assumption we made that some of the material could have been of aeolian origin was discounted as there is no evidence of wind-blown material in the stratigraphy of the deposit or in thin sections (see Section 5.3).

Sediment flows down slope and is deposited on the gentle gradients of the valley floor, mimicking the alluvial fan morphology (Figure 7.1). The sediment spreads out to create near-triangular, converging deposits lying on the valley floor (Figure 7.1). The bedrock was eroded initially to form an irregular surface (Figure 7.2); and the valley floor is an erosional surface where palaeo-channels cross-cut the surface, creating an irregular surface (Figures 7.2 and 7.3). A period of aggradation resulted in the accumulation of material on the hillslope and valley floor creating the Heelbo slope. Multiple events of sediment flow off the ridge have resulted in an accumulation of sediment on the valley floor, preserved as the stratigraphic horizons visible at present. These accreting layers would have resulted in an accumulation of sediment against the hillslope. The elongate deposits would account for the differences between the Area 1 and Area 2 deposits and the bone bed section.

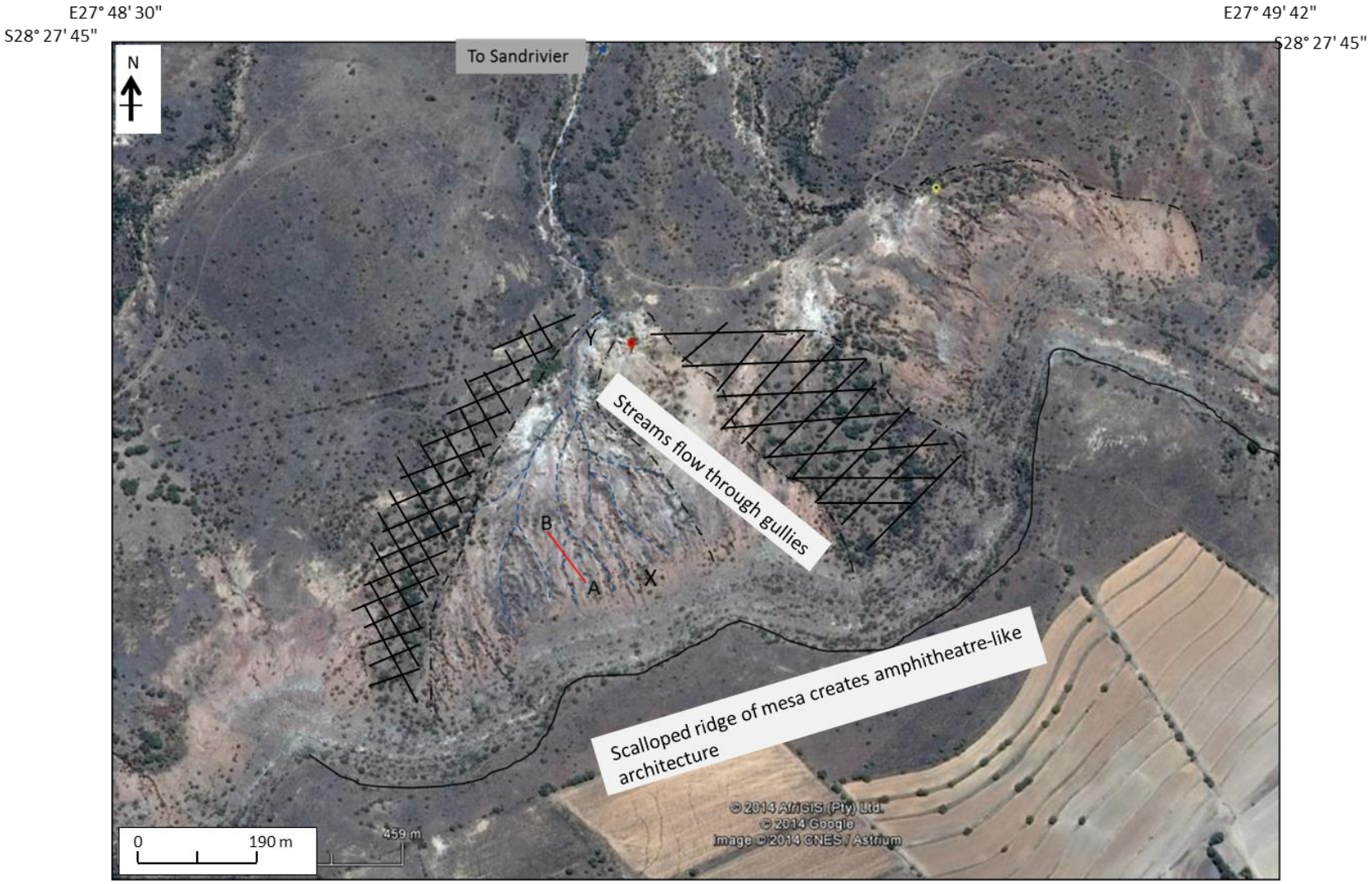


Figure 7.1 Google Earth image (2014) of the amphitheatre-like architecture of the crest of the mesa, that channels sediment flow downslope onto the valley floor. Shading lines indicate the basement highs perpendicular to the mesa, which confines sediment flow. Dashed blue lines indicate the possible position of palaeo-rills flowing off the mesa and flanks. Solid line marks the crest of the mesa. X-Y marks the position of the slope as described in Figure 7.2 and A-B marks position of palaeo-channel, described in Figure 7.3.

The palaeo-channel A-B (Figure 7.1) in the proximal section of the deposit is shown in cross section in Figure 7.2.

The mineralogy (Section 5.5) and thin-sections (Section 5.3) have shown the sediment on the hillslope to be similar to that of the bedrock sandstone that forms the underlying basement material. The samples all show a predominance of quartz material, with the bedrock characterised as arkose and the deposit as arkose to subarkose (Figure 5.26). Further support of the bedrock provenance is shown in the thin sections (see Chapter 5.3). There are no indications of equigranular, well-rounded, fine grains which could have been wind-transported. Instead the material appears to be mostly angular to sub-angular and moderate- to poorly-sorted (Section 5.4). The poor rounding of the material may reflect the resistance of the bedrock material to erosion over such short transport distances.

The elemental composition of the bedrock and the deposit show distinct similarities (see Figures 5.25 and 5.26). Overwhelmingly, the evidence suggests that the source material for the deposit is the mass-wasting and fluvial transport of the basement material from the mesa and its high-lying bedrock and undulating flanks.

7.3 HISTORY OF SEDIMENTATION AND PEDOGENESIS

The material from the crest and scarp have accumulated onto the talus and pediment slopes, to produce the sedimentary mantle present today. Periodically, channelised flow had the effect of incising the mantle, creating steep gullies (Figure 5.4), many of which were filled in the past before the modern gullies exposed the underlying stratigraphy. This reworking of the sediment also means that the deposit cannot be described as a simple colluvial mantle. Instead, sedimentation and pedogenesis are recorded in the sequence.

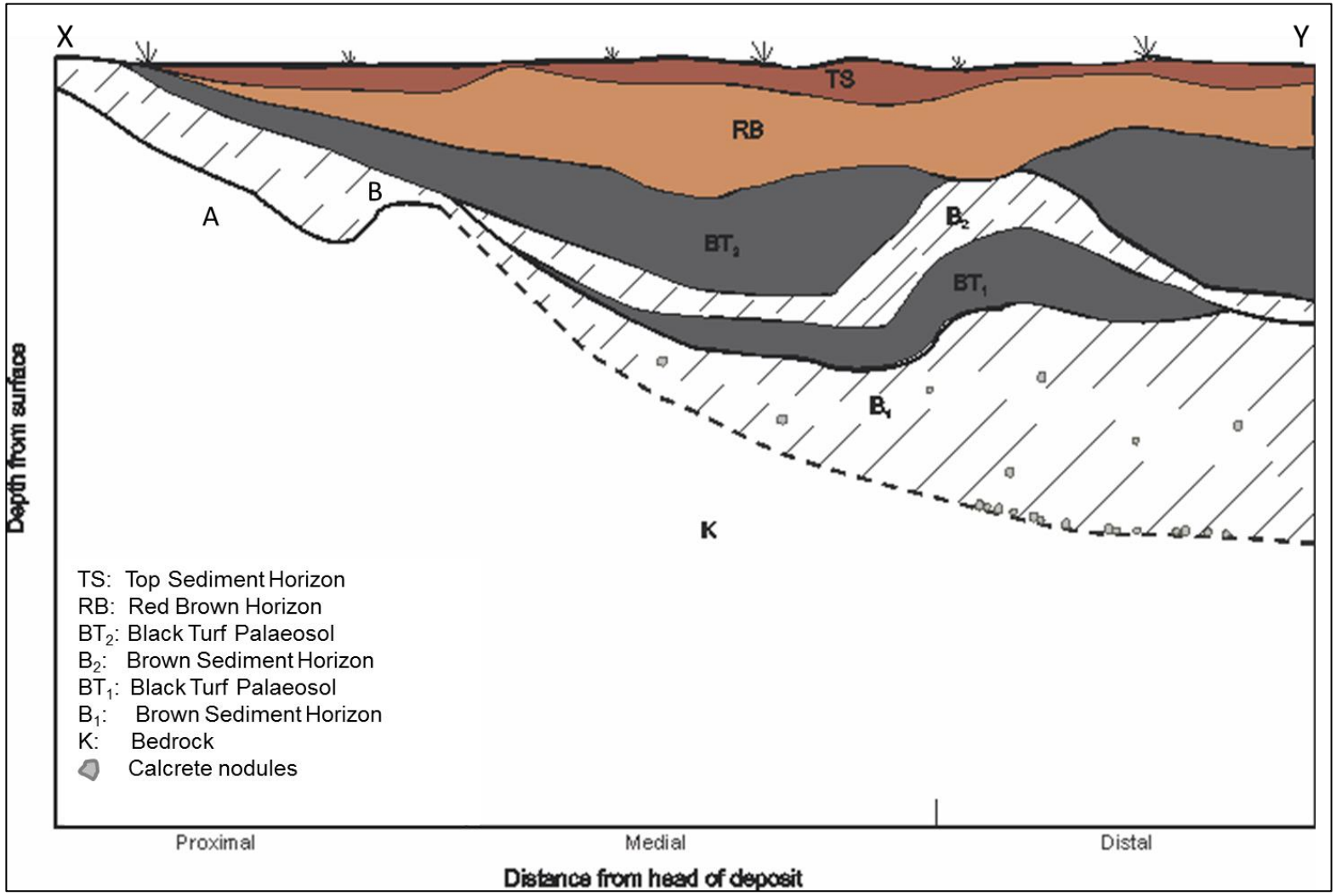
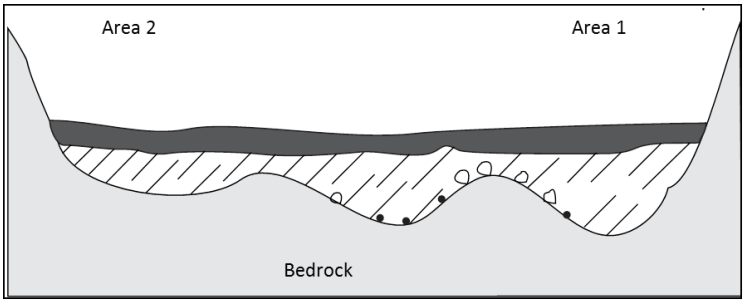
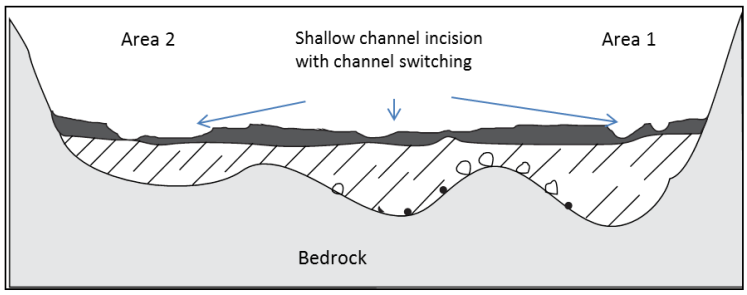


Figure 7.2 Schematic of the depositional sequence of the Heelbo deposit in Area 1. Undulating bedrock creates sediment traps and the dotted line indicates possible profile of bedrock surface, where exposure was limited. A-B marks the position of the cross-section through one of the palaeo-channel, and X-Y marks the location of the cross-section (see Figure 7.1). The key is in Figure 7.3

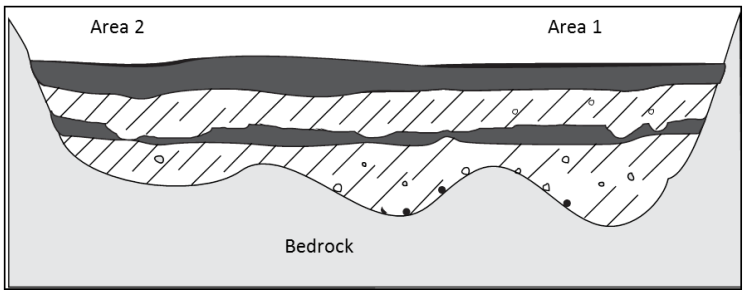


1. From 6 390 ± 740 years BP to onset of pedogenesis Deposition of B_1 horizon onto erosional surface bedrock. Formation of calcrete nodule in B_1 horizon. Undulating basement bedrock represents palaeo-stream channels flowing over surface. Remnant calcrete nodules and lag material at contact between bedrock and B_1 sediment horizon.

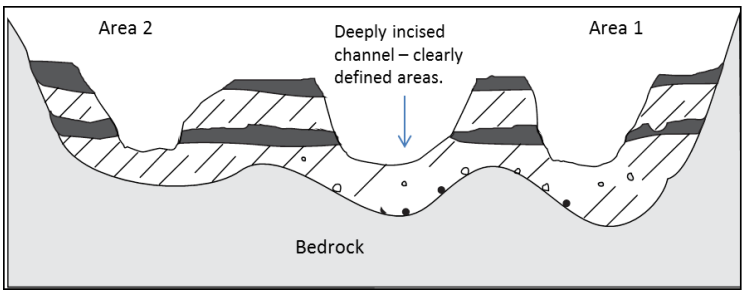
2. 5 030 ± 400 to 4 040 ± 320 years BP Pedogenesis of BT_1 palaeosol at Area 1 and Area 2, respectively.



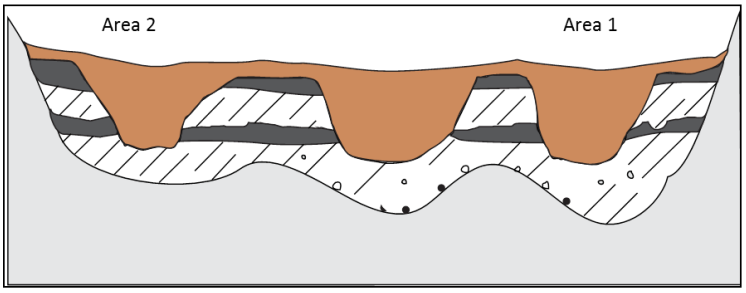
3. Between ~4 000 and 1 300 years BP Erosion of the BT_1 surface. Preferential erosion greater at Area 2 than Area 1.



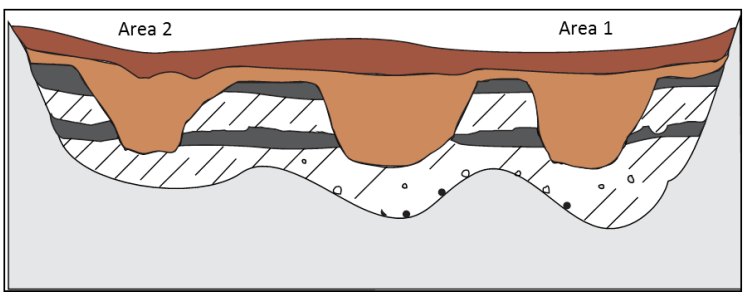
4. 1 300 ± 240 to 1 000 ± 210 years BP Deposition of B_2 horizon, marked by calcrete nodules and clasts incorporated into deposit, at Area 1. Pedogenesis of BT_2 palaeosol follows.



5. Between 1 000 and 400 years BP Erosion of BT_2 surface (to bedrock in some places). Channel migration occurs in each Area creating the palaeo-channels visible at present..



6. 400 ± 90 to 250 ± 170 years BP Deposition of RB horizon, infilling deeply-incised gullies, followed by a period of degradation with lateral migration and gully incision.



7. < 250 years BP Deposition of TS horizon which reflects last depositional event.

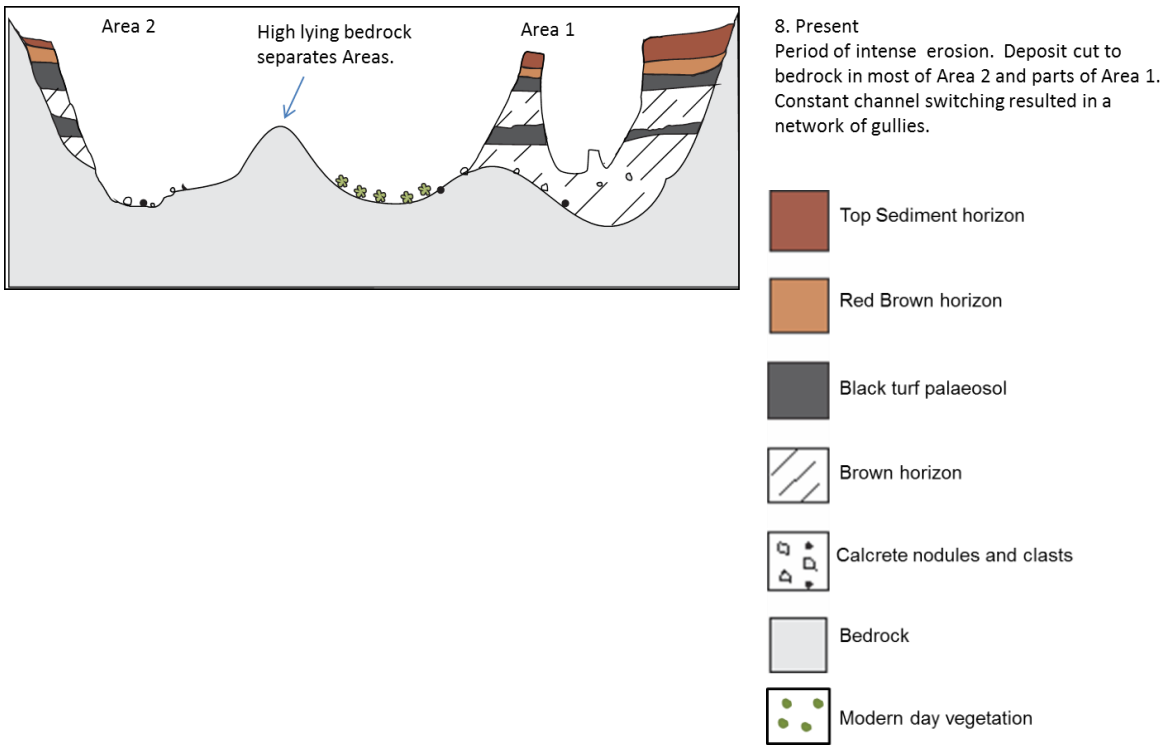


Figure 7.3. Schematic model to explain the history of deposition, erosion and pedogenesis in Areas 1 and 2 of the Heelbo deposit. Detailed explanations are provided in the text. The profile is drawn east to west to show the changes in Areas 1 and 2, rather than downslope.

The exposure of the underlying stratigraphy (as described in Chapter 3) indicates the presence of four distinct sedimentary horizons (TS, RB, B_2 and B_1) and two organic-rich palaeosols (BT_2 and BT_1). A schematic view of the depositional sequence is shown in Figure 7.2 and a summary of the depositional history is shown in Figure 7.3. The Brown horizon (B_1) lies unconformably on the underlying weathered Karoo bedrock. The erosional contact prior to the deposition of this horizon is reflected in the pebble-bed / conglomeratic basal contact between the bedrock and B_1 (Figure 5.3a and 5.3c) at Area 1. This basal material is possibly the remnants of previous horizons that may have been eroded during high-

energy flow regimes, leaving the coarse conglomeratic residue. Deposition of B_1 started prior to 6 390 ± 740 years BP in Area 1. Although the OSL age of B_1 in Area 2 is problematic, the unit is possibly contemporaneous with that of Area 1.

The presence of the calcrete nodules in the B_1 horizon suggests that aggradation of this unit occurred during a protracted dry period. The calcrete nodules are white, irregular shaped, hard concretions of calcium carbonate. The formation of calcrete nodules usually occurs in medium- to fine- textured soils that allow for the movement of groundwater (Wieder and Yaalon, 1982). However, these concretions may not be coeval with the sediment they are developed in.

The origins of pedogenic calcrete nodules are not well understood, but it is generally thought that calcium carbonate is leached from the soil profile by porewaters with relatively high dissolved CO_2 content (from plant decay and root respiration), and transported in solution down the soil profile (Rowe and Maher, 2000; Grevenitz, 2010). Reprecipitation of carbonate occurs, following this dissolution and eluviation, at some depth, usually >25 cm (Cerling and Quade, 1993; Royer, 1999; Rowe and Maher, 2000; Retallack, 2005), in the soil horizon. Once the soil solution becomes supersaturated with respect to calcite, precipitation of carbonate occurs. Supersaturation can result from several possible factors, including: 1) increases in the concentrations and activities of dissolved calcium and

carbonic acid owing to water loss by evaporation or evapotranspiration; 2) decreased $p(CO_2)$ leading to degassing of CO_2 from the soil solution; 3) and microbial activity (Cerling and Quade, 1993; Rowe and Maher, 2000). Estimates vary as to the amount of annual precipitation required for pedogenic carbonate formation but it generally lies in the range 400–750 mm (Cerling, 1984; Cerling and Quade, 1993; Royer, 1999; Rowe and Maher, 2000). Retallack (2005) showed that the depth to the carbonate nodular horizon can be correlated with mean annual precipitation (MAP) (Figure 7.4). This correlation showed that the horizon hosting carbonate nodules is deep in subhumid areas, but shallow in semi arid regions. The depth to B_1 at Heelbo is 50 – 100 cm and suggests a MAP of 400 – 600 mm (Figure 7.4 B), which is consistent with the mean annual precipitation of the region presently. However, rather than the actual amount of rainfall, a seasonally wet/dry climate, with a critical balance between rainfall and evaporation, is considered to be a key factor in driving calcrete formation (Rossinsky and Swart, 1993; Rowe and Maher, 2000). There is a greater concentration of CaO in the bedrock at Area 2 than Area 1 (Table 5.4) with marginally more Na_2O in the bedrock at Area 1 than Area 2.

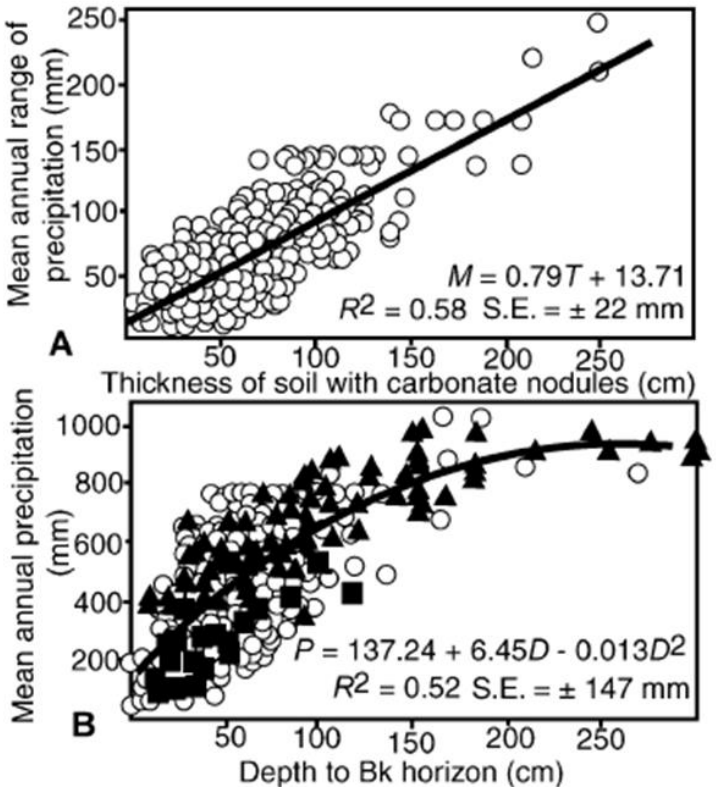


Figure 7.4 Correlation between (A) mean annual range of precipitation and thickness of soil with nodules and, (B) mean annual precipitation and depth to horizon hosting carbonate nodules (Retallack, 2005)

Overlying the B_1 horizon is the first of the two palaeosols – BT_1 (Figure 7.3). The BT_1 palaeosol is present in the medial and distal portions of the slope, occurring from site HB-06 to the base of the slope (Figure 5.7). The luminescence ages are 5030 ± 400 years BP for Area 1 and 4040 ± 320 years BP for Area 2.

The grain size in the BT_1 unit ranges from very-fine to fine sand. Root traces indicate that vegetation supported by this layer penetrated the underlying B_1 horizon. The high organic matter content, root traces and pedogenesis suggest a period of geomorphic and climatic stability that

would support the development of the palaeosol. The small calcrete clasts seen in the BT_1 layer are the remnant nodules that initially belonged to the B_1 horizon that have been incorporated into the palaeosol during pedogenesis. As the BT_1 palaeosol is superimposed on the underlying B_1 sedimentary layer, a possible scenario suggests that, during a dry climate regime, the sediment of B_1 was deposited on the footslopes of the mountain front; this was followed by the formation of the calcrete nodules in the B_1 horizon; a period of erosion followed during which the calcrete nodules were liberated into the sediment. A shift to a warmer, wetter climate led to the formation of the palaeosol (BT_1). A subsequent period of erosion and degradation, evidenced by the sharp erosional contact between BT_1 and B_2 (Figure 7.3) was followed by the deposition of B_2 and the formation of the BT_2 palaeosol.

The B_2 and BT_2 sedimentary units mimic the previous cycle in that the BT_2 palaeosol is interpreted as having been derived from the underlying B_2 horizon. This suggests that dry climates give way to warmer, wetter conditions which favour soil forming processes. Luminescence ages show that sedimentation at B_2 occurred at ~1000 ± 210 years BP at Area 1 and 1300 ± 240 years BP at Area 2. These ages indicate that pedogenesis occurred at the end of two pulsed events of sedimentation and that the B_2 horizon separating the palaeosols formed in a short-lived sedimentation event.

Wintle *et al*. (1995) reported a phase of Late Holocene colluviation and pedogenesis (Ntababomvu Pedoderm) at St Paul‘s Mission in northern Kwazulu-Natal, at 1770 ± 250, based on the average age of a range of luminescence dates. This age compares closely with the average age of the upper pedoderm at Blood River of 1740 ± 190 (Lyons *et al*., 2013) and falls within the period of B_2 sedimentation and BT_2 palaeosol formation at Area 2. Botha *et al*. (1994) reported a bulk organic matter radiocarbon age of 1420 ± 600 for the Ntababomvu 179 Pedoderm at St Paul's Mission which is consistent with the ages for the development of the BT_2 palaeosol at Heelbo. The age of the pedoderm has a large error (± 600 years which should possibly be regarded with caution) that places this deposit within the period of B_2 sedimentation, consistant with the Blood River event. as a result of this large error. This suggests that a phase of sedimentation followed by pedogenesis may have occurred regionally on hillslopes. The similar ages in widely separated sequences suggests that the drivers of the processes operating on the hillslopes are regional controls, such as climate.

The sharp, undulating upper contact between the BT_2 and RB horizon indicates another period of erosion and degradation (Figure 7.3). The thick RB horizon contains root traces and is present downslope at all the sites. Unlike the previous horizons, which are located only in the lower medial to distal part of the deposit, RB extends from the apex (Figure 7.2) onlapping the mountain front of the mesa. There are numerous clasts

incorporated into the RB layer that comprise both calcrete nodules as well as Karoo Supergroup sandstone clasts that were possibly incorporated during high-energy flow events. The RB unit shows evidence of early pedogenesis as seen by the presence of rhizocretions and carbonates in the unit and which are also present in the underlying units. RB is an immature, poorly developed soil that failed to develop fully as pedogenic conditions changed abruptly.

Rhizocretions are the nodules formed by the precipitation of cement (usually calcite) around roots that are preserved by these calcrete concretions. Rhizocretions are commonly seen in the distal sheet-flood facies of alluvial fans (Mack and Rasmussen, 1984). The size, shape and orientation of these depends on the root structures that once existed, for example small trees are indicated by rhizocretions greater than 20 cm in length (Mack and Rasmussen, 1984). If they exist in abundance they may cause the destruction of the original bedding, resulting in lamination and slickensiding owing to the collapse and compaction of roots. Rhizocretions assist in constraining the timing of sedimentation and pedogenesis as they form in relatively short periods of time in areas with high evaporation (Cerling, 1984; Mack and Rasmussen, 1984). Rhizocretions are found in the BT palaeosols as well as in the RB layer which suggests that RB is a pre-soil or very immature soil where pedogenesis was interrupted.

The TS horizon overlies the RB unit with a sharp contact (Figure 7.3). The TS layer is relatively thin and represents the youngest depositional event in the sequence. This unit supports the current vegetation cover and contains a large amount of organic material (Section 5.3). The TS horizon is also found at the proximal section of the deposit and extends for the full length of the hillslope. Rhizocretions are also seen in thin section (Figure 5.18) in this horizon, which suggests that, should conditions favour pedogenesis, the TS horizon may become a soil, given sufficient time and environmental stability. A depositional age for the TS layer could not be determined, as the unit was too thin to derive an accurate luminescence age and the contamination by modern carbon would negatively affect the radiocarbon age. However, the age of the unit is constrained by the age of the underlying RB horizon (250 ± 170 years BP) and is thus reported as < 250 years.

7.4 COMPARISON OF THE HEELBO DEPOSIT TO ALLUVIAL FAN TYPES

7.4.1 Alluvial Fan Morphology

Alluvial fans have been described extensively in the literature (see Chapter 2) as depositional landforms that occur where confined stream channels emerge from mountain catchment areas and, with the consequent loss of confinement, deposit their sediment load in fan-like

structures (Blissenbach, 1954; Bull, 1991; 1997; Harvey, 2002; 2011). This may occur at pediment-controlled mountain fronts or at fault-bounded mountain fronts as well as at the margins of subsiding basins. Alluvial fans generally have a conical surface form, with slopes radiating away from the apex and some fans may have a single stream source, whereas others have multiple sources where fan sediments have backfilled into mountain catchments (Harvey, 2002; 2011). The shape of the fans is controlled by the flow regime and the change from confined to unconfined flow. The spatial location ensures fluid gravity flows, sediment gravity flows (sheet floods, rock falls, rock slides, rock avalanches and debris flows) and fluvial processes of the deposit (Figure 7.5). The magnitude of sediment discharged onto a fan, its characteristics and distance from other alluvial fans along the mountain front control gross fan geometries (Allen and Hovius, 1998).

Alluvial fans can undergo continued expansion (aggradation), erosion (incision) or reach a state of equilibrium where the amount of sediment supplied to the surface of the fan equals that which is eroded away. Fans aggrade primarily during periods of high rainfall, tectonic activity and associated mass-wasting (Blair, 1987; Harvey, 2011). Alluvial fans also prograde basinwards through the building of depositional lobes on the fan surface. These lobes form where new fresh sediment leaves the channel and is deposited on the fan surface. These depositional lobes can migrate through time as a result of regional tilting, deflection of flow by fan-head

tilting, earthquakes or avulsion during floods (Wells and Dorr, 1987). Channels shift into the least aggraded part of the fan following the path of least resistance, which enables sediment to be distributed widely over the fan (Reneau *et al*., 1990; McCarthy *et al*., 1992). This channel shifting is the fundamental control maintaining the balance between erosion, deposition and weathering.

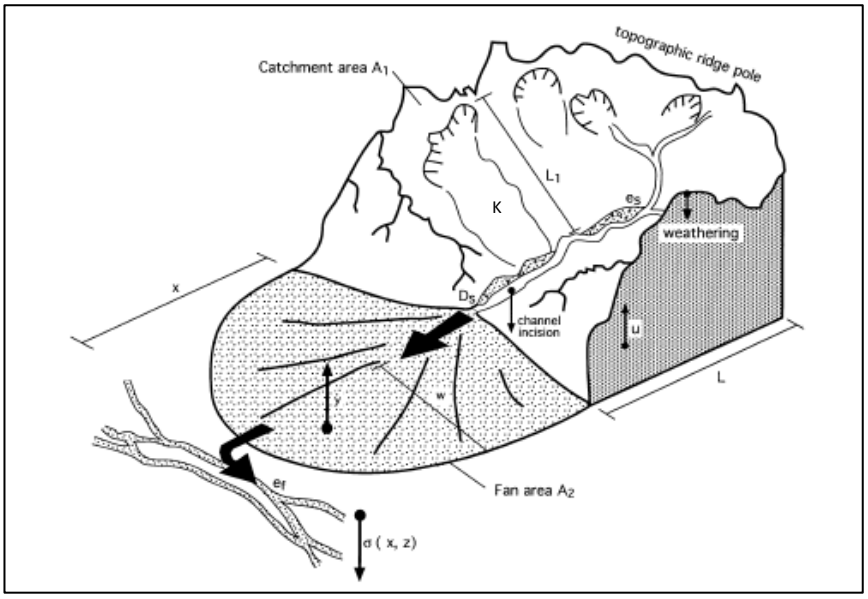


Figure 7.5 Factors controlling alluvial fan development: W – radius, x – length of fan, Y- fan depth, e_f – discharge into streams, e_s – small-scale discharge, D_s overall discharge, u – uplift, K - coefficient of catchment area, L_1 - upper length scale for landslides, A – catchment area and L – width of the catchment area (Allen and Hovius, 1998).

The Heelbo deposit resembles the alluvial fan morphology as it has a convex-up cross-fan profile with a concave-up radial profile (Figure 5.3). It is located on the foot slopes of a mountain front as the sediment radiates from multiple intersection points mid-way down the mountain (Figure 7.1). The deposit does not have a traditional fan-like shape as there is no single

confined feeder channel or a single apex. There are no well-defined lobes, but this may be as a result of erosion and channel-shifting of the sediment over time. However, it is possible to distinguish the separate regions of the deposit, referred to as Area 1 and Area 2, with the bone-bed section also defined as a separate depositional area. Channel-shifting could have resulted in these multiple lobes forming in each of the Areas 1 and 2.

The slope gradient of the present-day surface of the deposit is relatively steep, with an average slope of 10.20° (see Figure 5.1), which falls well within the accepted alluvial fan gradient of 1.5°- 25° or the accepted average of 2°-12° of typical fan slopes (De Chant *et al*., 1999; Saito and Oguchi, 2005). The deposit would have prograded basin-wards as the Brown (B_1 and B_2) horizons were deposited, and subsequent RB and TS deposits appear to offlap the mountain front (Figure 7.2) suggesting back-filling and reworking of the sediment.

7.4.2 Alluvial Fan Processes

As sediment moves from the apex of an alluvial fan, down-fan, a decrease in grain size is noted (Bull, 1972; Harvey 2011), although this is not always the case with steep fans. The primary controls on the fining of sediment are slope and distance from the head of the deposit and, as successive intersection points form, the focus of sedimentation shifts downslope

(Harvey, 1997, 2011). The fining rate is a measure of the efficiency with which the sorting processes operate (Blair and McPherson, 1994). The greater level of mixing of sand and fine material is seen in the proximal zones of the fans, whereas in the distal regions silt becomes dominant (Gerrard, 1992). The slope gradient and radius of the deposit also control fining. If the fan slope is too steep, there will be a rapid decrease in the grain size or poorer sorting; and the larger the fan, the slower the rate of sorting. The character of the deposit (facies) depends on the processes operating on the fan. Debris flow facies are characterised by matrix-supported gravels which are unsorted and massive. Sheet-flood facies tend to have thin gravel sheets of sand and silt; whereas channel facies are sand- to gravel- size and relatively well sorted, with channel scours. Debris flow fans are associated with small, rugged basins whereas fluvial-flow fans are associated with large, less rugged, basins (Lecce, 1990; De Haas *et al*., 2014; Šilhán, 2014).

Histograms were produced for each sample of the Top Soil (TS) (Figure 5.22) and Red Brown (RB) horizons (Figure 5.23). The proximal sections of both sedimentary units show that coarser material (as mass wasting under the force of gravity), would be more active on the steeper part of the slope. The smaller particles are transported downslope, leaving the larger particles to accumulate in the proximal reaches of the deposit. Further down the slope, beyond HB-05, mainly fine sediments have accumulated. The skewness of the grain size distribution suggests a dominance of

coarse material in the proximal section, with a slight shift to finer material down slope in both the RB and TS horizons.

Down-slope fining occurs in both the TS and RB horizons, but is more prominent in the TS horizon (Figure 7.6). This fining of grain sizes downslope concurs with the generally accepted description of debris flow fans (Blair and McPherson, 1994; Harvey, 2002; 2011).

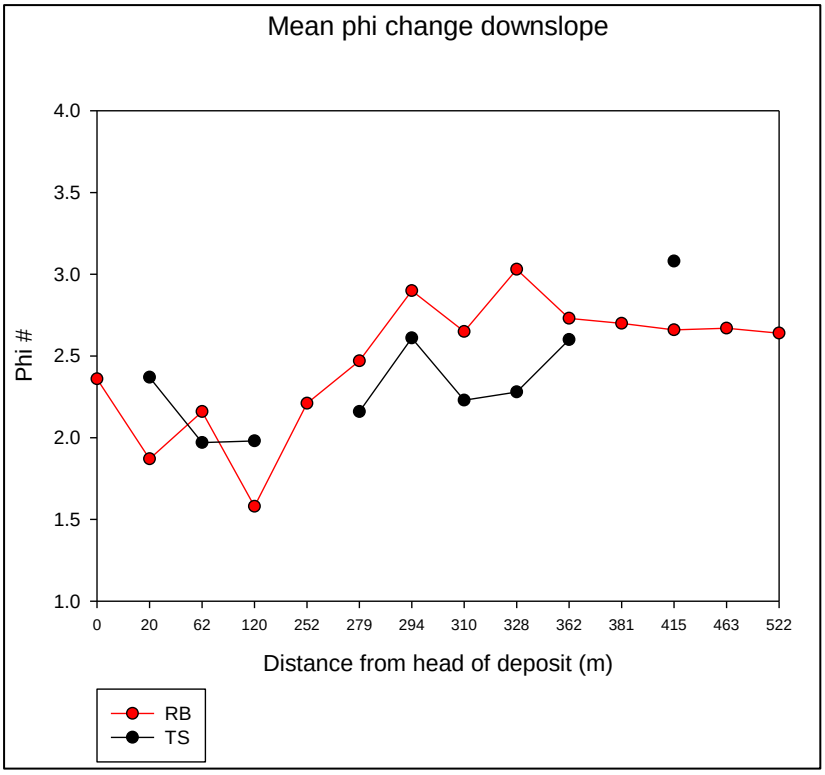


Figure 7.6 Mean phi changes of the TS and RB horizons. The greater the phi number the finer the grain size. The gaps in the TS profile are the samples that were discarded owing to clumping.

The Heelbo deposit superficially resembles the debris flow fans in the Blair and McPherson (1994) classification of alluvial fans and the modelling of

general fan slope deposition by De Chant *et al.* (1999), as the Heelbo deposit has a low gradient and relatively low head height. Average gradients for debris-flow fans range from 1.5° to 25° with the majority ranging between 2° and 12° (Rachocki, 1981; Blair and McPherson, 1994). The Heelbo gradient is 10.2°, which puts it well within the average range of a debris-flow fan. The relationship between the gradient of the present erosional surface and the grain size distribution is shown in Figure 7.7, showing the coarser material is found at steeper gradients and the finer material at the gentle gradients.

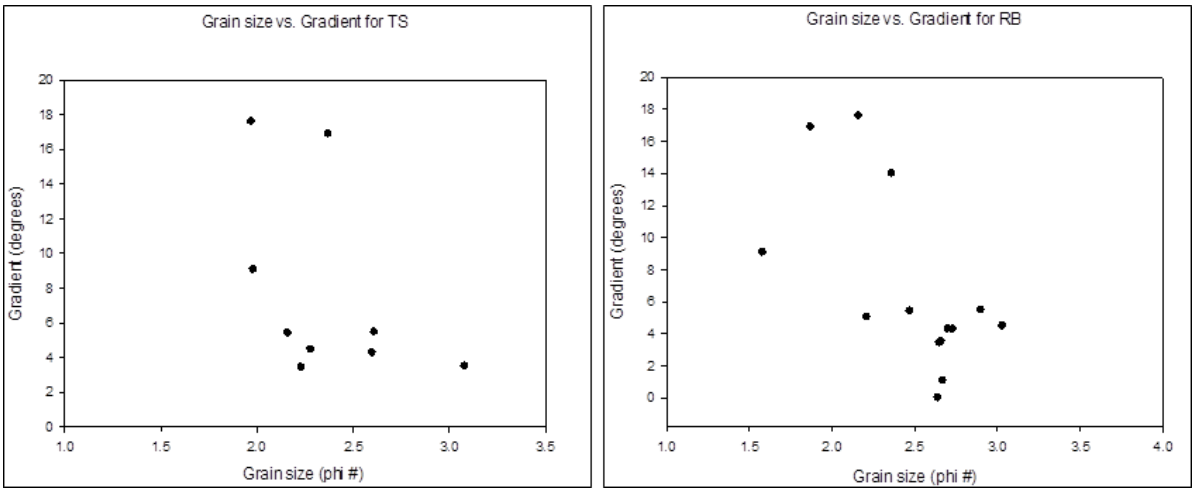


Figure 7.7 Change in mean grain size with slope gradient of the Top Sediment (TS) and Red Brown (RB) horizons with the regression line for each plot given.

The model suggested by De Chant *et al.* (1999) also assumes an ideal Blair and McPherson (1994) setting for a fan, i.e. a level fan depositional floor and unlimited space to spread out. The Heelbo deposit is formed on the foot slopes of the mountain and is laterally confined by basement highs. The pediment floor is not flat, but undulating and the hillslope

depositional events could not compensate for the change in plain topography as in the case of a talus sheet. The confinement of deposition is one of the reasons why the Heelbo deposit does not all elegantly into the different types of hillslopes as described in the literature. As the deposit matures, the underlying topography would have less of an influence on the hillslope morphology.

The gradient changes down slope have been noted in Figure 5.3 and similar to the classic morphology of an alluvial fan, it exhibits a concave-up form. Curry and Morris (2004) and Sass and Krautblatter (2007) have shown that talus slopes are relatively steep, steeper than the Heelbo slope (~30° in the case of Sass and Krautblatter, 2007) and exhibit constant gradients mostly independent of bedrock morphology. The slope gradient, together with the extensive channelisation, discounts the Heelbo slope as being a talus slope. The grain size is also too fine for the deposit to be classed as a talus as described by Sass and Krautblatter (2007).

One would expect the sediment grain size to decrease down the slope for an alluvial fan that slopes more gently towards the distal reach. The grain size does change with gradient, and this change, although small, still represents a fining down slope (Figure 7.6). Both the TS and RB horizons show a slight fining down the slope (Figure 7.6). However, the gently sloping gradients make up the majority of the profile, and this is where the

gully system cuts down through the sedimentary succession of the deposit.

7.4.3 Problems with the Classification of the Heelbo Deposit

From the preceding discussion the Heelbo deposit can clearly be defined as an alluvial fan, based on its morphology and the processes operating on the fan surface. However, unlike typical alluvial fans that have short radial lengths (< 1 km) and very steep slopes, the relatively fine-grained and low-sloping deposit at Heelbo would plot as an outlier on the classification trend as proposed by Blair and McPherson (1994). They suggested that many of the previously described alluvial fan deposits could be reclassified based on the morphology, hydraulic and sedimentary processes and resultant facies and facies assemblages. According to the classification diagram of modal texture vs. average depositional slope by McCarthy and Cadle (1995) (Figure 7.8), the steep gradients at Heelbo could only exist if the grain sizes from cobbles to medium-sized boulders (i.e. grain sizes >100 mm in diameter) were deposited. Alternatively, for the grain sizes measured at Heelbo, the slope gradient would need to be less than 0.05° (see Figure 7.8). As the gradient - grain size distribution relationship is central to identifying an alluvial fan (Blair and McPherson, 1994), the basis of the slope-grain size relationship observed in the Heelbo deposit suggests it cannot be classified as an alluvial fan. The

steep gradient of this fine-grained slope is a significant characteristic and is atypical of alluvial fans.

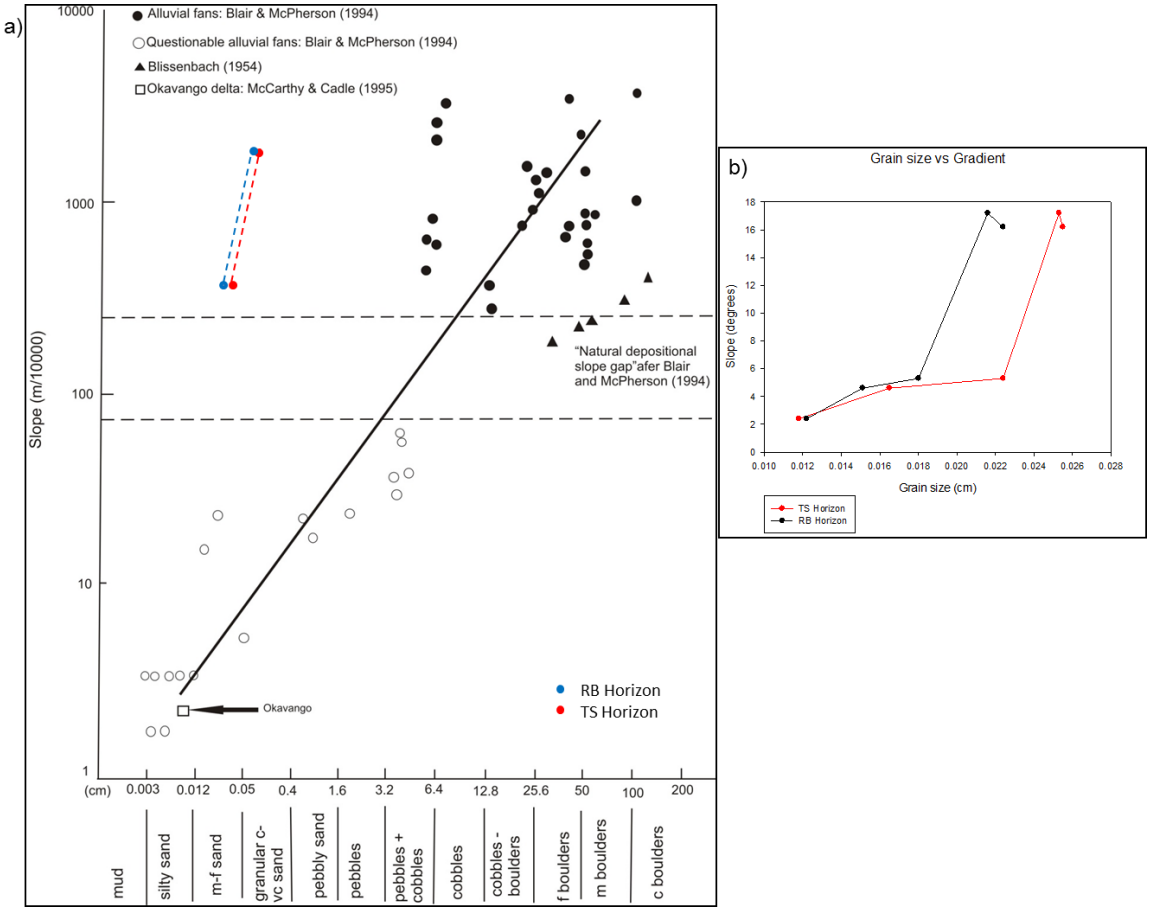


Figure 7.8 a) Modal textures versus average slope of alluvial fans showing the reclassification of deposits as true alluvial fans, the questionable fans as well as the Okavango Delta (modified after McCarthy and Cadle, 1995, p47 and Blair and McPherson, 1995, p584). Modal textures vs. average depositional slope of TS and RB are added to locate the position of the Heelbo deposit on the classification where the grain size ranges from silty, very-fine-sand to fine-medium-sand. b) An enlargement of the Heelbo samples is shown in the inset.

Where hillslope deposits appear to have the characteristics of an alluvial fan, but lack the distinct morphology of one, Bryan (1922) describes the feature as an alluvial slope (also described by Smith, 2000 and Kuhle and

Smith, 2001). The Heelbo deposit is composed of alluvium that dips away from the sides of the mesa and which merges with the broad valley floor. Such a feature could be referred to as a *bajada* or a coalesced alluvial fan (as described by Blair and McPherson, 1994; Harvey 1997; De Chant *et al*., 1999; Smith 2000). However, *bajadas* tend to have defined channelised, streamflow and gentle sloping fan-shaped deposits (Smith, 2000), which is not evident at Heelbo. Instead, Heelbo is best described by Bryan's (1922) usage of the term *alluvial slopes*, which is inclusive of alluvial fans and piedmont streams lacking fan morphology, as Heelbo has the characteristics that could distinguish it from an alluvial fan, as discussed previously. However, if an alluvial slope is defined as a piedmont plain that lacks the surface morphology of one or several coalesced alluvial fans (according to Hawley and Wilson, 1965), then the link to Heelbo would be tentative as there is little evidence of modern coalesced fans, although this could have been removed by the reworking of the deposit over time.

Smith (2000) noted, however, that the term alluvial slope is used to describe stream-flow-dominated piedmonts. Alluvial slopes are more likely to form than alluvial fans where mountain fronts, lack abrupt structural and topographic definition, which will most likely occur along tectonically inactive and embayed mountain fronts much like the Heelbo environment. Kuhle and Smith (2001) describe alluvial slope channels as steep and the ephemeral flows significant for sediment transport as rapid and shallow,

similar to what is described at Heelbo. Sediments on alluvial slopes are likely to be poorly sorted as a result of the flash-flood and unsteady flows. However, they will likely be better sorted than most alluvial fan deposits because sediment in the channels is more likely to be reworked and sorted by waning and subsequent flows and suspended load will be mostly deposited separately from bedload on interchannel floodplains than along with coarser sediment on sheet-flood fan lobes (Smith, 2000). As the poorly sorted material is located on relatively steep slopes it is more likely to be defined as an alluvial slope.

7.4.4 Grain size, Roundness, and Sorting

The TS and the RB sediments can be classified as mainly unimodal, which can be accounted for in the sand and silt composition of the bedrock, which is the source material for the sediment of the deposit. The unimodality position in the grain size spectrum of the sediments concurs with the fan in westernTransylvania, Romania, described by Pendea *et al.* (2008), that represents an alternation of slope deposits (coarse fan structures and reworked loess-like sediments) and paleosols. This may be further evidence that the processes operating on the fan described by Pendea *et al.* (2008) were very similar to those that produced the Heelbo deposit. The similar modalities of the TS and RB samples may also imply that both units formed under the same processes, i.e. suggesting that the

RB-forming environment only ceased very recently with the onset of drier conditions and subsequent gully formation.

The average roundness identified for the TS and RB samples is sub-angular / sub-rounded (Table 5.2 and 5.4) for most of the samples. There was little variation in roundness. The greater the radial extent of the fan, the greater the degree of rounding that can be expected. The short distances travelled by the particles (< 500 m) on the Heelbo deposit may contribute to the poor rounding of the particles.

The sorting of alluvial fan deposits varies widely. Blissenbach (1954) suggested that sorting of alluvial fan deposits is a function of: 1) the range in particle size of the material being transported, 2) the type of transporting and depositing agent and 3) the distance of transport. The sorting of the TS and RB horizons is poor. Baillie (1985) describes this as typical of colluvium - which is a poorly sorted mixture of clay, silt, sand, and gravel size particles, and is the result of the mass transport of the sediment down a hillslope (Botha, 1996). However, the existence of channelized deposition, as evidenced by the presence of palaeochannels (Section 5.3), discounts these units from being entirely colluvial.

Given the small scale of the deposit, it is possible that the poor sorting is a result of the less than 500 m distance travelled by - and the consequent little reworking - of the particles. Furthermore, most of the RB samples are

distinctly sub-angular/sub-rounded with a shift to more-rounded towards the base of the deposit, which may also reflect the transport history of the particles and suggests that these particles travelled short distances only. Chesworth (1973) and Martin and Chesworth (1992) claimed that the effect of parent material on soils is inversely related to time, and the end result of the chemical weathering of any rock type will be the residual system of SiO_2, Al_2O_3 and Fe_2O_3. The degree of weathering can be seen by the chemical index of alteration (CIA) or the plagioclase index of alteration (PIA). The CIA for the Heelbo deposit is generally similar or slightly higher than that of the source rock (Table 5.6). This is because the bedrock is a partly weathered sedimentary rock and the degree of weathering of the deposit would start from the bedrock value. The weathering values are moderate, indicating only a slight shift from low weathering conditions to conditions more conducive to chemical weathering, i.e. warmer, wetter environments. This does not exclude the possibility of *in-situ* weathering, which would also affect the sorting. The *in-situ* weathering would then lead to the grain size ranges becoming more diverse and the sorting of these grain sizes over short distances would be poor. However, over time *in situ* mechanical weathering would break down the lithics to the average grain size.

The degree of rounding and poor sorting in the channelized deposits could be caused by flash floods, i.e. floods that occur on a terrain that does not experience perennial fluvial activity. Evidence for flash flood events is

seen in the lag material of coarse grained material found at the base of the B horizons (see Figures 5.5a and b). The massive flood deposits coming off the ridge, which acts as a watershed, reflects periods of high rainfall, possibly after a protracted dry period or heavy, intermittent thunderstorms. The transport of this sediment by mass movement events is similar to the elongate debris-flow fans on the Torre del Loro Beach near Huelva, southwestern Spain, described by Moreno and Romero-Segura (1997). The deposition on the Spanish fan occurred during very intense and rare rainstorms which, in the Heelbo case, could have destabilised the heavily weathered and exposed sediment near the ridges' flanks.

7.4.5 Impact of vegetation on sheetflow versus concentrated channel flow

Smith (2000) suggested that vegetation may also play an important role in determining the degree of flow confinement and, therefore, favour the formation of alluvial slopes over alluvial fans. The gradient of the slope may not necessarily be governed by grain size alone. An explanation for the location of the fine sediments on the proximal steep slopes may be suggested by Abrahams and Parsons (1991). They investigated the relationship between infiltration and stone cover on a semi-arid hillslope in southern Arizona and found a negative correlation between infiltration, vegetation and stone cover and a positive correlation with shrub canopy. This arises from the fact that, under shrubs, fine sediment accumulates as

a result of differential splash; whereas between shrubs such sediments have been selectively removed by rain splash and overland flow, leaving behind a gravel lag. The effect of the shrub is to dissipate the kinetic energy of the raindrops and to inhibit surface sealing and, thus, to increase infiltration.

The sediment, in Abrahams and Parsons' (1991) study, consisting of 84% sand, 10% silt and 6% clay, is trapped by the shrub, and is not transported downslope. If this study is extrapolated to the Heelbo scenario, it implies then that the fine sediments may have been trapped and stabilised by a denser canopy of vegetation than exists on the Heelbo slopes presently. It also implies that, at the time of the sedimentary deposition event, the climate would have been temperate enough (warm and humid) to support the vegetation cover needed to trap the fine-grained sediments on the steep Heelbo slope.

In a laboratory experiment to simulate the channel dynamic, sediment transport and the slope of alluvial fans, Whipple *et al*. (1998) found that, in bed-load dominated systems, the slopes of the experimental fans were largely independent of grain size. The change from grain-size dependence to grain-size independent behaviour occurred at 160 μm. When the effect of vegetation on the sorting of grain sizes down slope was simulated in an experimental study, the results showed that vegetation has a direct effect on trapping finer grain sizes on the steeper slopes. Grasses

and shrubs are the dominant vegetation type of the Heelbo area with some scattered trees. The vegetation would then trap sediment as it moves down slope resulting in the poor sorting. Clarke *et al.* (2014) also showed that vegetation has a major influence on fan morphology and flow conditions; creating steeper and shorter fans, whilst also reducing the number of active channels, and lowering the lateral migration rate. Vegetation also impacted avulsion behaviour by reducing the frequency of avulsion events, but increasing the magnitude of the occurences of these avulsion events (Clarke *et al*., 2014).

The occurrences of vegetated alluvial fans that do not conform to the steep slope – fine grain size classification suggest that vegetation may not be the key driver of this relationship. Eriksson *et al*., (2008) noted that steep slopes can occur in pre-vegetational fluvial environments as described by the palaeohydrological data from the Waterberg Group. Therefore, if vegetation is a driver then all vegetated fans should deviate from this steep slope - grain size relationship, as is the case with Heelbo, which they do not. Therefore, another explanation for this relationship at Heelbo relates to the parent material. Depositionally, the particles at Heelbo are coarser, i.e. the large lithic blocks of shale and sandstone at Heelbo will need a high velocity flow to deposit it. During the intense periods of pedogenesis, these large lithic blocks would break down through mechanical weathering to smaller particles given a finer grain size trend which does not represent the depositional flow energy. Thus, the

grain size is removed from the depositional flow energy regime because of mechanical weathering during pedogenesis. This shows that for heavily pedogenic fans, with sedimentary sources, grain size is not a reliable indicator of depositional flow energy. De Haas *et al.* (2014) noted that for alluvial fans in the Atacama Desert, most coarse material in debris flows is deposited in on the proximal fan and coarse-grained debris flows have higher internal shear strength, and are thus more likely to halt on steeper, proximal slopes; whereas finer-grained debris flows are able to spread onto the distal fan. As fan width increases downslope, an increasing percentage of the fan surface has been inactive and thus subject to protracted weathering and reduction of the surface texture (De Haas *et al*., 2014). In a study on the Feather River Basin, Attal *et al*., (2015) found that, the coarseness of hillslope sediment increases with increasing mean hillslope gradient and erosion rate. They hypothesised that this is due to a decrease in residence time of rock fragments, causing particles to be exposed for shorter periods of time to mechanical weathering processes that can reduce grain sizes (Attal *et al*., 2015).

In summary, it is suggested that the Heelbo deposit is not a colluvial slope, as it has the overprint of alluvial processes on it. It can in part be described as an alluvial fan as it has most of the defining characteristics of a fan. However, a key feature of the fan classification is the relationship between grain sizes and slope gradient, and it is this relationship that separates Heelbo from previously described fans. Alternatively, Heelbo is

described as an alluvial slope where the fine grain size located on a steep slope is seen as a function of vegetation cover on the slope. However, Heelbo does not fully conform to the description of an alluvial slope either, in that it is not a coalesced alluvial fan lacking in fan morphology, and parent material, rather than vegetation appears to be the driver of the steep slope – fine grain sze anomaly. Therefore, Heelbo is best described as part of a continuum of hillslope deposits where colluvial and alluvial slopes are possible end-members and Heelbo is located somewhere along this continuum.

7.5 GULLY FORMATION AT HEELBO

7.5.1 Gully Morphology

The most noticeable feature of the Heelbo alluvial slope is the extensive network of gullies cutting into the deposit. These gullies range from a few centimetres in depth to more than 6 m and cut through the various stratigraphic horizons such that the preserved underlying stratigraphy as well as the bedrock is exposed. The gullies are described as a combination of immature V-shaped incisions located at the head of the deposit and mature U-shaped gullies in the distal portions which have eroded to bedrock level in some places (Figure 3.11). As described by Nordström (1988), Heelbo may be nearing the end of its cycle of erosion as 1) there is a steep slope above the gully heads (Figure 5.3), 2) a large

percentage of the gully heads have extended into the bedrock and 3) there is a predominance of rectangular cross-sections in the gully network (Figure 5.4). There also appears to be a decline in the rate of erosion, as some of the gullies appear to be infilling (Figure 7.2b). However, Nordström (1988) also noted that erosion tends to occur in cycles where periods of relative equilibrium are disturbed by periods of instability, which lead to either aggradation or degradation of the system. If Heelbo is at the end of an erosion cycle then the infilling of the valley floor signals a period of aggradation of sediment; and this could potentially lead to pedogenesis over time.

7.5.2 Possible Causes of the Gullies

7.5.2.1 Salinization of the sediment

As the horizons at Heelbo appear crusty and dispersive and were intensively gullied, displaying the characteristics of a sodic soil (Davies and Lacey, 2009), the SAR_s, EC and pH of the soils were determined to investigate their influence on the formation of the gullies. Sodic soils are soils that form mainly in arid to semi-arid regions when rain and irrigation waters are lost through evaporation or transpiration. Sodium salts then accumulate in the soil layers if they are not dissolved and are either leached to depth or exported in the drainage water (Rengasamy and Olssen, 1993). The hot climate regime at Heelbo is ideal for the formation

of sodic soils as the potential evapo-transpiration (PET) rate exceeds the rainfall rate. This dry environment possibly dates back to the formation of the lower Brown (B_1) horizon, as evidenced by the presence of calcrete nodules found in the horizon.

Based on the description of sodicity by Rengasamy and Churchman (1999), four of the samples (HB-04, HB05, HB-08, HB-12), taken from the profile down slope are defined as sodic, as these samples have a SAR_s > 3 and an EC <0.2 dS/m (Table 5.9). The rest of the samples are described as saline. Sodic soils have a high concentration of Na^+ in relation to other salts, whereas saline soils are considered to be inclusive of all dissolved salts, including Na, Ca and Mg (Rengasam and Churchman, 1999).

The vertical section at the base of the alluvial slope at Area 1 (see Figure 4.5) showed that all the horizons can be classified as sodic but that sodicity does not decrease with depth (Table 5.12) as it does in the soils of New South Wales as described by Rengasamy and Churchman (1999). A possible cause of the fluctuation of the SAR_s values is post-depositional alteration of the soils and each sample therefore reflects a different exposure event to sodic producing conditions.

The salinity effect: Saline soils have a relatively high concentration of dissolved salts such as sodium chloride (NaCl), calcium (Ca^{2+}),

magnesium (Mg^{2+}), sulphate (SO_4^{2-}) or bicarbonate (HCO_3^-) and other compounds and the salinity of soil is referred to in terms of total dissolved solids (TDS). Excess salt in the root zone prevents plant roots from withdrawing water from surrounding soils. This lowers the amount of water available to the plants. Therefore, excess salts in soil water can decrease plant-available water and cause plant stress (Warrence *et al*., 2002). This is significant on the Heelbo alluvial slope as both sodicity and salinity adversely affect the soil structure and reduce plant growth, leading to reduced slope stability. Soil salinity also causes fine particles to bind together into aggregates. This is beneficial in terms of soil aeration and root penetration and root growth; therefore initially soil salinity has a positive effect on aggradation and stabilization. The bulk of the samples measured at Heelbo should, therefore, provide greater soil stability on the slope. However, high levels of salinity can have a negative and possibly lethal effect on plant growth. Alternatively, the plant assemblages may change rather than be adversely affected by the lethal effects of increased salinity. Also, highly saline soils are likely to be dispersive and deflocculate easily in water (Warrence *et al*., 2002).

The sodicity effect: Sodic soils have high concentrations of sodium (Na^+) relative to concentrations of calcium (Ca^{2+}) and magnesium (Mg^{2+}) and the sodicity of the soil is expressed as the sodium adsorption ratio (SAR_s). Sodic soils are prone to soil dispersion and aggregate swelling. For Heelbo, this represents the four samples down slope (Table 5.10) and all

the samples in the vertical profile (Table 5.13). The forces that bind clay particles together are disrupted when too many large sodium ions come between them. When this separation occurs, the clay particles expand, causing swelling and soil dispersion (Pearson *et al*., 2003). Soil dispersion causes clay particles to block soil pores, resulting in reduced soil permeability.

The salts that contribute to salinity, such as calcium and magnesium, do not have the same effect as sodium as they tend to be smaller and cluster closer to the soil particles (Warrence *et al*., 2002). Ca and Mg will generally keep the soil flocculated because they compete for the same spaces as sodium to bind to clay particles. Therefore, increased amounts of calcium and magnesium can reduce the amount of sodium-induced dispersion. Calcium and magnesium usually precipitate out of the soil into carbonates and are replaced in the soil by sodium (Pitty, 1979; Hanson, 1993); therefore, at Heelbo the presence of calcrete nodules indicate that calcium and magnesium may have precipitated out to form calcrete nodules and were replaced by sodium ions.

7.5.2.2 Source of the Sodium / Salt

The change in a soil's sodicity or salinity can be 1) as a result of irrigation with saline water or secondary sodification resulting from human activity; 2) as a consequence of the nature of the parent material or 3) as a result

of rain water. Secondary sodicity is usually due to agricultural practices on land where irrigation water contains dissolved salts that accumulate in the soil and lead to conditions that the plants cannot tolerate (Rengasamy and Churchman, 1999; Seelig, 2000). The water dissolves these salts as it flows in rivers, over the ground surface, or though porous rocks and sediments (Rowell, 1994). If these salts are not washed away by rainwater, a sodicity or salinity problem could occur (Rowell, 1994), suggesting that this is why arid regions are mostly affected by this problem. The use of saline irrigation waters as the source of the sodium at Heelbo can be excluded, as the area is not currently being irrigated and has never been used for agricultural practices requiring irrigation. However, the southern slopes are farmed intensively and there may be some contamination through ground water flow. This cannot be proved conclusively as the water quality and movement of subsurface water from the southern slopes was not investigated as part of this research, and there was no indication of irrigation water interacting with surficial sediment at Heelbo. Also the length of time required to form a sodic soil would possibly exceed the length of time that agriculture has been practised in the region and the OSL dates position gully initiation before agriculture in the region.

The possibility of saline rainwater can be considered as a source of salts in the soil. Downes (1954) and Rengasamy and Olssen (1993) found that rain-borne salt has an important effect on soil salinization. In a study

based in Australia, they found that Na^+ input through rain varies between 0.6 and 130 kg/ha/year. The amount of salt deposited on an area depends on the proximity to the coast, the nature of the coastline, sources of local salt, the direction and intensity of prevailing winds and the distribution of rainfall throughout the year (Rengasamy and Olssen, 1993). Gunn and Richardson (1979) found that rainfall can account for the contribution of salt of both terrestrial and oceanic origin even in inland areas about 300 km from the coast. As Heelbo is 300-400 km from the coast, it is possible that saline rain water could contribute to the salinization of the soil – but the rainwater would need to be tested for accurate conclusions to be drawn. The topographic variance between Heelbo and the coast suggests that a seawater source of Na is unlikely and, if this were the mechanism, then all the soils in the area would be sodic.

The nature of the parent rock as a source for the salts is also a consideration. The mean Na level in the lithosphere is 2.8%, with the principal Na-bearing minerals being plagioclase and sodium feldspars, with 0.5-8.0% Na^+ (Rengasamy and Olssen, 1993). Most secondary sodium minerals are highly soluble in water. Gunn and Richardson (1979) found that in rocks in eastern Australia Na^+ was appreciably higher in the unweathered freshwater rocks than in those of marine origin. However, weathered sedimentary rocks of marine origin contain more Na^+ than those of freshwater origin. This suggests that mineral weathering can provide Na salts in the long term of soil formation which then accumulate

in less permeable soil layers. The effect of the parent material is not clear as the underlying Karoo sediments are not sodium-rich and there are no granitic rocks close to the area but the source rock is the weathered Elliot Formation sandstone which is of fluvial origin. The average concentration of Na of the deposit is 1.69 wt% which is derived from ~0.31 km^3 volume of sediment. Therefore, the average of 1.56 wt % of Na in the bedrock would require a volume of 0.28 km^3 of bedrock to supply the equivalent amount of Na to the deposit. As the volume of bedrock is much greater than 0.28 km^3 it is evident that the Na is derived locally and there is no external source of Na to the area. The most plausible source for sodicity of the soils is the evapo-transpiration of ground water from a shallow water table, as the ground water is discharged through the soil surface; dissolved salts precipitate and accumulate near the surface of the soil (Seelig, 2000).

7.5.2.3 Gullying through Piping

Although most studies link gully morphology to surface water flow, increasing attention is being paid to the significance of piping and tunnelling (see Valentin *et al*., 2005). Piping is an indicator of dispersive soils and an accumulation of free water in the subsoil, as these are the prerequisites for piping to occur. Piping or subterranean channels form when disaggregated particles are carried in suspension through the more permeable parts of the sedimentary structure. The removal of this material

can lead to subterranean erosion and possible collapse of the overlying structures. As the accumulated free water must have an outlet to flow to the main gully, piping provides an outlet for the accumulated free water and often causes tributary gullies to form (Thornes, 1980; Nordström, 1988; van Zijl, 2010). The Heelbo horizons are consolidated, porous sediments with a large number of open cavities and burrows that have not been filled, making it possible for water to move through them freely.

Soil piping refers to the formation of sub-surface pipes or tunnels owing to the erosive action of water moving through the soil. Piping, presumably initiated by water moving through pore spaces or dessication cracks, has the potential to provide subterranean networks with hydrological connectivity (Jones, 2010; Smart *et al*., 2012). Eventually the pipe may collapse completely, producing a line of sinks, which may then act as localised funnels to channel additional surface run-off into the subterranean pipe. Between the sinks, natural bridges remain for a while, before they too collapse and a gully is formed. The piping conditions may occur on a valley floor, floodplain or pediment as well as on hillslopes, badland ravines or mountains or gully channels and channel walls. In all these situations the basic conditions are the same: 1) enough water to saturate some part of the soil or bedrock above base level; 2) hydraulic head to move the water through a subterranean route; 3) presence of a permeable, erodible soil or bedrock above base level; and (4) an outlet for flow (Parker, 1963; Verachtert *et al*., 2010).

Parker (1963) noted that one factor common to practically all piped soils and rocks, except sand and gravel, is the presence of one or more of the swelling clays, most commonly montmorillonite, illite, mixed-layer montmorillonite and illite, and bentonite. Montmorillonite appears to be the most widely occurring and dominant of the swelling clays incorporated in rocks of piped areas as it changes in volume by about 700 percent between dry and saturated conditions. Such swelling clays upon drying out will shrink, and in the process the rocks containing them will become extremely hard and may crack both widely and deeply. Subsequently, upon wetting, the walls of the cracks will swell and the cracks will close until the clay dries out again. The more sodium the clay can hold the more infiltration and hydraulic conductivity will be reduced. Montmorillonite is most affected by sodium and kaolinite the least affected by it (Warrence *et al*., 2002). Montmorillonite is also most prone to swelling and dispersion and kaolinite least likely to swell and disperse (Pearson *et al.*, 2003).

The XRD analysis of the Heelbo samples identified montmorillonite in the assemblages (Figure 5.22) suggesting that this may add to the swelling and dispersion properties of the sediment in the deposit. The soils have also been shown to have a moderate to very high risk of swelling and crusting (Table 5.10). Montmorillonite acts as a cement when sediment is dried but as a lubricant when wet (Claridge, 1960). Thus, when water infiltrates, the montmorillonite swells and forces sediment apart, rendering the slope unstable and likely to collapse.

The presence of clays was also determined through XRF. The Al_2O_3 concentration in the source rock is high for a sandstone with an average of 8.92 wt% at Area 1 and 13.38 wt% at Area 2, which suggests that the feldspars have broken down to clays. Although this cannot be conclusive as the Al_2O_3 content could also reflect the presence of clays or feldspars.

Piping is evident throughout the Heelbo deposit (Figure 7.9) where small sinks have developed and the bridges between them are still stable. Over time these sinks merge laterally and the bridges between them collapse to form large holes, which are the start of gullies forming. Subterranean channels may also form, which will destabilise the overlying sediment, causing it to collapse.



Figure 7.9 Photos of piping at Heelbo where (a) a small sink formed which may eventually merge with other sinks surrounding it to form (b) a large cavity. Subterranean piping is seen at the bone bed(c) where the overburden begins to collapse (d).

7.5.2.4 Gullying as a result of base level changes

The lowering of base level is a cause of accelerated erosion in existing alluvial channels, and may be the cause of initiation of gullies (Begin, *et al*., 1981; Harvey, 2002). Knickpoints were identified at Heelbo which suggests that changes in the base level could have contributed to gully erosion on the slope. However, gully formation occurred after the recent sediments were deposited, which would have been in the last ~400 years. The knick points were buried and would have been excavated by gullying, and as it became exposed it would have appeared to be coeval with the

gullies. However, the gullies and the knickpoints are not concurrent, and are therefore not causal to gully formation. It is not possible that the knickpoints could have migrated significantly in this time, and can therefore not be the cause of gully formation

7.6 COMPARISON OF THE ^{14}C AND OSL AGES

The constraining of the timing of the deposition and pedogenesis of the deposit is critical to the reconstruction of the environmental history of the hillslope. Radiocarbon dating of the bulk organic rich sediment was selected as the independent age control for this project as Murray and Olley (2002) found that there was good agreement between ^{14}C and OSL ages for a number of depositional environments. However, the ages derived using the two techniques - radiocarbon and OSL dating – were not in agreement (Table 7.1).

Table 7.1 Comparison of calibrated radiocarbon and OSL ages

Sample Number	Location	Cal BP 2 σ (95.4 %)	Cal BP Median Probability	OSL Age (MAM)
OSL 7	Area 1 RB	328 – 374 394 – 396 440 – 546	493	400±90
OSL 8	Area 1 BT_2	2434 - 2757	2604	810±130
OSL 10	Area 1 BT_1	4976 – 5016 5031 – 5319 5427 - 5431	5163	5030±400
OSL 15	Area 2 BT_2	1593 – 1838 1854 - 1867	1739	4040±320
OSL 13	Area 2 BT_1	1882 – 2112 2123 - 2147	1996	1210±120

The OSL ages for OSL 7 and OSL 10 were similar to the median probability of the ^{14}C ages. However, there is no error calculated for the ^{14}C ages, therefore an accurate comparison is problematic. Soil organic matter is often considered unsuitable for ^{14}C dating (Wang *et al*., 1996). It is often difficult to trace the source of the original organic material found in the soil as fresh carbon is continually incorporated at varying rates into the soil (Wang *et al*., 1996). There are different decomposition rates for organic material which would result in a depletion of older organic matter and lead to an underestimation of the age. Carbon is also fixed in organic matter at different rates, depending on the uptake into the organism, either plant or animal (Ramsey, 2008). This uptake does involve some fractionation or preferential uptake of lighter isotopes. All radiocarbon ages were corrected for isotopic fractionation using the measured $^{12}C/^{13}C$ ratio and the ^{14}C ages of soil organic matter should therefore be interpreted as minimum ages (Wang, *et al*., 1996; Ramsey, 2008).

Despite the complications inherent in the radiocarbon dating technique, specifically around calibration of the ages, it is still considered valid for dating late Holocene sediments. A significant problem is that the low amount of residual radiocarbon (<3%, equivalent to ~30 000 BP) (Higham *et al*., 2009), may be significantly influenced by the trace presence of contaminating carbon of a more recent age. This contamination results in multiple populations being expressed (for example four 1 σ intercepts are recorded for OSL 10 (Table 7.1)); and the calibration programme cannot assign an error to the median probability. These multiple ages for one sample and the lack of an error margin suggests that multiple events are being dated. Therefore, comparing the radiocarbon ages relative to 1950 to the luminescence ages relative to 2013 is problematic as the techniques are dating separate events. It is acknowledged that the radiocarbon ages reflect a high precision of measurement but the samples collected may reflect a mixed-age organic sample and, therefore, the error of ±45 – 50 years is on the precision of the measurements and not reflective of the errors on the true age. Therefore, the ^{14}C ages were rejected in this project and were not used further in the discussion of the chronology of the Heelbo deposit. Instead, the OSL ages were examined carefully for their reliability in constraining the timing of the hillslope deposition.

The OSL ages proved to be more reliable despite partial bleaching in the samples which was corrected for by using the statistical minimum age model. OSL is considered suitable for dating colluvial sediment despite

their often short transport distances and possibly poor bleaching characteristics. Longer transport distances and low-energy flow regimes would increase the exposure time of the grains to sunlight. However, Pienaar *et al.* (2008) also noted that, if the intensity of soil erosion of colluvial sediment increases, and if during high magnitude flow events subsoil particles are mobilized that have not been bleached, then age overestimation may occur in OSL ages.

The OSL ages show that the BT palaeosols are two distinct units with more than 2 000 years of erosion and deposition separating them. This is important as only one BT horizon is visible in some sections of the deposit – or it is recorded as a thick horizon suggesting that either it is only one unit, or that the dividing horizon has eroded out. The identification of the two separate units suggests then that there may be a cyclical component to the deposition, pedogenesis and erosion on the slope.

The fairly good correspondence in the ages between the horizons at Area 1 and Area 2 and the bone bed supports the notion of Wallinga (2002) who suggests that the OSL dating of quartz grains using the SAR protocol is the most suitable technique for the luminescence dating of fluvial sediments. This supports the use of the OSL ages for the palaeo-environmental reconstruction of the alluvial slope, which is discussed in Chapter 8.

CHAPTER 8 PALAEOENVIRONMENTAL HISTORY OF THE HEELBO ALLUVIAL SLOPE

8.1 INTRODUCTION

Southern Africa is situated at the interface of tropical, subtropical and temperate climate systems and is influenced by a variety of atmospheric and oceanic circulation systems, and as such is in a critical location in the southern hemisphere for the study of environmental change over glacial-interglacial cycles (Chase and Meadows, 2007). Whilst palaeo-environmental research in southern Africa has been constrained by issues of access, lack of closed sites and difficulties in determining high-resolution chronologies, there have been significant advances in knowledge of regional palaeoclimates as a result of improved mapping techniques and field investigations and advancements in dating methodologies (Chase and Meadows, 2007).

Long, continuous palaeoclimatic records have been constructed by using sophisticated sampling techniques of sediments and precipitates from various sources (Holmgren *et al*., 1999; 2003) and regional syntheses of these data across South Africa have provided numerous scenarios of environmental change over the last 20 ka (Cockcroft *et al*., 1987; Deacon and Lancaster, 1988; Deacon, 1990; Partridge *et al*., 1990; Beaumont *et al*., 1992). However, little information exists in the scientific literature on the use of palaeosols for defining the depositional palaeo-environments in

South Africa (Botha, 1996). The reconstruction of the environmental history of the Heelbo alluvial slope will go some way to extending the Quaternary climate record and, in particular, the terrestrial record of environmental change in South Africa as this alluvial slope and the surrounding environment preserves a distinctive stratigraphic record that has, until now, not been fully described. This palaeo-environmental reconstruction extends the work started by Botha *et al*. (1994), and Botha (1996) in KwaZulu-Natal and the Free State and adds to the growing body of research on past climates in South Africa.

8.2 A RECORD OF CLIMATE CHANGE IN SOUTHERN AFRICA

The Holocene is defined as a post-glacial period in which interglacial conditions became established, and is considered to cover the last 11 500 years BP (Chase and Meadows, 2007). Northern and southern hemisphere climate changes are not always synchronous, and significant climatic events may not always be reflected in both records (Thomas, 2008). While evidence for climate change in the Late Quaternary in South Africa has been slow in coming, studies have shown that conditions in southern Africa were relatively arid, with the warmest period of the Holocene, recorded in southern Africa (prior to recent anthropogenic warming), being the Holocene Altithermal (HA) – broadly dated as 8 000 – 4000 years BP (Mayewski *et al*, 2004; Chase and Meadows, 2007). Thomas (2008) noted that the maximum solar radiation occurred around

10,500 years BP and high solar radiation resulted in maximum humidity and vegetation cover. Since the maximum, however, the climate has been getting generally cooler and drier and will continue to do so until it reaches the minimum approximately 1,000 years from the present (according to the model of Thomas, 2008). Thomas (2008) also added that, when solar radiation is at a maximum, the geomorphic work needed to destabilise hillslope sediment, such as at Heelbo, is much greater (at a maximum) as there is more vegetation cover, than during minimum solar radiation when the vegetation cover needed to stabilise the soil, is sparse.

Proxy records on past climates for southern Africa have been determined from a variety of techniques, including stable isotope analysis of speleothems (Talma and Vogel, 1992); pollen (Scott and Thackeray, 1987) and faunal analyses at archaeological sites (Klein *et al*., 1991); animal remains (Lee-Thorp and Beaumont, 1995); dissolved noble gas concentrations in artesian waters (Vogel, 1983; Heaton *et al*., 1986) and crater-lake sediments (Partridge *et al.*, 1993; 1997; Stuut *et al*., 2002). The best Holocene high-resolution, continuous, palaeoclimatic records available for southern Africa include the 200 ka Tswaing Crater record (Partridge, *et al*., 1993); the 25 ka Cold Air Cave record, the Cango Cave stalagmite record (covering 50 000 to 15 000 BP and 5000 BP to present) (Talma and Vogel, 1992, Holmgren *et al*., 1999); the tree-ring records covering the last 650 years (Holmgren *et al*., 1999); and more recently the dynamics of the winter rainfall zone (Chase and Meadows, 2007) and the

evidence of a 50-year large-scale cooling event in South Africa (Sundqvist, *et al*., 2013). However, it is worth noting that fluctuations in the early period of the climate record are more difficult to corroborate in southern Africa because of a lack of high-resolution data (Holmgren *et al*., 1999; Chase and Meadows, 2007; Huntley *et al*., 2014).

8.3 RECONSTRUCTION OF THE HEELBO PALAEO-ENVIRONMENT

8.3.1 Assumptions for Palaeo-environmental Reconstruction of the Heelbo Alluvial Slope

To reconstruct the palaeo-environment of the Heelbo alluvial slope certain assumptions were made:

1) The interlayered stratigraphy of the sediment horizons and the palaeosols reflect periods of aggradation, pedogenesis and erosion. Extreme sedimentation is assumed to have occurred during relatively arid climatic intervals, when a decrease in vegetation cover provided little surface protection. Calcrete formation marked these arid events, where when evaporation exceeded precipitation. In contrast, pedogenesis is assumed to have occured during humid intervals when vegetation cover was restored, the land was consequently stabilized, and the uppermost sands weathered to form soils.

2) Heelbo is described as an alluvial slope and the assumption is made that the environmental conditions that give rise to an alluvial slope are similar to those of alluvial fans, although the resultant feature may be

controlled by local conditions. Therefore, the cycles of climate cooling and warming may control the stability or instability of alluvial slope morphology. According to Harvey *et al.* (2005), Quaternary alluvial fans display a climatic control on fan morphology and sedimentary styles. Thus, a change in climate will force the alluvial fan / slope to change from an erosional to a depositional regime (or vice versa) which will, in turn, cause a change in the sedimentary environment. Other indications of climate change are visible, such as in calcrete formation, which is enhanced during dry periods, with little water available, and retarded during humid periods, when water is more readily available (Tooth *et al.*, 2001).

3) Clay mineral analysis can be used in palaeoclimatic reconstruction based on Singer's (1984) suggestions that clay minerals can be quantitatively related to climatic parameters such as precipitation and temperature. He also suggests that these minerals remain stable during weathering, after they have formed, provided there is a stable climate and no tectonic rejuvenation; and clay mineral assemblages throughout the weathering profile are uniform and are stable in a post-burial environment and these minerals display a uniform sensitivity towards environmental changes. Stoops *et al*. (2001) suggest that parent material is a more dominant factor than climate, in determining clay mineral assemblages. As the Heelbo alluvial slope is relatively young with a low level of diagenesis, the assertions suggested by Singer (1984) are considered valid for this reconstruction.

4) By constraining the timing of the deposition events either by dating organic matter (carbon) incorporated into the bulk sediment or by dating the burial period of the deposit through OSL, it is possible to relate the depositional history of the deposit to proxy records that exist for the given time.

8.3.2 Palaeo-environmental Significance of the Fan Mineralogy

Although mineralogy has been used to identify the source material of the deposit and to determine the extent of leaching, it can also be used to reconstruct the palaeo-environment of the alluvial slope.

Singer (1984) determined that relatively dry periods will produce clay mineral assemblages rich in chlorite and illite, whilst humid periods will produce kaolinite assemblages, and a strong seasonality with a more pronounced dry season might produce smectite. Alternatively, Le Roux (1972) completed an analysis of soils in a known climate by analysing extensively weathered, highly leached soils in KwaZulu-Natal from a humid climate and determined that kaolinite was the dominant mineral and that many of the clay minerals displayed a chlorite component. A similar study by Retallack (2001) of present-day basaltic soils in Hawaii showed that where annual precipitation is lower than 1000 mm, smectite is the dominant clay mineral produced, whilst kaolinite is produced where precipitation is 1000-2000 mm. He concluded that clay minerals formed in

wetter climates usually belong to the 1:1 layer group, whereas 2:1 layer clays are more likely to form in climates with less available water. In the lacustrine sediments of Lake Baikal it was determined by Fagel *et al.* (2003) that the average clay composition showed no significant changes through glacial-interglacial stages. Thus, it can be seen that, at its present level, clay mineral analysis is capable of giving only a broad palaeoclimate reconstruction (Singer, 1984; Zhou and Keeling, 2013; Raigemborn *et al*., 2014), which should be supplemented by other proxies.

XRD analysis of the Heelbo sediment identified quartz, muscovite, plagioclase, calcite and dolomite as the non-clay minerals and a mixed-layered chlorite / smectite assemblage and montmorillonite as the clay minerals. However, neither illite nor K-feldspar was identified in the mineral assemblage. Smectite is more commonly found under surface conditions and illite can recrystallise from smectite upon burial (Pusch and Karnland, 1996; Moore and Reynolds, 1997; Nesse, 2000) in the presence of sufficient K^+ (Nesse, 2000). The availability of K^+ in the deposit suggests that, over time, illite has recrystallised from smectite. Muscovite, which is present in the Heelbo mineral assemblage, is the only source of K^+ in the Heelbo palaeosols. Under sufficiently high temperatures, smectite would start converting to illite, which would then be found in the Heelbo deposit, which it is not. Thus it is more likely that the formation of the mixed layered clay mineral is due to the weathering of sedimentary material i.e. it is detrital. This is supported by Velde (1992) who found

corrensite (the trioctahedral form of dioctahedral tosudite) to be stable in all physical environments where clays exist, and thus capable of forming in sedimentary rocks and weathering environments.

A study similar to the Heelbo alluvial slope study was carried out on the Permian red beds from Lisbon Valley, Utah, by Morrison and Parry (1986). The clay mineral assemblage comprises smectite with minor amounts of chlorite, illite and corrensite, where smectite occurs in low-permeability arkosic sandstones and corrensite in permeable aeolian and marine sandstones. It was determined that the smectite most likely formed owing to the interaction of high-pH solutions with the host rock, whilst corrensite could have formed at any time after deposition. However, since corrensite is produced at temperatures of ~100˚C (Morrison and Parry, 1986), this implies either a burial depth of 3-4 km or the presence of a local thermal anomaly. Furthermore, upon deeper burial, corrensite typically is replaced by chlorite (Morrison and Parry, 1986).

In another study focusing on red beds in Argentina (Manassero, 1997), two palaeo-depositional environments were identified; these were an alluvial fan system and a sandy braided river system. Two clay assemblages were identified in the study region, one rich in smectite owing to the alteration of volcanic rocks located within the middle sandy braid-plain and the upper floodplain sequence and the other rich in

kaolinite, produced by the weathering of acid plutonic rocks within the middle sandy braid-plain of the sequence (Manassero, 1997).

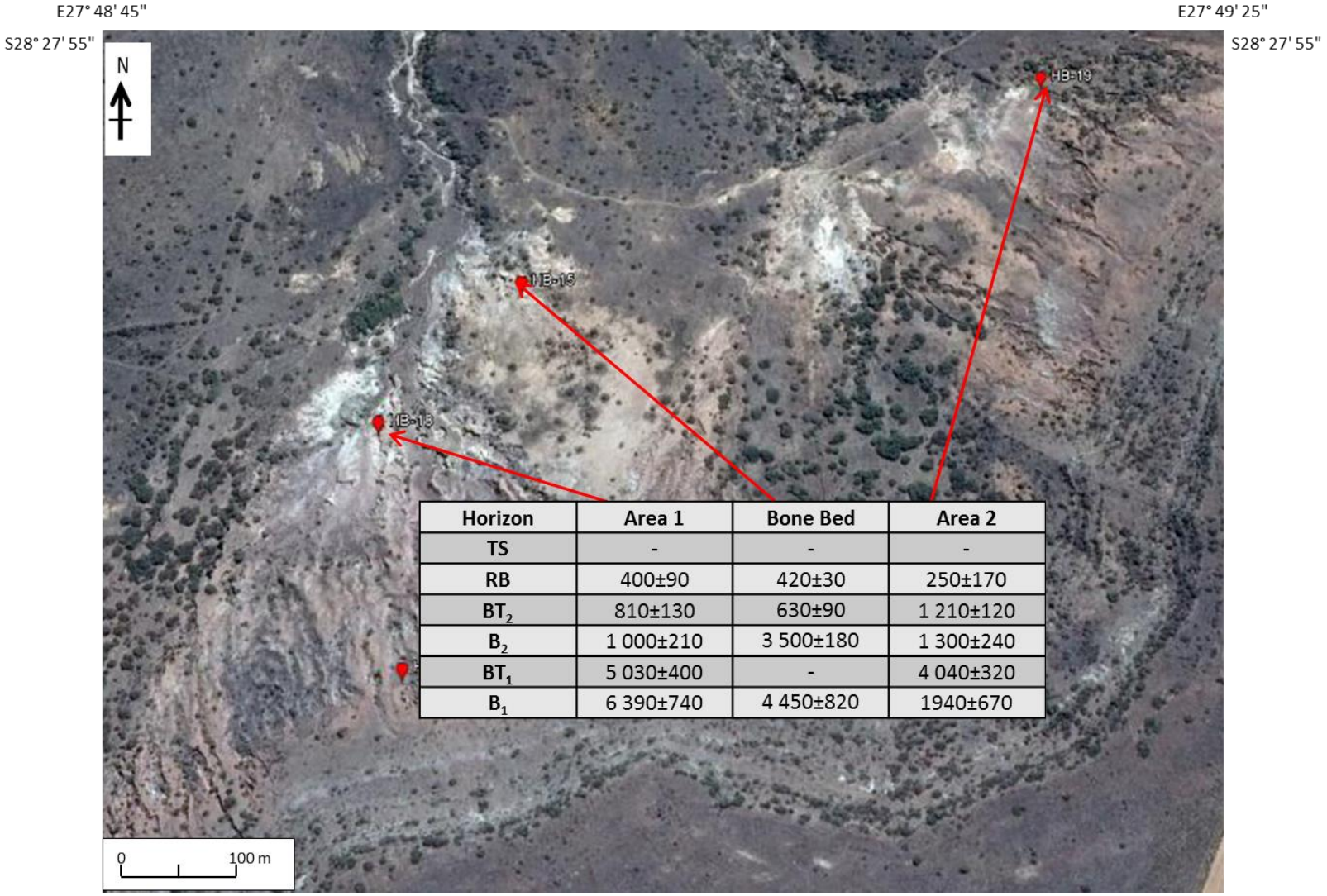
Particularly in the case of smectite, it is often difficult to determine whether minerals are authigenic or detrital. Detrital minerals can undergo differentiation in the form of selective erosion, size sorting or differential flocculation during transport, which will alter the composition at the deposition site. Finally, there is not necessarily a simple relationship between clay mineral formation and climatic factors. Once again using smectite as an example, smectites can be formed in semi-arid or tropical areas, depending on the topography and drainage conditions (Singer, 1984). Furthermore, Timms and Acworth (2002) determined that weathering in seasonally arid climates produces smectite from Ca-feldspar and/or illite from K-feldspar.

8.3.3 Depositional History

The Heelbo sediments and palaeosols were deposited within the late Holocene within the past 7 000 years, and significantly, all after the end of the last Ice Age. The OSL ages for the interlayered sediments and palaeosols for the hillslope are shown in Figure 8.1.

The Heelbo alluvial slope lies unconformably on an erosional bedrock surface and it has been shown that the weathered bedrock sediment is the

source material for the Heelbo deposit. The characteristics of the palaeosols and sedimentary horizons and the cross-cutting relationships between the stratigraphic units were used for relative dating and to describe the depositional history of the slope deposit (Figure 8.2).



Horizon	Area 1	Bone Bed	Area 2
TS	-	-	-
RB	400±90	420±30	250±170
BT_2	810±130	630±90	1 210±120
B_2	1 000±210	3 500±180	1 300±240
BT_1	5 030±400	-	4 040±320
B_1	6 390±740	4 450±820	1940±670

Figure 8.1 OSL ages for Area 1 and 2 and the bone bed. The OSL ages for the B_1 horizon at the head of the slope are also shown.

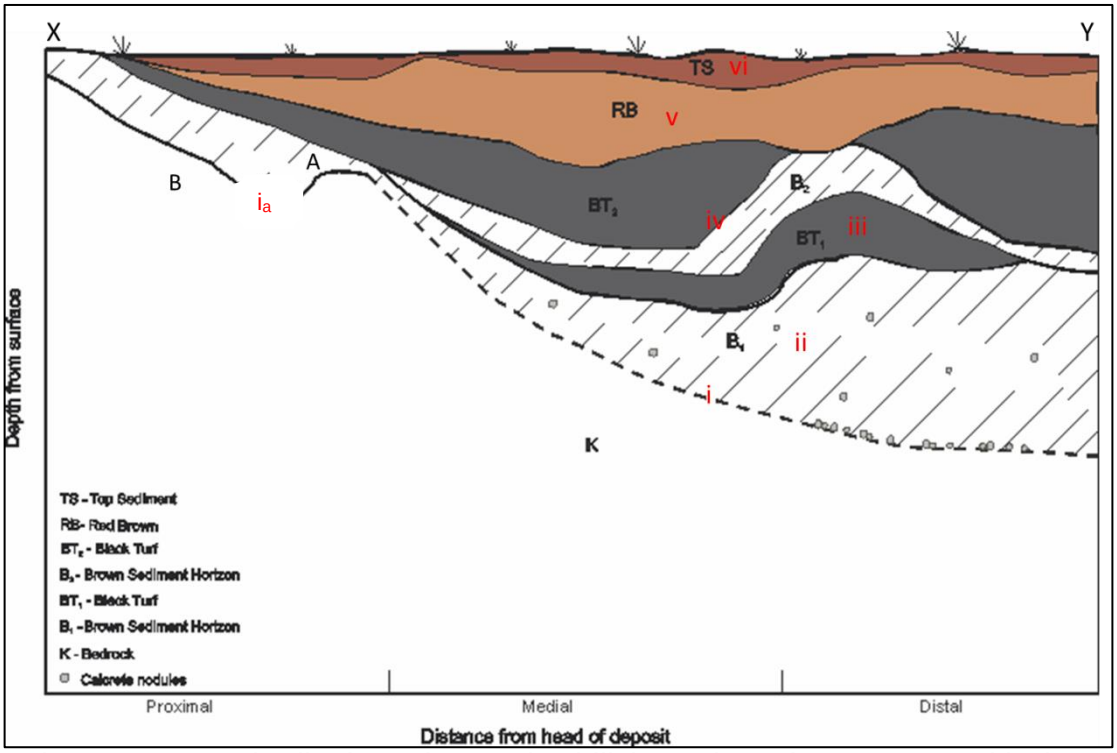


Figure 8.2 Longitudinal section of the hillslope deposit at Area 1 with the depositional history shown in red numerals with explanations in text. Dashed lines represent estimated position of bedrock.

i) The eroded bedrock surface forms the unconformable base of the Heelbo hillslope deposit. The position of the bedrock is estimated as it is only rarely exposed in the gullies. A palaeo-channel was identified between A-B, which eroded the bedrock and created an irregular rock surface (see i_a in Figure 8.2). Sediment collected in these undulating surfaces until such time as hillslope processes could remove it downslope. Unfortunately, the OSL ages for the sediment at the head of the deposit were unreliable (possibly as a result of bioturbation – see Chapter 6), and it was not possible to date the timing of this sediment accumulation. The underlying bedrock is an erosional surface and there were probably

numerous episodes of sedimentation before the first preserved sediment horizon (B_1) was deposited.

ii) Deposition of weathered bedrock material began around ~7000 years ago to form B_1 in Area 1 and ~4500 years ago in the bone bed (Figure 8.1). The ages for B_1 in Area 2 are stratigraphically inverted and not used in this discussion. The bone bed appears as a separate lobe, slightly north and downslope of Area 1, which would account for the timing of deposition in this area. There was a time-lag before material coming off the hillslope reached the bone bed site, further downslope.

The most recent African Humid Period (AHP) occurred between ~9000 and 6000 years BP, but continuous high-resolution marine sediment records indicate an extended duration from 12300 to 5500 years BP (deMenocal *et al*., 2000; Cole *et al*., 2009). The AHP is characterised by the North African Sahara Desert being completely vegetated with annual grasses and shrubs (deMenocal *et al*., 2000). Burrough and Thomas (2013) suggest that the southern African region experienced great environmental and climatic variability during the AHP. Data from the Makgadikgadi Basin (Figure 8.3) suggests that a period of marked hydrological dynamism was followed by mid-Holocene aridity (Burrough and Thomas, 2013). The B_1 horizon formed towards the end of this extended warm, humid period. The accumulation of sediment on the lower slopes would have required an initial humid period to weather the

bedrock and a subsequent shift to more arid conditions to allow sheet wash from rainstorm events to transport the weathered material downslope and deposit it as a thick succession on the gentler, stable slopes. This aridity is reflected in the formation of calcrete nodules within the B_1 horizon, and the absence of palaeosol formation (i.e. presence of vegetation). Flash flood events are recorded in the lag material located between the B_1 and BT_1 horizons in sections of the deposit. The size of the clasts (~2 cm diameter) suggests a high-energy flow regime to move the material down slope. The lag material is only found in the medial and distal slopes (see Figure 5.6).

The Boomplaas and Wonderkrater (Figure 8.3) records indicate that maximum warming of the Holocene Altithermal (HA) occurred around 7000 – 4500 cal yr BP (Scott and Thackeray, 1987; Thackeray, 1990). Records from Uitenhage suggest that this HA occurred between 8 000 and 4 500 cal yr BP, with temperatures 2-3 °C higher than present conditions (Heaton *et al*., 1983). At Stampriet (Figure 8.3) the warmest temperatures occurred between 9500 and 6000 cal yr BP (Stute and Talma, 1997). The OSL ages for B_1 at Heelbo locate the depositional period of this horizon within the Holocene Altithermal period.

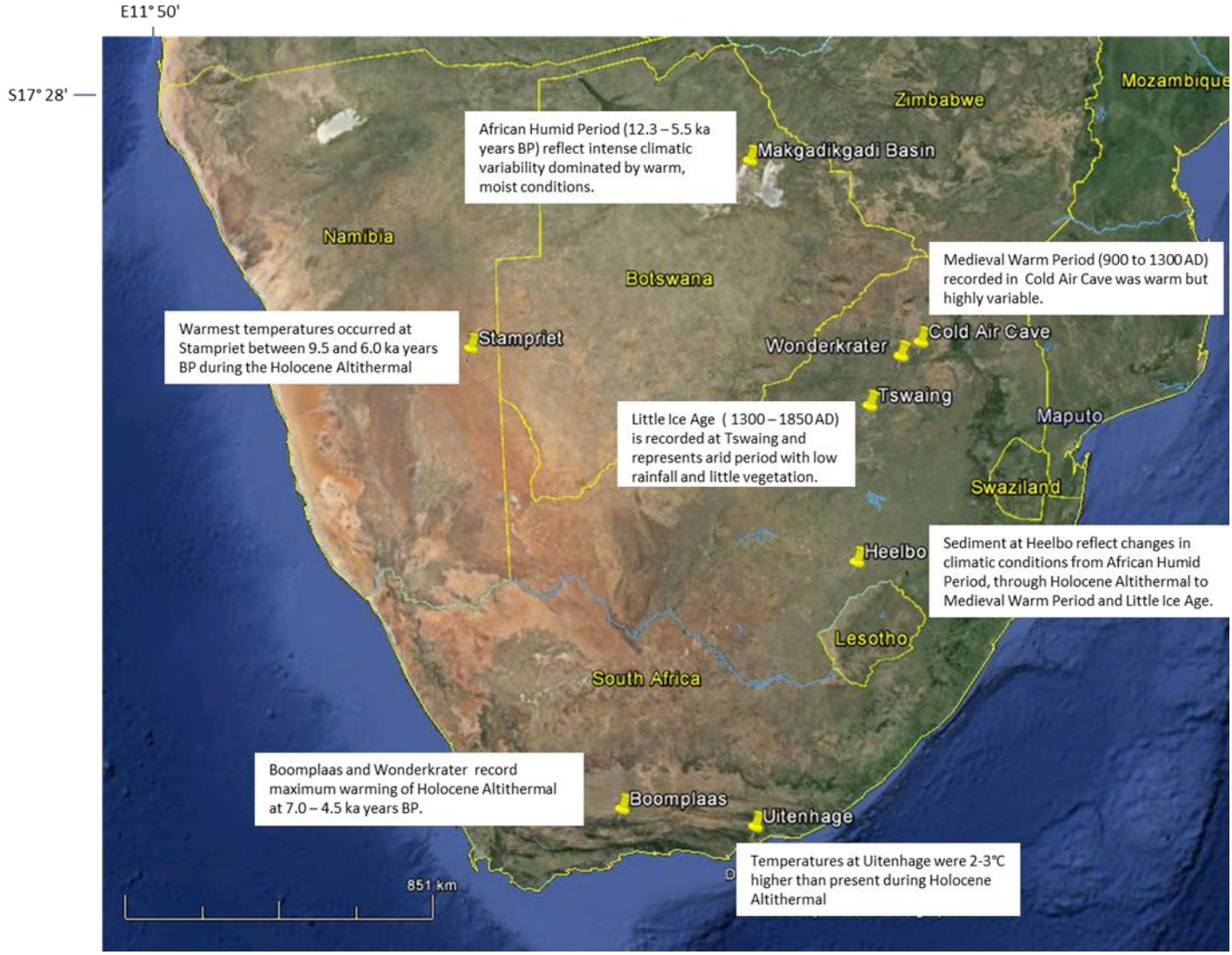


Figure 8.3 Google Earth (2014) image showing location of the southern African sites that record climatic periods reflected in the Heelbo sedimentary deposit.

iii) Around ~5 000 years BP, the shift to warmer, moist, conditions gave rise to the development of a soil (BT_1) with stable environmental conditions capable of sustaining increased vegetation growth and stability on the slope. The vegetation was incorporated into the sediment to create the palaeosol (BT_1), over a short period of time. Partridge (1990) noted that in the eastern parts of SA, maximum warming occurred from 8 000 – 5 000

years BP, with wetter conditions being established during the latter part of that period. This would coincide with the change in climate from hot and dry during B_1, to warm and wet during BT_1. Pedogenesis in BT_1 is synchronous between Area 1 and 2 (Figure 8.1).

iv) Around ~1 000 years BP, a second episode of deposition started with B_2 followed by BT_2, less than 100 years later (Figure 8.2). Unlike the B_1 horizon, there are only a small number of scattered, detrital calcrete nodules in the B_2 horizon. If the formation of the calcrete nodules is synchronous with the deposit in which they are found, it would suggest that B_1 experienced a drier climate than B_2. However, this is speculation until the concretions can be dated and proved to have formed *in situ*. As with the first cycle, pedogenesis occured as organic matter was incorporated into the sediment to form the BT_2 palaeosol. A period of weathering and erosion caused the incision of the newly deposited horizon as well as the underlying units (Figure 8.2). The avulsion of the channelised flow is indicated by the position of the palaeochannels. Gullying deepened and widened the channels and underground piping resulted in the overlying sediment collapsing and further widening the gullies. The relatively drier conditions made the soil more vulnerable to erosion, as rainfall began to decrease, such that, when wetter conditions returned, erosion and, therefore, piping and gullying increased.

Deposition of the B_2 horizon and soil formation at BT_2 was synchronous with the shift to warmer and drier conditions of the Medieval Warm Period (MWP). The Medieval Warm Period is a well-documented climatic period from about 900 to 1 300 AD (Broecker, 2001; Wanner *et al*., 2008). Four centuries of variable but generally warmer conditions are recorded with the highest temperatures occurring in the 10th and 11th centuries (Tyson and Lindesay, 1992). Evidence for the MWP in southern Africa is increasing and the importance of this climatic event on landscape dynamics is becoming apparent (Gillson and Ekblom, 2009). Evidence suggests that the MWP was warmer and wetter in the summer rainfall zone (SRZ), for example the Makapans Valley speleothem record) (Holmgren *et al*., 2003). However, it is unclear whether these warm, wet conditions were widespread across southern Africa and rainfall may have been more regionally variable (Lyons *et al*., 2013). Scott *et al*. (2012) demonstrated this regional variability in a recent synthesis of pollen data from across southern Africa.

The alternating brown (B_1 and B_2) and black turf (BT_1 and BT_2) deposits (Figure 8.2) seemingly reflect alternating dry and wet cycles within the depositional history. The period of aridity, reflected in the B_1 horizon extended to the Heelbo alluvial slope, and created the chemical precipitates in the B_1 unit. When wetter conditions returned, vegetation growth created the organic-rich BT_1 palaeosol which overlies B_1. Arid climates, as a result of the decreased vegetation cover and sediment

yield, and increased hill slope instability, may lead to alluvial slope development if any alluviation factors exist within an area (e.g. high/low relief contrasts). Wetter climates may result in increased sheet-flow fan and flood deposits from previous debris flow deposits and the change from drier conditions can lead to these alluviation conditions (Chamyal *et al.,* 2003). High rates/intensities of precipitation in this way can destabilise hill slopes and lead to increased sediment supply for alluvial slope deposition and to incision once the sediment supply decreases (Leigh and Webb, 2006).

v) Deposition of the RB horizon occurred ~420 to 250 years BP and filled some of the gullies. In the proximal slope the RB unit is thick, and becomes thinner towards the distal reaches. The estimated timing of the RB sequence coincides with the transition from the Medieval Warm Period (MWP) (AD 700 – 1300) to the Little Ice Age (LIA) (AD 1300 – 1850) (Mann, 2002). The MWP was generally warmer, but highly variable, where overall warm periods were punctuated by short cold periods, based on the Cold Air Cave record (Figure 8.3) (Holmgren *et al*., 1999). Therefore, it is possible that arid periods occurred during MWP, resulting in aggradation of slope and the higher temperatures, and rainfall produced fine-grained deposits. The RB horizon is synchronous with this MWP/LIA transition where a combination of declining temperatures and decreasing precipitation resulted in the destabilisation of the landscape and accounted for the period of erosion which followed the RB horizon. During the

MWP/LIA transition hillslopes changed from long-term sedimentation to net erosion and gully incision. This incision period between the RB and TS units could possibly have been halted around ~AD 1760, reflected in the deposition of the TS horizon. The LIA (AD 1300 – 1850) represents an arid period of low rainfall and little vegetation during which regional thunderstorms produced short, intense, run-off events (Matthews and Briffa, 2005), which resulted in the removal of sediment of the RB horizon to be deposited as gully infill. The timing of the LIA is recorded in the dated RB sequence and the shift towards a drier climatic regime is supported by Thomas (2008) as well as by the Tswaing Crater (Figure 8.3) record (Partridge *et al*., 1993).

vi) The TS horizon records the last episode of deposition on the hillslope deposit, post-250 years ago. The TS unit has begun to fill the gullies and, as with the RB horizon, it is thickest in the proximal slope, gradually thinning out towards the distal margins. The TS unit possibly reflects the climate shift towards its present day aridity. The present climate reflects arid conditions in a summer rainfall zone and the deposition of the modern horizon, although not well defined, has already begun.

The reconstruction of the palaeo-environmental history of the hillslope deposit suggests a change in climatic conditions from the African Humid Period (AHP), through the Holocene Altithermal (HA) to the Medieval Warm Period (MWP) and the Little Ice Age (LIA). An uncertainty with this

reconstruction is that southern African climates do not necessarily respond to periods of global warming and cooling in a uniform or globally representative way (Chase, 2010). Instead local climates may be controlled by a wide variety of forcing mechanisms. Evidence suggests that there is also no linear relationship between regional palaeo-environments and global conditions (Chase, 2010) and, therefore, it is not possible to accurately construct southern African palaeo-environmental histories solely by comparison with existing records. However, the reconstruction of the Heelbo history is supported by the mineralogy and sedimentary characteristics as well as high resolution geochronology.

CHAPTER 9 CONCLUSIONS

The relatively small alluvial slope succession located on the hillslopes of the remnant Karoo mesa on the farm Heelbo in the Eastern Free State provided an opportunity to describe and reconstruct the depositional and palaeo-environmental history of the deposit. An integrated analysis of the sedimentology, stratigraphy, mineralogy and geochronology formed the basis of the palaeo-environmental reconstruction of this hillslope deposit. This research has shown that alluvial fans and slopes with high sedimentary lithic input and some degree of pedogenesis will have deceptive grain size trends that are too fine for the corresponding depositional slope on which they form.

9.1 SUMMARY OF KEY FINDINGS

1. The Heelbo alluvial slope is a relatively small deposit derived from weathering and transportation of the underlying Elliot Formation bedrock. The ridge extends in a northwest, southeast direction for 1 450 m; the deposit rises only 60 m above the valley floor and spreads across the mountain front for ~ 500 m. The mineralogy of the Elliot Formation bedrock is mainly quartz and muscovite as non-clay minerals and montmorillonite and a mixed-layered chlorite/smectite mineral as the clays. Similarly, the alluvial slope mineralogy identified the mineral assemblage quartz, plagioclase, muscovite and calcite/dolomite with the clay mineral

fraction also represented by montmorillonite and a mixed-layered chlorite/smectite mineral. Ethylene-glycol-solvated samples produced very small shifts of less than 1˚ 2θ in the 001 peak, thus it is likely that the mixed-layer chlorite/smectite (C/S) mineral contains a higher proportion of chlorite than smectite. XRF analysis indicates very high SiO_2 and Al_2O_3 together with significant amounts of K_2O, NaO, CaO and FeO and very little MgO and MnO. Thin sections also reveal that the bedrock material is similar to the slope material, except where the bedrock appears as mature sandstone. The slope is immature sediment, although with a well-developed soil texture with secondary porosity. Lithic fragments indicate the source rocks as the subarkoses of the upper Elliot Formation in the Karoo Supergroup and these fragments commonly display Fe-oxide coatings. Calcite was visible in only two of the thin sections, thus it is likely due to a diagenetic overprint that is constrained by depth from the surface or time and not to specific layers.

The bedrock is described as mostly lithic arkose whereas the slope material is mainly lithic-subarkose to subarkose. The lithic material in the sediment appears to be the sand- and mud-stone of the bedrock that has been incorporated into the deposit. There is no evidence in thin section or in the mineralogy of windblown material having contributed to the deposit. The grains are sub-angular, sub-rounded and poorly sorted, which suggests a local provenance for the sediment.

2. The stratigraphy comprises six distinct sedimentary units with B_1, B_2, RB and TS representing sediment horizons and BT_1 and BT_2 interlayered palaeosols. Although one BT layer is visible across most of the deposit, the presence of another BT horizon in sections of the deposit and the ages of the palaeosols indicate there were two distinct cycles of pedogenesis in the sequence.

3. Heelbo is defined as an alluvial slope. Samples from the units were subjected to granulometric analysis to determine the grain size distribution down slope. The mainly unimodal distribution of the grain size supports the finding that there was only one source for the deposit. Grain size distribution histograms revealed that coarse material is abundant in the proximal slope but grain size decreases downslope. This is true for both the TS and RB horizons that were sampled.

The fine sand to silt grains found on a steep slope (~ 10°) locates Heelbo outside the scope of traditionally describe alluvial fans, colluvial or talus slopes. Some of the differences to previously described hillslopes include the absence of an incising feeder channel but rather an amphitheatre-like architecture, and the confined deposition of sediment. The fining of grain sizes down the slope of the alluvial fan is illustrated in Figure 7.5, and confirms the existence of down slope fining and, hence, the possibility of this being described as an alluvial fan; although, it is acknowledged that this is a characteristic of a number of fluvial sedimentary systems.

The deposit is described as an alluvial slope as it lacks the distinctive fan morphology (see Bryan, 1922) and has formed on a mountain front that lacks abrupt structural and topographic definition (see Smith, 2000). However, it is possible that a continuum of hillslope deposits may exist and Heelbo plots somewhere along this continuum rather than as an end member, as many factors may play a role in governing the defining of hillslope deposits.

4. The hillslope deposit is intensively gullied and the morphology of the gullies is described as mature and continuous gully networks with V-shapes profiles in the proximal slope, becoming combined V- and U-shaped profiles in the medial and distal sections. The degree of cation exchange in the soil as measured by the sodium adsorption ratio (SAR_s), as well as pH and electrical conductivity were determined to identify the cause of gullying on the slope. The cause of the gullies was related to the SAR_s, which determined that the soils could be described as mainly saline with a few sodic samples down the slope profile, and mainly sodic within a vertical section of the slope. This implies that gullying can and does occur in non- / slightly-sodic environments just as it would in sodic soil. Furthermore the high clay content, especially the presence of smectite which has significant shrinking and swelling properties, found in the sediment destabilises the soils and causes it to be washed away. Notwithstanding the sodicity index, the dispersion tests show that the soil is highly dispersive and is easily eroded, leaving behind a network of

gullies. The extreme piping in the deposit suggests that this dispersive nature of the soil is the primary cause of the gullies.

It was also shown that the gullies could not be caused by a change in base level. As the Sandrivier became deeply incised, a knickpoint was created which migrated upstream, but this is not contemporary with gully formation and therefore no causal relationship exists between the knickpoint and the gullies.

5. The sequence was dated using both radiocarbon and optically stimulated luminescence dating techniques. The OSL ages indicate that the alluvial slope was deposited possibly within the last ~7 000 years. The palaeosols were dated as ~5 000 and 1 200 years, respectively. The palaeosols were shown to have at least 3-4 ka years of erosion and deposition between them and the ages between the two Areas appear to correlate. However, the ^{14}C ages proved to be unreliable, possibly as a result of modern carbon contamination in the bulk sediment sample. The OSL ages were therefore used in the reconstruction, as these were considered suitable for constraining the timing of deposition of the sediment.

6. The reconstruction of the depositional environment indicates that the Heelbo succession was established under semi-arid conditions as evidenced by the formation of calcrete nodules within the B_1 horizon, some

calcrete found in B_2 and the presence of rhizocretions in RB, which all formed during periods of limited water availability.

The palaeoenvironment during deposition was one of strong seasonality with a pronounced dry season and low rainfall based on the conditions and environments for smectite formation and the lack of kaolinite within the mineral assemblage. The BT_1 and BT_2 palaeosols were formed under different conditions when water and organic matter were available. This probably occurred during the rain- season when sediments became water-logged due to a high proportion of clays. The BT palaeosols are generally more clay-rich than the B sediment and, together with the lack of calcrete formation within the palaeosols, strongly suggests a wetter climate during pedogenesis, shifting towards drier conditions eventually.

The interlayered sediment and palaeosol horizons suggest some cyclicity in the deposition, pedogenesis and erosion history of the alluvial succession. The reconstruction suggests that there were lengthy dry periods with intermittent short periods of high rainfall reflected in flash flood events. The alluvial slope has experienced climatically controlled histories of erosion, sedimentation and pedogenesis. Extreme sedimentation is assumed to have occurred during relatively arid climatic intervals, when decreased vegetation cover provided little surface protection. In contrast pedogenesis occurs during humid intervals when

vegetation cover is restored, the land stabilizes and the uppermost gravely sands weather to form soils.

9.2 IMPORTANCE OF THIS STUDY AND SUGGESTIONS FOR FUTURE RESEARCH

The identification of a previously undescribed type of hillslope deposit is one of the most important issues raised. A review of the literature highlights the problems with defining a hillslope deposit based on characteristics of gradient, grain-size distribution and morphology. Current research suggests that assigning the descriptor "alluvial fan" to most hillslope deposits is incorrect and that slopes can be reassigned as colluvial mantles, talus slopes and alluvial slopes amongst others. This study highlights the problematic nature of defining hillslope deposits and suggests the possibility of a continuum as deposits change morphology from one form to another. These changes may be driven by external forcing such as climate or by localised forcing such as vegetation, mineralogy or topography.

An expansion of a similar integrated study on slopes similar to Heelbo is required. Such slopes have been identified in the Free State area (see map in APPENDIX A), at Loskop Dam (Mpumalanga), and Diepdrift (Limpopo). Initial studies suggest fine grained sediments are located on steep slopes at these sites, but the bedrock geology, vegetative cover and morphologies are different. But this expanded study would confirm (or

disprove) the existence of a hillslope continuum or establish whether Heelbo is in fact a new class of landform. Either way the issue that may be the most pertinent is the understanding of the processes that allow for the production of steep fine-grained slopes that still conform to alluvial fan processes.

Gully erosion was considered to be an agricultural and land-use problem but the soil properties of Heelbo has shown that gullying occurs in non-sodic soils and that the clay mineralogy is also a determining factor in gully formation. This is an important finding as it may influence how gullies are managed and treated in areas where soil stability is critical, i.e. farming or rangelands. An extension of this work would be to do a clay mineral investigation in other soils where gullying occurs in the absence of a sodic source and determine if the clay minerals are indeed a major contributing factor.

Robust chronologies are critical for palaeo-environmental reconstructions especially in fluvial environments. However, research has shown that fluvial environments are often difficult to date. The contamination of modern carbon often leads to an underestimation in the ^{14}C ages especially in bulk sediment samples, and problem with partial bleaching plagues OSL ages. However, the dating of the Heelbo succession has added to the growing number of successfully dated fluvial sequences in South Africa, and combined with the depositional history, adds to the

palaeo-environmental record of the country. The climate reconstruction confirms that the region is becoming drier and that these semi-arid conditions occurred on a cyclical basis, although the overwhelming trend is towards drier conditions.

The bone bed is an interesting feature of this area. The study of the fossils was considered outside the scope of this project. However, the bone bed is located within the BT_1 horizon in an adjacent lobe, separate from Area 1. While the stratigraphy and field descriptions of the two sections correlate well, the ages suggested that localised factors control the timing of the deposition in separate areas and those climatic controls may overprint these localised conditions.

The palaeo-environmental reconstruction of this region suggests that the sedimentary units were deposited in dry climatic regimes and the palaeosols where formed when more water was available. The trend towards a semi-arid climate in the region is concordant with predictions of future climate change that suggests southern Africa will be desiccated and experience water stress in the future (Hulme *et al*., 2001).

REFERENCES

Abrahams, A.D. and Parsons, A.J. (1991). Relationship between infiltration and stone cover on a semiarid hillslope, Southern Arizona. *Journal of Hydrology*, **122,** 49-59.

Adamiec, G. and Aitken, M.J. (1998). Dose-rate conversion factors: update. *Ancient TL*, **16**, 37-49.

Aguilar, J., Dorronsoro-Fdez, C., Fernández, J., Dorronsoro Diaz, C., Martin, F. and Dorronsoro, B. (2002). Soil Microscopy: Interactive multimedia programme for self-studying soil thin section description. Department of Pedology, Faculty of Science, University of Granada, Spain. [www] http://edafologia.ugr.es/index/index.htm (14 September 2012).

Aitken, M.J. (1985). *Thermoluminescence Dating*. Academic Press, London, 359p.

Aitken, M.J. (1998). *An introduction to optical dating .The Dating of Quaternary Sediments by the Use of Photon-Stimulated Luminescence.* Oxford University Press, Oxford, 267p.

Aitken, M.J. and Xie, J. (1990). Moisture correction for annual gamma dose. *Ancient TL*, **8**, 6-9.

Alkan, M., Demirbas, Ö., Celikcapa, S. and Dogan, M. (2004). Sorption of acid red 57 from aqueous solution onto sepiolite. *Journal of Hazardous Materials*, **116,** 135-145.

Allen, P.A. and Hovius, N. (1998). Sediment supply from landslide dominated catchments: implications for basin-margin fans. *Basin Research*, **10**, 19-35.

Allison, R.J. and Thomas, D.S.G. (1993). The sensitivity of landscapes. In: Thomas, D.S.G. and Allison R.J. (Eds), *Landscape Sensitivity*, John Wiley and Sons Ltd., 1-6.

Amézketa, E. (1999). Soil aggregate stability: A review. *Journal of Sustainable Agriculture*, **14** (2), 83-151.

Anstey, R.L. (1965). Physical characteristics of alluvial fans. U.S. Army Natick Laboratory, Technical Report ES20, 109.

Armitage, S.J., Duller, G.A.T. and Wintle, A.G. (2000). Quartz from southern Africa: Sensitivity changes as a result of thermal pretreatment. *Radiation Measurements*, **32**, 571-577.

Armstrong, A.S.B. and Tanton, T.W. (1992). Gypsum applications to aggregated saline sodic clay topsoils. *Journal of Soil Science*, **43**, 249–260.

Armstrong-Altrin, J.S., Lee, Y.I., Verma, S.P. and Ramasamy, S. (2004). Geochemistry of sandstones from the Upper Miocene Kudankulam Formation, Southern India: Implications for provenance, weathering, and tectonic setting. *Journal of Sedimentary Research*, **74**(2), 285–297.

Attal, M., Mudd, S., Hurst, M.D., Weinman, B., Yoo, K. and Naylor, M. (2015). Impact of change in erosion rate and landscape steepness on hillslope and fluvial sediments grain size in the Feather River Basin (Sierra Nevada, California. *Earth Surface Dynamcs*, **3**, 201-222.

Avery, D.M. (1993). Last Interglacial and Holocene altithermal environments in South Africa and Namibia: Micromammalian evidence. *Palaeogeography, Palaeoclimatology, Palaeoecology,* **101**, 221-228.

Baillie, I. (1985). Comment on "The palaeoenvironmental interpretation of colluvial sediments and palaeosols of the Late Pleistocene hypothermal in southern Africa". *Palaeogeography, Palaeoclimatology, Palaeoecology*, **52**, 153-163.

Ballantyne, C. K. and Harris, C. (1994). *The Periglaciation of Great Britain*. Cambridge University Press, Cambridge.

Bateman, M.D., Frederick, C.D., Jaiswal, M.K. and Singhvi, A.K. (2003). Investigations into the potential effects of pedoturbation on luminescence dating. *Quaternary Science Reviews,* **22**, 1169-1176.

Bates, R.L. and Jackson, J.A. (1987). *Glossary of Geology* (3rd edition). American Geological Institute, Alexandria, Virginia.

Beaumont, P.B., Miller, G.H. and Vogel, J.C. (1992). Contemplating old clues to the impact of future greenhouse climates in South Africa. *South African Journal of Science*, **88**, 490--498.

Beavis, S. (2000). Structural controls on the orientation of erosion gullies in mid-western New South Wales, Australia. *Geomorphology*, **33**, 59-72.

Beckedahl, H.R. and De Villiers, A.B. (2000). Accelerated erosion by piping in Eastern Cape, *South African Geographical Journal*, **87**(3), 157-162.

Begin, Z.B., Meyer, D.F. and Schumm, S.A. (1981). Development of longitudinal profiles of alluvial channels in response to base-level lowering. *Earth Surface Processes and Landforms*, **6** (1), 49-68.

Beinart, W. (1984). Soil erosion, conservationism and ideas about development: a southern African exploration, 1900-1960. *Journal of Southern African Studies*, **11(1)**, 52-83.

Bell, F.G. and Walker, D.J.H. (2000). A further examination of the nature of dispersive soils in Natal, South Africa. *Quarterly Journal of Engineering Geology and Hydrogeology*, **33**, 187-199.

Bennett, H.H. (1939). *Soil Conservation*. McGraw-Hill, New York.

Berjak, M., Fincham, R.J., Liggitt, B. and Watson, H.K., (1986). Temporal and spatial dimensions of gully erosion in northern Natal, South Africa. Proceedings of an International Symposium of the International Society for Photogrammetry and Remote Sensing and the Remote Sensing Society. Edinburgh, pp. 583–593.

Billi, P. and Dramis, F. (2003). Geomorphological investigation on gully erosion in the rift valley and the northern highlands of Ethiopia, *Catena*, **50**, 353-368.

Birkeland, P.W. (1990). Soil-geomorphic research – a selective overview. *Geomorphology*, **3**, 207-224.

Blair, T.C. (1987). Sedimentary processes, vertical stratification sequences, and geomorphology of the Roaring River alluvial fan, Rocky Mountain National Park, Colorado. *Journal of Sedimentary Petrology*, **57**, 845-862.

Blair, T.C. and McPherson, J.G. (1994). Alluvial fans and their natural distinction from rivers based on geomorphology, hydraulic processes, sedimentary processes, and facies assemblages. *Journal of Sedimentary Research*, **A64**, 450-489.

Blair, T.C. and McPherson, J.G. (1995). Reply: alluvial fans and their natural distinction from rivers based on morphology, hydraulic processes, sedimentary processes, and facies assemblages. *Journal of Sedimentary Research*, **A65**, 583–586.

Blank, R.R., Young, J.A. and Lugaski, T. (1996). Pedogenesis on talus slopes, the Buckskin range, Nevada, USA. *Geoderma*, **71**, 121-142.

Blissenbach, E. (1954). Geology of alluvial fans in semi-arid regions. *Geological Society of America Bulletin*, **65**, 175-189.

Bloem, A.A. and Laker, M.C. (1994). Criteria for adaptation of the design and management of centre-pivot irrigation systems to the infiltrability of soils. *Water SA*, **20**, 127-132.

Blong, R.J. (1970). The development of discontinuous gullies in a pumice catchment. *American Journal of Science*, **268**, 369-383.

Blott, S.J. (2010). GRADISTAT, Version 8.0.

Blott, S.J. and Pye, K. (2001). Gradistat: A grain size distribution and statistics package for the analysis of unconsolidated sediments. *Earth Surface Processes and Landforms*, **26**, 1237-1248.

Bocco, G. (1991). Gully Erosion: Processes and Models. *Progress in Physical Geography*, **15*(4)***, 392-406.

Boothroyd, J.C. (1972). Coarse-grained sedimentation on a braided outwash fan, northeast Gulf of Alaska. University of South Carolina Coastal Research Division Technical Report 6, 127.

Bordy, E.M., Hancox, P.J. and. Rubidge, B.S. (2004a). Basin development during the deposition of the Elliot Formation (Late Triassic - Early Jurassic), Karoo Supergroup, South Africa. *South African Journal of Geology*,**107**, 397-412.

Bordy, E.M., Hancox, P.J. and Rubidge, B.S. (2004b). Fluvial style variations in the Late Triassic-Early Jurassic Elliot Formation, main Karoo Basin, South Africa. *Journal of African Earth Sciences*, **38**, 383-400.

Botha, G.A., (1996). Memoir 83: The geology and palaeopedology of late quaternary colluvial sediments in northern Kwazulu-Natal. Council for Geosciences, Pretoria.

Botha, G.A., and Partridge, T.C. (2000). Colluvial Deposits. In: Partridge, T.C., Maud, R.R. (Eds.), *The Cenozoic Geology of Southern Africa*. Oxford University Press, New York, 88-99.

Botha, G.A., Scott, L., Vogel, J.C. and von Brunn, V. (1992). Palaeosols and palaeoenvironments during the Late Pleistocene Hypothermal in northern Natal. *South African Journal of Science*, **88**, 508–512.

Botha, G.A., Wintle, A.G. and Vogel, J.C. (1994). Episodic Late Quaternary palaeogully erosion in northern KwaZulu/Natal, South Africa. *Catena,* **23**, 327-340.

Bøtter-Jensen, L., McKeever, S.W.S. and Wintle, A.G. (2003a). Optically Stimulated Luminescence Dosimetry. Elsevier Science, The Netherlands, 355p., ISBN: 0-444-50684-5.

Bøtter-Jensen, L., Andersen, C.E., Duller, G.A.T. and Murray, A.S. (2003b). Developments in radiation, stimulation and observation facilities in luminescence measurements. *Radiation Measurements,* **37**, 535-541.

Broecker, W.S. (2001). Was the medieval warming global? *Science*, **291**, 1497–1499.

Bronick, C.J. and Lal, R. (2005). Soil structure and management: A review. *Geoderma*, **124**, 3-22.

Bryan, K. (1922). Erosion and sedimentation in the Papago country, Arizona, with a sketch of the geology. *US Geological Survey Bulletin*, **730**, 19-90.

Bull, W.B. (1972). Recognition of alluvial fan deposits in the stratigraphic record. In: Rigby, K.J. and Hamblin, W.K. (Eds), *Recognition of Ancient Sedimentary Environments*. Special Publication of the Society of Economic Paleontologists and Mineralogists.

Bull, W.B. (1991). *Geomorphic Responses to Climate Change.* Oxford University Press, Oxford.

Bull, W.B. (1997). Discontinuous ephemeral streams. *Geomorphology*, **19**, 227-276.

S.L. Burrough, S.L. and Thomas, D.S.G. (2013). Central southern Africa at the time of the African Humid Period: a new analysis of Holocene palaeoenvironmental and palaeoclimate data. *Quaternary Science Reviews,* **80**, 29–46.

Butler, R.J. (2005). The 'fabrosaurid' ornithischian dinosaur of the Upper Elliot Formation (Lower Jurassic) of South Africa and Lesotho. *Zoological Journal of the Linnean Society*, **145**, 177 – 218.

Catuneanu, O., Hancox, P.J. and Rubidge, B.S. (1998). Reciprocal flexural behaviour and contrasting stratigraphies: a new basin development model for the Karoo retroarc foreland system, South Africa. *Basin Research*, **10**, 417- 439.

Cerling, T.E. (1984). The stable isotopic composition of modern soil carbonate and its relationship to climate. *Earth and Planetary Science Letters*, **71**, 229-240.

Cerling, T.E. and Quade, J. (1993). Stable Carbon and Oxygen Isotopes in Soil Carbonates. In: Swart, P.K., Lohmann, K.C., McKenzie, J. and Savin, S., (Eds), *Climate Change in Continental Isotopic Records* American Geophysical Union, Washington, D. C. doi:10.1029/GM078p0217.

Chamyal, L.S., Maurya, D.M. and Raj, R. (2003). Fluvial systems of the drylands of western India: a synthesis of Late Quaternary environmental and tectonic changes. *Quaternary International*, **104**, 69-86.

Chappell, C. (1992). The Ecology of sodic sites in the Eastern Transvaal lowveld. M.Sc. thesis (unpubl). University of the Witwatersrand, Johannesburg, South Africa.

Chase, B.M. (2010). South African palaeoenvironments during marine oxygen isotope stage 4: A context for the Howiesons Poort and Still Bay industries. *Journal of Archaeological Science*, **37**, 1359-1366.

Chase, B.M. and Meadows, M.E. (2007). Late Quaternary dynamics of southern Africa's winter rainfall zone. *Earth-Science Reviews*, **84**, 103-138.

Chesworth, W. (1973). The parent rock effect in the genesis of soil. *Geoderma*, **10**, 215-225.

Chorom, M., Rengasamy, P. and Murrary, R.S. (1994). Clay dispersion as influenced by pH and net particle charge of sodic soils. *Australian Journal of Soil Research*, **32**, 1243-1252.

Chu, S.Y., Nordberg, H., Firestone, R.B. and Ekström, L.P. (1999). Isotope Explorer, Version 2.23.

Claridge, G.G.C. (1960). Clay minerals, accelerated erosion, and sedimentation in the Waipaoa River catchment, New Zealand. *Journal of Geology and Geophysics*, **3** (2), 184-191.

Clarke, L., McLelland, S. and Coulthard T. (2014) Investigating the impact of vegetation on alluvial fans using laboratory experiments. *Geophysical Research Abstracts*, **16**, EGU General Assembly.

Clarke, M.L., Vogel, J.C., Botha, G.A. and Wintle, A.G. (2003). Late Quaternary hillslope evolution recorded in eastern South African colluvial badlands. *Palaeogeography, Palaeoclimatology, Palaeoecology,* **197**, 199-212.

Cockcroft, M.J., Wilkinson, M.J. and Tyson, P.D. (1987). The application of a present-day climatic model to the late Quaternary in southern Africa. *Climate Change,* **10**, 161-181.

Cole, J.M., Goldstein, S.L., deMenocal, P.B., Hemming, S.R., Grousset, F.E. (2009). Contrasting compositions of Saharan dust in the eastern Atlantic Ocean during the last deglaciation and African Humid Period. *Earth and Planetary Science Letters*, **278**, 257-266.

Cooke, R.U. and Warren, A. (1973). *Geomorphology in Deserts*. Batsford Ltd, London.

Crouch, R.L. and Blong, R.J. (1989). Gully sidewall classification: methods and applications, *Zeitschrift fur Geomorphologie N.F.,* **3**, 291-305.

Curry, A.M. and Morris, C.J. (2004). Lateglacial and Holocene talus slope development and rockwall retreat on Mynydd Du, UK. *Geomorphology*, **58**, 85-106.

Curtin, D., Steppuhn, H. and Selles, F. (1994). Effects of magnesium on cation selectivity and structural stability of sodic soils. *Soil Science Society of America Journal*, **58**, 730-737.

Dardis, G.F. (1988). Colluvial stratigraphy in southwestern Transkei. In Beckedahl H.R., Moon B.P. and Dardis, G.F. (Eds), *South African Landscapes: A Geomorphological Field Guide:* Post Symposium Field Excursion Guide Book, Symposium on the Geomorphology of Southern Africa, 8-26.

Davies, J. G., Waskom, R. M., Bauder, T. A. and Cardon, G. E. (2007). Managing Sodic Soils. http://www.greenhouse.colostate.edu/pubs/crops/00504.html (13/05/2010)

Davies, S. and Lacey, A. (2009). Identifying dispersive soils, *Farmnote 386*, Department of Agriculture and Food, Government of Western Australia.

Davis, W.M. (1898). *Physical Geography*. Ginn and Company, Boston, 432pp.

Deacon, J. (1990). Changes in the archaeological record in South Africa at 18000 BP. In Gamble. C. and Softer, O. (Eds.), *The World at 18,000 BP*, vol. 2. Unwin Hyman. London, 170-188.

Deacon, J. and Lancaster, N. (1988). *Late Quaternary Paleoenvironments of Southern Africa.* Clarendon Press, Oxlbrd.

De Chant, L.J., Pease, P.P. and Tchakerian, V.P. (1999). Modelling alluvial fan morphology. *Earth Surface Processes and Landforms*, **24**, 641-652.

De Haas, T., Ventra, D., Carbonneau, P.E., and Kleinhans, M.G. (2014). Debris-flow dominance of alluvial fans masked by runoff reworking and weathering. *Geomorphology,* **217**, 165–181.

De Meis, M. R. and de Moura, J. R. (1984). Upper Quarternary sedimentation and hillslope evolution: Southeastern Brazilian Plateau. *American Journal of Science*, **284**, 241-254.

DeMenocal, P., Ortiz, J., Guilderson, T., Adkins, J., Sarnthein, M., Baker, L. and Yarusinsky, L. (2000). Abrupt onset and termination of the African Humid Period: Rapid climate responses to gradual insolation forcing. *Quaternary Science Reviews*, **19**, 347-361.

Deschamps, C. (2006). A comparison of the biogeographical and geomorphological characteristics of gullied and non-gullied valley head mires in eastern Lesotho. Masters dissertation (unpubl). University of the Witwatersrand, Johannesburg, 252pp.

Descroix, L., González Barrios, J.L., Viramontes, D., Poulenard, J., Anaya, E., Esteves, M and Estrada, J. (2008). Gully and sheet erosion on subtropical mountain slopes: Their respective roles and the scale effect. *Catena*, **72**, 325–339.

Dexter, A.R. (1988). Advances in characterization of soil structure. *Soil and Tillage Research,* **11**, 199-238.

Dimoyiannis, D.G., Tsadilas, C.D. and Valmis, S. (1998). Factors affecting aggregate instability of Greek agricultural soils. *Communications in Soil Science and Plant Analysis,* **29**, 1239-1251.

Dlamini, P., Orchard, C., Jewitt, G., Lorentz, S., Titshall, L. and Chaplot, V. (2010). Controlling factors of sheet erosion under degraded grasslands in the sloping lands of Kwa-Zulu Natal, South Africa. *Agricultural Water Management*, DOI:10.1016/j.agwat.2010.07.016.

Dobbie, P. (2001). *Poverty and the drylands*. Challenge Paper 2, UNDP Drylands Development Centre, Nairobi.

Dosseto, A., Hesse, P.P., Maher, K., Fryirs, K. and Turner, S. (2010). Climatic and vegetation control on sediment dynamics during the last glacial cycle. *Geology*, **38** (5), 395–398.

Downes, R. G. (1954). Cyclic salt as a factor in soil genesis. *Australian Journal of Agricultural Research*, **5**, 448-64.

Duller, G.A.T. (2004). Luminescence dating of Quaternary sediments: recent advances. *Journal of Quaternary Science*, **19(2)**, 183-192.

Duller, G.A.T. (2008). Single grain optical dating of Quaternary sediments: why aliquot size matters in luminescence dating. *Boreas*, **37**, 589-612.

Dye, P.J. (1977). Vegetation – Environment relationships on Rhodesian sodic soils. M.Sc. thesis (unpubl). University of the Witwatersrand, Johannesburg, South Africa.

Embrechts, J. (1986). Pedogenesis in relation to landscape development in a humid subequatorial climate (Yaounde, Cameroon). *Academiae Analecta*, **48**, 1–41.

Eriksson, M.G., Olley, J.M. and Payton, R.W. (2000). Soil erosion history in central Tanzania based on OSL dating of colluvial and alluvial hillslope deposits. *Geomorphology*, **36** (1–2), 107–128.

Eriksson, P.G. (1985). The depositional environment of the Elliot Formation in the Natal Drakensberg and north-east Orange Free State. *Transactions Geological Society of South Africa*, **88**, 19–26.

Eriksson, P., Long, D., Bumby, A., Eriksson, K., Simpson, E., Catuneanu, O., Claassen, M., Mtimkulu, M., Mudziri, K., Brümer, J. and Van der Neut, M. (2008). Palaeohydrological data from the c. 2.0 to 1.8 Ga Waterberg Group, South Africa: discussion of a possibly unique Palaeoproterozoic fluvial style. *South African Journal of Geology*, **111**, 281-304.

Etemad-Saeed, N., Hosseini-Barzia, M. and Armstrong-Altrin, J.S. (2011). Petrography and geochemistry of clastic sedimentary rocks as evidences for provenance of the Lower Cambrian Lalun Formation, Posht-e-badam block, Central Iran. *Journal of African Earth Sciences*, **61** (2), 142–159.

Evans, J.E. (1991). Facies relationships, alluvial architecture, and paleohydrology of a Paleogene, humid-tropical alluvial-fan system: Chumstick Formation, Washington State, U.S.A. *Journal of Sedimentary Petrology*, **61**, 732-755.

Faber, T.H. and Imeson, A.C. (1982). Gully hydrology and related soil properties in Lesotho. In: Walling D.E. (Ed), *Recent Developments in the Explanation and Prediction of Erosion and Sediment Yield*, Proceedings of the Exeter Symposium, July, IAHS Pub no. 137, International Association of Hydrological Sciences, 135-144.

Fagel, N., Boski, T., Likhoshway, L. and Oberhaensli, H. (2003). Late Quaternary clay mineral record in Central Lake Baikal (Academician Ridge, Siberia). *Palaeogeography, Palaeoclimatology, Palaeoecology*, **193**, 159-179.

Firth, C.R. and Whitlow, R. (1991). Patterns of gullying in Zimbabwe. *Geojournal*, **23(1)**, 59-67.

Folk, R..L. (1980). *Petrology of sedimentary rocks*, Hemphill Pub. Co.

Folk, R.L. and Ward, W. C. (1957). Brazos River Bar: A study in the significance of grain size parameters. *Journal of Sedimentary Petrology,* **27,** 3-26.

Foster I.D.L., Rowntree, K.M., Boardman, J. and Mighall, T.M. (2012). Changing sediment yield and sediment dynamics in the Karoo Uplands, South Africa; Post-European impacts. *Land Degradation and Development,* **23**, 508–522.

Fox, R. (2000). Agriculture and rural development. In: Fox, R., and Rowntree, K. (Eds) *The geography of South Africa in a changing world*, Oxford University Press, Cape Town, 211–232.

Francus, P. and Asikainen, C.E. (2001). Sub-sampling unconsolidated sediments: a solution for the preparation of undisturbed thin-sections from clay-rich sediments. *Journal of Paleolimnology*, **26**, 323-326.

Frankl, A., Poesen, J., Deckers, J., Haile, M. and Nyssen, J. (2012). Gully head retreat rates in the semi-arid highlands of Northern Ethiopia. *Geomorphology*, **173-174**, 185-195.

Frankl, A., Deckers, J., Moulaert, L., van Damme, A., Haile, M., Poesen, J. and Nyssen, J. (2014). Intergrated solutions for combatting glly erosion in areas prone to soil piping: Innovations from the drylands of northern Ethiopia. *Land Degradation and Development*, DOI: 10.1002/ldr.2301

Frenkel, H., Goertzen, J.O. and Rhoades, J.D. (1978). Effects of clay type and content, exchangeable sodium percentage, and electrolyte concentration on clay dispersion and soil hydraulic conductivity. *Soil Science Society of America Journal*, **48**, 32-39.

Fuchs, M. and Lang, A. (2009). Luminescence dating of hillslope deposits – A review. *Geomorphology*, **109**, 17-26.

Garland, G. and Broderick, D. (1992). Changes in the extent of erosion in the Tugela catchment, *South African Geographical Journal*, **74**, 1944-1981.

Garland, G., Hoffman, T. and Todd, S. (2000). Soil degradation. In: Hoffman, T., Todd, S., Ntshona, Z. and Turner, S. (Eds), *Land degradation in South Africa*. Department of Environmental Affairs and Tourism, Pretoria.

Galbraith R.F. (1988). Graphical display of estimates having differing standard errors. *Technometrics*, **30**, 271-281.

Galbraith R.F. (1994). Some applications of radial plots. *Journal of the American Statistical Association,* **89**, 1232-1242.

Galbraith, R.F. and Green, P.F. (1990). Estimating the component ages in a finite mixture. International Journal of Radiation Applications and Instrumentation. Part D. *Nuclear Tracks and Radiation Measurements*, **17**, 197-206.

Galbraith, R.F. and Laslett, G.M. (1993). Statistical models for mixed fission track ages. *Nuclear Tracks and Radiation Measurements*, **21**, 459-470.

Galbraith, R.F., Roberts, R.G., Laslett, G. M., Yoshida, H. and Olley, J.M. (1999). Optical dating of single and multiple grains of quartz from Jinmium rock shelter, northern Australia: Part I, experimental design and statistical models. *Archaeometry*, **41**, 339-364.

Galbraith, R.F., Roberts, R.G. and Yoshida, H. (2005). Error variation in OSL palaeodose estimates from single aliquots of quartz: a factorial experiment. *Radiation Measurements* **39**, 289-307.

Gerrard, J. (1992). *Soil Geomorphology*: *An Integration of Pedology and Geomorphology*. Chapman and Hall, London.

Guérin, G., Mercier, N., Nathan, R., Adamiec, G. and Lefrais, Y. (2012). On the use of the infinite matrix assumption and associated concepts: A critical review. *Radiation Measurements*, **47**, 778-785.

Gillson, L. and Ekblom, A. (2009) Untangling anthropogenic and climatic influence on riverine forest in the Kruger National Park, South Africa. *Vegetation History and Archaeobotany*, **18** (2), 171–185.

Godfrey-Smith, D.I., Huntley, D.J. and Chen, W.H. (1988). Optical dating studies of quartz and feldspar sediment extracts. *Quaternary Science Reviews,* **7**, 373-380.

Godwin, H. (1962). Half-life of radiocarbon. *Nature,* **195**, 984.

Graf, W.L. (1988). *Fluvial Processes in Dryland Rivers*. Blackburn Press, New Jersey.

Grevenitz, P. (2010). The character and genesis of pedogenic calcrete in southern Australia. Unpublished PhD thesis, University of Wollongong Australia.

Grissinger, E.H. (1996). Rill and Gullies Erosion. In: Agassi, M. (Ed.), *Soil Erosion,Conservation, and Rehabilitation.* Marcel Dekker, Inc., New York, NY, U.S.A., 153-167.

Guérin, G., Mercier, N., Nathan, R., Adamiec, C. and Lefrais, Y. (2012). On the use of the infinite matrix assumption and associated concepts: A critical review. *Radiation Measurements*, doi:10.1016/j.radmeas.2012.04.004.

Gunn, R. H., and Richardson, D. P. (1979). The nature and possible origins of soluble salts in deeply weathered landscapes of eastern Australia. *Australian Journal of Soil Research,* **17**, 197-215.

Hamer, J.M.M., Sheldon, N.D., Nichols, G.J. and Collinson, M.E. (2007). Late Oligocene–Early Miocene paleosols of distal fluvial systems, Ebro Basin, Spain. *Palaeogeography, Palaeoclimatology, Palaeoecology* , **247**, 220-235.

Hanson, B. (1993). Reclaiming sodic and saline soils. Drought Tips, **92,** 33.

Hanvey, P.M., Dardis, G.F. and Beckedahl, H.R. (1991). Soil erosion on a sub-tropical coastal dune complex, Transkei, southern Africa. *Geojournal*, **231(1)**, 41-48.

Harvey, A.M. (1984). Aggradation and dissection sequences on Spanish alluvial fans: influence on morphology development. *Catena*, **11**, 289-304.

Harvey, A.M. (1997). The role of alluvial fans in arid zone fluvial systems. In: Thomas, D.S.G. (Ed.), *Arid Zone Geomorphology*, 2nd edition. Wiley, Chichester, 231–259.

Harvey, A.M. (2002) Effective timescales of coupling in fluvial systems. *Geomorphology*, **44** (3-4), 175-201.

Harvey, A.M. (2011). The coupling status of alluvial fans and debris cones: a review and synthesis. *Earth Surface Processes and Landforms*, **37**, 64–76.

Harvey, A.M., Mather A. E. and Stokes, M. (2005). Alluvial fans: geomorphology, sedimentology, dynamics - Introduction: A review of alluvial-fan research. *Geological Society, London, Special Publications,* **251**, 1-7.

Harvey, A.M. and Wells, S.G. (1994). Late Pleistocene and Holcene changes in hillslope sediment supply to alluvial fan systems, California. In: Millington, A.C. and Pye, K. (Eds), *Environmental Change in Drylands: Biogeographical and Geomorphological Perspectives.* New York, Wiley and Sons, 67-84.

Hawley, J.W. and Wilson, W.E. (1965). Quaternary geology of the Winnemuca area, Nevada. *Desert Research Institute Technical Report*, **5**, 66.

Heaton, T.H.E., Talma, A.S. and Vogel, J.C. (1986). Dissolved gas paleotemperatures and ^{18}O variations derived from groundwater near Uitenhage. *Quaternary Research*, **25**, 79-88.

Heede, B.H. (1976). Gully Development and Control: the Status of our Knowledge, USDA Forest Service Research Paper, RM-169, May 1976.

Herron, M.M. (1988). Geochemical classification of terrigenous sands and shales from core or log data. *Journal of Sedimentary Petrology*, **58** (5), 820-829.

Higham, T., Brock, F., Peresani, M., Broglio, A., Wood, R. and Douka, K. (2009). Problems with radiocarbon dating the Middle to Upper Palaeolithic transition in Italy. *Quaternary Science Reviews,* **28**, 1257–1267.

Hillel, D. (1980). *Fundamentals of Soil Physics*. Academic Press Inc., New York.

Hiller, N. and Stavrakis, N. (1984). Permo-Triassic fluvial systems in the southeastern Karoo Basin, South Africa. *Palaeogeography, Palaeoclimatology, Palaeoecology,* **45**, 1-21.

Hodgson, G. and Dixon, J.A. (1988). Measuring economic losses due to sediment pollution: logging versus tourism and fisheries. *Tropical Coastal Area Management*, 5–8.

Holmes, P. and Barker, C.H. (2006). Geological and geomorphological controls on the physical landscape of the Free State. *South African Geographical Journal*, **88** (1), 3-10.

Holmes, P.J., Thomas, D.S.G., Bateman, M.D., Wiggs, G.F.S. and Rabumbulu, M. (2012). Evidence for land degadation from aeolian sediment in the west-central Free State Province, South Africa. *Land Degradation and Development,* **23**, 601-610.

Holmgren, K., Karlen, W., Lauritzen, S-E., Lee-Thorp, J.A., Partridge, T.C., Piketh, S., Repinski, P., Stevenson, C., Svanered, O. and Tyson, P.D. (1999). A 3000-year high-resolution record of palaeoclimate for north-eastern South Africa. *The Holocene*, **9**, 295-309.

Holmgren, K., Lee-Thorp, J.A. Cooper, G.R.J., Lundblad, K., Partridge, T.C., Scott, L., Sithaldeen, R., Talma, A.S. and Tyson, P.D. (2003). Persistent millennial-scale climatic variability over the past 25,000 years in southern Africa. *Quaternary Science Reviews*, **22**, 2311-2326.

Hooke, R.L. (1968). Discussion: model geology: prototype and laboratory streams. *Geological Society of America Bulletin*, **79**, 391-394.

Hua, Q. (2009). Radiocarbon: A chronological tool for the recent past. *Quaternary Geochronology*, **4**, 378–390.

Hulme, M., Doherty, R., Ngara, T., New, M. and Lister, D. (2001). African climate change: 1900–2100. *Climate Research, **17**, 145–168.*

Huntley, B., Midgley, G.F., Barnard, P., Valdes, P.J. (2014). Sub-orbital climatic variability and centres of biological diversity in the Cape region of southern Africa. *Journal of Biogeography*, **41**, 1338–1351.

Huntley, D.J., Godfrey-Smith, D.I. and Thewalt, M.L.W. (1985). Optical dating of sediments. *Nature*, **313**, 105-107.

Imeson, A.C. and Kwaad, F.J.P.M. (1980). Gully types and gully prediction, *Geografisch Tijdschrift*, **14 (5)**, 430-441.

IUSS Working Group WRB., 2007. World Reference Base for Soil Resources 2006, first update 2007, World Soil Resources Reports No.103. FAO, Rome.

Jacobs, Z. (2004). Development of luminescence techniques for dating Middle Stone Age sites in South Africa. Unpublished PhD thesis, University of Wales, Aberystwyth.

Jain, M., Murray, A.S. and Bøtter-Jensen, L. (2004). Optically stimulated luminescence dating: How significant is incomplete light exposure in fluvial environments. *Quaternaire*, **15**, 143-157.

Johnson, R.F. (1988). *A history of climate and marine productivity from sediment off the west coast of southern Africa*. Final Report, National Programme for Weather, Climate and Atmosphere Research. FRD, Pretoria, 6 pp.

Johnson, M.R., van Vuuren, C.J., Visser, J.N.J., Cole, D.I., de V. Wickens, H., Christie, A.D.M., Roberts, D.L. and Brandl, G. (2006). Sedimentary rocks of the Karoo Supergroup. In: Johnson, M.R., Anhaeusser, C.R. and Thomas, R.J. (Eds.), *The Geology of South Africa*. The Geological Society of South Africa, Council for Geosciences, Pretoria, 461-500.

Jones, J.A.A. (2010). Soil piping and catchment response. *Hydrological Processes,* **24**, 1548–1566.

Kakembo, V. (1997). A reconstruction of the history of land degradation in relation to land use change and land tenure in Peddie district, former Ciskei. MSc thesis (unpubl.), Rhodes University.

Kakembo, V., Xanga, W.W. and Rowntree, K. (2009). Topographic thresholds in gully development on the hillslopes of communal areas in Ngqushwa Local Municipality, Eastern Cape, South Africa. *Geomorphology*, **110**, 188 – 194.

Keay-Bright, J. and Boardman, J. (2006). Changes in the distribution of degraded land over time in the central Karoo, South Africa. *Catena,* **67**, 1-14.

Keay-Bright, J. and Boardman, J. (2009). Evidence from field-based studies of rates of soil erosion on degraded land in central Karoo, South Africa. *Geomorphology*, **103**, 455-465.

Keefer, D.K., Moseley, M.E. and deFrance, S.E. (2003). A 38 000-year record of floods and debris flows in the Ilo region of southern Peru and its relation to El Niño events and great earthquakes. *Palaeogeography, Palaeoclimatology, Palaeoecology,* **194** (1-3), 41-77.

Khomo, L. M. and Rogers, K. H. (2005). Proposed mechanism of the origin of sodic patches in the Kruger National Park, South Africa. *African Journal of Ecology*, **43**, 29-34.

Kim, J.C. (2009). Geochronology and geochemical characteristics of sediments at the Jeongokri archaeological site, Korea. Unpublished PhD Dissertation, Seoul National University, Korea

Kim, S.B. (1995). Discussion: alluvial fans and their natural distinction from rivers based on morphology, hydraulic processes, sedimentary processes, and facies assemblages. *Journal of Sedimentary Research*, *Section A, Sedimentary Petrology and Processes*, **65**, 706-708.

King, L.C. (1953). Canons of Landscape Evolution. *Geological Society of America Bulletin*, **64** (7), 721-752.

King, L.C. (1967). *South African Scenery: A Textbook of Geomorphology*. (3rd edition). Oliver and Boyd, Edinburgh and London.

King, L.C. (1982). *The Natal Monocline: explaining the origin and scenery of Natal, South Africa* (2nd edition). University of Natal Press, Pietermaritzburg, 134pp.

Kirkby, M.J. and Bracken, L.J. (2009). Gully processes and gully dynamics. *Earth Surface Processes and Landforms*, **34**, 1841-1851.

Klein, R.G., Cruz-Uribe, K., Beaumont, P.B. (1991). Environmental, ecological, and paleoanthropological implications of the Late Pleistocene mammalian fauna from Equus Cave, northern Cape Province, South Africa. *Quaternary Research*, **36**, 94-119.

Knighton, A.D. (1989). River adjustment to changes in sediment load: the effects of tin mining on the Ringarooma River, Tasmania,1875– 1984. *Earth Surface Processes and Landforms*, **14**, 333– 359.

Kuhle, A.J. and Smith, G.A. (2001). Alluvial-slope deposition of the Skull Ridge Member of the Tesuque Formation, Española Basin, New Mexico. *New Mexico Geology,* **23** (2), 30-37.

Kumari,K, and Kumar, B. (2009). Basics of Radiocarbon. *Manthan International Journa*l, **9**, 18-20.

Laker, M.C. (2004). Advances in soil erosion, soil conservation, land suitability evaluation and land use planning research in South Africa, 1978-2003. *South African Journal of Plant and Soil,* **21**, 345-368.

Lang, A. (2003). Phases of soil erosion-derived colluviation in the loess hills of South Germany. *Catena*, **51**, 209-221.

Lang, A. (2013). Luminescence, Colluvial Sediments. *Encyclopeadia of Scientific Dating Methods*, DOI: 10.1007/978-94-007-6326.5_4-2.

Leeder, M.R. (1978). A quantitative stratigraphic model for alluvium, with special refernce to channel deposit density and interconnectedness. In: Miall, A.D., *Fluvial Sedimentology*, *Can. Soc. Petrol. Geol. Mem*., **5**, 587-596.

Lee-Thorp, J.A., Beaumont. PB. (1995). Vegetation and seasonality shift during the late Quaternary deduced from $^{13}C/^{12}C$ ratios of grazers at Equus Cave, South Africa. *Quaternary Research*, **43**, 426-432.

Leigh, D.S. and Webb, P.A. (2006). Holocene erosion, sedimentation, and stratigraphy at Raven Fork, Southern Blue Ridge Mountains, USA. *Geomorphology*, **78**, 161–177.

Leopold, L.B. and Miller, J.P. (1956). Ephemeral streams - Hydraulic factors and their relation to the drainage net. U.S. Geological Survey Professional Paper, 282A.

Leopold, L.B., Wolman, M.G. and Miller, J. (1964). *Fluvial Processes in Geomorphology*. W.H. Freeman and Company, San Francisco.

LeRoux, J. (1972). Quantitative clay mineralogical analysis of highly weathered Natal soils. *Proceedings of the South Africa Sugar Technologists' Association*. June 1972, 201-203.

Levy, G.J. (1988). The effects of clay mineralogy and exchangeable cations on some of the hydraulic properties of soils. D.Sc.(Agric.) thesis, University of Pretoria.

Li, G., Klik, A., and Faqi, W. (2004). Gully erosion features and its causes of formation on the (Yuan) land in the Loess Plateau, China. In: Li, Y., Poesen, J., Valentin, C. (Eds.), *Gully Erosion Under Global Change*. Sichuan Science and Technology Press, Chengdu, China, pp. 131– 142.

Libby, W.F. (1955). *Radiocarbon Dating* (2nd edition). University of Chicago Press, Chicago.

Liggitt, B. (1988). An investigation into soil erosion in the Mfolozi catchment. MSc thesis (unpubl). University of Natal, Pietermaritzburg.

Lucas, S.J. and Hancox, P.J. (2001). Tetrapod-based correlation of the non-marine Upper Triassic of southern Africa. *Albertiana*, **25**, 5-9.

Lurie, J. (1994). *South African Geology.* Lupon Publishing, Johannesburg.

Lyons, R., Tooth, S. and Duller, G.A.T. (2013). Chronology and controls of donga (gully) formation in the upper Blood River catchment, KwaZulu-Natal, South Africa: Evidence for a climatic driver of erosion. *The Holocene*, **23** (12), 1875-1887.

Mack, G.H. and Rasmussen, K.A. (1984). Alluvial-fan sedimentation of the Cutler Formation (Permo-Pennsylvanian) near Gateway, Colorado. *Geological Society of America Bulletin*, **95** (1), 109-116.

Manassero, M.L. (1997). Sedimentology of the Upper Cretaceous Red Beds of Angostura Colorada Formation in the western sector of the North Patagonian Massif, Argentina. *Journal of South American Earth Sciences*, **10:1**, 81-90.

Mann, M.E. (2002). Little Ice Age. *Encyclopedia of Global Environmental Change*, **1**, 504-509.

Martin, I.P. and Chesworth, W. (Eds) (1992). *Weathering, Soils & Paleosols*. Elsevier Science Publishers, Amsterdam, Netherlands, 618pp.

Matthews, J.A. and Briffa, K.R. (2005). The 'Little Ice Age': Re-evaluation of an evolving concept. *Geografiska Annaler*, **87**, 17-37.

Mayewski, P.A., Rohling, E.E., Stager, J.C., Karlen, W., Maasch, K.A., Meeker, L.D., Meyerson, E.A., Gasse, F., van Kreveld, S., Holmgren, K., Lee-Thorp, J., Rosqvist, G., Rack, F., Staubwasser, R.R. Steig, E.J. (2004). Holocene climate variability. *Quaternary Research*, **62**, 243-255.

McBride, M. B. (1994). *Environmental Chemistry of Soils*. Oxford University Press, Oxford.

McCarthy, T.S. and Cadle, A.B. (1995). Discussion: Alluvial fans and their natural distinction from rivers based on morphology, hydraulic processes, sedimentary processes, and facies assemblages. *Journal of Sedimentary Research*, **A65(3)**, 581-583.

McCarthy, T.S., Ellery, W.N. and Stanistreet, I.G. (1992). Avulsion mechanisms on the Okavango Fan, Botswana: the control of a fluvial system by vegetation. *Sedimentology*, **39**, 779-795.

McCarthy, T.S., Stanistreet, I.G., Cairncross, B. (1991). The sedimentary dynamics of active fluvial channels on the Okavango Fan, Botswana. *Sedimentology*, **38**, 471–487.

Meadows, M.E. (2003). Soil erosion in the Swartland, Western Cape Province, South Africa: implications of past and present policy and practice. *Environmental Science and Policy*, **6**, 17-28.

Medinski, T.V. (2007). Soil Chemical and physical properties and their influence on the plant species richness of arid South-West Africa. MSc thesis (unpubl). University of Stellenbosch.

Mejdahl, V. (1979) Thermoluminescence dating: beta-dose attenuation in quartz. *Archaeometry*, **21** (1), 61–72.

Middleton, N. And Thomas, D. (Eds) World Atlas of Desertification (2nd edition). UNEP, Edward Arnolds, London.

Mills, H.H. and Allison, J.B. (1995). Weathering rinds and the evolution of piedmont slopes in the southern Blue Ridge Mountains. *Journal of Geology*, **103**, 379-394.

Mills, A.J., Fey, M.V., Gröngröft, A., Petersen, A. and Medinski, T.V. (2006). Unravelling the effects of soil properties on water infiltration: segmented quantile regression on a large data set from arid southwest Africa. *Australian Journal of Soil Research*, **44**, 783–797.

Moeletsi, M.E., Walker, S. and Landman, W.A. (2011). ENSO and implications on rainfall characteristics with reference to maize production in the Free State Province of South Africa. *Physics and Chemistry of the Earth, Parts A/B/C*, **36**, 715-726.

Montgomery, D. (2007). Soil erosion and agricultural sustainability. *Proceedings of the National Academy of Sciences*, **104**, 13268-13272.

Moore, D.M. and Reynolds, R.C. (1997). *X-Ray Diffraction and the Identification and Analysis of Clay Minerals.* Oxford University Press, Oxford, New York.

Moreno, C. and Romero-Segura M.J. (1997). The development of small-scale sandy alluvial fans at the base of a modern coastal cliff: process, observations and implications. *Geomorphology*, **18**, 101-118.

Morgan, R.P.C. (2005). *Soil Erosion and Conservation* (3rd edition). Blackwell, UK.

Morrison, S.J. and Parry, W.T. (1986). Dioctahedral corrensite from Permian red beds, Lisbon Valley, Utah. *Clays and Clay Minerals*, **34**, 613-624.

Murray, A.S. and Olley, J.M. (2002). Precision and accuracy in the optically stimulated luminescence dating of sedimentary quartz: a status review. *Geochronometria,* **21**, 1-16.

Murray A.S., Olley J.M. and Caithcheon G.G. (1995). Measurement of equivalent doses in quartz from contemporary water-lain sediments using optically stimulated luminescence. *Quaternary Science Reviews (Quaternary Geochronology,)* **14**, 365-371.

Murray, A.S. and Wintle, A.G. (2000). Luminescence dating of quartz using an improved single-aliquot regenerative-dose protocol. *Radiation Measurements*, **32**, 57-73.

Nayak, P.S. and Singh, B.K. (2007). Instrumental characterization of clay by XRF, XRD and FITR. *Bulletin of Material Science*, **30 (3)**, 235-238.

Nelson, P.N., Baldock, J.A. and Oades, J.M. (1998). Changes in dispersible clay content, organic carbon content, and electrolyte composition following incubation of sodic soil. *Australian Journal of Soil Research*, **36**, 883-897.

Nemec, W. and Postma, G. (1993). Quaternary fans in southwestern Crete: Sedimentation processes and geomorphic evolution. In: Marzo, M. and Puigdefábregas, C. (Eds.), *Alluvial Sedimentation*, *Special Publication of the International Association of Sedimentologists*, **17**, 235-276.

Nesbitt, H.W., Markovics, G. and Price, R.C. (1980). Chemical processes affecting alkalis and alkaline earths during continental weathering. *Geochimica et Cosmochimica Acta*, **44**, 1659–1666.

Nesbitt, H.W. and Young, G.M. (1982). Early Proterozoic climates and plate motions inferred from major element chemistry of lutites. *Nature*, **299**, 715–717.

Nesbitt, H.W. and Young, G.M. (1996). Petrogenesis of sediments in the absence of chemical weathering: effects of abrasion and sorting on bulk composition and mineralogy. *Sedimentology*, **43**, 341–358.

Nesse, W.D. (2000). *Introduction to Mineralogy*. Oxford University Press, New York.

Nicholas, A.P and Quine, T.A. (2007). Crossing the divide: Representation of channels and processes in reduced-complexity river models at reach and landscape scales. *Geomorphology*, **3-4**, 318-339.

Nichols, G., (2009). *Sedimentology and Stratigraphy* (2nd edition). Wiley-Blackwell. United Kingdom, 419 pp.

Nordström, K. (1988). Gully erosion in the Lesotho lowlands – A geomorphological study of the interactions between intrinsic and extrinsic variables. Department of Physical Geography, Uppsala University, UNGI Rapport No. 69. ISBN 91-506-0707-3.

Oades, J.M. and Waters, A.G. (1991). Aggregate hierarchy in soils. *Australian Journal of Soil Research*, **29**, 815-828.

Ollerhead, J., Huntley, D.J. and Berger, G.W. (1994). Luminescence dating of sediments from Buctouche Spit, New Brunswick. *Canadian Journal of Earth Science*s, **31**, 523-531.

Olley, J.M., Caitcheon, G. and Murray, A. (1998). The distribution of apparent dose as determined by optically stimulated luminescence in small aliquots of fluvial quartz: implications for dating young sediments. *Quaternary Geochronology,* **17**, 1033-1040.

Olley, J.M., Caitcheon, G. and Roberts, R. (1999). The origin of dose distributions in fluvial sediments, and the prospect of dating single grains of quartz from fluvial deposits using OSL. *Radiation Measurements*. **30**, 207–217.

Olley, J.M., Murray, A. and Roberts, R.G. (1996). The effects of disequilibrium in the Uranium and Thorium decay chains on burial dose rates in fluvial sediments. *Quaternary Science Reviews (Quaternary Geochronology)*, **15**, 751-760.

Olley, J. M., Pietsch, T. and Roberts, R. G. (2004). Optical dating of Holocene sediments from a variety of geomorphic settings using single grains of quartz. *Geomorphology*, **60**, 337-358.

Oostwoud-Wijdenes, D.J.O., Poesen, J., Vandekerckhove, L., Nachtergaele, J. and De Baerdemaeker, J. (1999). Gully-head morphology and implications for gully development on abandoned fields in a semi-arid environment, Sierra De Gata, Southeast Spain. *Earth Surface Processes and Landforms*, **24**, 585-603.

Page, K., Frazier, P., Pietsch, T. and Dehaan, R. (2007). Channel change following European settlement: Gilmore Creek, south-eastern Australia. *Earth Surface Processes and Landforms*, **32**, 1398-1411.

Parker, G. G., (1963). Piping, A geomorphic agent in landform development of the drylands. In: *Land Erosion, Precipitation, Hydrometry, Soil Moisture* (Proceedings of the IUGG General Assembly of Berkeley), pp. 103-113: IAHS Publ. no. 65.

Parker, G. (1999). Progress in the modeling of alluvial fans. *Journal of Hydraulic Research*, **7** (6), 805-825.

Partridge, T.C. (1998). Of diamonds, dinosaurs, and diastrophism: 150 million years of landscape evolution in southern Africa. South African Journal of Geology, **101**, 167-184.

Partridge, T.C. and Maud, R.R. (1987). Geomorphic evolution of southern Africa since the Mesozoic. *South African Journal of Geology*, **90**, 179-208.

Partridge, T.C. and Maud, R.R. (2000). Macroscale geomorphic evolution of southern Africa. In: Partridge, T.C. and Maud, R.R. *The Cenozoic of Southern Africa*. Oxford University Press, New York, 3-18.

Partridge, T.C., Avery, D.M., Botha, G.A., Brink, J.S., Deacon, J., Herbert, R.S., Maud, R.R., Scholtz, A., Scott, L., Talma, A.S. and Vogel, J.C. (1990). Late Pleistocene and Holocene climatic change in southern Africa, *South African Journal of Science*, **86**, 302-306.

Partridge, T.C., Kerr, S.J., Metcalfe, S.E., Scott, L., Vogel, J.C. (1993). The Pretoria Saltpan: A 200,000 year South African lacustrine sequence. *Palaeogeography, Palaeoclimatology, Palaeoecology*, **101**, 317-337.

Partridge, T.C., Demenocal, P.B., Lorentz, S.A., Paiker, M.J., Vogel, J.C. (1997). Orbital forcing of climate over South Africa: A 200,000-year rainfall record from Pretoria Saltpan. *Quaternary Science Reviews*, **16**, 1125-1133.

Paton, T.R., Humphreys, G.S., Mitchell, P.S. (1995). *Soils: A New Global View*. UCL Press, London.

Pearson, F.J., Arcos, D., Bath, A., Boisson, J.-Y., Fernández, A.M., Gäbler, H.-E., Gaucher, E., Gautschi, A., Griffault, L., Hernán, P. and Waber, H.N. (2003). Mont Terri Project – Geochemistry of Water in the Opalinus Clay Formation at the Mont Terri Rock Laboratory: Bern, Switzerland, Federal Office for Water and Geology (FOWG). Geology Series 5.

Pederson, J. Pazzaglia, F and Smith, G. (2000). Ancient hillslope deposits: Missing links in the study of climate controls on sedimentation. *Geology*, **28(1)**, 27-30.

Pendea, I.F., Gray, J.T., Ghaleb, B., Tantau, I., Badarau, A.S. and Nicorici, C. (2008). Episodic build-up of alluvial fan deposits during the Weichselian Pleniglacial in the western Transylvanian Basin, Romania and their palaeoenvironmental significance. *Quaternary International,* **198**, 98-112. doi:10.1016/j.quant.2008.05.002.

Pettijohn, F.J., Potter, P.E and Siever, R. (1972). *Sand and Sandstone*. Springer-Verlag, New York, 618p.

Pienaar, M., Woodborne, S. and Wadley, L. (2008). Optically stimulated luminescence dating at Rose Cottage Cave. *South African Journal of Science*, **104**, 65-69.

Pitty, A. F. (1979). *Geography and soil properties*. Methuen & CO LTD, Britain, 287pp

Poesen, J. and Govers, G. (1990). Gully Erosion in the Loam Belt of Belgium: Topology and Control Measures. In: Boardman, J., Foster, I.D.I. and Dearing, J.A. (Eds), Soil *Erosion on Agricultural Land.* John Wiley and Sons, Chichester.

Poesen, J., Nachergaele, G., Verstraeten, G., Valentin, C. (2003). Gully erosion and environmental change: importance and research needs. *Catena*, **50**, 91-133.

Porat, N. (2006). Use of Magnetic Separation for Purifying Quartz for Luminescence Dating. *Ancient TL*, **24**, 33–36.

Powers, J.S. and Schlesinger, W.H. (2002). Relationships among soil carbon distributions and biophysical factors at nested spatial scales in rain forests of northeastern Costa Rica. *Geoderma* **109**, 165– 190.

Prescott, J.R. and Hutton, J.T. (1994). Cosmic ray contributions to dose rates for luminescence and ESR dating: large depths and long-term time variations. *Radiation Measurements*, **23**, 497-500.

Prescott J.R. and Hutton J.T. (1995). Environmental dose rates and radioactive disequilibrium from some Australian luminescence dating sites. *Quaternary Science Reviews (Quaternary Geochronology)* **14**, 439-448.

Prescott J.R. and Stephan L.G. (1992). The contribution of cosmic radiation to the environmental dose for thermoluminescent dating. Latitude, altitude and depth dependences. *PACT,* **6**, 17-25.

Preusser, F., Degering, D., Fuchs, M., Hilgers, A., Kadereit, A., Klasen, N., Krbetschek, M. R., Richter, D. and Spencer, J. Q. G. (2008). Luminescence dating: basics, methods and applications. *Quaternary Science*, **57**, 95-149.

Price-Williams, D. And Watson, A. (1982). New observations on the prehistory and palaeoclimate of the Late Pleistocene in southern Africa. *World Archaeology* , **13**, 372–381.

Price-Williams, D., Watson, A. And Goudie, A.S. (1982). Quaternary colluvial stratigraphy, archaeological sequences and palaeoenvironment in Swaziland, southern Africa. *Geographical Journal,* **148**, 50–67.

Prosser, I.P. and Slade, C.J. (1994). Gully formation and the role of valley-floor vegetation, southeastern Australia. *Geology*, **22**, 1127–1130.

Pusch, R. and Karnland, O. (1996). Physico/chemical stability of smectite clays. *Engineering Geology*, **41**, 73-85.

Rachocki, A.H. (1981). *Alluvial Fans*. J. Wiley and Sons, New York, 161pp.

Rahman, W.A. and Rowell, D.L. (1979). The influence of magnesium in saline and sodic soils: A specific effect or problem of cation exchange? *Journal of Soil Science*, **30**, 535-546.

Raigemborn, M.S., Gómez-Peral, L.E., Krause, J.M. and Matheos, S.D. (2014). Controls on clay minerals assemblages in an early paleogene nonmarine succession: Implications for the volcanic and paleoclimatic record of extra-andean Patagonia, Argentina. *Journal of South American Earth Sciences,* **52**, 1-23.

Ramsey, B.C. (2008). Radiocarbon dating: revolutions in understanding. *Archaeometry*, **50,** 249–275.

Reimer, P.J., Baillie, M.G.L., Bard, E., Bayliss, A., Beck, J.W., Bertrand, C.J.H., Blackwell, P.G., Buck, C.E., Burr, G.S., Cutler, K.B., Damon, P.E., Edwards, R.L., Fairbanks, R.G., Friedrich, M., Guilderson, T.P., Hogg, A.G., Hughen, K.A., Kromer, B., McCormac, F.G., Manning, S., Bronk Ramsey, C., Reimer, R.W., Remmele, S., Southon, J.R., Stuiver, M., Talamo, S., Taylor, F.W., van der Plicht, J. and Weyhenmeyer, C.E. (2004). IntCal04 terrestrial radiocarbon age calibration, 0–26 cal kyr BP. *Radiocarbon*, **46**, 1029–1058.

Reimer, P.J., Bard, E. Bayliss, A., Beck, J.W., Blackwell, P.G., Ramsey, C.B., Buck, C.E., Cheng, H., Edwards, R.L., Friedrich, M. Grootes, P.M., Guilderson, T.P., Haflidason, H., Hajdas, I., Hatté, C., Heaton, T.J., Hoffmann, D.L., Hogg, A.G., Hughen, K.A., Kaiser, K.F., Kromer, B., Manning, S.W., Niu, M., Reimer, R.W., Richards, D.A., Scott, E.M., Southon, R., Staff, R.A., Turney, C.S.M. and van der Plicht, J. (2013). Intcal13 and Marine13 radiocarbon age calibration curves 0–50,000 years cal BP. *Radiocarbon*, **55**, 1869-1887.

Reneau, S.L., Dietrich, W.E., Donahue, D.J., Jull, A.J.T. and Rubin, M. (1990). Late Quaternary history of colluvial deposition and erosion in hollows, central California Coast Ranges. *Geological Society of America Bulletin*, **102**, 969-982.

Reneau, S.L., Dietrich, W.E., Rubin, M., Donahue, D.J. and Jull. A.J.T.1989). Analysis of hillslope erosion rates using dated colluvial deposits. *Journal of Geology*, **97** (1), 45-63.

Rengasamy, P. and Churchman, G.J. (1999). Cation exchange capacity, exchangeable cations and sodicity. In: Peverill, K. I., Sparrow, L. A. and Reuter, D. J. *Soil Analysis: An Interpretational Manual*. CISRO Publishing, Australia, 147-157.

Rengasamy, P. and Olssen, K.A. (1993). Irrigation and Sodicity. *Australian Journal of Soil Research*, **31**, 821-837.

Retallack, G.J. (2001). *Soils of the Past: A Introduction to Palaeopedology (2nd edition)*. Blackwell Science, Oxford.

Rienks, S.M., Botha, G.A. and Hughes, J.C. (2000). Some physical and chemical properties of sediments exposed in a gully donga in northern KwaZulu-Natal, South Africa and their relationship to the erodibility of the colluvial layers. *Catena*, **39**, 11–31.

Roberts, R. G., Galbraith, R. F., Yoshida, H., Laslett, G. M. and Olley, J. M. (2000). Distinguishing dose populations in sediment mixtures: a test of single-grain optical dating procedures using mixtures of laboratory-dosed quartz. *Radiation Measurements,* **32,** 459-465.

Rodnight, H. (2006). Developing a Luminescence Chronology for Late Quaternary Fluvial Change in South African Floodplain Wetlands. Ph.D. dissertation (unpubl). University of Aberystwyth, Wales.

Rodnight, H., Duller, G.A.T., Wintle, A.G. and Tooth, S. (2006). Assessing the reproducibility and accuracy of optical dating of fluvial deposits. *Quaternary Geochronology*, **1** (2), 109–120.

Roering, J.J., Kirchner, J.W. and Dietrich, W.E. (2001). Hillslope evolution by non-linear, slope-dependent transport: Steady state morphology and equilibrium adjustment timescales. *Journal of Geophysical Research*, **106**(B8), 16499-16513.

Rollinson, H.R. (1993). *Using Geochemical Data: Evaluation, Presentation, Interpretation*. Longman, England.

Rooyani, F. (1985). A note on soil properties influencing piping at the contact zone between albic and argillic horizons of certain duplex soils (Aqualfs) in Lesotho, southern Africa. *Soil Science*, **139**, 517-522.

Rossinsky Jr, V. and Swart, P.K., 1993. Influence of climate on the isotopic composition of calcretes. In: Swart, P.K., Lohmann, K.C., McKenzie, J. and Savin, S. (Eds.), Climate Change in Continental Isotopic Records, *American Geophysics Union Geophysics Monograph,* **78**, 67–75.

Rowe, P.J. and Maher, B.A. (2000). 'Cold' stage formation of calcrete nodules in the Chinese Loess Plateau: evidence from U-series dating and stable isotope analysis. *Palaeogeography, Palaeoclimatology, Palaeoecology*, **157**, 109–125.

Rowell, D. L. (1994). *Soil Science: Methods and Applications*. Longman Group Limited, United Kingdom, 350pp.

Rowntree, K.M., 1988: Equilibrium concepts, vegetation change and soil erosion in semi-arid areas: some considerations for the Karoo. In Dardis, G.F. and. Moon, B.P. (Eds.), *Geomorphological Studies in Southern Africa,* Balkema, Rotterdam, Netherlands, 175-185.

Rowntree, K.M. (1991). Morphological characteristics of gully networks and their relationships to host materials, Baringo district, Kenya. *Geojournal*, **23**(1), 19-27.

Rustomji, P. and Pietsch, T. (2007). Alluvial sedimentation rates from southeastern Australia indicate post-European settlement landscape recovery. *Geomorphology*, **90**, 73-90.

Rydgren, B. (1990). A geomorphological approach to soil erosion studies in Lesotho – case studies of soil erosion and land use in the southern Lesotho lowlands. In: Strömquist, L. (Ed.). *Monitoring soil loss at different observation levels: Case studies of soil erosion in the Lesotho lowlands*. Uppsala University, Department of Physical Geography, UNGI Rapport nr. 74. ISBN 91-506-0791-X, 39-89.

Saito, K. and Oguchi, T. (2005). Slope of alluvial fans in humid regions of Japan, Taiwan and the Philippines. *Geomorphology*, **70**, 147-162.

Saito, K., Yamada, M., Hashimoto, A. and Oguchi, T. (2003). Slope of alluvial fans in Death Valley, California. *Occasional Paper of Department of Geography*, Saitama University, **23**, 29-40.

Samadi, M., Germishuyse, T. and van der Walt, T. (2005). *Understanding South African Soils*. ARC-Institute for Soil, Climate and Water, Pretoria.

Sass, O. and Krautblatter, M. (2007). Debris flow-dominated and rockfall-dominated talus slopes: Genetic models derived from GPR measurements. *Geomorphology*, **86**, 176-192.

Schaetzl, R.J. and Anderson, S. (2005). *Soil: Genesis and Geomorphology*. Cambridge University Press, UK.

Scott, L. (1996) Palynology of hyrax middens: 2000 years of palaeo-environmental history in Namibia. *Quaternary International*, **33**, 73–79.

Scott, L. (1999). Vegetation history and climate in the Savanna biome South Africa since 190,000ka: A comparison of pollen data from the Tswaing Crater (the Pretoria Saltpan) and Wonderkrater. *Quaternary International*, **57/58**, 215-223.

Scott, L. (2000). Pollen. In: Partridge, T.C. and Maud, R.R. (Eds), *The Cenozoic of Southern Africa*, Oxford University Press, Oxford.

Scott, L., Holmgren, K., Talma, A.S., Woodborne, S. and Vogel, J.C. (2003). An interpretation of the Wonderkrater spring sediments and vegetation change in the savanna biome, Limpopo Province, South Africa, *South African Journal of Science*, **99**, 484-488.

Scott, L., Neumann, F.H., Brook, G.A., Bousman, C.B., Norström, E. and Metwally, A.A. (2012). Terrestrial fossil-pollen evidence of climate change duing the last 26 thousand years in southern Africa. *Quaternary Science Reviews*, **32**, 100-118.

Scott, L. and Thackeray, J.F. (1987). Multivariate analysis of late Pleistocene and Holocene pollen spectra from Wonderkrater, Transvaal, South Africa. *South African Journal of Science,* **83**, 93-98.

Seelig, B. D. (2000). Salinity and Sodicity in North Dakota Soils. http://www.ag.ndsu.edu/pubs/plantsci/soilfert/eb57-1.htm. (07/04/2008).

Shakesby, R.A. and Whitlow, R. (1991). Perspectives on prehistoric and recent gullying in central Zimbabwe. *GeoJournal,* **23**, 49-58.

Shichi, T. and Takagi, K. (2000). Clay minerals as photochemical reaction fields. *Journal of Photochemistry and Photobiology C: Photochemical Reviews*, **1**, 113-130.

Showers, K.B. (1989). Soil erosion in the kingdom of Lesotho: origins and colonial response: 1830s–1950s. *Journal of Southern African Studies*, **15**, 263–286.

Showers, K.B. (2005). *Imperial Gullies*. Ohio University Press. Athens, Ohio.

Šilhán, K. (2014). Chronology of processes in high-gradient channels of medium-high mountains and their influence on the properties of alluvial fans. *Geomorphology*, **206**, 288–298.

Singer, A. (1984). The palaeoclimatic interpretation of clay minerals in sediments - A review. *Earth Science Reviews*, **21**, 251-293.

Smart, R.P., Holden, J., Dinsmore, K.J., Baird, A.J., Billett, M.F., Chapman, P.J. and Grayson, R. (2013). The dynamics of natural pipe hydrological behaviour in blanket peat. *Hydrological Processes*, **27**, 1523–1534.

Smith, G. A. (2000). Recognition and significance of streamflow-dominated piedmont facies in extensional basins. *Basin Research*, **12**, 399-411.

Smith, R and Kitching, J. (1997). Sedimentology and vertebrate taphonomy of the *Tritylodon* Acme Zone: a reworked palaeosol in the Lower Jurassic Elliot Formation, Karoo Supergroup, South Africa. *Palaeogeography, Palaeoclimatology, Palaeoecology*, **131** (1-2), 29-50.

Soil Survey Staff. (1999) *Soil Taxonomy: A basic system of soil classification for making and interpreting soil surveys* (2nd edition). United States Department of Agriculture, Natural Resources Conservation Service.

Soleimani, B. (2009). Palaeoclimate reconstruction during Pabdeh, Gurpi, Kazhdumi and Gadvan Formations (Cretaceous – Tertiary) based on clay mineral distribution. *International Journal on Environmental Science and Engineering*, **1:2**, 59-63.

Sparks, D. L. (1995). *Environmental Soil Chemistry*. Academic Press Inc., San Diego, 267pp

Spooner, N. (1994). The anomalous fading of infrared-stimulated luminescence from feldspars. *Radiation Measurements*, **23**, 625-632.

Sonneveld, M.P.W., Everson, T.M. and Veldkamp, A. (2005). Multi-scale analysis of soil erosion dynamics i Kwa-Zulu Natal, South Africa. *Land Degradation and Development*, **16**, 287-301.

Stanistreet, I.J. and McCarthy,T.S.(1993). The Okavango Fan and the classification of subaerial fan systems. *Sedimentary Geology*, **85**, 115-133.

Stern, R. (1990). Effects of soil properties and chemical ameliorants on seal formation, runoff and erosion. D.Sc.(Agric.) thesis, University of Pretoria.

Stocking, M.A. (1978). Interpretation of stone lines, *South African. Geographical Journal*, **60**, 121-134.

Stokes, S. (1992). Optical dating of young (modern) sediments using quartz: results from a selection of depositional environments. *Quaternary Science Reviews* **11**, 153-159.

Stokes, S., Thomas, D.S.G. and Washington, R. (1997). Multiple episodes of aridity in southern Africa since the last interglacial period. *Nature*, **388**, 154-158.

St-Onge, G., Stoner, J.S. and Hillaire-Marcel, C. (2003). Holocene paleomagnetic records from the St. Lawrence Estuary, eastern Canada: centennial-to millennial-scale geomagnetic modulation of cosmogenic isotopes. *Earth and Planetary Science Letters,* **209**, 113–130.

Stoops, G., Marcelino, V. A. and Mees, F. (2010). *Interpretation of Micromorphological Features of Soils and Regolith.* Elsevier, Amsterdam.

Stoops, G., van Ranst, E. and Verbeek, K. (2001). Oedology of soils within the spray zone of the Victoria Falls (Zimbabwe). *Catena*, **46**, 63-83.

Stuiver, M. and Polach, H.A. (1977). Discussion: reporting of ^{14}C data. *Radiocarbon* **19**, 355–363.

Stute, M. and Talma, A.S. (1997) Glacial temperatures and moisture transport regimes reconstructed from noble gas and δ18O, Stampriet aquifer, Namibia. Isotope Techniques in the Study of Past and Current Environmental Changes in the Hydrosphere and the Atmosphere. IAEA Vienna Symposium, 1997, Vienna, 307-328.

Stuut, J.-B.W. et al. (2002) A 300 kyr record of aridity and wind strength in southwestern Africa: inferences from grain-size distributions of sediments on Walvis Ridge, SE Atlantic. *Marine Geology*, **180** (1-4), 221-233.

Summerfield, M. A. (1991). Sub-aerial denudation of passive margins: Regional elevation versus local relief models, *Earth Planetary Science Letters*, **102**, 460–469.

Sumner, M.E. (1993). Sodic soils - New perspectives. *Australian Journal of Soil Research***, 31** (6) 683 – 750.

Sundqvist, H.S., Holmgren, K., Fohlmeister, J., Zhang, Q., Bar-Matthews, M., Spotl, C. and Kornich, H. (2013). Evidence of a large cooling between 1690 and 1740 AD in southern Africa, *Scientific Reports*, **3**, 1767; DOI:10.1038/srep01767.

Talma, A.S. and Vogel, J.C. (1992). Late Quaternary palaeotemperatures derived from a speleotherm from Cango Caves, Cape Province, South Africa, *Quaternary Research*, **37**, 203-213.

Taylor, R.E. (1987). *Radiocarbon Dating: An Archaeological Perspective*. Academic Press, London, 212 pp.

Thackeray, J.F. (1990) Temperature indices from Late Quaternary sequences in South Africa: comparisons with the Vostok core. *South African Geographical Journal*, **72**, 47–49.

Thomas, M.F. (2008) Understanding the impacts of Late Quaternary climate change in tropical and sub-tropical regions. *Geomorphology*, **101**, 146-158.

Thomas, M.F., Thorp, M.B. (1980). Some aspects of the geomorphological interpretation of Quaternary alluvial sediments in Sierra Leone. Z. *Geomorphology*, Suppl. **36**, 140–161.

Thomsen, K. J., Murray, A. S. and Bøtter-Jensen, L. (2005). Sources of variability in OSL dose measurements using single grains of quartz. *Radiation Measurements,* **39,** 47-61.

Thomsen, K.J., Murray, A.S., Bøtter-Jensen, L. And Kinaham, J. (2007). Determination of burial dose in incompletely bleached fluvial samples using single grains of quartz. *Radiation Measurements*, **42**, 370-379.

Thornes, J.B. (1980). Erosional processes of running water. In: Kirkby, M.J. and Morgan. R.P.C. (Eds), *Soil Erosion*. Chinchester, Wiley. 129-182.

Timms, W. and Acworth, R.I. (2002). Origin, lithology and weathering characteristics of Upper Tertiary – Quarternary clay aquitard units on the Lower Murrumbidgee alluvial fan. *Australian Journal of Earth Sciences*, **49**, 525 – 537.

Tisdall, J.M. and Oades, J.M. (1982). Organic matter and water-stable aggregates in soils. *Journal of Soil Science*, **33**, 141-163.

Tomita, Y. (1951). On the geomorphological classification of fans in Taiwan (Formosa). *Journal of Geography (Tokyo)*, **60**, 2 –9 (in Japanese with English abstract).

Tooth, S., Brandt, D., Hancox, P.J. and McCarthy, T.S. (2004). Geological controls on alluvial river behaviour: a comparative study of three rivers on the South African Highveld. *Journal of African Earth Sciences,* **38,** 79–97.

Tooth, S., McCarthy, T.S., Brandt, D., Hancox, P.J. and Kendall, G.J. (2001) Controls on Late Quaternary river channel and alluvial fan activity in the semi-arid Steelpoort region, Mpumalanga/Northern Province, South Africa. Dryland Change 2001 International Conference, Upington, Northern Cape, South Africa, 30 August–2 September 2001, p.52.

Tooth, S., McCarthy, T.S., Brandt, D., Hancox, P.J., Morris, R. (2002). Geological controls on the formation of alluvial meanders and floodplain wetlands: the example of the Klip River, eastern Free State, South Africa. *Earth Surface Processes and Landforms*, **27**, 797–815.

Torri, D. and Borselli, L. (2003). Equation for high-rate gully erosion. *Catena,* **50**, 449-467.

Torri, D. and Poesen, J. (2014). A review of topographic threshold conditions for gully head development in different environments. *Earth Science Reviews*, **130**, 73-85.

Toya, H., Machida, H., Naito, H., Hori, N. (1971). Distribution of alluvial fans in Japan. In: Yazawa, D., Toya, H., Kaizuka, S. (Eds.), *Alluvial Fans*. Kokon Shoin, Tokyo, pp. 97– 120 (in Japanese).

Tyson, P.D. and Lindesay, J.A. (1992). The climate of the last 2000 years in southern Africa. *Holocene*, 2 (3), 271-278

Tyson, P.D. and Preston-Whyte, R.A., 2000: *The Weather and Climate of Southern Africa*. Oxford University Press, Oxford.

UNEP (1992). *World Atlas of Desertification*. Edward Arnold, London.
UNEP/ISRIC. (1990). *World map on status of human-induced soil degradation*. UNEP, Nairobi.

Valentin, C., Poesen, J. and Li, Y. (2005). Gully erosion: Impacts, factors and control. *Catena*, **63**, 132-153.

Valentine, K.W.G and Dalrymple, J. B. (1976). Quaternary buried palaeosols: A critical review. *Quaternary Research,* **6**, 209-222.

Vandenberghe, D., (2004). Investigation of the Optically Stimulated Luminescence Dating Method for Application to Young Geological Samples. PhD Dissertation (Unpubl). University Of Gent, Netherlands.

Van Deventer, P.W., Bennie, A.T.P. and Hattingh, J.M. (2002). Influence of stones on infiltration and runoff. In: Van Deventer, P.W., Bennie, A.T.P. and Hattingh, J.M. (Eds.), *Hydraulic properties of stony soils*. Draft final report to WRC.

Van Olphen, H. (1977). *An Introduction to Clay Colloid Chemistry*. 2nd edition. Wiley-Interscience Publications, New York. 318p.

Van Wambeke, A. (1992). *Soils of the Tropics*. McGraw-Hill, New York.

Van Zijl, G.M. (2010). An investigation of the soil properties controlling gully erosion in a sub-catchment in Maphutseng, Lesotho. Ph.D. dissertation (unpubl.). Stellenbosch University, South Africa.

Velde, B. (1992). *Introduction to Clay Minerals: Chemistry, origins, uses and environmental significance*. Chapman and Hall, London.

Verachtert, E., Van Den Eeckhaut, M., Poesen, J. and Deckers, J. (2010). Factors controlling the spatial distribution of soil piping erosion on loess-derived soils: A case study from central Belgium. *Geomorphology*, **118**, (3–4), 339–348.

Verster, E. and van Rooyen, T.H. (1999). Palaeosols on a fluvial terrace at Driekop, Northern Province, South Africa as indicators of climatic changes during the Late Quaternary. *Quaternary International*, **57/58**, 229-235.

Viljoen, M. J., Franey, N. J., Coward, D. and Wedepohl, C. (1993). Classification of vegetation degrading in the north-eastern Transvaal using SPOT imagery. *South African Journal of Science,* **89**, 429-431.

Visser, J.N.J. and Botha, B.J.V. (1980). Meander channel, point bar, crevasse splay, and aeolian deposits from the Elliot Formation in Barkly Pass, North-Eastern Cape. *Transactions of the Geological Society of South Africa*, **83**, 55-62.

Vogel, J.C. (1983). Isotopic evidence for past climates and vegetation of southern Africa. *Bothalia,* **14**, 391-394.

Wallinga, J. (2002). Optically stimulated luminescence dating of fluvial deposits: A review. *Boreas,* **31**, 303-322.

Wang, Y., Amundson, R. and Trumbore, S. (1996). Radiocarbon dating of soil organic matter. *Quaternary Research*, 45 (3), 282–288.

Wanner, H., Beer, J., Butikofer, J., Crowley, T.J., Cubasch, U., Fluckiger, J., Goosse, H., Grosjean, M., Joos, F., Kaplan, J.O., Kuttel, M., Muller, S.A., Prentice, I.C., Solomina, O., Stocker, T.F., Tarasov, P., Wagner, M. and Widmann, M. (2008). Mid- to Late Holocene climate change: An overview. *Quaternary Science Reviews*, **27**, 1791–1828.

Warrence, N., Bauder, J.W. and Pearson, K.E. (2002). Basics of Salinity and Sodicity Effects on Soil Physical Properties. Department of Land Resources and Environmental Sciences, Montanta State University-Bozeman.

Wasson, R.J., Mazari, R.K., Starr, B. and Clifton, G. (1998). The recent history of erosion and sedimentation on the Southern Tablelands of Southeastern Australia: sediment flux dominated by channel incision. *Geomorphology*, **24**, 291–308.

Watson, A., Price-Williams, D. and Goudie, A.S. (1984). The palaeoenvironmental interpretation of colluvial sediments and palaeosols of the Late Pleistocene hypothermal in southern Africa. *Paleaogeography, Palaeoclimatology, Palaeoecology*, **45**, 225-249.

Watson, H.K. (1996). Short and long term influence on soil erosion of settlement by peasant farmers in KwaZulu-Natal. *South African Geographical Journal*, **78** (1), 1–6.

Watson, H.K. (1997). Geology as an indicator of land capability in the Mfolozi area, KwaZulu-Natal. *South African Journal of Science*, **93**, 39–44.

Watts, C.W., Dexter, A.R., Dumitru, E. and Arvidsson, J. (1996). An assessment of the vulnerability of soil structure to destabilization during tillage. Part I. A laboratory test. *Soil & Tillage Research*, **37**, 161-174.

Webster, R. (1965). A catena of soils on the northern Rhodesian plateau. *Journal of Soil Science*, **16**, 31–43.

Wells, N.A. and Dorr, J.A. (1987). Shifting of the Kosi River, northern India. *Geology*, **15**, 204-207.

Western Fertilizer Handbook. (1995). Produced by the Soil Improvement Committee of the California Fertilizer Association. Interstate Publishers Inc., Sacramento, California.

Whipple, K.X., Parker, G., Paola, G. and Mohrig, D. (1998). Channel dynamics, sediment transport, and the slope of alluvial fans: Experimental study. *Journal of Geology*, **106**(6), 677-694.

Wieder, M. and Yaalon, D.H. (1982). Micromorphological fabrics and developemental stages of carbonate nodular forms related to soil characteristics. *Geoderma*, **28**, 203-220.

Wilkinson, M.T. and Humphreys, G.S. (2005). Exploring pedogenesis via nuclide- based soil production rates and OSL-based bioturbation rates. *Australian Journal of Soil Research*, **43**, 767-779.

Wintle, A.G. (1997). Luminescence dating: laboratory procedures and protocols. *Radiation Measurements*, **27**, 769-817.

Wintle, A.G., Botha, G.A., Li, S.H. and Vogel, J.C. (1995a). A chronological framework for colluviation during the last 110 kyr in KwaZulu/Natal. *South African Journal of Science*, **91**, 134-139.

Wintle, A.G., Botha, G.A., Li, S.H. and Vogel, J.C. (1995b). Evaluation of luminescence-dating procedures applied to late-Holocene colluvium near St Paul's Mission, Natal, South Africa. *The Holocene*, **5** (1), 97-102.

Wintle, A.G., Li, S.H. and Botha, G.A. (1993). Luminescence dating of colluvial deposits from Natal, South Africa. *South African Journal of Science*, **89**, 77-82.

Wintle, A.G. and Murray, A.S. (2006). A review of quartz optically stimulated luminescence characteristics and their relevance in single-aliquot regeneration dating protocols. *Radiation Measurements*, **41**, 369-391.

www.weathersa.co.za. Accessed 14 April 2013.

Yadav, J.S.P. and Girdhar, I.K. (1981). The effect of different magnesium-calcium ratios and sodium adsorption values of leaching water on the properties of calcareous soils versus non-calcareous soils. *Soil Science*, **131**, 194-198.

Young, A. (1976). *Tropical Soils and Soil Survey.* Cambridge University Press, U.K.

Zhang, X.C. and Norton, L.D. (2002). Effect of exchangeable Mg on saturated hydraulic conductivity, disaggregation and clay dispersion of disturbed soils. *Journal of Hydrology*, **260**, 194-205.

Zhou, C.H. and Keeling, J. (2013). Fundamental and applied research on clay minerals: From climate and environment to nanotechnology. *Applied Clay Science,* **74**, 3–9.

Zimmerman, D.W. (1971). Thermoluminescent dating using fine grains from pottery. *Archaeometry*, **13**, 29-52.

APPENDIX A

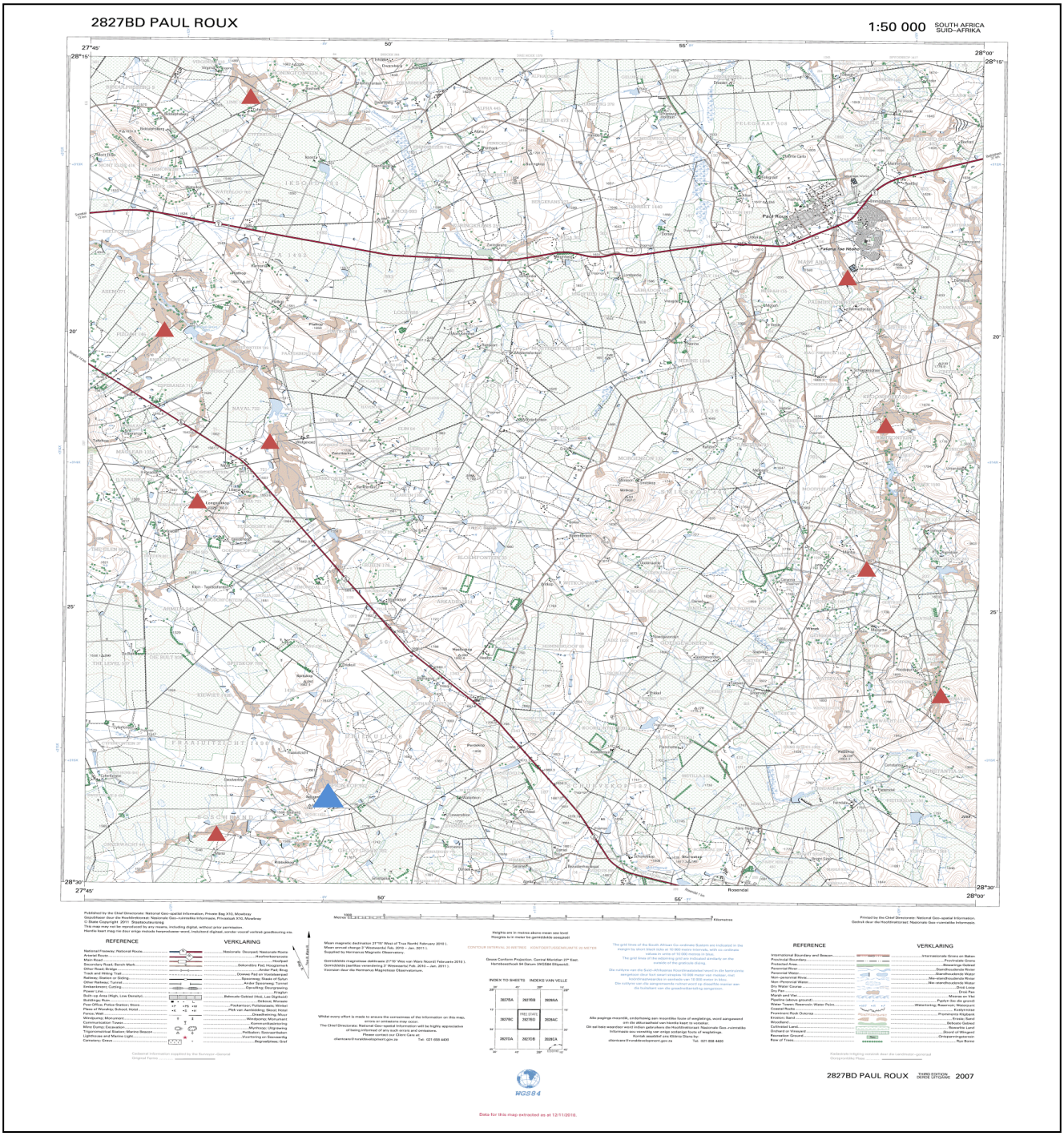
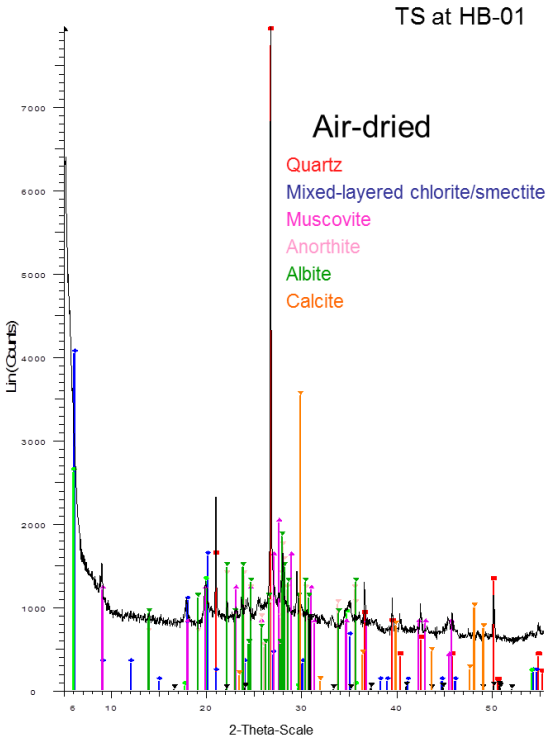
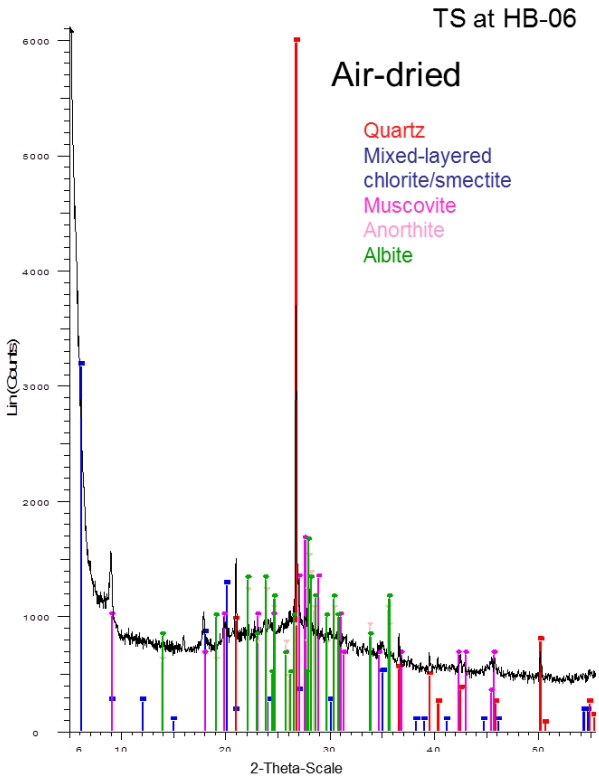


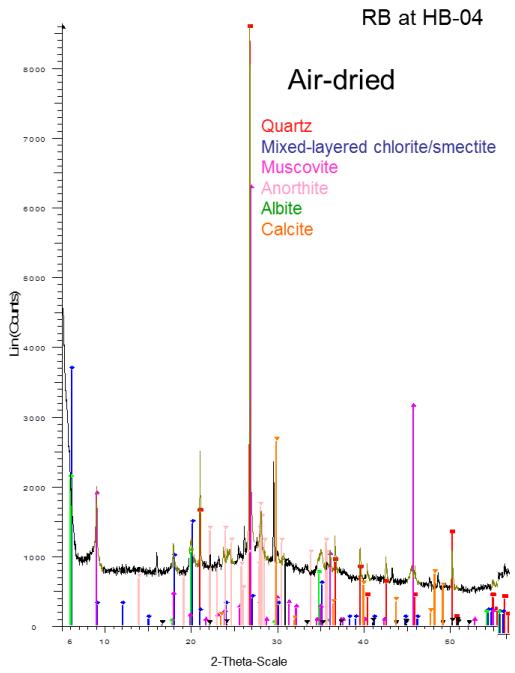
Figure A.1 1:50000 map of 2827 BD Paul Roux with numerous, discontinuous erosional sites (red markers). These are sites for future research to compare the Heelbo deposit to. Heelbo is shown by blue marker.

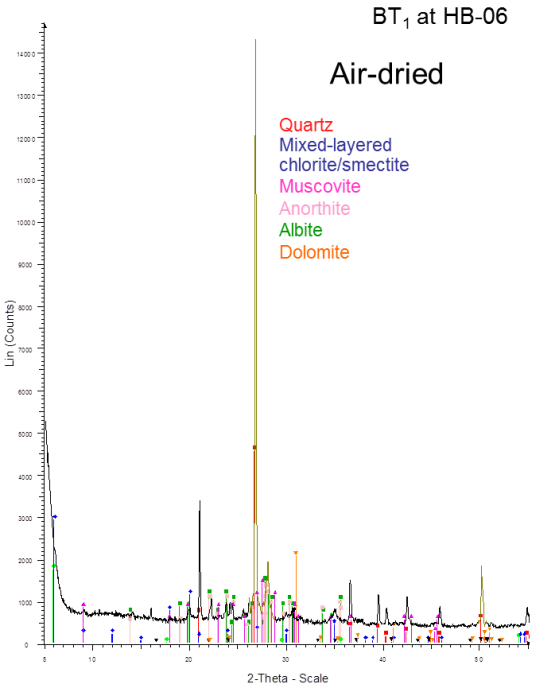
APPENDIX B

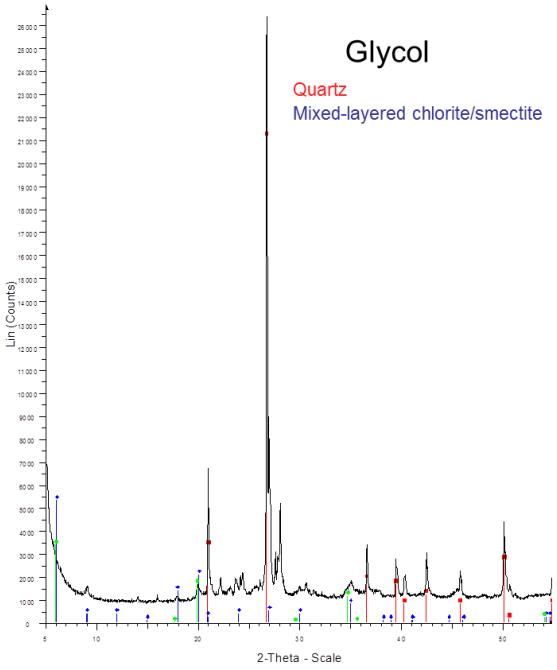
XRD patterns for mineral identification. The principle minerals are identified on each pattern in the colour of the peaks.

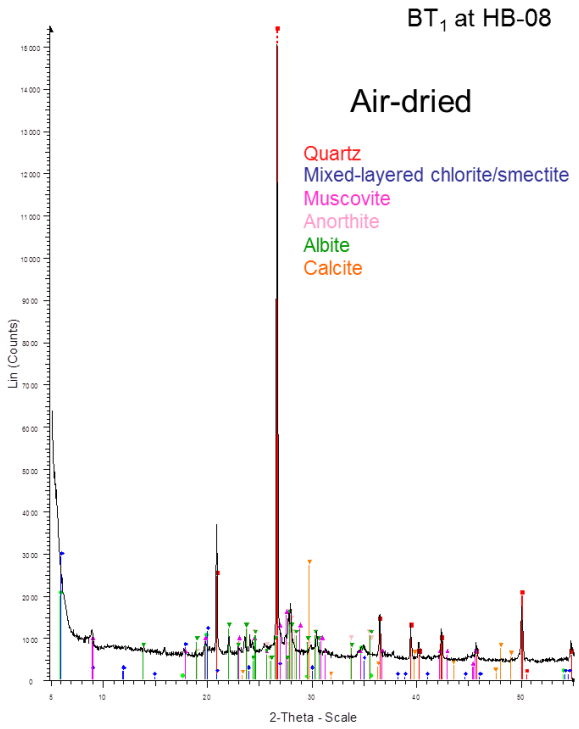


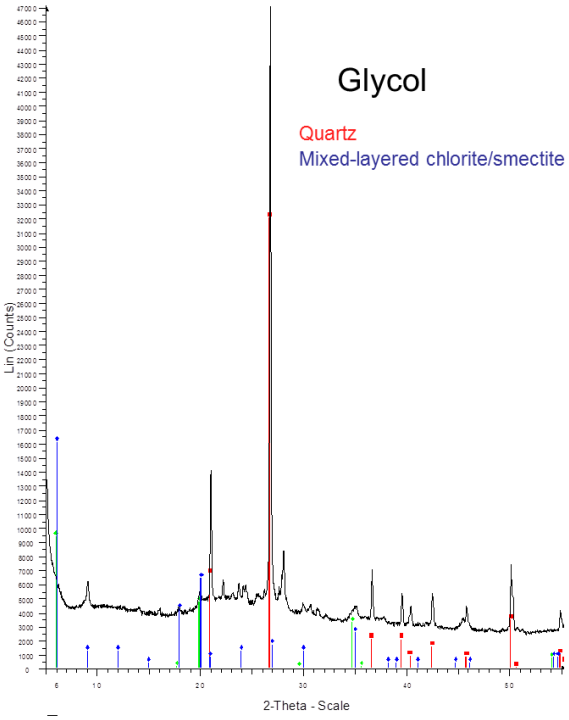


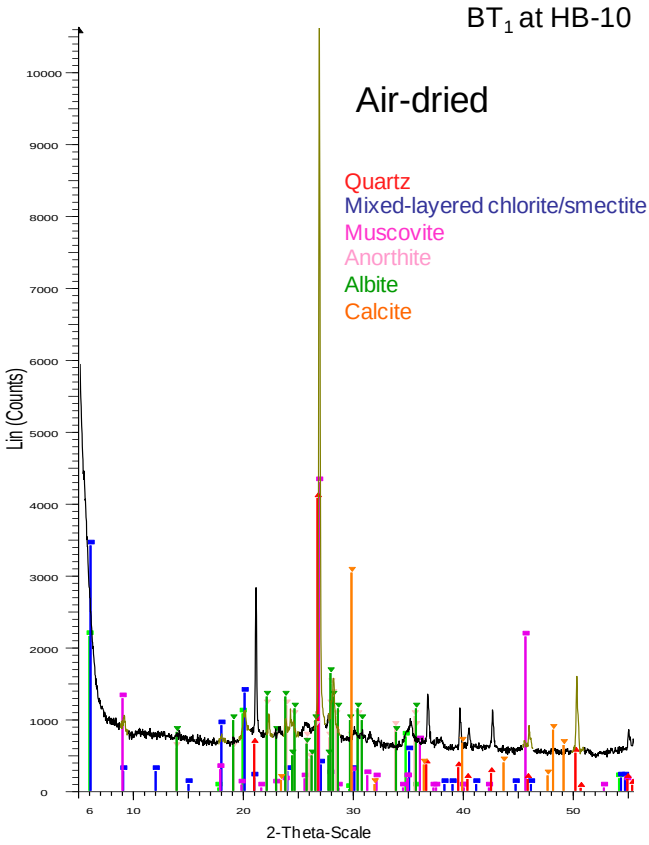

RB at HB-04
Air-dried
Quartz
Mixed-layered chlorite/smectite
Muscovite
Anorthite
Albite
Calcite
Lin(Counts)
2-Theta-Scale


BT1 at HB-06
Air-dried
Quartz
Mixed-layered chlorite/smectite
Muscovite
Anorthite
Albite
Dolomite
Lin (Counts)
2-Theta - Scale

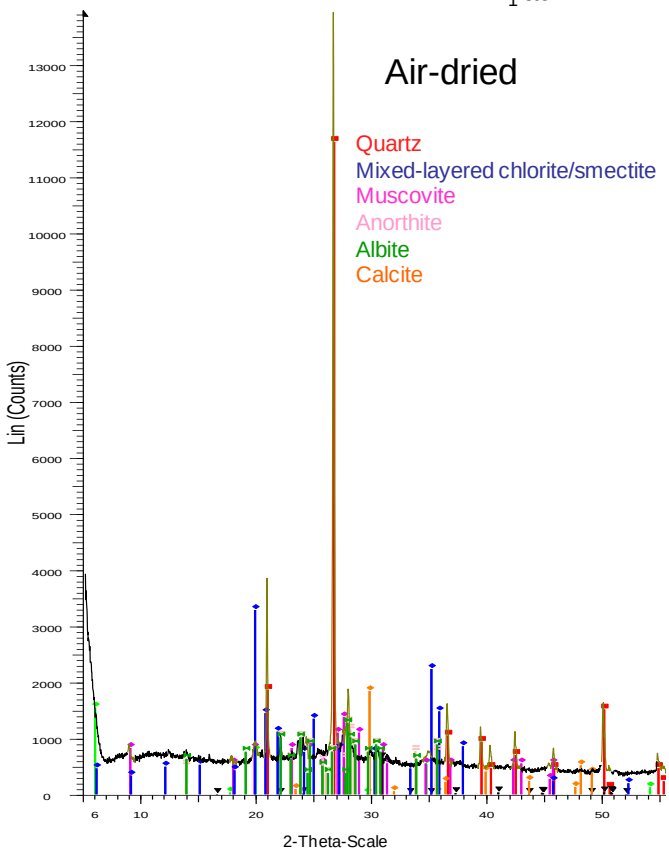

Glycol
Quartz
Mixed-layered chlorite/smectite
Lin (Counts)
2-Theta - Scale


BT1 at HB-08
Air-dried
Quartz
Mixed-layered chlorite/smectite
Muscovite
Anorthite
Albite
Calcite
Lin (Counts)
2-Theta - Scale

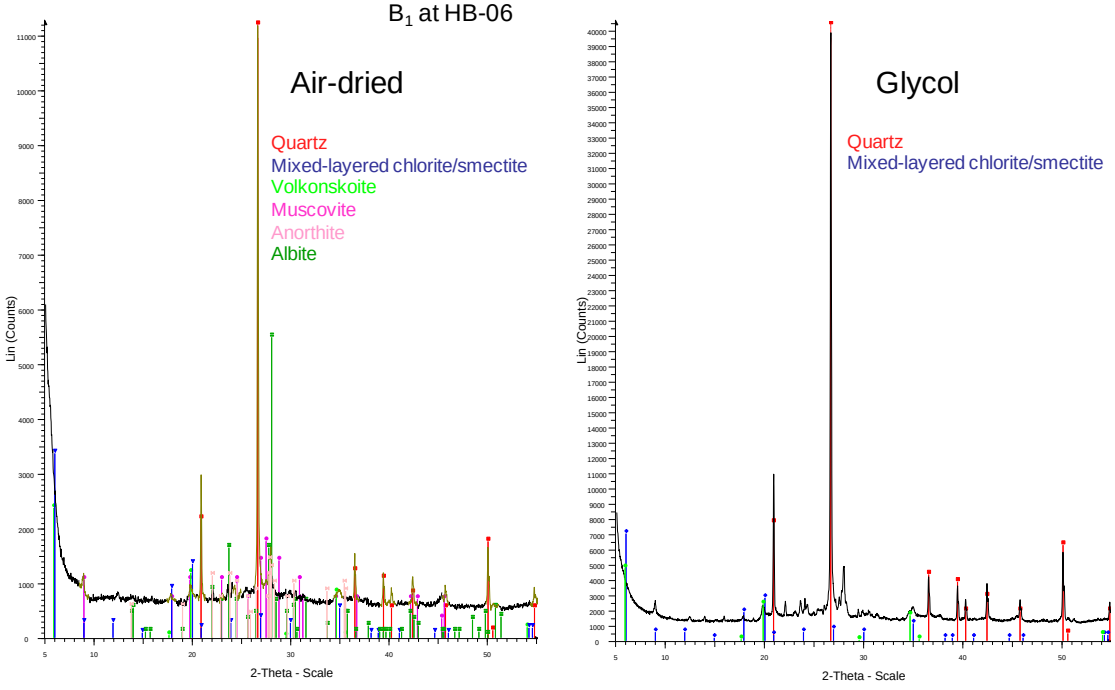

Glycol
Quartz
Mixed-layered chlorite/smectite
Lin (Counts)
2-Theta - Scale


BT1 at HB-10
Air-dried
Quartz
Mixed-layered chlorite/smectite
Muscovite
Anorthite
Albite
Calcite
Lin (Counts)
2-Theta-Scale

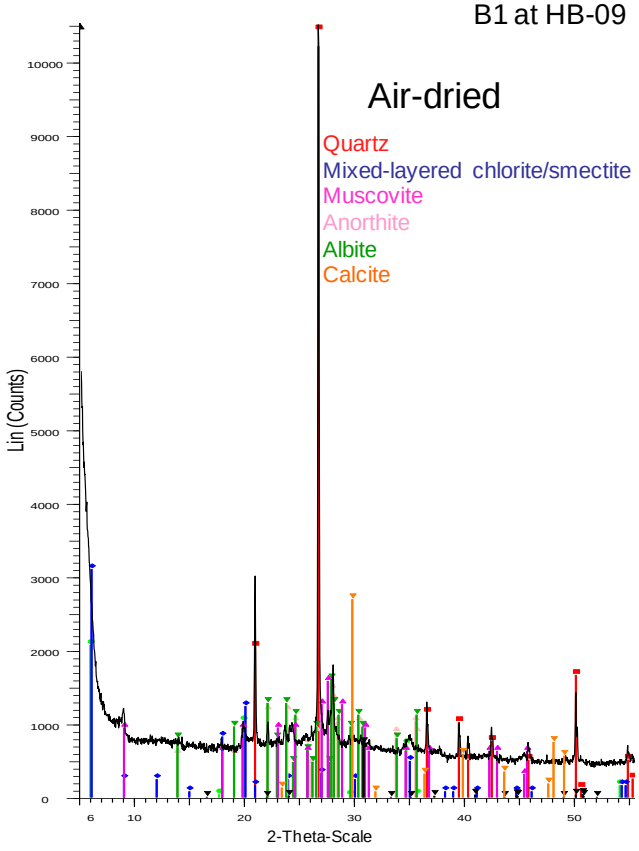
BT_1 at HB-11



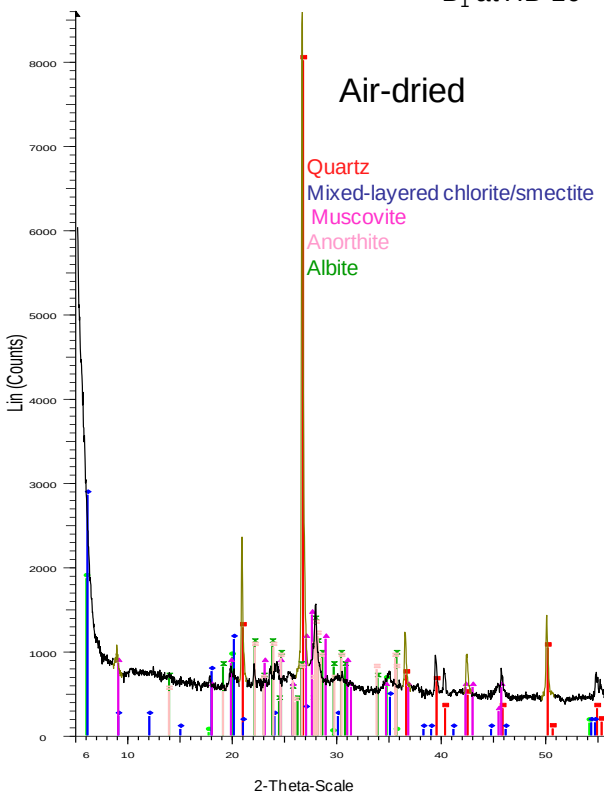
B_1 at HB-06

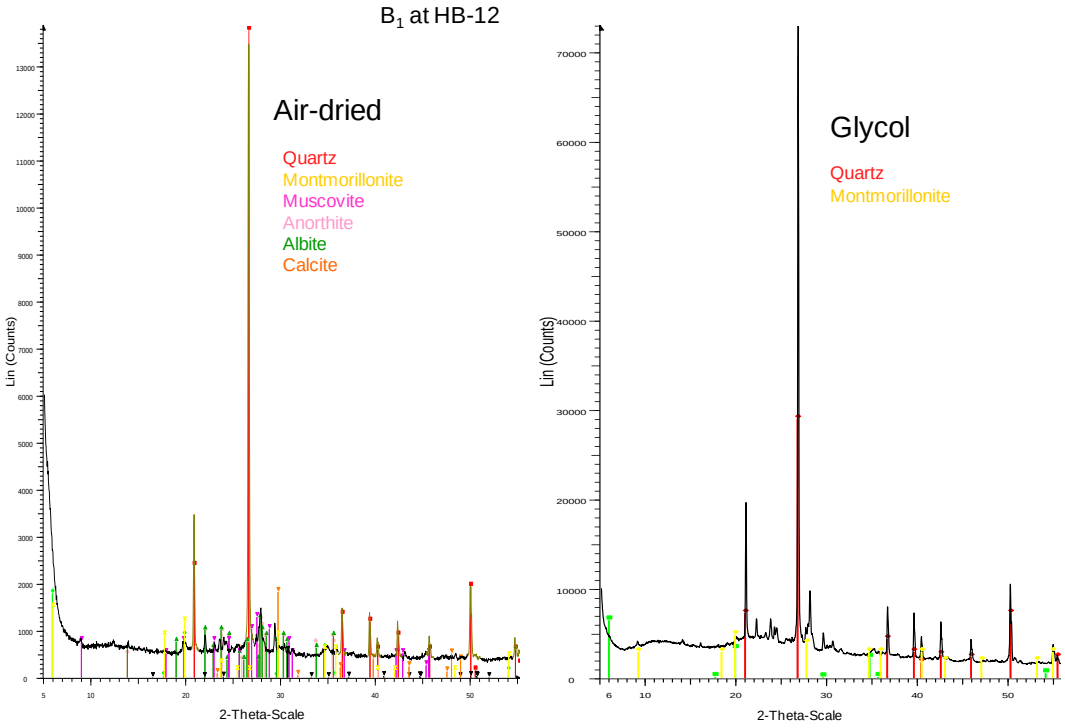


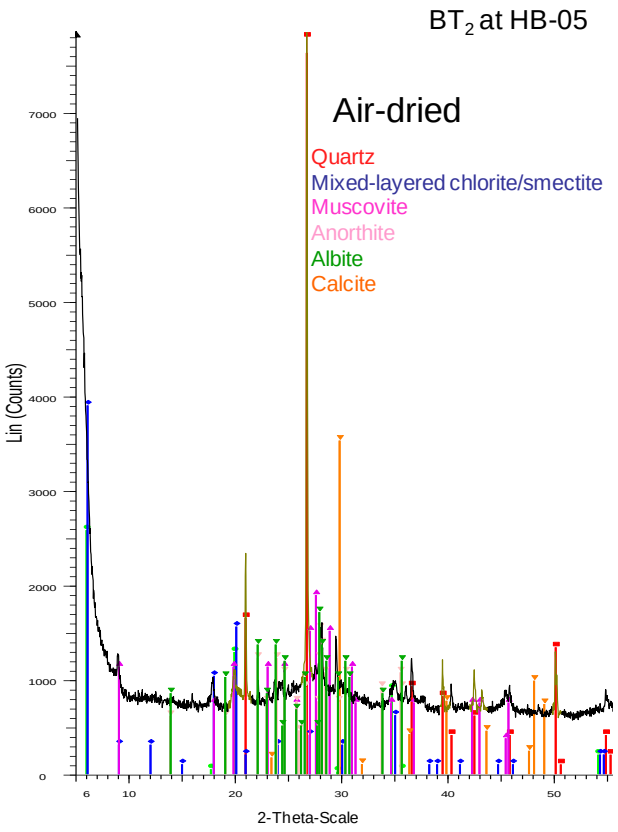
B1 at HB-09

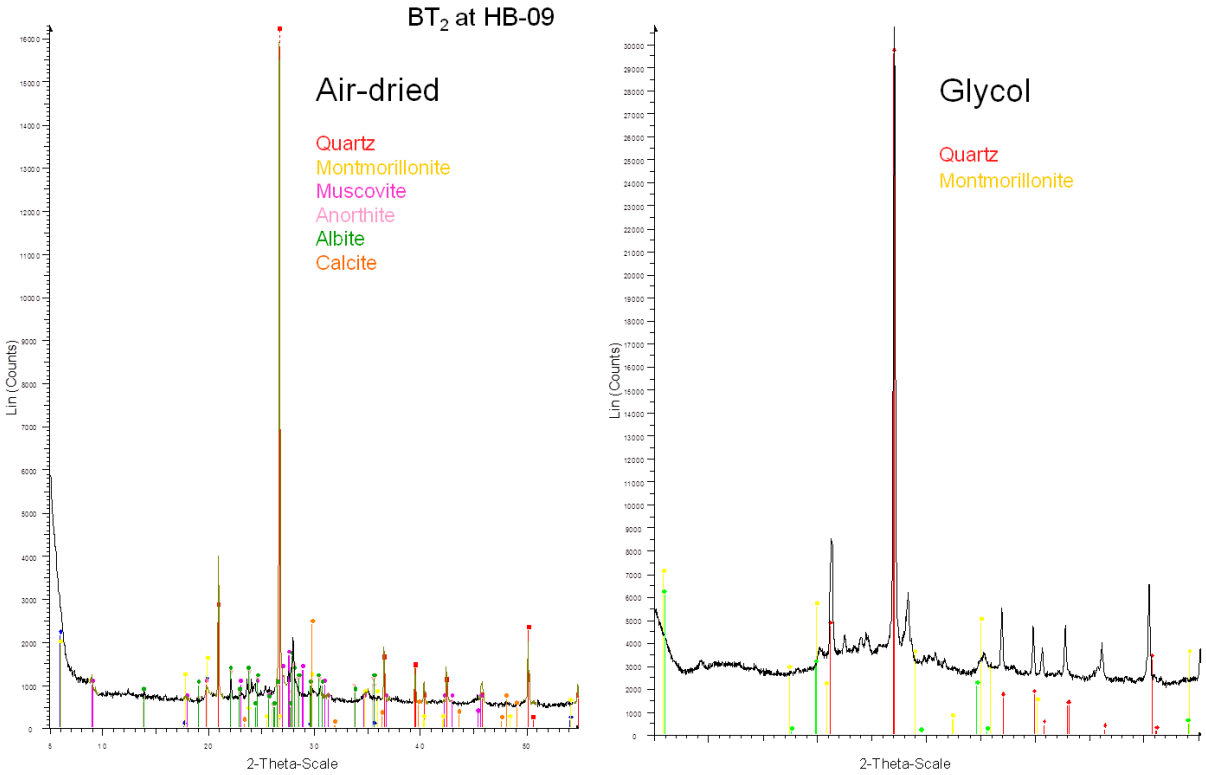


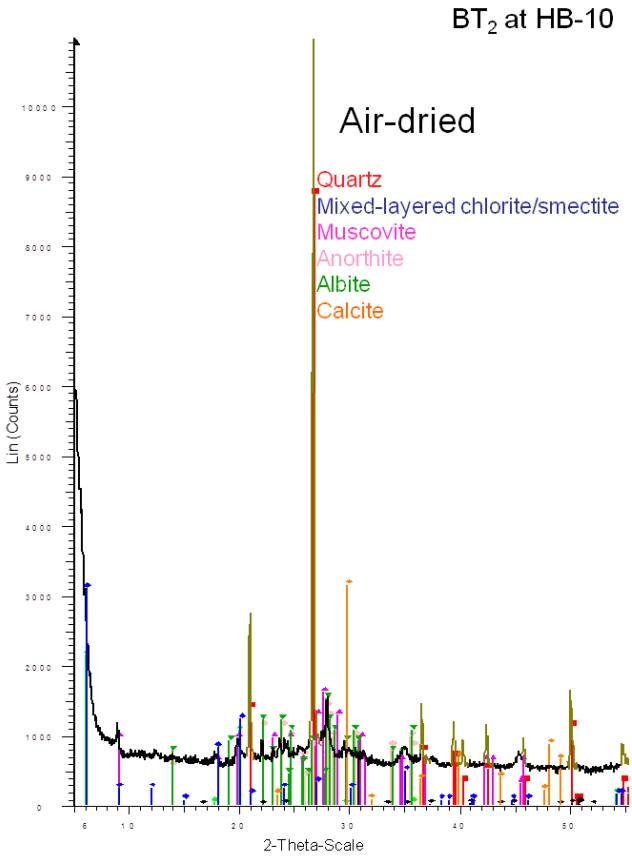
B_1 at HB-10



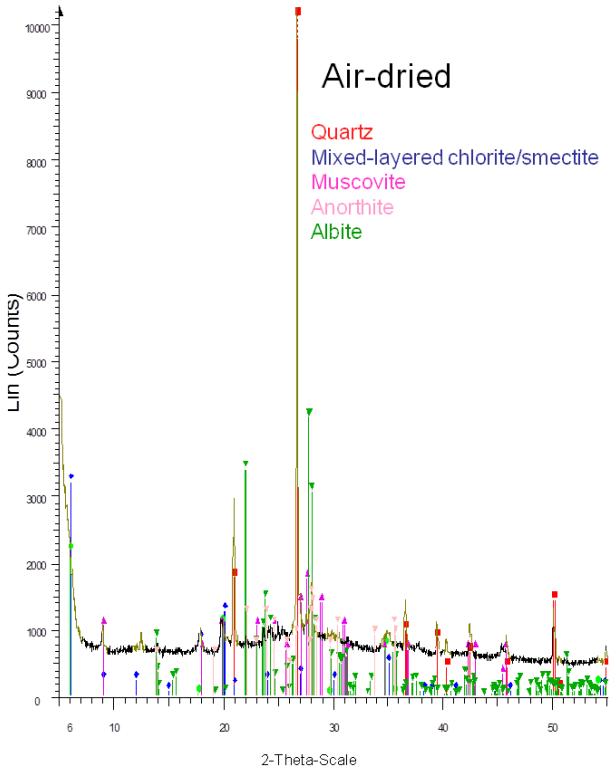

B1 at HB-12
Air-dried
Quartz
Montmorillonite
Muscovite
Anorthite
Albite
Calcite
Lin (Counts)
2-Theta-Scale
Glycol
Quartz
Montmorillonite
Lin (Counts)
2-Theta-Scale


BT2 at HB-05
Air-dried
Quartz
Mixed-layered chlorite/smectite
Muscovite
Anorthite
Albite
Calcite
Lin (Counts)
2-Theta-Scale

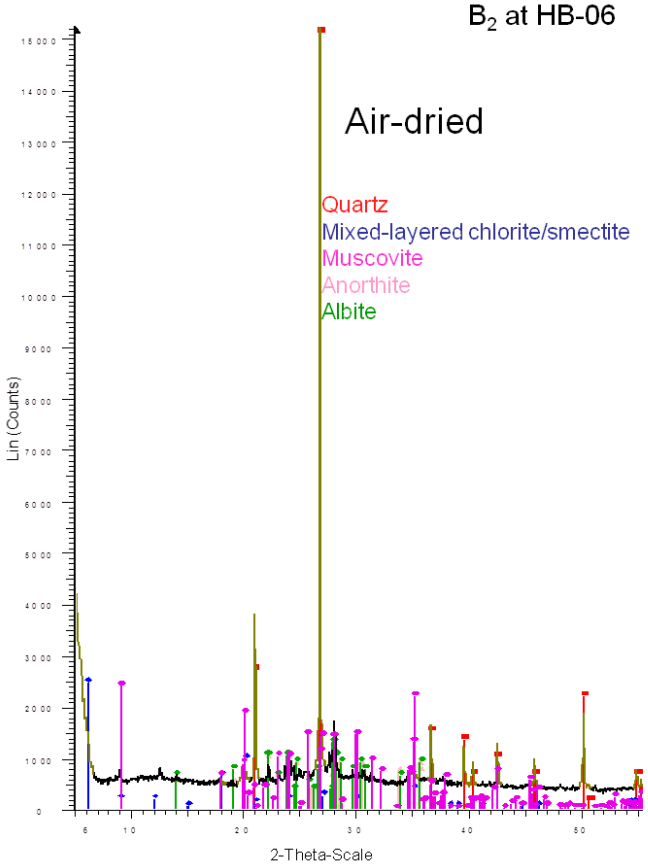

BT2 at HB-09
Air-dried
Quartz
Montmorillonite
Muscovite
Anorthite
Albite
Calcite
Lin (Counts)
2-Theta-Scale
Glycol
Quartz
Montmorillonite
Lin (Counts)
2-Theta-Scale


BT2 at HB-10
Air-dried
Quartz
Mixed-layered chlorite/smectite
Muscovite
Anorthite
Albite
Calcite
Lin (Counts)
2-Theta-Scale

B_2 at HB-05



B_2 at HB-06



APPENDIX C

Table C.1 Dose rate for the thorium and uranium series (Adamiec and Aitken, 1998, 43)

	Th-232	**U-238**	**U-235**	**Nat. U**
1. Abundance by weight	100%	99.29%	0.71%	-
2. Half life (Ga)	14.05	4.468	0.704	-
3. Parent Activity (Bq mg^{-1})	4.06	12.4	80	12.9
4. Activity Share in nat. U	-	95.6%	4.4%	-
Dose-rate (Gy ka-1) per ppm				
5. alpha, full series	0.732	2.685	16.6	2.78
6. alpha, pre-Rn	0.305	1.146	(16.6)	1.26
7. beta, full-series	0.0273	0.143	0.515	0.146
8. beta pre-Rn	0.0091	0.057	(0.515)	0.060
9. gamma, full serie	0.0476	0.112	0.269	0.113
10. gamma, pre-Rn	0.0178	0.0025	(0.269)	0.0044
Dose-rate (Gy ka-1) per unit specific activity (Bq kg-1				
11. Divide lines 5-10 by	4.06	12.4	80	12.9

Table C.2 Dose rate data for potassium and rubidium (Adamiec and Aitken, 1998, 44)

	K-40	**Rb-87**
1. Natural abundance (mg/g)	0.119	283
2. Half-life (Ga)	1.277	47.5
3. Average energy per disintegration (MeV)	β: 0.501 γ: 0.156	β: 0.082
4. Specific activity (Bq kg^{-1}) for concentration of 1% natural K and 50 ppm natural Rb	β: 270 γ: 32.5	β: 0.45.29
5. Dose-rate (Gy ka^{-1}) for concentrations of 1% natural K and 50 ppm natural Rb	β: 0.782 γ: 0.243	β: 0.019
6. As in 5 but for 1% K_2O and 50 ppm Rb_2O	β: 0.649 γ: 0.202	β: 0.017

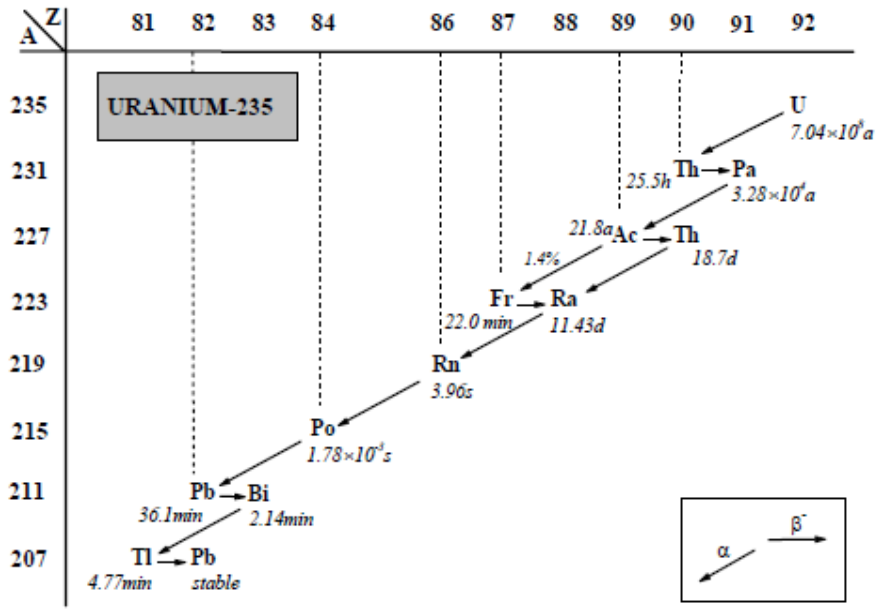


Figure C.1 Decay series for ^{235}Uranium with branching of a probability less than 1% omitted (modified from Chu *et al.*, 1999; Vandenberghe, 2004).

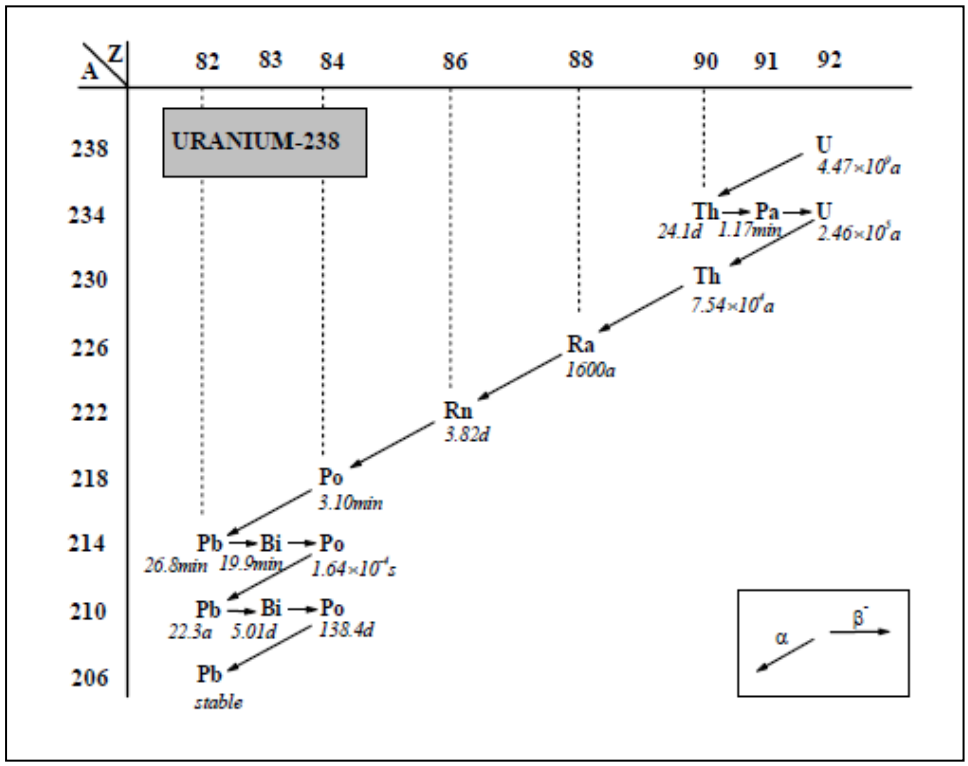


Figure C.2 Decay series for ^{238}Uranium with branching of a probability less than 1% omitted (modified from Chu *et al.*, 1999; Vandenberghe, 2004).

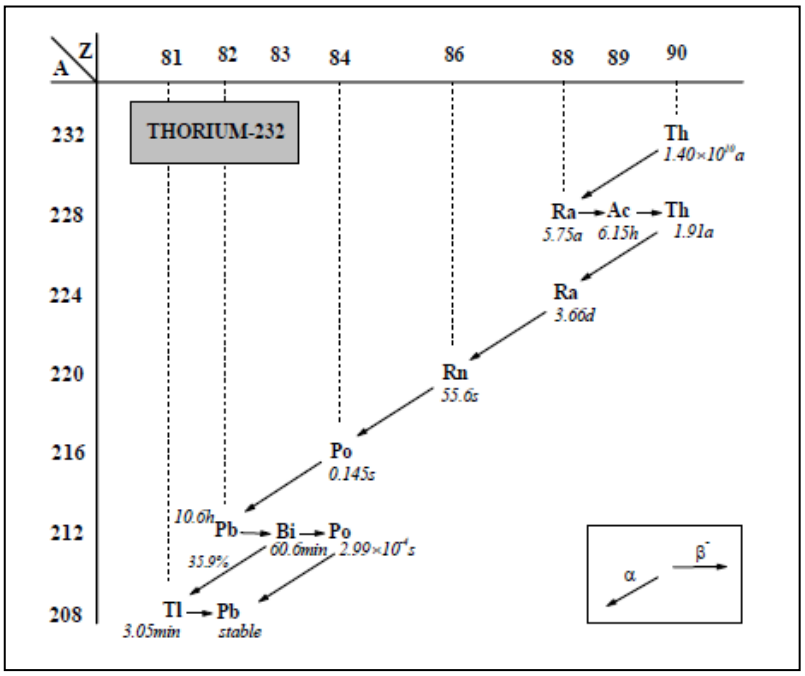


Figure C.3 Decay series for ^{232}Thorium with branching of a probability less than 1% omitted (modified from Chu *et al.*, 1999; Vandenberghe, 2004).

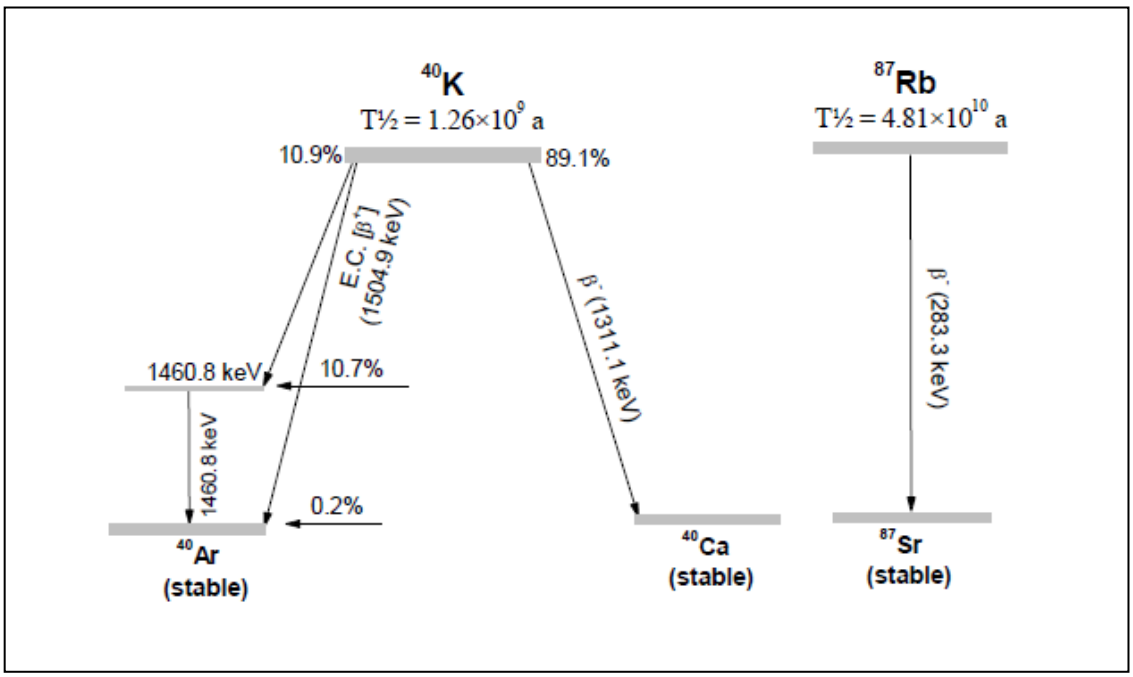


Figure C.4 Decay series for ^{40}K and ^{87}Rb (modified from Chu *et al.*, 1999; Vandenberghe, 2004).

APPENDIX D

A working example of the calculations to derive the total dose rate (D_r). The conversion rates are given in APPENDIX C. The example is based on the U, Th and K values of sample OSL3 given below:

	Th (ppm)	Unat (ppm)	K (%)
OSL3	9.66±0.24	2.69±0.04	1.64±0.028

1. Calculating the Beta Dose Rate

Beta dose rate from U ($Gy.ka^{-1}$) (2.69 x 0.146) 0.393 ± 0.006

Beta dose rate from U error ($Gy.ka^{-1}$) (0.393x 0.04/2.69)

Beta dose rate from Th ($Gy.ka^{-1}$) (9.66 x 0.0273) 0.264 ± 0.007

Beta dose rate from Th error ($Gy.ka^{-1}$) (0.264x0.24/9.66)

Beta dose rate from K ($Gy.ka^{-1}$) (1.64 x 0.782) 1.282 ± 0.022

Beta dose rate from K error ($Gy.ka^{-1}$) (1.282*0.028/1.64)

Total beta dose rate ($Gy.ka^{-1}$) (0.393+0.264+2.422) 3.079±0.024

Total beta dose rate error ($Gy.ka^{-1}$) ($\sqrt{(0.006^2+0.007^2+0.022^2)}$)

The attenuated beta dose rate is calculated using the beta attenuation factor (Table 6.6) for the grain size 180-212µm.

Total beta dose rate ($Gy.ka^{-1}$) (3.079*0.879) **2.706±0.024**

Total beta dose rate error ($Gy.ka^{-1}$) $(2.706* (0.004/0.879)^2+(0.024/3.079)^2)$

The total beta dose rate is then corrected for water content where the water content measured in the laboratory was applied:

Total beta dose rate (Gy/ka) (2.706/(1 + (1.25 x 0.129)) **2.330 ± 0.080**

Total beta dose rate error (Gy/ka) (2.330 x $\sqrt{((0.0375/1.125)^2 + (0.024/2.706)^2)}$ *

2. Calculating the Gamma Dose Rate

Gamma dose rate from U (Gy/ka) (2.69 x 0.113) 0.304 ± 0.005
Gamma dose rate from U error (Gy/ka) (0.304 x 0.04/2.69)

Gamma dose rate from Th (Gy/ka) (9.66 x 0.0476) 0.460 ± 0.011
Gamma dose rate from Th error (Gy/ka) (0.460 x 0.24/9.66)

Gamma dose rate from K (Gy/ka) (1.64 x 0.243) 0.399 ± 0.003
Gamma dose rate from K error (Gy/ka) (0.399 x 0.028/1.64)

The total gamma dose rate was calculated by combining the calculated gamma dose rates for each element.

Total gamma dose rate (Gy/ka) (0.304+0.460+0.399) 1.163 ± 0.018

Total gamma dose rate error (Gy/ka) ($\sqrt{(0.005^2 + 0.017^2 + 0.003^2)}$)

The total gamma dose rate was then corrected for water content, as with the beta dose rate:

Total gamma dose rate (Gy/ka) (1.163 / 1 + (1.14 x 0.129))

1.014 ± 0.035

Total gamma dose rate error (Gy/ka)

(1.014 x $\sqrt{(0.0342/1.114)^2+(0.018/1.163)^2}$) *

*The error calculations above include the terms (0.0375/1.125) and (0.0342/1.114) and are derived from the propagation of the error on the water content through the applied equation.

3. Determining the Cosmic Dose Rate

The cosmic dose rate was calculated from the co-ordinates and considering the overburden, according to Prescott and Hutton (1994). The cosmic dose rate (in $Gy.ka^{-1}$) is given in Table 6.7.

Total cosmic dose rate (Gy/ka) for OSL3 **0.34 ± 0.02**

Error on total cosmic dose-rate (Gy/ka)

TOTAL DOSE-RATE for Sample OSL3 **3.20 ± 0.16**